Effects of Warming on the Phenology of Photosynthesis of Eastern White Pine and Implications for the Use of Remote Sensing in a Changing Climate

by

Emmanuelle Fréchette

A thesis submitted in conformity with the requirements
for the degree of Doctor of Philosophy

Cell and Systems Biology
University of Toronto

Effects of Warming on the Phenology of Photosynthesis of Eastern White Pine and Implications for the Use of Remote Sensing in a Changing Climate

Emmanuelle Fréchette

Doctor of Philosophy

Cell and Systems Biology
University of Toronto

2019

Abstract

In northern trees, temperature and photoperiod control the beginning and end of the photosynthetically active season. Climate warming could extend the length of the photosynthetically active season, while photoperiod could potentially prevent trees from benefitting from warmer temperatures. Changes in the length of the photosynthetically active season can be estimated with the photochemical reflectance index (PRI), which detects xanthophyll cycle pigments involved in non-photochemical quenching (NPQ), a process affecting photosynthetic efficiency. In overwintering conifers, sustained NPQ replaces xanthophyll cycle-mediated NPQ, likely causing seasonal variations in the relationship between PRI and photosynthetic efficiency.

To better understand the impacts of climate warming on the spring and autumn photosynthesis of conifer forests, we investigated 1) the potential for enhanced photosynthesis during warmer springs and autumns in *Pinus strobus* L. and 2) seasonal variations in the relationship between PRI and the photosynthetic efficiency of needles.

During simulated summer-autumn and winter-spring transitions, PRI variation mainly reflected constitutive carotenoid pigment pool adjustments. During spring, differences in the timing of pigment pool adjustments and photosynthetic recovery impaired the relationship between PRI and photosynthesis. NPQ mechanisms and energy sinks undetected by PRI, such as electron transport around photosystem I, also impaired the relationship between PRI and photosynthesis.

In *P. strobus* seedlings from provenances located along a 1000 km latitudinal gradient, we observed differences in the phenology of photosynthesis, suggesting genetic controls of photosynthesis by photoperiod, with stronger controls during autumn than spring. The PRI could effectively track seasonal variations in energy partitioning, as well as carotenoid pigment pool sizes indicative of cold stress.

Photosynthesis in *P. strobus* might be enhanced during warmer springs and autumns, however, photoperiodic regulation of photosynthesis is to be expected during autumn. The interpretation of the PRI in evergreens should take into account alternative energy sinks, especially under cold spring and autumn conditions.

Acknowledgments

I would like to express my deepest gratitude to all of the people who made the completion of this work possible.

First of all, I wish to thank my thesis advisor Dr. Ingo Ensminger. Ingo, thank you for introducing me to the field of plant physiology all those years ago, and infecting me with your passion for the topic. I am grateful for your time, dedication, mentoring and guidance. Thank you for the hours spent discussing experiments, data, results and manuscripts, and for challenging me every step of the way. Thank you for reading, re-reading, and commenting countless versions of my written work. Ingo, thanks for everything!

I would also like to express my gratitude to the other members of my thesis advisory committee, Dr. Greg Vanlerberghe and Dr. Yuhong He, for taking the time to meet with me regularly throughout the years, and providing valuable feedback on my work. I am also grateful to Dr. John Gamon for hosting me in his laboratory at the University of Alberta during the summer of 2012, and for sharing helpful insight and advice on everything remote sensing!

Then I would like to thank my friends and colleagues from the Ensminger lab, for their constant support and presence. Particularly, thanks to Dr. Christine Chang, for your friendship, help with experiments, support in the field, motivational beer-drinking sessions and so much more. Thanks to Dr. Laura Junker, for guidance in the lab, help with our less-than-perfect HPLC, and German-style good times. Also, special thanks to all of those who provided invaluable assistance in the laboratory or out in the field: Chris Wong, Attey Rostami, Dhyani Patel, Alyssa Molinaro, Tarek Bin Yameen, Daniel Marsden, Chris Juliao, Kayla Dias, Maha Munawar, Claire Depardieu, Petra d'Odorico and Sharad Baral.

I must also thank UTM staff for their instrumental help with research projects: Lisa Cheung and Windsor Chan for providing assistance with laboratory equipment and experiments, Mirek Szreder and Andrew Veglio for repairing failing equipment more than once, Christine Tan and Tom Silver for ensuring proper functioning of our growth chambers. I am also

grateful to the staff of Koffler Scientific Reserve at Joker's Hill, particularly Stephan Schneider and John Jensen for ensuring proper functioning of our T-FACE arrays and providing all-season assistance in the field. Also, thanks to CSB's Ian Buglass for your help with everything administrative and quick email replies.

Last but not least, I am deeply grateful to my family and friends for their constant support throughout the years. Thanks to my mother, Nicole, for teaching me to dream big and believe that everything is possible. Thanks to my sisters Isabelle and Catherine for the support and encouragements, and for the visits to Ontario! Also, special thanks to my son Félix for giving me the last boost of motivation needed to complete this work and for daily reminders of what is really important. Finally, to Nicolas, who has been my rock and biggest cheerleader, thank you! Your love, (almost) infinite patience and support have been vital through it all.

I acknowledge financial support from the Natural Sciences and Engineering Research Council of Canada (NSERC), the Canada Foundation for Innovation (CFI), the University of Toronto Center for Global Change Science (CGCS), the Department of Cell and Systems Biology (CSB) at the University of Toronto and Ontario Graduate Scholarships (OGS).

Table of Contents

List of Tables

List of Figures

List of Abbreviations

A	CO_2 assimilation (in μmol CO_2 $m^{-2}s^{-1}$)
AIC	Akaike information criterion
ANOVA	analysis of variance
AT	ambient temperature
ATP	adenosine triphosphate
α	leaf absorptance
α_1	winter parameter value of the spring logistic function
α_2	early summer plateau value of the spring logistic function
α_3	late summer plateau value of the autumn logistic function
β_1	spring transition midpoint in DOY of the logistic function
β_2	autumn transition midpoint in DOY of the logistic function
Car	total carotenoids (in mmol mol Chl^{-1})
CBF	core binding factor
CCI	chlorophyll/carotenoid index
CET	cyclic electron transport rate (in μmol electron $m^{-2}s^{-1}$)
Chl	total chlorophylls (in μmol g fresh $weight^{-1}$)
CO_2	carbon dioxide
DEPS	de-epoxidation status of the xanthophyll cycle (in mol mol Chl^{-1})
DNA	deoxyribonucleic acid
DOY	day of year
δ_1	spring transition normalized slope coefficient of the logistic function
δ_2	autumn transition normalized slope coefficient of the logistic function

ΔPRI	difference between PRI of dark-adapted needles and PRI measured at high light
ELIP	early light-induced protein
ET	elevated temperature (+1.5°C/+3°C; day/night)
ETR_I	electron transport rate of photosystem I (in μmol electron $m^{-2}s^{-1}$)
ETR_{II}	electron transport rate of photosystem II (in μmol electrons $m^{-2}s^{-1}$)
EVI	Enhanced Vegetation Index
F_o	minimal fluorescence of dark-adapted needles
F_m	maximum fluorescence of dark-adapted needles
F_m'	maximum fluorescence of light-adapted needles
F_o'	minimal fluorescence of light-adapted needles
F_s	yield of fluorescence of light-adapted needles
F_v/F_m	maximum quantum yield of photosystem II
f_{PAR}	fraction of radiation absorbed by leaves
$\Phi_{f,D}$	fraction of light quenched by fluorescence and sustained NPQ
Φ_{NA}	fraction of overall P700 that cannot be oxidized by a saturation pulse due to a lack of electron acceptors
Φ_{ND}	fraction of overall P700 oxidized due to a lack of electron donors
Φ_{NPQ}	fraction of light quenched via dynamic NPQ
Φ_{PSI}	effective quantum yield of photosystem I
Φ_{PSII}	effective quantum yield of photosystem II; fraction of absorbed light used for photochemistry
GPP	gross primary productivity
g_s	stomatal conductance (in mmol H_2O $m^{-2}s^{-1}$)
HPLC	high-performance liquid chromatography
IPCC	Intergovernmental Panel on Climate Change
LD/HT	long day / high temperature (summer) seedlings

LHC	light-harvesting complexes
LP	local provenance
LP/AT	local provenance exposed to ambient temperature
LP/ET	local provenance exposed to elevated temperature
LUE	light-use efficiency of photosynthesis
LUE_A	light-use efficiency of CO_2 assimilation (in mol CO_2 mol quanta^{-1})
NADPH	nicotinamide adenine dinucleotide phosphate hydrogen
NDVI	Normalized Difference Vegetation Index
NP	northern provenance
NP/AT	northern provenance exposed to ambient temperature
NP/ET	northern provenance exposed to elevated temperature
NPQ	non-photochemical quenching
P	P700 signal
P700	reaction centre chlorophyll a molecule in association with photosystem I
PAR	photosynthetically active radiation
P_m	difference between fully reduced and fully oxidized P700
P_m'	maximum change of the P700 signal upon application of a saturating pulse
P_o	minimal P700 signal
PPFD	photosynthetic photon flux density (in μmol quanta $m^{-2}s^{-1}$)
PRI	photochemical reflectance index
PS	photosystem
PTFE	polytetrafluoroethylene
PTOX	plastid terminal oxidase
Q_A	primary quinone Q_A
qE	energy-dependent quenching
qI	sustained quenching

qN	non-photochemical quenching
qP	photochemistry
qT	state transition quenching
R_{531}	reflectance at 531 nm
R_{570}	reflectance at 570 nm
R_{645}	reflectance at 645 nm
RC	reaction centre
ROS	reactive oxygen species
SD/HT	short day / high temperature (warm autumn) treatment seedling
SD/LT	short day / low temperature (cold autumn) treatment seedling
SOD	start of downregulation
SOR	start of recovery
SP	southern provenance
SP/AT	southern provenance exposed to ambient temperature
SP/ET	southern provenance exposed to elevated temperature
Sp_C	cold spring treatment seedlings
Sp_W	warm spring treatment seedlings
Su	summer-acclimated seedlings
T-FACE	Temperature Free-Air-Controlled Enhancement
VAZ	total xanthophyll cycle pigments (in mmol mol Chl^{-1}).
Wi	winter-acclimated seedlings
1-qP	excitation pressure of photosystem II

Statement of Co-authorship

At the time of the submission of this thesis, Chapter 1, a literature review, is in preparation for submission to a peer-reviewed journal. Chapter 2, an original research paper, was published in the peer-reviewed journal *Tree Physiology* in February 2016. Chapter 3, an original research paper, was published in the peer-reviewed *Journal of Experimental Botany* in September 2015. Chapter 4, an original research paper, is in preparation for submission to a peer-reviewed journal. I was the primary author of all chapters of this thesis and for all research projects reported here, I was responsible for project design, execution and data analysis. Projects were carried out under the supervision of my thesis advisor, Dr. Ingo Ensminger. Contributions were made by fellow Ph.D. students at the University of Toronto at Mississauga, Dr. Christine Chang (Chapters 2, 3 and 4), Dr. Laura Junker (Chapter 3) and Christopher Wong (Chapter 3). A full description of author contributions for each manuscript is presented below.

Chapter 1

I had the lead writing the manuscript with editorial input from Dr. Ensminger.

Chapter 2

Dr. Chang, Dr. Ensminger and I initially planned the experiment and elaborated the experimental setting together. Dr. Chang and I set up and ran the growth chamber experiments together, and shared the work collecting the data. I analyzed samples and data myself, and wrote the manuscript with advice and guidance from Dr. Ensminger, who read and commented on versions of the manuscript. Dr. Junker elaborated the HPLC method that I used for photosynthetic pigment analysis.

Chapter 3

Dr. Ensminger and I initially planned the experiment and elaborated the experimental setting. I collected the majority of the data myself, and Christopher Wong collected the light-response curves to assess short-term PRI, fluorescence and gas exchange responses. Dr. Chang helped with HPLC analysis. I analyzed the data myself, and wrote the manuscript with advice and guidance from Dr. Ensminger.

Chapter 4

Dr. Ensminger and I designed the study. I performed field measurements and samplings with the assistance of Dr. Chang. I performed pigment analyses, data analyses and I had the lead on writing the manuscript with input from Dr. Ensminger.

Chapter 1

1 Introduction: The Photochemical Reflectance Index as a Tool to Assess Changes in the Spring and Autumn Phenology of Photosynthesis of Evergreen Conifers Under Climate Warming

1.1 Context

In boreal forests, cold temperature is the most important climatic constraint to photosynthesis (Nemani *et al.* 2003; Öquist and Hüner 2003). The timing and duration of the photosynthetically active season are tightly coupled with that of the warm season, characterized by above-zero temperature and the absence of a snow cover. During the last decades, northern ecosystems have experienced the fastest warming compared to other regions of the globe, particularly during winter and spring (IPCC 2014). Indeed, in the last 30 years warming has extended the thermal potential growing season by 10.5 days, yet, the photosynthetic growing season has not matched that pace, with an extension of only 6.7 days (Barichivich *et al.* 2013). This indicates that vegetation is unable to fully exploit warmer temperatures in the spring and/or autumn. Several authors have postulated that photoperiodic control of spring and autumn phenology is constraining additional carbon uptake at the ends of the growing season (Körner and Basler 2010, Way and Montgomery 2014). As climate warms, photoperiod remains unaltered, resulting in shifted timing of the two environmental signals. Yet, the effects of this asynchrony on the phenology of photosynthesis in the spring and autumn are largely misunderstood. Myneni *et al*. (1997) estimated that during spring a week difference in canopy development can account for up to 20% of the inter-annual variability in forest net primary productivity. Changes in phenology associated with climate warming of northern forests will, therefore, directly affect global carbon cycling.

Although substantial developments have been made in assessing growing season length using remote sensing of forests dominated by deciduous vegetation, important limitations remain for the transfer of these techniques to coniferous forests. In deciduous forests,

growing season phenology is typically monitored with vegetation greenness indices derived from spectral reflectance data, most commonly the normalized difference vegetation index (NDVI) or enhanced vegetation index (EVI; Garrity *et al*. 2011, Sonnentag *et al*. 2012). Greenness indices, however, present important limitations in forests dominated by evergreen trees, which show little variation in canopy greenness throughout the year (Guyon *et al*. 2011, Hufkens *et al*. 2012, Melaas *et al*. 2013; Walther *et al.* 2016), making it difficult to detect the beginning and, particularly, the end of the photosynthetically active season. An alternative to greenness indices for the detection of the "invisible" phenology of evergreen conifers is the use of indices that actually track the efficiency of photosynthesis, such as the photochemical reflectance index (PRI). The biological basis of PRI is its capacity to detect the spectral signature of pigments involved in the dissipation of excess light, and, hence, the efficiency of photosynthesis (Gamon *et al*. 1992, 1997, Peñuelas *et al*. 1995).

The PRI has been used successfully to assess the efficiency of photosynthesis in a wide range of plant functional types and growing conditions (Garbulsky *et al*. 2011). However, recent studies on evergreen conifers suggest that changes in energy partitioning occurring during the spring and autumn seasons result in discrepancies between the PRI and the efficiency of photosynthesis, and that the size of leaf carotenoid pigment pools appears to be the main driver of PRI changes over seasonal timespans (Busch *et al.* 2009, Porcar-Castell *et al.* 2012; Wong and Gamon 2015a,b). More recently, the chlorophyll/carotenoid index (CCI), which tracks seasonal changes in leaf carotenoid pigment pools, has been proposed as a new way to assess the phenology of photosynthesis (Gamon *et al.* 2016). Indeed, since carotenoid pigments are upregulated with environmental stress, including cold stress occurring during winter, detecting the variations in their pool sizes might be the key to a better understanding of the spring and autumn phenology of photosynthesis. The suitability of the PRI and CCI to track variations in photosynthesis during those transitionary seasons needs to be clarified. This will allow more accurate assessment of growing season length conifer-dominated ecosystems in current and future climates, and, in turn, of the overall effects of warming on the carbon budget of northern forests.

1.2 Seasonal acclimation of photochemical and non-photochemical processes

For photosynthesis to occur, solar energy trapped by the photosystems (PS) is used to transfer electrons through an electron transport chain (Fig. 1.1). Electrons are initially donated by water when it is oxidized by PSII, and in the process protons are released into the lumen. Donated electrons reduce plastoquinone (PQH_2), which transfers electrons to the cytochrome b_6f, and delivers protons into the lumen, creating an electrochemical proton gradient across the thylakoid membrane. Electrons are then transferred to PSI via plastocyanin. PSI reduces $NADP^+$ to NADPH in the stroma with ferrodoxin (Fd) and flavoprotein ferrodoxin-NADP reductase (FNR). ATP synthase produces ATP as protons diffuse back through it into the stroma. The reducing power (NADPH) and chemical energy (ATP) resulting from the light reactions of photosynthesis are then used to fix carbon dioxide (CO_2) in the Calvin-Benson cycle to produce carbohydrates to sustain plant growth and metabolism (Fig 1.1; Hall and Rao 1986).

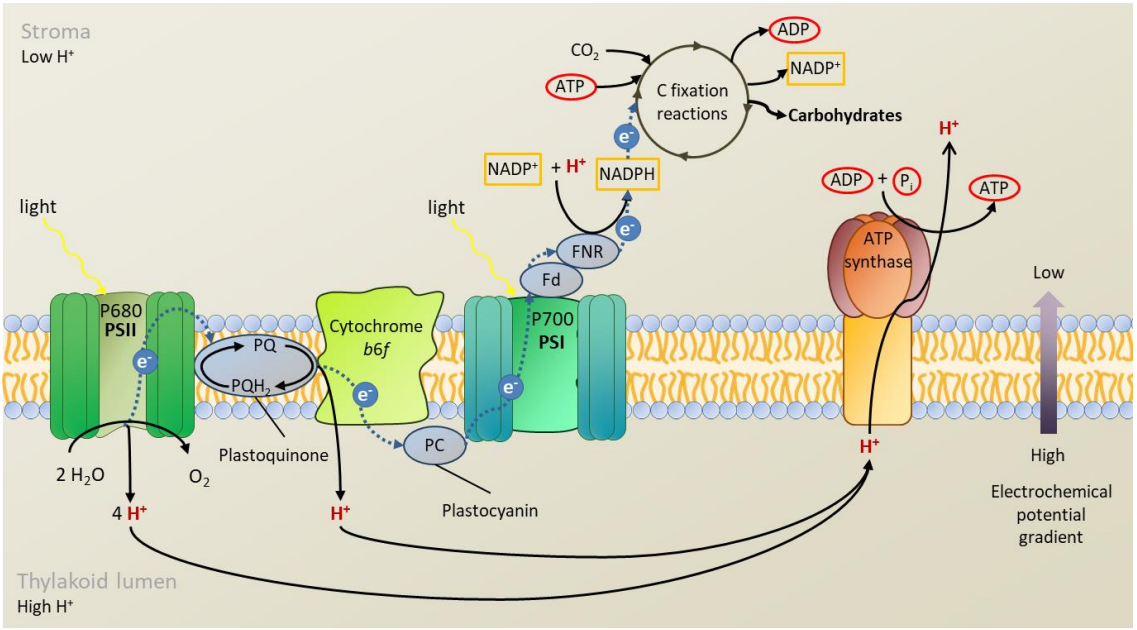

Figure 1.1 Electron and proton transport in the thylakoid membrane. Electrons released by water oxidation at PSII are transferred to PSI via plastoquinone (PQ), the cytochrome b_6f, and plastocyanin. At PSI, NAP^+ is converted into NADPH via the action of ferrodoxin (Fd) and flavoprotein ferrodoxin-NADP reductase (FNR). ATP synthase produces ATP as protons diffuse from the lumen into the stroma. NADPH and ATP are then used to fix CO_2 in the Calvin-Benson cycle for carbohydrate production (modified from Govindjee *et al.* 2017).

Over the course of days and seasons, plants harvest more light than can be used for photosynthesis. Indeed, not every photon trapped by the photosystems is destined to photosynthetic purposes. Plant exposure to solar energy is constantly changing, and environmental stresses continuously act on their metabolic sink capacity (Ensminger *et al*. 2006). Whenever light intensity increases or reducing power decreases via limitations in metabolism, photosynthesis may become light-saturated (Kanervo *et al*. 2005; Ensminger *et al.* 2006). This is because the processes involved in light absorption and energy transfer happen at a much faster timescale than electron transport and metabolism (Hüner *et al*. 1998). When more electrons are produced through light absorption than can be sent to the electron transport chain, accumulation of reduced components may occur. Such accumulation can be harmful, as it may cause photooxidative damage by reactive oxygen species (ROS; Barber and Andersson 1992). One strategy to avoid the production of ROSs is to maintain photostasis, i.e. a balance between the amount of absorbed energy and the amount used for photochemistry (Ensminger *et al*. 2006). This is accomplished with the regulation of light-use efficiency (LUE; Monteith 1972, 1977). Such regulation is achieved with the partitioning of absorbed light energy between photochemistry (qP) and non-photochemical quenching (NPQ or qN; Demmig-Adams & Adams 2006a, Ensminger *et al.* 2006; Fig. 1.2).

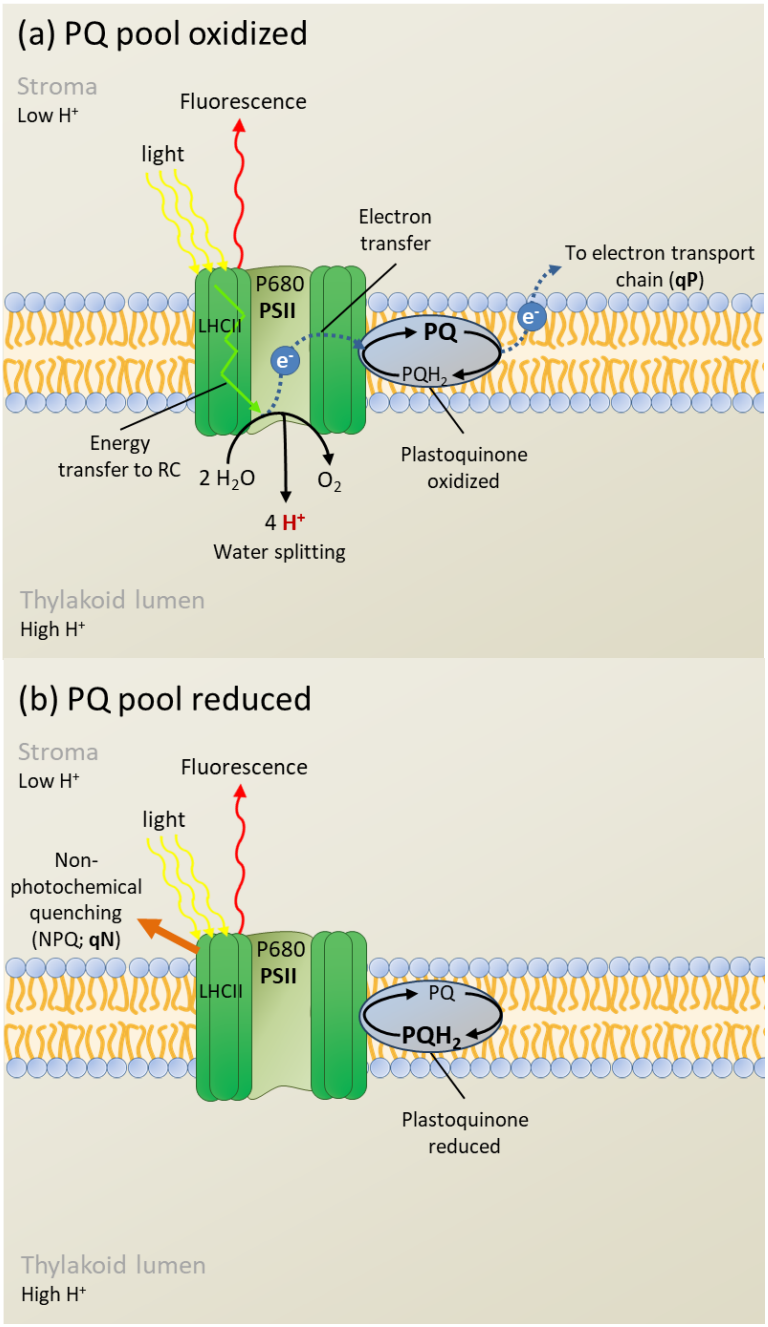

Figure 1.2 Light energy absorbed by chlorophylls in the light harvesting centers of PSII (LHCII) can be quenched via one of three alternative pathways: (1) excited chlorophyll can re-emit a photon to return to its ground state in a process known as fluorescence; (2) energy of the excited state can be used for photochemical reactions in a process known as photochemistry (qP; panel a), given that the components of the electron transport chain are oxidized and able to accept electrons; (3) excited chlorophyll can return to its ground state by converting its excitation energy into heat in a process known as non-photochemical quenching (NPQ; qN; panel b) in the case that the components of the electron transport chain are reduced and unable to accept electrons (modified from Govindjee *et al*. 2017; Demmig-Adams and Adams 2006).

In higher plants, NPQ has two main components, energy-dependent quenching (qE) and sustained quenching (qI), which differ in terms of their relaxation kinetics in darkness following a period of illumination (Demmig-Adams & Adams 2006a, Verhoeven 2014).

Energy-dependent quenching (qE)

The major and fastest component of NPQ is the pH- or energy-dependent component, qE (Müller *et al*. 2001, Demmig-Adams and Adams 2006a). This component is triggered at a timescale of seconds by light-induced proton transport across the thylakoid membrane, which creates a pH gradient and conformational change of PSII (Ruban *et al*. 2012). Additionally, xanthophyll cycle pigments are de-epoxidated, i.e. the pigment violaxanthin is converted into antheraxanthin and zeaxanthin (Fig. 1.3, Niyogi *et al*. 2005, Demmig-Adams & Adams 2006a). The de-epoxidation state of the xanthophyll cycle (DEPS) is commonly expressed as the ratio of foliar zeaxanthin and anteraxanthin to violaxanthin (Thayer and Björkman 1990). When the xanthophyll cycle is de-epoxidated, xanthophyll pigments are unable to pass their excitation energy to chlorophyll *a*, and energy transfer to the PSII reaction centre (RC) is reduced, thereby protecting PSII against over-excitation and photo-damage (Demmig-Adams *et al*. 2012). This process occurs at a timescale of minutes and is quickly reversible upon dark-relaxation (Müller *et al*. 2001).

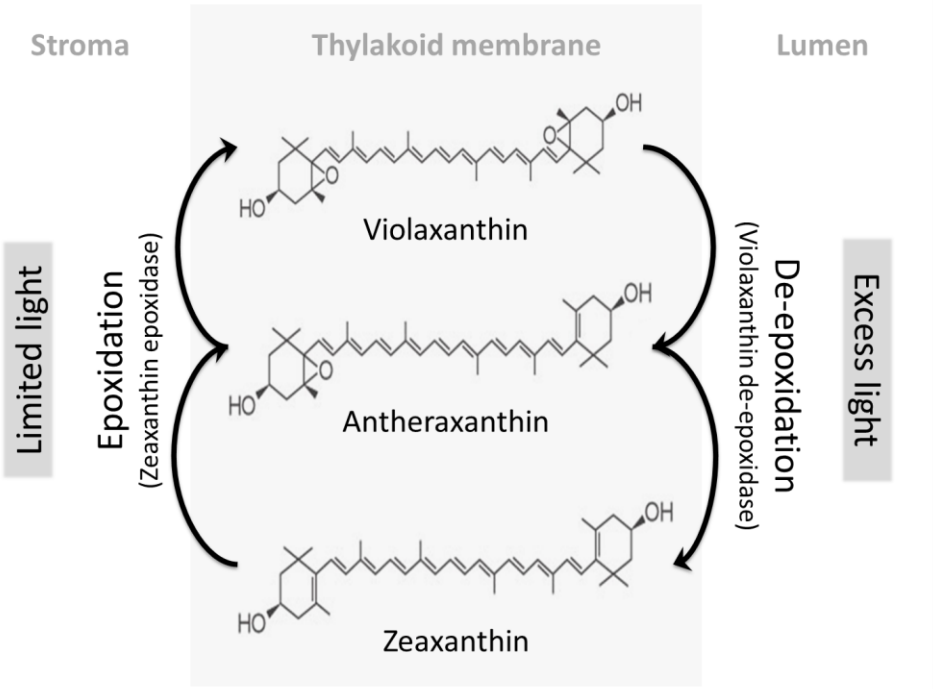

Figure 1.3 In plant leaves, as excess light conditions create the need for energy-dependent quenching (qE), xanthophyll cycle pigments are de-epoxidated within the thylakoid membrane. The de-eopxidation of xanthophyll pigments involves the conversion of the pigment violaxanthin into the energy-quenching pigment zeaxanthin via the intermediate pigment antheraxanthin. Under limited light conditions, zeaxaxanthin is re-converted back to violaxanthin (modified from Demmig-Adams 1990).

In addition to xanthophyll pigments, the thylakoid protein PsbS, which is part of the light harvesting complex (LHC) II family, was shown to function as a lumen pH sensor, playing a crucial role in the induction of energy dissipation (Verhoeven 2004). In evergreen conifers, qE is the main NPQ component during summer, allowing them to cope with diurnal fluctuations in light intensity.

Sustained quenching (qI)

The other major component of NPQ is referred to as sustained quenching, or qI, and replaces qE under prolonged and severe light stress (Müller *et al*. 2001, Demmig-Adams and Adams 2006a). The qI type quenching involves the upregulation of xanthophyll cycle pigments and the retention of zeaxanthin upon dark-relaxation, securing the photochemical system in a state of sustained dissipation of energy. When qI occurs concomitantly with cold

acclimation, such as in overwintering evergreen conifers, it involves a complete reorganization of the photosynthetic apparatus and changes in the composition of the thylakoid membrane (Ottander *et al*. 1995, Ensminger *et al*. 2004). The number of PSII reaction centre (RC) complexes declines considerably, and this includes reductions of the protein D1 (Ensminger *et al*. 2004, Verhoeven 2014), which was reported to be maintained in a phosphorylated state (Ebbert *et al*. 2005) under cold conditions. The physical size of the light-harvesting complexes (LHC) II also decreases, which involves the degradation of a fraction of the antenna chlorophyll content (Ottander *et al*. 1995). In the light-harvesting complex of PSII (LHCII), the early light-induced protein (ELIP) and the PsbS protein are upregulated (Verhoeven 2014), along with photoprotective pigments such as lutein and β-carotene (Adams & Demmig-Adams 1994, Filella *et al*. 2009). The light-harvesting complexes are also reorganized into large aggregates that are highly efficient in excess energy quenching (Ottander *et al*. 1995). These aggregates consist of chlorophylls and xanthophylls bound to thylakoid polypeptides, together with LHCII components, but also bind with polypeptides from the PSI complex (Öquist and Hüner 2003).

In evergreen conifers, qI gradually replaces qE during autumn as photosynthesis is downregulated in response to declining air temperature and shortening photoperiod (Öquist and Hüner 2003, Chang *et al*. 2015). There is evidence that evergreens have the ability to shift between qI and qE during winter (Ensminger *et al*. 2006). In early spring, most biochemical processes associated with qI are maintained as cold temperatures and excess light maintain a high demand for photoprotection. Upon warming of air temperature to above 0˚C, however, DEPS significantly declines, and the fraction of chlorophyll pigments increases and the photosynthetic apparatus is restructured (Ensminger *et al*. 2004). In Scots pine (*Pinus sylvestris* L.), the protein composition of the thylakoid membrane is to a large extent dependent on air temperature (Ensminger *et al*. 2004). Soil temperature also plays an important role in the recovery of photosynthesis, as it controls liquid water availability (Ensminger *et al*. 2004). Increased electron sink capacity due to warm air and soil conditions in late spring allows the complete recovery of photosynthesis and the full relaxation of qI.

Other NPQ mechanisms and energy sinks

In addition to qE and qI a number of NPQ mechanisms and energy sinks may contribute to the preservation of photostasis throughout the year. These mechanisms include state transitions (Minagawa 2013), PSII and PSI reaction centre quenching (Öquist and Hüner 2003), cycling electron transport around PSI (Johnson 2011), ROS scavenging by carotenoid pigments (Krieger-Liszkay 2008, Jahns and Holzwarth 2012), the Mehler reaction (Asada 2000) and the malic valve (Hossain and Dietz 2016). These mechanisms and energy sinks are in no way exclusive but work together as highly integrated photoprotective responses modulated by the physiological state of the plant, the duration and intensity of light stress, the time of day, and also the time of year.

State transitions

State transitions (qT) are a dynamic and rapid way of balancing light absorption. They involve the reversible dissociation of a peripheral fraction of the LHCII antenna complex, and association with either PSI or PSII (Minagawa 2013; Fig. 1.4). Lunde *et al*. (2000) demonstrated the activation of a protein kinase to be responsible for the phosphorylation of LHCII and the detachment of the mobile antenna complex. The redistribution of antenna proteins helps balance the absorption properties of the two photosystems at low light intensities, i.e. in early mornings, late afternoons and cloudy periods of the day (Kanervo *et al*. 2005). The qT component of NPQ is not considered to significantly contribute to photoprotection at high light intensities (Busch *et al*. 2007, Kanervo *et al*. 2005).

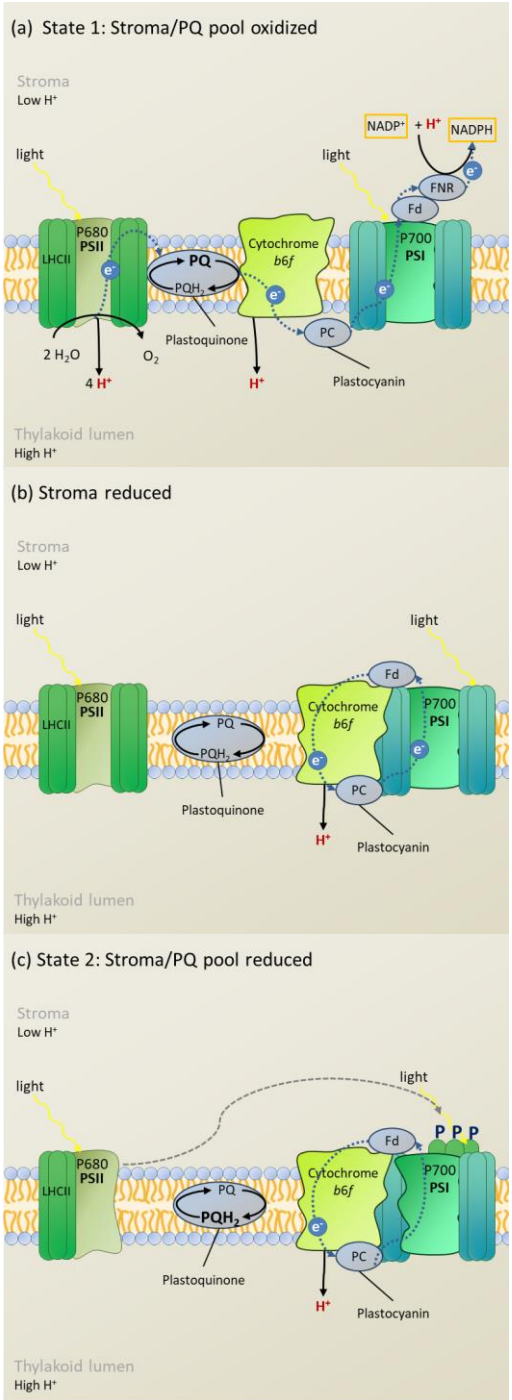

Figure 1.4 State transitions is a mechanism that helps maintain an energy balance between PSII and PSI. (a) When the stroma and PQ pool are oxidized, LHCII are bound to PSII and electron flow proceeds linearly to generate NADPH and a proton gradient across the thylakoid membrane. (b) When the stroma is reduced, cyclic electron flow is induced and the cytochrome b_6f complex and FNR associate with PSI to form a super-supercomplex. (c) If both the stroma and PQ pool are reduced, the lateral migration of phosphorylated LHCII to the periphery of PSI can occur to deliver more energy to PSI (modified from Minagawa 2013; Govindjee *et al*. 2017).

PSII and PSI reaction centre quenching

In addition to energy dissipation of excess light in the PSII antenna, efficient NPQ can occur within reaction centres (RCs) and play a significant role in photoprotection. RC quenching is induced when the primary quinone Q_A is over-reduced and NPQ via the enzyme-dependent xanthophyll cycle is restricted such as is the case under cold conditions (Ivanov *et al*. 2008). In winter-acclimated evergreen needles, it was proposed that the small number of remaining PSII RCs might act as important non-radiative quenchers (Öquist and Hüner 2003). Indeed, PSII RCs can be reversibly interconverted to a state of photochemical energy transduction, upon a decrease of excitation pressure and the oxidation of Q_A during spring. PSI RCs remain largely intact during winter, and since P700 efficiently quenches chlorophyll fluorescence (Bulter 1978), PSI may also be important for the quenching of excess light energy during winter (Öquist and Hüner 2003).

Cyclic electron transport around PSI

Under certain conditions, electron flow may occur from the reducing side of PSI via plastoquinone and cytochrome b_6f and back to P700. This cyclic electron flow occurs along with proton pumping into the lumen, which can be used for the production of ATP without oxidating water or reducing $NADP^+$ (Fig. 1.5; Johnson 2011). Additionally, the enhancement of the electrochemical gradient resulting from proton pumping into the lumen was shown to induce NPQ (Johnson 2011). While PSII is severely photoinhibited during winter, PSI is reportedly much less sensitive to cold stress (Ivanov *et al*. 2001). A drastic reduction of linear electron flow occurs between PSII and PSI under cold conditions, while cyclic electron transport around PSI is enhanced (Ivanov *et al*. 2001). Authors have suggested that PSI photochemistry during winter supplies the ATP required to maintain the integrity of chloroplasts under conditions of impaired linear electron transport, and may support recovery from winter stress during spring (Huang *et al*. 2011).

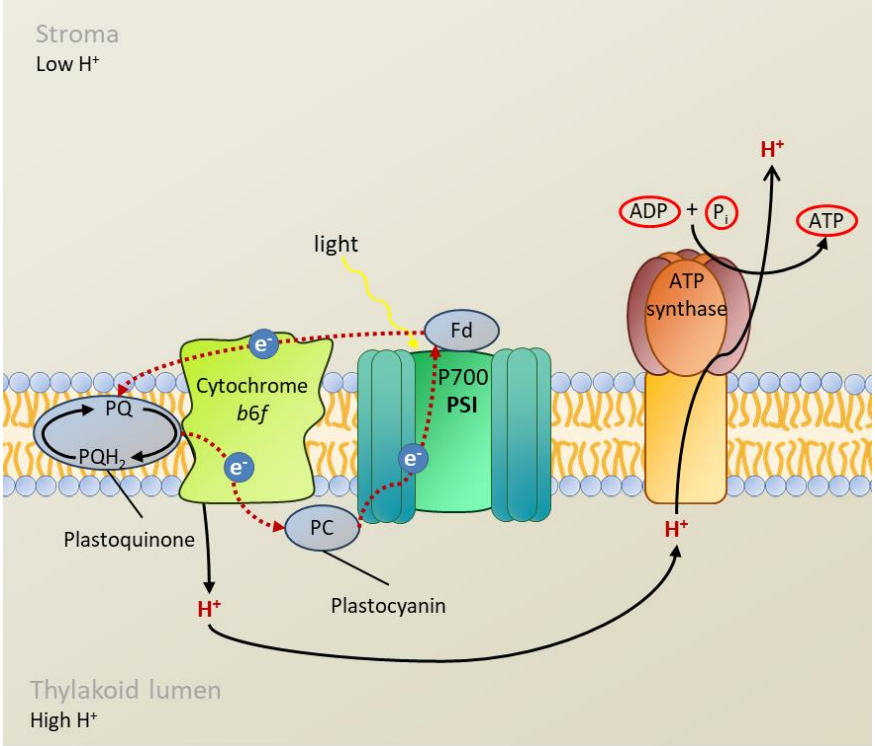

Figure 1.5 Under conditions suppressing linear electron transport, PSI may accept electrons from plastocyanin and transfer them back to cytochrome b_6f instead of transferring them to NADPH as is the case with linear electron transport (modified from Johnson 2011; Govindjee *et al*. 2017).

ROS scavenging by carotenoid pigments

As mentioned earlier, when more electrons are produced through light absorption than can be sent to the electron transport chain, the accumulation of reduced components may produce harmful ROSs (Barber and Andersson 1992). The carotenoid pigments lutein and β-carotene act as important ROS scavengers, with lutein having the ability to quench both the ^{3}Chl and ^{1}Chl*states (Dall'Osto *et al*. 2006, Avenson *et al*. 2009, Jahns and Holzwarth 2012), and β-carotene quenching the singlet oxygen generated via the triplet state of the primary electron donor pheophytin (Young and Frank 1996, Trebst 2003, Telfer 1994, 2005, 2014, Krieger-Liszkay 2008). This indicates that these pigments can act as efficient quenchers of excess energy. In overwintering conifers, the contents of both pigments are generally upregulated during autumn and peak during winter (Ottander *et al*. 1995, Chang *et*

al. 2015), suggesting a key role of these pigments in photoxidative damage avoidance under cold conditions.

The Mehler reaction

Under light conditions that are in excess of the amount of energy required to fuel photosynthesis, O_2 may constitute an important sink for excess excitation energy in a process referred to as the Mehler reaction (Asada 2000). Under conditions of excess light conditions causing an accumulation of reduced components on the electron transport chain, O_2 can be reduced by electrons produced by ferrodoxin at PSI to form a superoxide. The superoxide is then reduced by superoxide dismutase to form H_2O_2. This H_2O_2 is then rapidly scavenged at the site of its generation by the action of ascorbate peroxidase to form water and oxidized ascorbate, thereby preventing components of the electron transport chain from becoming over-reduced (Asada 2000).

The malate valve

The malate/oxaloacetate (OAA) shuttle, or malate valve, exports reducing equivalents out of the chloroplast to be used by processes such as oxidative electron transport in mitochondria, cytosolic enzymatic reactions, and photorespiratory metabolism in peroxisomes (Taniguchi and Miyake 2012). Under periods of stress, it also functions as a safety valve by removing excess reducing equivalents from the chloroplast, thereby maintaining the redox status of the stroma. The malate valve is composed of a malate/OAA exchanger situated in the chloroplast inner envelope membrane as well as isozymes of malate dehydrogenase (MDH) located in the stroma and cytosol. Using NADPH, stromal OAA is reduced to malate by NADP-MDH, allowing the shuttling of reductants from the chloroplast. Malate is subsequently exported to the cytosol by a malate/OAA transporter. In the cytosol, NAD-MDH produces NADH by oxidizing the exported malate to OAA, which is then sent back to the stroma by the malate/OAA transporter in exchange for malate from the stroma (Taniguchi and Miyake 2012).

1.3 Will warmer spring and autumns result in longer photosynthetic seasons in northern latitude forests?

Tree acclimation to warmer conditions through phenotypic plasticity

At northern latitudes, the length of the photosynthetically active season of trees is controlled by two environmental factors: temperature and photoperiod (Fig. 1.6), with individual tree species differing in their responses to each signal (Green 2007, Way and Montgomery 2015). The seasonal course of temperature varies greatly from one year to another, and sensitivity to photoperiod prevents plants from tracking temperature at the wrong time of year (Körner and Basler 2010), which can be lethal to active buds and other tissues. Körner and Basler (2010) reported long-lived, late-successional species to be generally sensitive to photoperiod, while shorter-lived, early-successional species generally adopt a more risky life-strategy and respond mainly to variations in air temperature.

The rise in atmospheric CO_2 concentrations due to fossil fuel burning and land use change is expected to increase global mean temperature by 2 to 5°C by 2100, with warming expected to be more severe at higher latitudes, and during winter (IPCC 2014). Climate envelope models predict a northward shift of the range of suitable conditions for tree species in the next decades in response to warming (Rehfeldt *et al.* 2012). As suitable conditions shift, trees can adjust to novel climatic conditions by either adapting through natural selection (Liepe *et al.* 2015) or migrating to follow conditions to which they are adapted (Savolainen *et al.* 2007; Hamann and Aitken 2013). Alternatively, plants may acclimate to novel conditions through phenotypic plasticity, i.e. the range of observable traits a single genotype can express as a function of its environment (Nicotra *et al.* 2010, Franks *et al*. 2013, Beever *et al.* 2016). In the case of long-lived tree species, phenological responses to rapid climate warming will depend largely on the degree of phenotypic plasticity exhibited in response to temperature and photoperiod, and the extent to which species rely on photoperiodic cues for determining phenology (Ensminger *et al*., 2015). For instance, species that are highly sensitive to photoperiod will not be able to track climate warming, thereby preventing a lengthening of the photosynthetically active season, unless they exhibit enough phenotypic plasticity to acclimate to new conditions (Fig. 1.6; Nicotra *et al*. 2010). In addition, epigenetic variation, i.e. variation arising from heritable changes in gene function that do not

result from changes in DNA sequence, is likely to play an important role in the phenotypic plasticity and adaptive capacity of trees (Bräutigam *et al*. 2013).

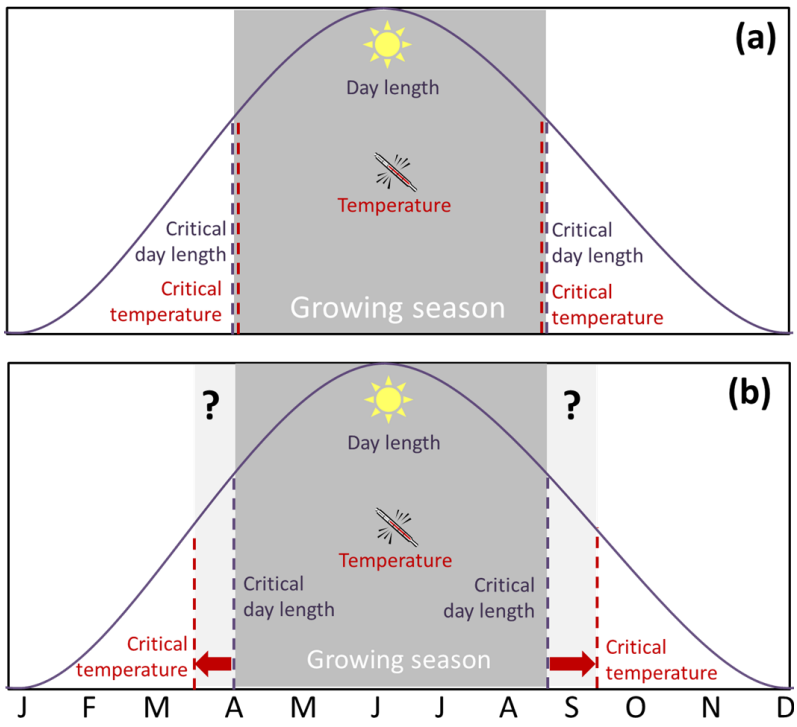

Figure 1.6 The spring and autumn phenology of photosynthesis is regulated by temperature and photoperiod. As climate warms, the timing of the critical temperature thresholds will shift while the timing of the critical photoperiod thresholds will remain unchanged. Species will benefit from warmer temperatures only if they are not constrained by photoperiod.

Temperature and photoperiod control the length of the photosynthetically active season of trees

Temperature

At temperate and boreal latitudes, low temperature is a major constraint on conifer photosynthesis, which decreases upon exposure to cold autumn days before being completely suppressed at subfreezing temperatures during winter (Lloyd *et al*. 2002, Ensminger *et al*. 2004). During autumn, cold temperature imposes limitations on the light reactions of photosynthesis by decreasing fluidity of the thylakoid membrane (Vogg *et al*. 1998), and inhibiting regeneration of the PSII RC protein D1 (Kanervo *et al*. 1997). In

addition, low temperature inhibits carbon fixation in the Calvin-Benson cycle by hindering the regeneration of ribulose 1,5-biphosphate (RuBP), and reducing the efficiency of Ribulose-1,5-bisphosphate carboxylase/oxygenase (Rubisco) carboxylation (Sage 2002). At the same time, plant exposure to low temperatures inhibit plant water uptake (Kauffman 1975, Kramer 1983), cell division and differentiation (Rossi *et al*. 2008), and the enzymatic reactions essential to growth and metabolism (Hüner *et al.* 1998). Slowed down growth and metabolism results in decreased sink capacity for photosynthates (Ensminger *et al*. 2006), which creates an imbalance between light absorption and its utilization in carbon fixation and other metabolic pathways (Öquist and Hüner 2003, Verhoeven 2014). Such imbalance causes the buildup of a pH gradient across the thylakoid membrane, which triggers NPQ as a way to safely dissipate excess light energy as heat rather than being transferred to oxygen and resulting in ROS production. As mentioned earlier, NPQ during summer and early autumn is mainly facilitated by energy-dependent quenching (qE), but is gradually replaced by sustained quenching (qI) with prolonged cold stress in late autumn and winter (Demmig-Adams and Adams 2006a). Prolonged exposure to cold temperatures also results in plant cold acclimation, which involves biochemical alterations in lipids, proteins, amino acids, and carbohydrates (Öquist and Hüner 2003). Indeed, accumulation of reduced components on the electron transport chain are sensed by the redox state of the plastoquinone (PQ) pool (Hüner *et al*. 1998, Ensminger *et al*. 2006). The PQ pool acts as a primary cold sensor, transducing the redox state of the electron transport chain into biochemical signals that regulate the transcription of genes involved in photosynthesis and cold acclimation in the chloroplast and the nucleus (Ensminger *et al*. 2006).

During spring, the recovery of photosynthesis in conifers was reported to be closely linked to the increase of air temperature above 0°C (Tanja *et al*. 2003, Sevanto *et al.* 2006) which facilitates biochemical reactions involved in repair and reorganization of the photosynthetic apparatus (Ensminger *et al*. 2004, 2006). Spring in northern climates is characterized by large day-to-day variation in air temperature, and in conifers, photosynthesis recovers quickly and opportunistically with increasing air temperature. Conversely, photosynthesis can rapidly revert back to a downregulated state with the occurrence of cold episodes (Ensminger *et al*. 2004, 2008, Zarter *et al*. 2006). While temperature was established as a dominant factor in the timing of the spring recovery and autumn downregulation of

photosynthesis, the effects of photoperiod appear to be prevalent during autumn, and vary widely among species.

Photoperiod

Photoperiod induces physiological changes in plants during late summer and autumn. Short photoperiod, or longer nights, results in a temporary period of sugar starvation at the end of the night in *Arabidopsis* (Gibon *et al*. 2009) and *Populus* (Hoffman *et al*. 2010). Sugar starvation during long nights causes hormonal inhibition of growth the next day (Paparelli *et al*. 2013), reduced rate of starch turnover, and a decrease in protein and amino acid content of leaves (Gibon *et al*. 2009). Growth inhibition can, in turn, induce the downregulation of photosynthesis through feedback response to reduced sink capacity for photosynthates (Savitch *et al*. 2002, Ensminger *et al*. 2006). Decreasing photoperiod also causes phytochromes to activate a cold response pathway mediated by the CBF transcription factors (Lee and Thomashow 2012, Maibam *et al*. 2013), resulting in enhanced freezing tolerance.

The sensitivity of photosynthetic downregulation to photoperiod seems to vary among species. For instance, Lundmark *et al*. (1998) reported the timing of photosynthetic downregulation in field-grown Norway spruce (*Picea abies*) to vary from one year to another as a function of air temperature, suggesting little photoperiod sensitivity of photosynthesis in that species. Similarly, Stinziano *et al.* (2015) did not conclude to photoperiodic regulation of the autumn decline of photosynthetic capacity of *Picea abies*. In contrast, Bauerle *et al.* (2012) observed peaks in photosynthetic capacity just after the summer solstice, and declines with decreasing photoperiod in 23 temperate and boreal tree species from the genera *Acer*, *Betula*, *Gleditsia*, *Fraxinus*, *Paulownia*, *Prunus* and *Quercus*, which points to photoperiodic regulation of photosynthesis at the end of the growing season. During the spring season, however, there is little evidence of photoperiodic control of photosynthesis in temperate and boreal trees.

Potential for increased photosynthetically active seasons in a future climate

Studies have investigated the potential for elongated photosynthetically active seasons in trees exposed to warmer autumn and spring conditions. For instance, under controlled conditions Busch *et al.* (2007) reported that warmer autumn temperature does not increase photosynthetic carbon uptake but instead enhanced NPQ of excess light energy via the xanthophyll cycle in Jack pine (*Pinus banksiana* Lamb.). Recently, Chang *et al.* (2015) reported that an additional 1.5°C/3°C (day/night) above ambient field temperature was not enough to delay photosynthetic downregulation in Eastern white pine (*Pinus strobus* L.) seedlings, while Stinziano *et al*. (2015) observed delayed photosynthetic downregulation in Norway spruce (*Picea abies*) seedlings exposed to a +4°C warming treatment.

During spring, warming experiments both in the field and controlled environments have confirmed earlier recovery of photosynthesis with elevated spring temperature. A whole-tree chamber experiment recently revealed that a heating treatment of 2.8-5.6°C advanced the onset of photosynthetic recovery by approximately 8 days, and the completion of the recovery of photosynthesis by 22 days in Norway spruce (*Picea abies* (L.) H. Karst; Hall *et al.* 2013, Wallin *et al.* 2013). In another study, the spring recovery of photosynthesis of field grown Norway spruce (*P. abies*) was mainly controlled by air temperature and the frequency of severe night frosts, with artificial soil heating having little effect on the timing of photosynthetic recovery (Bergh and Linder 1999). The delaying effect of intermittent frost on the recovery period photosynthesis was also reported by Ensminger *et al.* (2008) for Scots pine (*P. sylvestris*) in controlled environments.

1.4 Tracking the light-use efficiency of photosynthesis with the PRI

Uncertainties in using LUE limit model estimates of GPP through remote sensing

A commonly used approach for modelling photosynthesis or gross primary productivity (GPP) of plant canopies is the light-use efficiency model (Monteith 1972, 1977). According

to this model, GPP is a function of incident photosynthetically active radiation (PAR), the fraction of this radiation that is actually absorbed by leaves (f_{PAR}), and the light-use efficiency of photosynthesis (LUE):

$$\mathrm{GPP} = \mathrm{PAR} \cdot f_{\mathrm{PAR}} \cdot \mathrm{LUE} \qquad \text{Equation 1.1}$$

The first term of the equation, PAR, can be measured with light intensity sensors such as those commonly installed at weather stations. The second term, f_{PAR}, can be estimated with remotely sensed vegetation indices. For instance, the Normalized Difference Vegetation Index (NDVI) or the Enhanced Vegetation Index (EVI) are normalized differences between the amount of near infrared radiation and the amount of red light reflected by vegetation, and are commonly determined from satellite or aircraft imagery (Garbulsky *et al*. 2011).

The third term of the LUE model, LUE, is the most challenging to measure, thereby introducing the greatest amount of uncertainty in the model. This is because photosynthesis is highly variable through space and time, and influenced by a large number of biotic and abiotic factors. Greenness indices are useful measures of potential photosynthesis in the absence of constraints on photosynthesis. Indeed, these indices can identify the presence of vegetation on a landscape, or describe the timing of leaf development and senescence in forests dominated by deciduous vegetation. However, in many ecosystems, asynchrony between green canopy development and photosynthetic activity limits the usefulness of greenness indices for the assessment of LUE. This is particularly the case in evergreen conifer-dominated forests, which remain green in the winter when trees downregulate photosynthesis. The photochemical reflectance index (PRI) is a promising alternative to greenness indices to track the LUE of evergreen conifers. The PRI is a vegetation index that reflects the dynamics of the xanthophyll cycle which is linked to heat dissipation, and thus, the actual LUE of photosynthesis.

The PRI as a proxy of xanthophyll cycle dynamics

As mentioned earlier, under conditions of excess light PSII is protected against over-excitation and photo-damage by qE type quenching. This involves the rapid de-epoxidation of xanthophyll cycle pigments, i.e. the conversion of violaxanthin into antheraxanthin and zeaxanthin (Niyogi *et al*. 2005, Demmig-Adams & Adams 2006a), which facilitate the safe

dissipation of excess light energy as heat. Changes in the de-epoxidation state of the xanthophyll cycle cause a change in leaf spectral reflectance. This is because the pigments violaxanthin and antheraxanthin present higher absorption coefficients than zeaxanthin (Middleton *et al*. 2009). These changes are detectable in two narrow waveband absorption features at 505 and 531 nm. In order to quantify these changes, the band at 531 nm (R_{531}) is compared to a xanthophyll-insensitive reference band at 570 nm (R_{570}; Fig. 1.7), yielding the PRI (Gamon *et al*. 1992, 1997, Peñuelas *et al*. 1995):

$$\text{PRI} = \frac{R_{531} - R_{570}}{R_{531} + R_{570}} \qquad \text{Equation 1.2}$$

Gamon and colleagues (1992) initially found a strong correlation between diurnal variations of LUE and PRI in sunflower (*Helianthus annuus*) canopies. Since then the relation between PRI and LUE was documented in a wide range of plant functional types at the leaf (e.g. Stylinski *et al*. 2000, Moran *et al*. 2000, Sims and Gamon 2002, Guo and Trotter 2006, Inoue and Peñuelas 2006, Mõttus *et al.* 2017, 2018), canopy (e.g. Nichol *et al*. 2000, 2006, Strachan *et al*. 2002, 2008, Nakaji *et al*. 2007, 2008, Peguero-Pina *et al*. 2008, Springer *et al*. 2017) and landscape (e.g. Rahman *et al*. 2004, Drolet *et al*. 2005, Garbulsky *et al*. 2008, Goerner *et al*. 2008, 2009, Markiet *et al.* 2017) levels. A meta-analysis by Garbulsky *et al*. (2011) reported PRI to account for 42%, 59% and 62% of the variability of LUE at the leaf, canopy and landscape levels, respectively, with unique exponential relationships for all vegetation types studied. The analysis also revealed a high degree of functional convergence of the biochemical, physiological and structural components that affect the photosynthetic efficiencies of leaves, canopies and landscapes.

In boreal evergreen conifers, the relation between PRI and LUE was documented in species such as Douglas fir (*Pseudotsuga menziesii* [Mirb.] Franco; Hall *et al*. 2008, Hilker *et al*. 2008, Cheng *et al*. 2009, Hilker *et al*. 2009, Middleton *et al*. 2009), Scots pine (*Pinus sylvestri*s L.; Nichol *et al*. 2002, Louis *et al*. 2005, Filella *et al*. 2009, Porcar-Castell *et al*. 2012, Hmimina *et al*. 2015, Mõttus *et al.* 2017, 2018), jack pine (*Pinus banksiana* Lamb.; Rahman *et al*. 2001, Drolet *et al*. 2008, Busch *et al*. 2009, Springer *et al.* 2017), lodgepole pine (*Pinus contorta* Doug.; Wong and Gamon 2015a, b), ponderosa pine (*Pinus ponderosa* Doug.; Wong and Gamon 2015a, b), red spruce (*Picea rubens* Sarg.; Richardson *et al*. 2001), white spruce (*Picea glauca* (Moench) Voss; Springer *et al.* 2017), black spruce

(*Picea mariana* Mill.; Rahman *et al*. 2001, Drolet *et al*. 2008, Springer *et al.* 2017), and balsam fir (*Abies balsamea* L.; Richardson *et al*. 2001).

1.5 The challenges of using the PRI to detect LUE of evergreen needles in the cold

Seasonal variations in NPQ mechanisms

In evergreen conifers, some authors have reported the PRI to be effective at tracking seasonal variations in photosynthesis such as its spring activation both at the canopy (Nichol *et al*. 2002, Louis *et al*. 2005) and leaf levels (Wong and Gamon 2015a), while others have reported a breakdown of the relationship between the PRI and photosynthetic efficiency under cold conditions. For instance, Busch *et al*. (2009) reported that leaf-level PRI could not explain variations in the quantum yield of PSII of *P. banksiana* seedlings exposed to simulated spring treatments. In the field, Porcar-Castell *et al*. (2012) observed a good correlation between PRI and NPQ in needles of mature *P. sylvestris* trees during most of the year, but a decoupling in the relationship during early spring when needles were deeply downregulated. Both authors suggested that the spring decoupling might be due to the activation of NPQ mechanisms that operate independently of dynamic, zeaxanthin-regulated NPQ. One such mechanism might be sustained quenching, which is dominant in winter-acclimated needles, but not reflected by PRI (Porcar-Castell *et al*. 2012).

Seasonal variation in photosynthetic pigment pools

Other authors have reported variations in PRI to be controlled to a greater extent by variations in chlorophyll and carotenoid pigment pool sizes than dynamic operation of the xanthophyll cycle. For instance, Filella *et al*. (2009) reported PRI to be strongly controlled by the carotenoid (Car) to chlorophyll (Chl) ratio and β-carotene to Chl ratio in *P. sylvestris* saplings exposed to various light treatments. Similarly, Gamon and Berry (2012) observed the occurrence of both dynamic and sustained pigment effects on PRI along a canopy light gradient, with sustained pigment effects accounting for most of the PRI variability within the canopy. In field grown *P. sylvestris*, Porcar-Castell *et al*. (2012) found a stronger correlation between PRI and VAZ Chl^{-1} than DEPS at a seasonal scale, while Wong and

Gamon (2015a) observed Car Chl^{-1} to match PRI more closely than DEPS throughout the year.

1.6 Tracking plant stress with the CCI

In the last years, the chlorophyll/carotenoid index (CCI), which tracks seasonal changes in leaf chlorophyll to carotenoid pigment ratios, has been proposed as a new way to assess the photosynthetic capacity of evergreen conifers remotely. Indeed, authors have suggested that the important variations in pigment pool sizes that evergreens experience seasonally might be the key to detecting the phenology of photosynthesis in those species. In order to quantify these changes, the band at 531 nm (R_{531}) is compared to a band in the red region of the spectrum at 645 nm (R_{645}), which is expected to vary with leaf concentrations of carotenoid pigments (Fig. 1.7). The CCI is formulated as follows (Gamon *et al*. 2016):

$$\mathrm{CCI} = \frac{R_{531} - R_{645}}{R_{531} + R_{645}} \qquad \text{Equation 1.3}$$

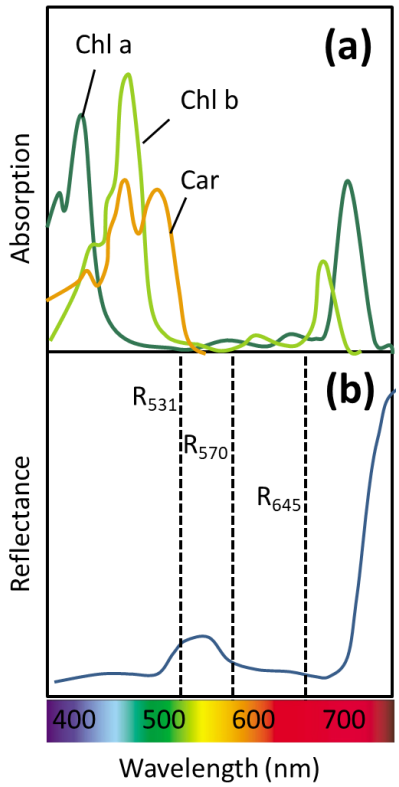

Figure 1.7 Absorption spectra of chlorophyll a (Chl a), chlorophyll b (Chl b) and carotenoids (Car, panel a) and reflectance spectrum of green vegetation (panel b). Variations in the de-epoxidation state of the xanthophyll cycle cause a change in leaf spectral reflectance at 531 nm (R_{531}). The PRI is calculated by comparing R_{531} to the xanthophyll-insensitive band at 570 nm (R_{570}). The CCI tracks variations in carotenoid pigments by comparing R_{531} with a band in the red region of the spectrum at 645 nm (R_{645}).

Both PRI and CCI are calculated using bands of the spectrum located on either side of the green reflectance 'bump' (i.e. 531 and 570 nm for PRI, 531 nm and 645 nm for CCI). Both indices, therefore, compare reflectance in the blue, i.e. the chlorophylls and carotenoids absorption region of the spectrum, with the reflectance in the orange and red regions of the spectrum, where absorption is limited to chlorophylls. Because CCI is integrated using reflectance at 645 nm, which is more strongly absorbed by chlorophylls, an enhanced sensitivity to chlorophyll pool sizes is expected with the CCI, and, in turn, enhanced sensitivity to seasonal variations in carotenoid pigment pool sizes.

The upregulation of carotenoid pigment pools under cold conditions is well documented in evergreen conifers (e.g. Adams and Demmig-Adams 1994, Ottander *et al.* 1995, Chang *et al.* 2015). This is because carotenoids play a two-fold role in photoxidative damage

avoidance under cold stress by (1) being active thermal energy quenchers (Niyogi et al. 2005, Demmig-Adams and Adams 2006b) and (2) being important reactive oxygen species (ROS) scavengers (Jahns and Holzwarth 2012; Trebst 2003; Telfer 1994, 2005, 2014). Detecting the upregulation of carotenoid pigment pools might, therefore, help identify periods of plant stress which generally coincide with photosynthetic downregulation. At this time the suitability of the CCI to track variations in photosynthesis during spring was evaluated by (Gamon *et al.* 2016) at the leaf level in ponderosa pine (*P. ponderosa*) as well as in stands dominated by eastern and western Hemlock (*Tsuga canadensis* (L.) Carrière and *T. heterophylla* (Raf.) Sarg.), red spruce (*P. rubens*), Loblolly pine (*Pinus taeda L.*) and Douglas fir (*P. menziesii*). Gamon *et al.* (2016) reported a close relationship between the CCI and the seasonal patterns of daily gross primary productivity of evergreen conifer stands measured by eddy covariance. Another recent study by Springer *et al*. (2017) reported effective tracking of photosynthetic phenology by the CCI in potted black spruce (*P. mariana*), white spruce (*Picea glauca*), and jack pine (*P.banksiana*). At this time the suitability of the CCI as a proxy for photosynthesis needs to be validated in more species, spatial and temporal scales as well as growth conditions.

1.7 Thesis framework

Uncertainties regarding the relationship between the PRI and photosynthetic efficiency of evergreen conifers during spring and autumn currently limit the use of this index for tracking the seasonality of photosynthetic efficiency in conifer-dominated forests, in addition to poor understanding of the effects of warmer spring and autumn conditions on the physiology of evergreen conifers. The research presented in this thesis aims to (1) elucidate the effects of warming on photosynthesis in *P. strobus* during spring and autumn (2) clarify the relationship between xanthophyll cycle dynamics, LUE of photosynthesis and PRI in *P. strobus* during spring and autumn and (3) determine whether intraspecific variation affects the response of *P. strobus* to climate warming. The experiments presented in the following chapters were designed to test the following hypotheses:

1. Given the strong control of air temperature on photosynthesis, warmer temperatures during spring and autumn have the potential to extend the photosynthetically active season. However, photoperiodic constraints on the initiation of photosynthetic

recovery in the spring and, particularly, photosynthetic downregulation in the autumn might prevent trees from benefiting from warmer conditions during those seasons, partly offsetting any potential for prolonged carbon gain due to warm temperatures.

2. During spring and autumn, NPQ mechanisms that are independent of zeaxanthin-regulated qE type NPQ might be an important proportion of total NPQ. Since these zeaxanthin independent mechanisms are undetected by the spectral bands used to integrate the PRI, photochemical quenching and LUE are likely overestimated by the PRI during those seasons.

3. Because genotypic characteristics determine phenology, yearly photosynthetic capacity will not increase linearly with an increase in temperature. Both temperature and photoperiodic cues might be necessary to initiate photosynthetic recovery in the spring and photosynthetic downregulation in the autumn. When transferred to a common garden, tree seedlings adapted to northern and southern conditions will face photoperiodic constraints on photosynthesis, unless they exhibit enough phenotypic plasticity to acclimate to local temperature and photoperiod regimes.

These hypotheses were tested with three sets of experiments:

The experiment presented in Chapter 2 was designed to study the downregulation of photosynthesis during a simulated summer-autumn transition, shifts in energy partitioning during the transition, as well as variations in the strength of the relationship between LUE and the PRI. The main aims of the experiment were to shed light on the main sources of PRI variation at a seasonal timescale, and identify the NPQ mechanisms likely to introduce a discrepancy in the PRI-LUE relationship during autumn. In order to clarify the roles of cold temperature and shortened photoperiod on photosynthetic downregulation, we shifted *P. strobus* seedlings from a long day and warm temperature summer treatment to either a short day and cold temperature treatment or a short day and warm temperature treatment. In both cases, we characterized the transition of seedlings with photosynthetic gas exchange, chlorophyll fluorescence, leaf pigment analysis and leaf-level spectral reflectance.

The experiment presented in Chapter 3 was designed to study the recovery of photosynthesis during a winter-spring transition, shifts in energy partitioning during the transition, as well as variations in the strength of the relationship between LUE and the PRI. The experiment allowed the identification of NPQ mechanisms and electron sinks likely to be responsible for the discrepancy between PRI and LUE during spring. In this experiment, we shifted winter-acclimated *P. strobus* seedlings to either a cold or a warm spring treatment. The recovery of seedlings was characterized with photosynthetic gas exchange, chlorophyll fluorescence, leaf pigment analysis and leaf-level spectral reflectance.

The experiment presented in Chapter 4 was designed to assess the photosynthetic performance during spring and autumn of *P. strobus* seedlings under the projected temperature for 2050 in southern Ontario. This experiment also aimed to elucidate the roles intraspecific variation on the response of photosynthesis to warming during spring and autumn, as well as to evaluate and compare the suitabilities of the PRI and of the CCI to track variations in photosynthesis during spring and autumn. To do so, *P. strobus* provenances from local, northern and southern sites of were grown in a field environment and exposed to either ambient or elevated air temperature using temperature free-air-controlled enhancement (T-FACE) infrared warming arrays. Over the course of 1.5 year, the physiological state of seedlings was monitored using photosynthetic gas exchange, chlorophyll fluorescence, leaf pigment analysis and leaf-level spectral reflectance.

Finally, Chapter 5 summarizes the main findings of my doctoral research as well as their implications for the fields of global change science, plant physiology and remote sensing.

Chapter 2

2 Photoperiod and temperature constraints on the relationship between the photochemical reflectance index (PRI) and the light-use efficiency of photosynthesis in *Pinus strobus*

Fréchette E, Chang CY, Ensminger I (2016) Photoperiod and temperature constraints on the relationship between the photochemical reflectance index (PRI) and the light-use efficiency of photosynthesis in *Pinus strobus*. Tree Physiology 36(3):311-324.

Status: published.

2.1 Abstract

The photochemical reflectance index (PRI) is a proxy for the activity of the photoprotective xanthophyll cycle and photosynthetic light-use efficiency (LUE) in plants. Evergreen conifers downregulate photosynthesis in autumn in response to low temperature and shorter photoperiod, and the dynamic xanthophyll cycle-mediated non-photochemical quenching (NPQ) is replaced by sustained NPQ. We hypothesized that this shift in xanthophyll cycle dependent energy partitioning during the autumn is the cause for variations in the PRI-LUE relationship. In order to test our hypothesis we characterized energy partitioning and pigment composition during a simulated summer-autumn transition in a conifer and assessed the effects of temperature and photoperiod on the PRI-LUE relationship. We measured gas exchange, chlorophyll fluorescence and leaf reflectance during the photosynthetic downregulation in *Pinus strobus* L. seedlings exposed to low temperature/short photoperiod or elevated temperature/short photoperiod conditions. Shifts in energy-partitioning during simulated autumn where observed when the pools of chlorophylls decreased and pools of photoprotective carotenoids increased. On a seasonal timescale, PRI was controlled by carotenoid pool sizes rather than xanthophyll cycle dynamics. PRI variation under cold autumn conditions mainly reflected long-term pigment pool adjustments associated with sustained NPQ, which impaired the PRI-LUE relationship. Exposure to warm autumn conditions prevented the induction of sustained NPQ but still impaired the PRI-LUE relationship. We therefore conclude that alternative zeaxanthin-independent NPQ mechanisms, which remain undetected by the PRI, are present under both cold and warm autumn conditions, contributing to the discrepancy in the PRI-LUE relationship during autumn.

2.2 Introduction

Boreal forests represent a substantial carbon sink (Ciais *et al*. 1995, Myneni *et al*. 2001, Pan *et al*. 2011) and changes in their capacity to sequester carbon through photosynthesis have the potential to significantly affect the global carbon budget (Bonan 2008). Photosynthesis is governed by a number of biotic and abiotic factors, making carbon sequestration highly variable through space and time. A number of vegetation indices have been developed in an effort to capture that variability (Ustin *et al*. 2006). For instance, greenness indices such as the normalized difference vegetation index (NDVI) are commonly used to track phenology and seasonal dynamics of photosynthesis of deciduous biomes. Greenness indices, however, provide measures of potential and not actual photosynthesis, because of differences in timing between greening and ecosystem carbon uptake (Garbulsky *et al*. 2011). This is particularly true for conifer-dominated boreal biomes, since evergreen conifers retain needles but downregulate photosynthesis during winter. Seasonal dynamics in photosynthesis in evergreen conifers are mainly controlled by adjustments in the light-use efficiency of photosynthesis (LUE; Demmig-Adams & Adams 2006a), i.e. the amount of assimilated CO_2 per mole of absorbed photosynthetically active radiation. Regulation of LUE is achieved via changes in energy partitioning of absorbed light energy between photochemistry (qP) and non-photochemical quenching (NPQ or qN; Müller *et al*. 2001, Demmig-Adams & Adams 2006a).

Over the course of days and seasons, plants harvest more light than can be used for photosynthesis. The absorption of excess light can be harmful, as it may cause photooxidative damage by reactive oxygen species (ROS; Barber and Andersson 1992). Non-photochemical quenching (NPQ) can dissipate excess excitation energy and contribute to photoprotection and avoid ROS formation. In higher plants, NPQ has two main components, according to their relaxation kinetics in darkness following a period of illumination. The major and fastest component is the pH- or energy-dependent component, qE (Müller *et al*. 2001, Demmig-Adams and Adams 2006a). This component is triggered at a timescale of seconds by light-induced proton transport across the thylakoid membrane, which creates a pH gradient and conformational change of photosystem (PS) II (Ruban *et al*. 2012). In addition, the de-epoxidation of the xanthophyll cycle pigments, i.e. the conversion of the pigment violaxanthin into antheraxanthin and zeaxanthin (Demmig-Adams & Adams

2005, Niyogi *et al*. 2005) occurs at a timescale of minutes and is quickly reversible upon dark-relaxation (Müller *et al*. 2001). The other major component of NPQ is called qI, and replaces qE under prolonged and severe light stress (Müller *et al*. 2001, Demmig-Adams and Adams 2006a). The qI type quenching involves the upregulation of xanthophyll cycle pigments and the retention of zeaxanthin upon dark-relaxation. When qI occurs concomitantly with cold acclimation, such as in overwintering evergreen conifers, it involves a reorganization of PSII core units (Verhoeven 2014), a decrease in the abundance of the PSII protein D1, a partial degradation of chlorophylls (Ensminger *et al*. 2006, Demmig-Adams & Adams 2006a) and the upregulation of photoprotective pigments such as lutein and β-carotene (Adams & Demmig-Adams 1994, Filella *et al*. 2009). Hereafter we refer to the rapidly induced and reversed quenching mechanisms associated to qE type quenching as dynamic NPQ, and to the sustained photoprotective mechanisms associated with qI type quenching and cold acclimation as sustained NPQ.

Changes in the de-epoxidation state (DEPS) of xanthophyll cycle pigments modify leaf spectral reflectance at 531 nm. The photochemical reflectance index (PRI) is derived by comparing this shift at 531 nm to the xanthophyll-insensitive band at 570 nm (Gamon *et al*. 1992, 1997, Peñuelas *et al*. 1995). At diurnal timescales, the relationship between PRI and dynamic NPQ (and hence, LUE) has been confirmed in various plant species at the leaf level, but also at the stand- and ecosystem-levels (Garbulsky *et al*. 2011). More recently, studies have reported PRI variations over seasonal timescales, and revealed that PRI varies not only with dynamic NPQ, but also as a result of long-term adjustments of plant pigment pools associated with sustained NPQ (Sims & Gamon 2002, Stylinsky *et al*. 2002, Garrity *et al*. 2011). For instance, Gamon & Berry (2012) observed the occurrence of both dynamic and sustained pigment effects on PRI along a canopy light gradient, with sustained pigment effects accounting for most of the PRI variability within the canopy.

Other studies have documented long-term PRI variation (over weeks or months) caused by changes in pigment pools in desert and dry shrub species (Sims & Gamon 2002), chaparral evergreen shrubs (Stylinski *et al*. 2002), deciduous (Garrity *et al*. 2011) and evergreen trees (Filella *et al*. 2009). In boreal evergreens, significant adjustments in chlorophylls and carotenoid pool sizes occur during the autumn downregulation of photosynthesis and concomitant transition from dynamic to sustained NPQ. For instance, at seasonal timescales

authors have reported PRI variation to be attributable to the ratio of carotenoids per chlorophylls rather than xanthophyll cycle activity in lodgepole and ponderosa pine (*P. contorta* D. and *P. ponderosa* Laws.; Wong & Gamon 2015b) and Scots pine (*P. sylvestris* L.; Porcar-Castell *et al*. 2012). In addition, authors have observed a discrepancy between PRI and variations in photosynthesis during early spring, when excess energy was predominantly dissipated via sustained NPQ in Scots pine (*P. sylvestris* L.; Porcar-Castell *et al*. 2012) and Eastern white pine (*P. strobus* L.; Fréchette *et al*. 2015). Despite these recent observations, it is still unclear by which mechanism adjustments in pigment pools affect PRI and LUE during the autumn downregulation of photosynthesis.

The transition from dynamic to sustained NPQ is strongly influenced by growth temperature, and anticipated future warmer autumns will likely affect the PRI-LUE relationship. For instance, Busch *et al*. 2007 recently reported that warmer temperature during simulated autumn did not increase photosynthetic carbon uptake in Jack pine (*P. banksiana*) but instead enhanced NPQ and hence increased dissipation of excess light energy, indicating limitations of photosynthesis from photoperiodic control. We hypothesize that the transition of dynamic to sustained NPQ is a major cause for the observed variation in the PRI-LUE relationship and that it will likely be affected by a warmer climate.

In the present study, we aimed to provide physiological mechanisms responsible for the variations in the PRI-LUE relationship previously reported at seasonal timescales. *P. strobus* seedlings were shifted from warm temperature and long photoperiod to short photoperiod and either low or elevated temperature to (1) investigate the effect of elevated autumn temperature on the transition from dynamic to sustained NPQ in needles; (2) characterize temperature and photoperiod induced changes in needle pigment composition, LUE and PRI at diurnal and seasonal timescales; and (3) assess which physiological factors affect the PRI-LUE relationship on a seasonal basis.

2.3 Materials and Methods

Plant material and growth conditions

Three-year-old Eastern white pine (*P. strobus*) seedlings were obtained in April 2011 and 2012 from a local seed orchard (Ontario seed zone 37, Somerville Seedlings, Everett, Ontario, Canada), planted in a mixture of sand and sphagnum peat moss (1:2 v/v) and fertilized with 28:10:10 (N:P:K) mineral fertilizer (Miracle-Gro, Scotts, Marysville, OH, USA). Seedlings were kept outside in an experimental garden at the University of Toronto at Mississauga (Ontario, Canada) until transferred to environmental growth chambers (Biochambers, Winnipeg, Canada) during July. The seedlings were acclimated for 6 weeks to simulated summer conditions with long days and high temperature (LD/HT; 14h photoperiod; 22/15˚C day/night) and then exposed for 36 days of simulated cold or warm autumn conditions. The cold autumn simulation consisted of short days and low temperature (SD/LT; 8h photoperiod; 12/5˚C day/night) and the warm autumn simulation consisted of short days and high temperature (SD/HT; 8h photoperiod; 22/15˚C day/night). Under LD/HT, SD/LT and SD/HT, seedlings were exposed to a light intensity of 1500 μmol quanta $m^{-2}s^{-1}$, with a period of 30 minutes at 400 μmol quanta $m^{-2}s^{-1}$ at the beginning and end of the day. Seedlings acclimated to LD/HT conditions were sampled and measured one day prior to transfer to autumn conditions (day 0), followed by sampling and measurements of SD/LT and SD/HT seedlings on days 1, 4, 8, 16, 26 and 36 of the experiment. All measurements and sampling were performed on current-year needles of the top portion of the leader shoot. Two independent experiments were performed in two consecutive years, using identical settings and protocols, with rotations of treatments between the chambers to minimize chamber-specific effects.

Chlorophyll-fluorescence measurements

At each time point chlorophyll-fluorescence was used to assess energy partitioning (Dual-PAM-100, Walz, Effeltrich, Germany). A saturating light pulse was applied to dark-adapted (pre-dawn) needles for determination of F_o and F_m (minimal and maximal fluorescence). Maximum quantum yield of PSII was measured as defined by Genty *et al*. (1989):

$$F_v/F_m = \left(\frac{F_m - F_o}{F_m}\right) \quad \text{Equation 2.1}$$

The needles were then exposed to a sequence of 2.5-min intervals with actinic light of increasing intensity (0-2000 μmol quanta $m^{-2}s^{-1}$), each step followed by a 400 ms saturating pulse of 10000 μmol quanta $m^{-2}s^{-1}$ for determination of F_m' (maximal fluorescence of light-adapted needles), and a weak pulse of far-red light for determination of F_o' (minimal fluorescence of light-adapted needles). Energy partitioning using the parameters Φ_{PSII}, Φ_{NPQ} and $\Phi_{f,D}$ was calculated according to Hendrickson *et al*. (2004). Effective quantum yield of PSII of a light-adapted sample (Φ_{PSII}) reflects the proportion of light absorbed by PSII, which is used for photochemistry and was calculated as:

$$\Phi_{PSII} = 1 - \frac{F_s}{F_m'} \quad \text{Equation 2.2}$$

where F_s is the yield of steady state fluorescence in a light-adapted sample recorded immediately before the saturation pulse. The proportion of light that is absorbed by PSII antenna and quenched via dynamic NPQ (Φ_{NPQ}) was calculated as:

$$\Phi_{NPQ} = \frac{F_s}{F_m'} - \frac{F_s}{F_m} \quad \text{Equation 2.3}$$

The proportion energy quenched by fluorescence and sustained NPQ ($\Phi_{f,D}$) and, therefore, remains unchanged with short-term variations in light intensity, was calculated as:

$$\Phi_{f,D} = \frac{F_s}{F_m} \quad \text{Equation 2.4}$$

The electron transport rate of PSII (ETR_{II}, in μmol electron $m^{-2}s^{-1}$) was calculated according to Genty *et al*. (1989):

$$ETR_{II} = \Phi_{PSII} \cdot I \cdot 0.5 \cdot \alpha \quad \text{Equation 2.5}$$

where I is the intensity of the actinic light (μmol quanta $m^{-2}s^{-1}$), 0.5 is a factor that accounts for the energy distribution between PSII and PSI and assumes even distribution of excitation energy between the two photosystems (Maxwell and Johnson, 2000), and α is the absorptance, i.e. the fraction of incident light absorbed by leaves. Values of α were calculated as α = 1 – transmittance – reflectance. Given the thickness of pine needles,

transmittance was assumed to be 0 and reflectance was measured with a Unispec-SC spectrometer over the 400-700 nm wavelengths range (Huang *et al*. 2012).

The excitation pressure of PSII was calculated as 1–qP according to Hüner *et al*. (1998) with :

$$qP = \frac{F_{m}\prime - F_{s}}{F_{m}\prime - F_{o}\prime} \qquad \text{Equation 2.6}$$

Photosynthetic gas exchange measurements

To assess variations in photosynthetic activity at a seasonal timescale, photosynthetic gas exchange was measured at each time point (GFS-3000, Walz, Effeltrich, Germany). Measurements started 2 hours after the lights were turned on. A bundle of attached needles was oriented to form a flat plane and inserted in the leaf cuvette. CO_2 concentration in the cuvette was set to 400 ppm, cuvette temperature was set to growth temperature and humidity was set 60% RH. Net CO_2 assimilation (A) and stomatal conductance (g_s) were measured at growth light intensity (1500 µmol quanta $m^{-2}s^{-1}$) once steady-state assimilation was achieved. Immediately after the measurements, needles were detached from the seedling and measured for surface area using the Winseedle software package (Regent Instruments Inc., Québec, Canada). The light use efficiency of CO_2 assimilation (LUE_A, in mol CO_2 mol^{-1}) was calculated as the ratio of assimilation (in µmol CO_2 $m^{-2}s^{-1}$) and the intensity of the actinic light (in µmol quanta $m^{-2}s^{-1}$) during measurements.

Spectral reflectance measurements

To assess variations in PRI at a seasonal timescale, at each time point needle spectral reflectance was measured with a Unispec-SC spectrometer (UNI007, PP Systems, Haverhill, MA, USA). The spectrometer was connected to a bifurcated fiberoptic (UNI400) and a leaf clip (UNI500) maintaining the fiberoptic on the needle surface at a fixed angle of 60° relative to needle axis (2 mm diameter spot size). Needle reflectance was computed by dividing each needle scan by the radiance obtained from a white reflectance standard (Spectralon, Labsphere, North Sutton, NH, USA) taken immediately before each needle measurement. Dark current instrument noise was subtracted from white standard and needle

radiance measurements. Reflectance was measured on needles of the topmost part of the leader shoot. Needles were in bundles of approximately 10-15 needles arranged in parallel to form a single layer flat plane. For each measurement, 30 scans were averaged, followed by interpolation of the ~3.3 nm resolution output of the spectrometer to 1 nm bandwidths. Finally, PRI was calculated according to Peñuelas *et al*. (1995):

$$\mathrm{PRI} = \frac{R_{531} - R_{570}}{R_{531} + R_{570}} \qquad \text{Equation 2.7}$$

where R_{531} and R_{570} represent needle reflectance at 531 and 570 nm, respectively. At each time point, reflectance was measured at pre-dawn and at midday. In order to compare PRI variation at a seasonal timescale, we used pre-dawn PRI measurements to separate the effects of sustained and dynamic pigment variations on PRI (Gamon & Berry 2012).

Measurements of light-response curves

To assess energy partitioning, LUE_A and PRI at a diurnal timescale, light response curves were measured on day 0 as well as on day 16 of the experiment. A pre-dawn dark-adapted bundle of needles was exposed to 10-minute steps of increasing actinic light intensity (0-2000 μmol quanta $m^{-2}s^{-1}$). At each light step, Φ_{PSII}, Φ_{NPQ} and $\Phi_{f,D}$ were recorded with the Dual-PAM-100. Then, assimilation was measured with the GFS-3000 and LUE_A was calculated, with measurement and cuvette conditions identical to those used for assessing variation of photosynthetic activity at a seasonal timescale (see above). Finally, spectral reflectance was assessed using the Unispec-SC, with 3 scans averaged at each light step. To assess the range of diurnal PRI variation, we calculated ΔPRI as the difference between PRI dark-adapted needles and PRI measured at 2000 μmol quanta $m^{-2}s^{-1}$ according to Gamon & Berry (2012).

Pigment analysis

Needle samples for pigment analysis were collected after at least 2 hours of exposure to growth light (1500 μmol quanta $m^{-2}s^{-1}$). The samples were immediately frozen in liquid nitrogen and stored at -80°C. The needles were then ground to a fine powder in liquid nitrogen. Pigments were extracted in dim light conditions in 98% methanol buffered with

2% 0.5M ammonium acetate for 2 hours. The extracts were filtered through a 0.2 µm PFTE filter prior to high-performance liquid chromatography (HPLC) analysis. HPLC analysis was performed with an Agilent system (Agilent Technologies, Santa Clara, CA, USA) consisting of a quaternary pump, autosampler set to 4 °C, column oven set to 25°C and photodiode array detector recording absorption at the wavelengths of 450 nm and 656 nm and separated using a reverse-phase C_{30}-column (5 µm, 250*4.6 mm; YMC Co. Ltd., Kyoto, Japan) protected by a 20*4.6 mm guard column. Three solvents, i.e. A: 100% methanol, B: 60% methanol buffered with 0.2% ammonium acetate and C: 100% methyl-tert-butyl-ether, were used to run a gradient starting with 40% A and 60% B. First solvent B was gradually replaced by solvent A to a minimum of 5% B. Then, solvent A was gradually replaced by solvent C until the solvent mixture consisted of 13.7% A, 5% B and 81.3% C. Finally, solvent C was replaced by solvent A until the mixture consisted of 95% A, and 5% B. Every run was followed by a 20 min reconditioning phase with the initial solvent concentrations. For calibration and peak detection, commercially available standards were obtained from Sigma Aldrich (St. Louis, MO, USA) and DHI Lab products (Hørsholm, Denmark). Peak detection and pigment quantification was performed using ChemStation software (Agilent Technologies, Santa Clara, CA, USA).

Total chlorophylls (Chl) were determined as the sum of chlorophyll a and b concentration on a fresh weight basis (µmol g^{-1}) and the ratio of chlorophyll a/b was expressed in mol mol^{-1}. The concentration of carotenoid pigments was normalized to chlorophyll levels and was expressed in mmol mol^{-1}. Total carotenoids (Car) were expressed as the sum of violaxanthin, antheraxanthin, zeaxanthin, neoxanthin, lutein, α-carotene and β-carotene concentrations. Total xanthophylls were expressed as the sum of violaxanthin, antheraxanthin, zeaxanthin, neoxanthin and lutein. Total xanthophyll cycle pigments (VAZ) were calculated as the sum of violaxanthin, antheraxanthin and zeaxanthin. DEPS was expressed according to Thayer and Björkman (1990) as:

$$\mathrm{DEPS} = \frac{0.5A+Z}{V+A+Z} \qquad \text{Equation 2.8}$$

Statistical analyses

For seasonal time series, the effects of treatments on individual parameters at each time point were estimated using mixed model analysis of variance (ANOVA). The mixed model analysis included the data of two independent experiments. Each experiment was included in the mixed model as a random effect. The mixed model analysis was performed using the difflsmeans function in the lmerTest package, using R version 3.1.1 (R Core team, 2014).

In order to evaluate the strength of the relationship between PRI and physiological parameters both at diurnal and seasonal timescales, we obtained R^2 values from linear regressions with log-transformed variables and considered the slope significantly different from zero when $P<0.05$. Regressions were performed using GraphPad Prism 6 software version 6.05 (GraphPad Software, Inc., La Jolla, CA, USA).

Finally, for the estimation of the best predictors for PRI at a seasonal timescale, we pooled data from both treatments and used mixed regression models and the Akaike information criterion (AIC) scores as a measure of model goodness of fit using the lmer function in the lme4 package in R version 3.1.1 (R Core team, 2014). ΔAIC values were calculated by subtracting the AIC score of each predictor model from the AIC score of the null model. Predictors were ranked according to ΔAIC values, with high ΔAIC representing high goodness of fit. Each experiment was included as a random effect to account for the two independent sets of experiments in both years. Significance of predictors was calculated comparing the null model to the predictor model using ANOVA.

2.4 Results

Short term variations in energy partitioning, photosynthesis and PRI

After 16 days of acclimation to SD/LT and SD/HT conditions, the seedlings exhibited different responses to increasing light intensity compared to LD/HT conditions (Fig. 2.1). Assimilation (*A*) in LD/HT seedlings was approximately 9 μmol CO_2 $m^{-2}s^{-1}$ at 2000 μmol quanta $m^{-2}s^{-1}$ light intensity. In the SD/HT seedlings *A* was about half the rate observed in LD/HT seedlings and in SD/LT seedlings the rate was decreased to merely 25% of LD/HT values (Fig. 2.1A). The higher maximum rate of *A* in LD/HT seedlings was accompanied by

a lower light compensation point (20.4 ±4.3 μmol quanta $m^{-2}s^{-1}$) compared to SD/LT (45.7 ±1.1 μmol quanta $m^{-2}s^{-1}$) and SD/HT (44.2 ±2.8 μmol quanta $m^{-2}s^{-1}$) seedlings. Compared to LD/HT, LUE_A was considerably lower in both SD/LT and SD/HT with similar values across the full range of light intensities (Fig. 2.1B). Assessing changes in energy partitioning via chlorophyll-fluorescence revealed a different pattern. The short term light response of SD/HT seedlings revealed Φ_{PSII}, Φ_{NPQ} and $\Phi_{f,D}$ values similar to LD/HT seedlings, whereas SD/LT seedlings showed decreased values for Φ_{PSII} and Φ_{NPQ} (Fig. 2.1C,D,E). In SD/LT seedlings $\Phi_{f,D}$ was approximately twice as high as in LD/HT seedlings and SD/HT seedlings. PRI only slightly decreased in SD/HT seedlings compared to LD/HT seedlings, but was considerably lower in SD/LT seedlings. In addition, the range of diurnal PRI variation differed between treatments; with a ΔPRI (PRI at 0 minus PRI at 2000 μmol quanta $m^{-2}s^{-1}$) of -0.033 in LD/HT seedlings, a ΔPRI of -0.014 in SD/LT seedlings, and a ΔPRI of -0.031 in SD/HT seedlings (Fig. 2.1F).

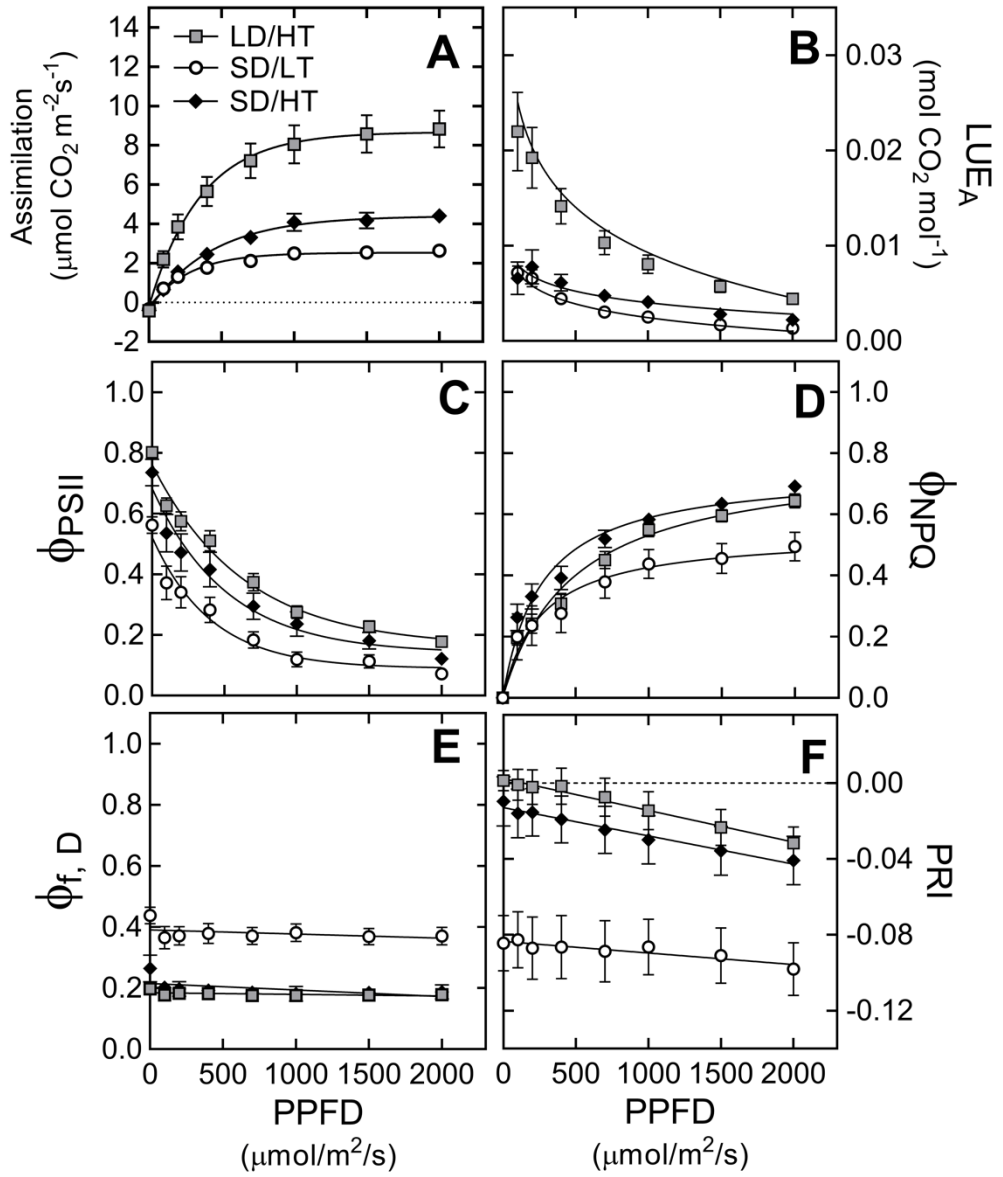

Figure 2.1 Response to light in *P. strobus* seedlings acclimated to LD/HT, SD/LT or SD/HT conditions for A) photosynthetic CO_2 assimilation; B) LUE_A, light use efficiency of CO_2 assimilation; C) Φ_{PSII}, fraction of absorbed light used for photochemistry, D) Φ_{NPQ}, fraction of light quenched via dynamic NPQ; E) $\Phi_{f,D}$, fraction of the sum of fluorescence and sustained NPQ and F) PRI, photosynthetic reflectance index. Each data point represents n=6 seedlings ±SE.

At a diurnal timescale, the relationship between PRI and *A* (R^2=0.47; P<0.001) or LUE_A (R^2=0.52; P<0.001, Fig 2.2a,b) was significant in LD/HT seedlings. However, the strength of the relationship between PRI and *A* was reduced by approximately half in SD/HT seedlings (R^2=0.18; P=0.01), and became non-significant in SD/LT seedlings (R^2=0.06,

P=0.587; Fig 2.2a). Upon acclimation to SD/LT or SD/HT, the relationship between LUE_A and PRI became non-significant in both treatments (Fig. 2.2B). In LD/HT seedlings we also observed significant relationships between PRI and both Φ_{PSII} and Φ_{NPQ} (R^2=0.66; *P*<0.001 and 0.59; *P*<0.001, respectively). Under cold conditions, the relationship between PRI and Φ_{PSII} became non-significant (R^2=0.05, *P*=0.187) whereas the relationship between PRI and Φ_{NPQ} remained significant (R^2=0.24, *P*=0.003; Fig. 2.2C,D). In LD/HT, SD/LT and SD/HT seedlings we also recorded significant relationships between PRI and $\Phi_{f,D}$ (Fig. 2.2E).

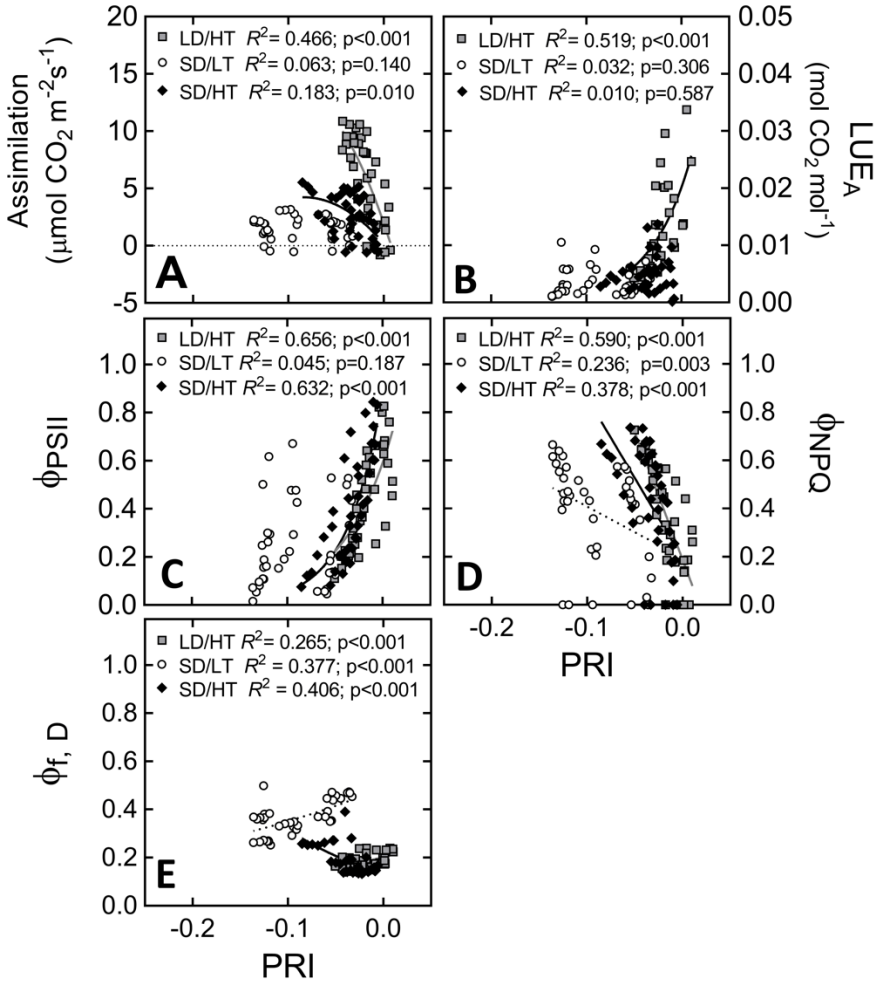

Figure 2.2 Relationship between PRI and A) photosynthetic CO_2 assimilation; and B) LUE_A, the light use efficiency of CO_2 assimilation; and C) Φ_{PSII}, fraction of absorbed light used for photochemistry, and D) Φ_{NPQ}, fraction of light quenched via dynamic NPQ; and E) $\Phi_{f,D}$, sum of fluorescence and sustained NPQ on *P. strobus* seedlings acclimated to LD/HT, SD/LT or SD/HT conditions. The relationships were considered significant when p<0.05.

Seasonal variation in energy partitioning and suppression of the induction of sustained NPQ under elevated autumn temperature

Upon transfer to SD/LT and SD/HT, a clear response of energy partitioning to shorter photoperiod and temperature was observed, indicated by changes in the proportion of absorbed light used for photochemistry (Φ_{PSII}), dynamic NPQ (Φ_{NPQ}), and the sum of fluorescence and sustained NPQ ($\Phi_{f,D}$) at different light intensities (Fig. 2.3). In SD/LT seedlings, Φ_{PSII} sharply declined on the first day of exposure to cold temperature and short photoperiod at all light intensities (Fig. 2.3A,C,E,G). Over the first 4 days of SD/LT, we observed a shift from a system primed to allocate most of the absorbed energy to photochemistry, to a system dissipating most of the absorbed energy via NPQ. Following this shift, excess energy was quenched in equal proportions via Φ_{NPQ}, and $\Phi_{f,D}$. This pattern did persist throughout the initial downregulation of photochemistry (days 0-4), and until the end of the experiment. By contrast, in SD/HT seedlings we observed only a minor decline of Φ_{PSII} after day 1 of exposure to short photoperiod (Fig. 2.3B,D,F,H). This decline occurred at the expense of Φ_{NPQ} while $\Phi_{f,D}$ remained unchanged over the 36 days of the experiment. In both treatments, Φ_{PSII} decreased with increasing light intensity at the expense of Φ_{NPQ}. Light intensity did not affect $\Phi_{f,D}$ (Fig. 2.3B,D,F,H).

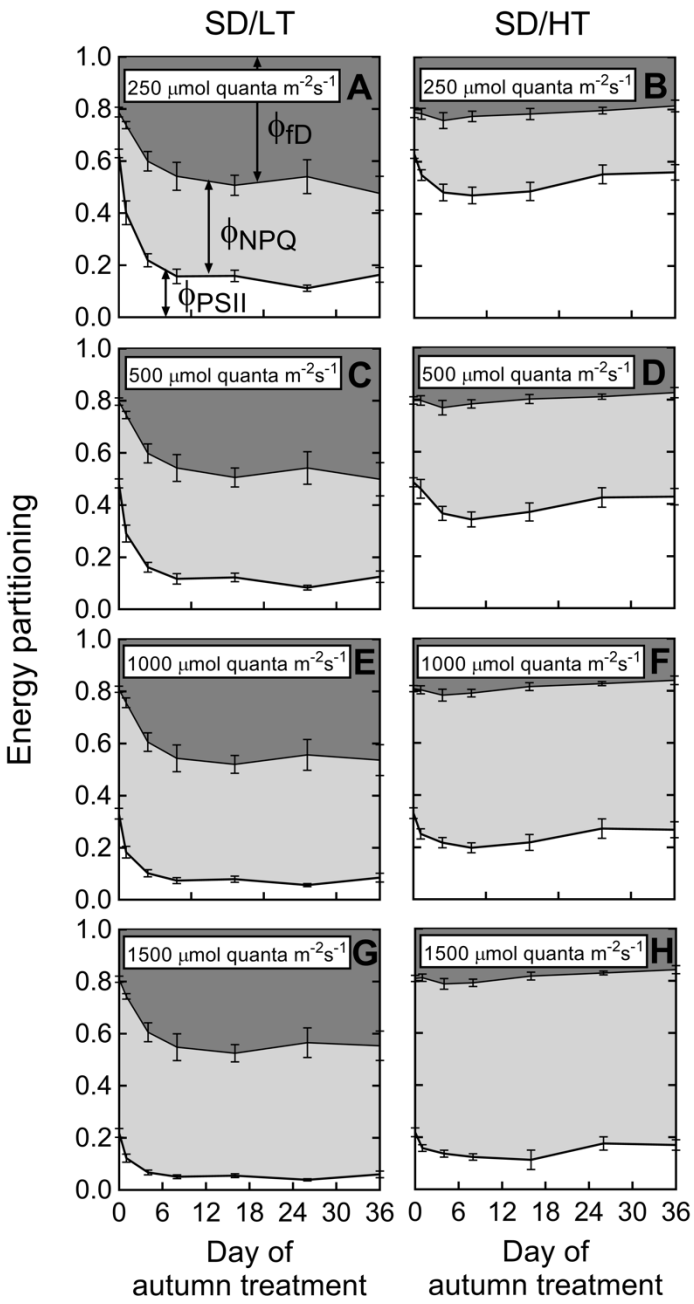

Figure 2.3 Time course of energy partitioning characteristics of *P. strobus* needles exposed to LD/HT, SD/LT or SD/HT conditions. Areas in white represent Φ_{PSII}, fraction of absorbed light used for photochemistry; areas in light grey represent Φ_{NPQ}, dynamic NPQ, and areas in dark grey represent $\Phi_{f,D}$, sum of fluorescence and sustained NPQ. Measurements taken at 250, 500, 1000 and 1500 μmol quanta $m^{-2}s^{-1}$ light intensity. Left and right panels present the SD/LT and SD/HT conditions, respectively. Each data point represents n=10 seedlings ±SE.

Downregulation of photosynthesis and seasonal variation in PRI

Consistent with the pattern revealed by energy partitioning, we observed a downregulation of photosynthetic activity over the 36 days of SD/LT or SD/HT (Fig. 2.4). We observed a maximum quantum yield of PSII (F_v/F_m) of about 0.8 in LD/HT seedlings, and a decrease of F_v/F_m of approximately 50% over the first 16 days of exposure to cold temperature and short photoperiod (Fig. 2.4A). In contrast, short photoperiod alone (warm treatment) had only little effect on F_v/F_m over the experiment (Fig. 2.4A). The excitation pressure of PSII (1-qP) rose on day 1 in both treatments, but was significantly higher in SD/LT seedlings from day 16 to 36 of the experiment (Fig. 2.4B).

Both the electron transport rate (ETR_{II}) and light use efficiency of CO_2 assimilation (LUE_A) in seedlings decreased by about half of LD/HT values after only one day of exposure to SD/LT (Fig. 2.4C,D). Short photoperiod alone also caused both ETR_{II} and *A* to decrease quickly, as was indicated in SD/HT seedlings on day 1 of the experiment. However, the magnitude of this decrease was smaller in SD/HT seedlings, where ETR_{II} partially recovered after day 16, while LUE_A remained low and did not recover during the experiment (Fig 2.4c,d). Exposure to both SD/LT and SD/HT caused an overall decline in stomatal conductance (g_s) over the 36 days of the experiment (Fig. 2.4E).

PRI gradually decreased in both SD/LT and SD/HT seedlings, however, PRI in SD/LT seedlings was consistently lower than SD/HT seedlings (Fig 2.4f). Mean PRI was -0.023 under LD/HT conditions, but decreased to -0.100 in SD/LT seedlings and -0.044 in SD/HT seedlings by the end of the experiment (Fig. 2.4F).

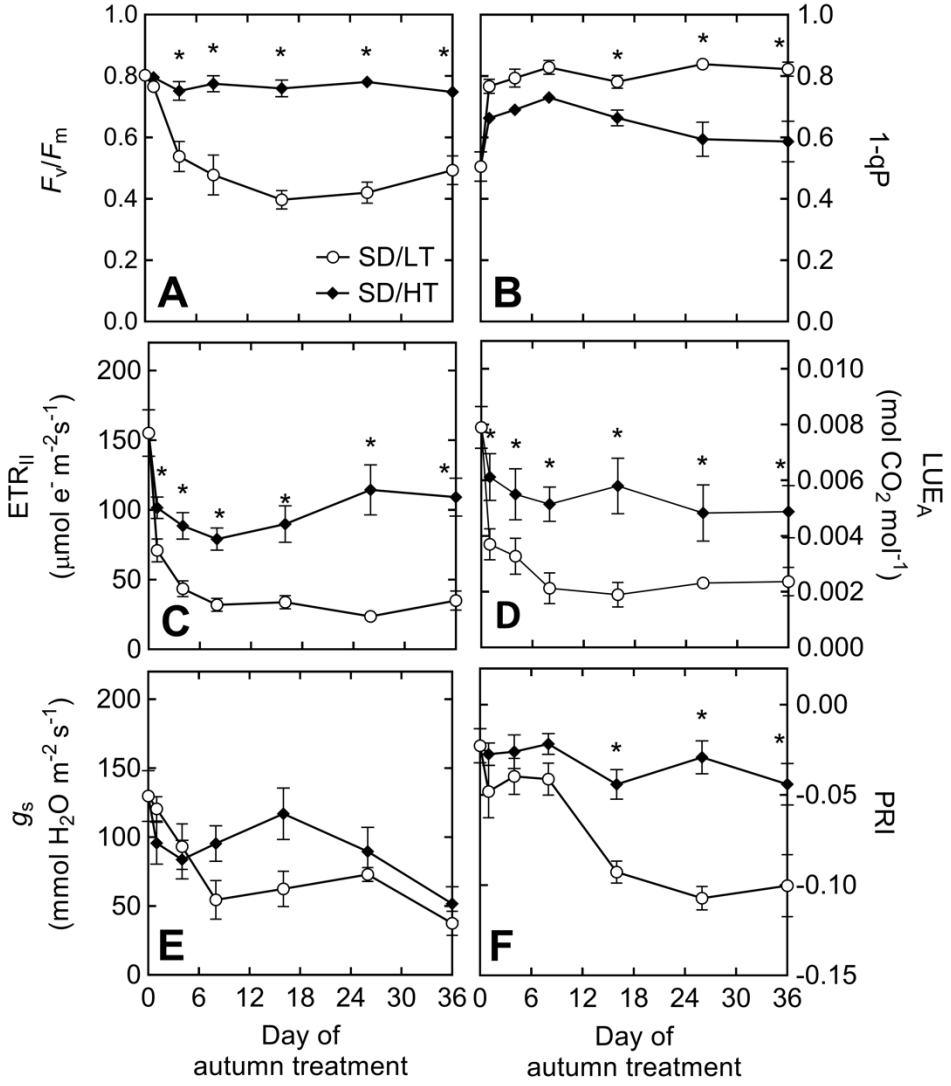

Figure 2.4 Time course of photosynthetic downregulation in *P. strobus* exposed to LD/HT, SD/LT or SD/HT conditions. A) F_v/F_m, maximum quantum yield of PSII; B) 1-qP, excitation pressure of the reaction centres of PSII; C) ETR_{II}, electron transport rate at 1500 µmol quanta $m^{-2}s^{-1}$ light intensity; D) LUE_A, light use efficiency of CO_2 assimilation at 1500 µmol quanta $m^{-2}s^{-1}$; E) g_s, stomatal conductance at 1500 µmol quanta $m^{-2}s^{-1}$ light intensity and F) PRI. Each data point represents n=10 seedlings ±SE and asterisks indicate significant differences (α = 0.05) between treatments at a given time point.

Seasonal variation in pigments

Upon transfer to simulated autumn growth conditions, we observed a clear response of photosynthetic pigment composition in both treatments (Fig. 2.5). Chlorophylls (Chl) quickly decreased on day 1 when seedlings were shifted to both SD/LT and SD/HT (Fig. 2.5A). The initial decline was more pronounced in SD/LT seedlings, where almost half of the Chl pool was lost within the first 24 hours of the experiment (Fig. 2.5A). A moderate recovery in Chl was observed after day 1 in both treatments, followed by a second phase during which values decreased and then remained constant following day 16 of the experiment (Fig. 2.5A). A similar trend was observed with a consistently larger Chl pool size in SD/HT seedlings (Fig. 2.5A). The ratio of chlorophyll a to b (Chl a/b) was consistently lower in SD/LT seedlings from day 8 of the experiment (Fig. 2.5B).

The ratios of carotenoids Chl^{-1} and xanthophylls Chl^{-1} gradually increased in both treatments during the experiment, with consistently higher values in SD/LT seedlings (Fig. 2.5C,D). In LD/HT seedlings, the amount of zeaxanthin Chl^{-1} was low but exposure to SD/LT resulted in a steady increase of zeaxanthin Chl^{-1} over the entire experiment, with approximately half of the increase occurring on day 1 (Fig. 2.5E). In contrast, levels of zeaxanthin Chl^{-1} in SD/HT seedlings remained low throughout the entire experiment (Fig. 2.5E). This pattern was somewhat similar to the changes observed in DEPS over the course of the experiment. In both treatments, DEPS initially increased on days 0-4. Interestingly, DEPS then retained the increased values for the rest of the experiment in SD/LT seedlings with values around 0.6-0.7, but in SD/HT seedlings DEPS gradually decreased after day 8 to values similar to those recorded at the beginning of the experiment (Fig. 2.5F).

In both treatments, the amount of lutein Chl^{-1} progressively increased during the experiment, with an increase by almost 150% in SD/LT and by about 80% in SD/HT seedlings (Fig. 2.5G; Table 2.S1). In contrast, equal increases were observed for β-carotene Chl^{-1} in both treatments. We observed a sharp increase on day 1 of the experiment and then β-carotene Chl^{-1} progressively increased until day 36, with similar levels in both treatments (Fig 2.5h; Table 2.S1).

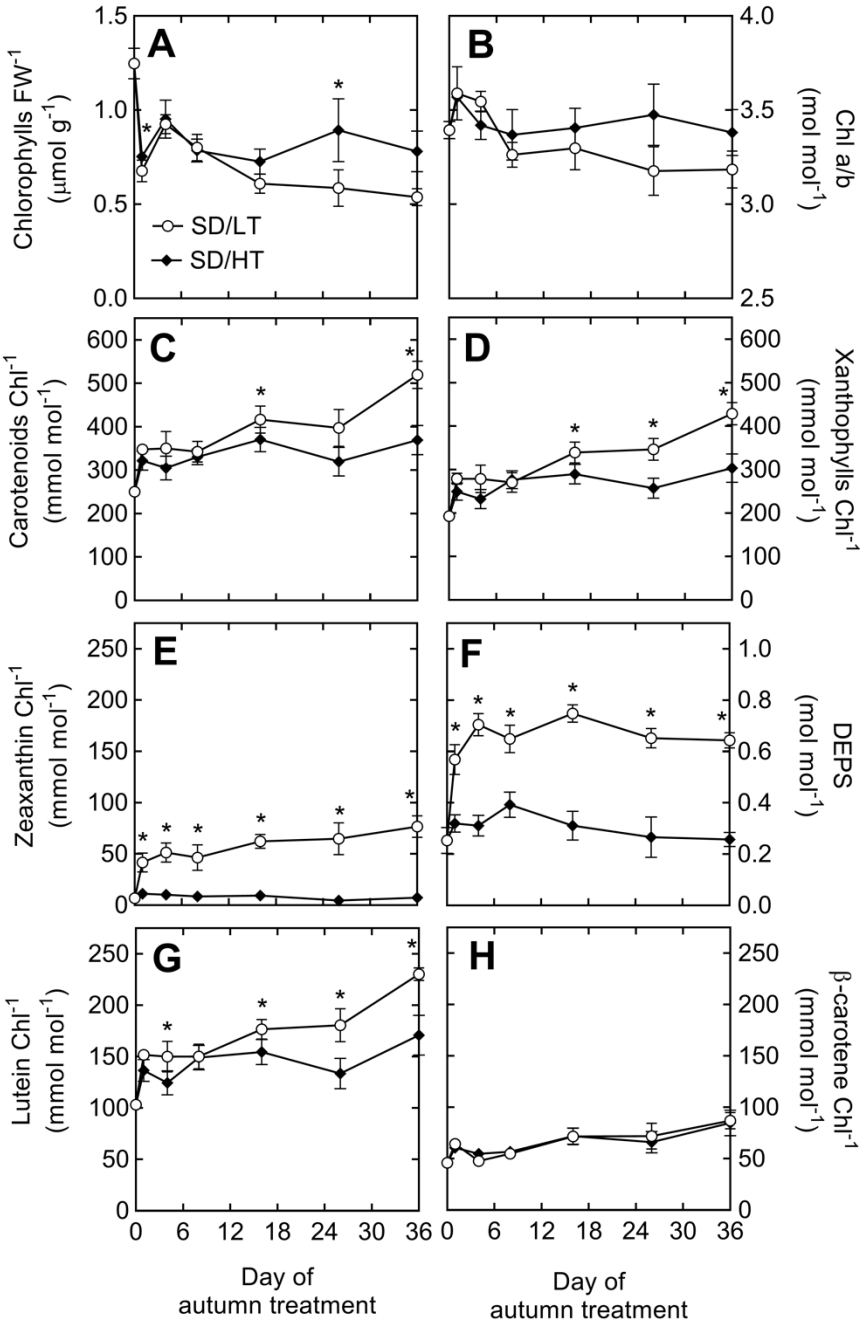

Figure 2.5 Time course of photosynthetic pigment dynamics in *P. strobus* needles exposed to LD/HT, SD/LT or SD/HT conditions. A) amount of Chl a+b FW^{-1} B) ratio of Chl a to Chl b; C) amount of carotenoids Chl^{-1}; D) amount of xanthophylls Chl^{-1}; E) amount of zeaxanthin Chl^{-1}; F) de-epoxidation state of the xanthophyll cycle; G) amount of lutein Chl^{-1}; H) amount of β-carotene Chl^{-1}. Each data point represents n=10 seedlings ±SE and asterisks indicate significant differences ($\alpha = 0.05$) between treatments at a given time point.

Relationship between seasonal changes in energy partitioning and PRI

Figure 2.6 shows the relationship between PRI and parameters of light energy utilization by the seedlings. During days 0-4, we observed a relationship between LUE_A and PRI, with an R^2 of 0.55 (P<0.001) in SD/LT seedlings, and 0.41 (P<0.001) in SD/HT seedlings (Fig. 2.6A). In SD/LT seedlings, the relationship was lost during days 8-36, with an R^2 of only 0.01 (P=0.57) but it remained significant in SD/HT seedlings, with an R^2 of 0.17 (P=0.008; Fig. 2.6B). The fraction of light used for photochemistry (Φ_{PSII}) correlated significantly with PRI, with an R^2 of 0.38 (P<0.001) in SD/LT seedlings and an R^2 of 0.39 (P<0.001) in SD/HT seedlings (Fig. 2.6C). After day 8 this relationship was no longer observed in SD/LT seedlings, but was retained in SD/HT seedlings (Fig. 2.6D). Both the fraction of light quenched via sustained NPQ (Φ_{NPQ}) and the sum of fluorescence and sustained NPQ ($\Phi_{f,D}$) showed a poor relationship with PRI during the entire experiment.

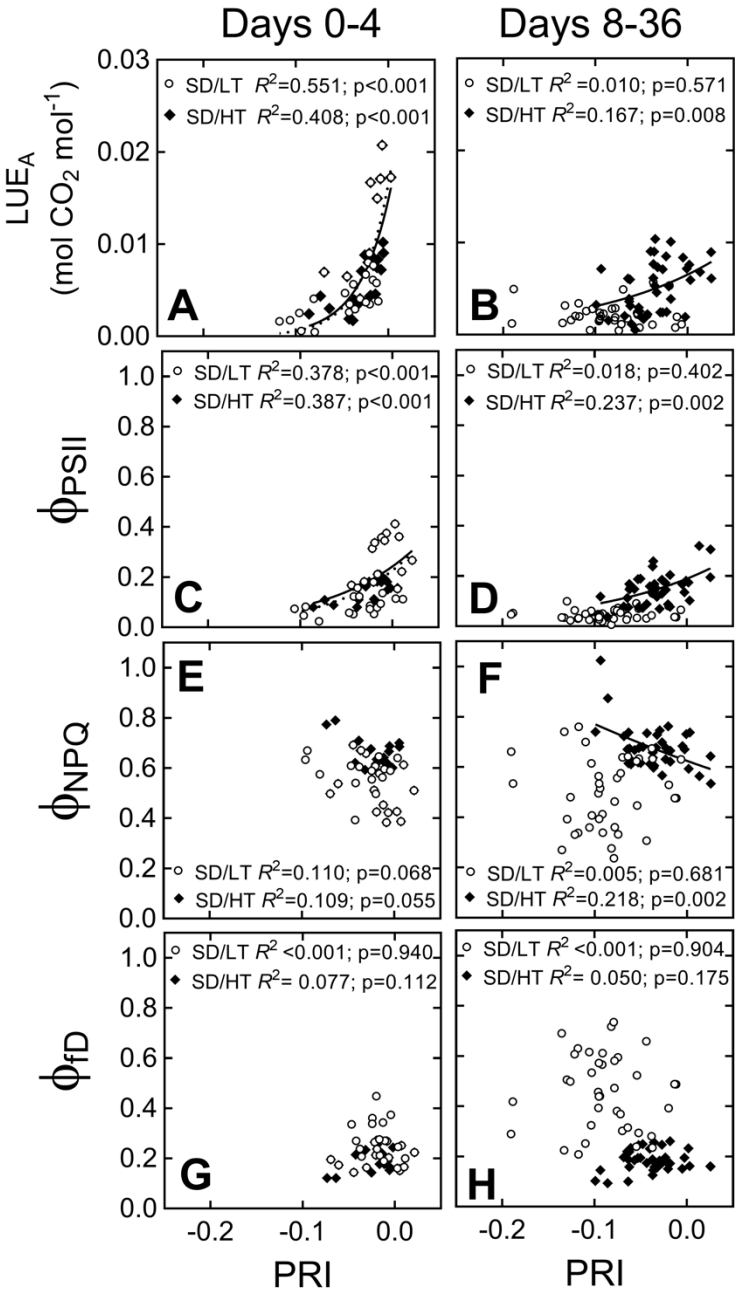

Figure 2.6 Relationship between PRI and LUE_A, the light use efficiency of CO_2 assimilation (A-B), Φ_{PSII}, fraction of absorbed light used for photochemistry (C-D), Φ_{NPQ}, fraction of absorbed light quenched via dynamic NPQ (E-F); and $\Phi_{f,D}$, the sum of fluorescence and sustained NPQ (G-H) at 1500 μmol quanta $m^{-2}s^{-1}$ during the downregulation of photosynthesis of *P. strobus* exposed LD/HT, SD/LT or SD/HT conditions. The relationships were considered significant when $p<0.05$. Left and right panels present data from days 0-4 and days 8-36 of the experiment, respectively.

Relationship between seasonal pigment changes and PRI

Figure 2.7 shows the relationship between PRI and key pigment parameters. The de-epoxidation state of the xanthophyll-cycle (DEPS) correlated significantly with PRI during days 0-4, with R^2 values of 0.73 (P<0.001) and 0.70 (P<0.001) in SD/LT and SD/HT seedlings, respectively (Fig. 2.7A). However, the correlation was lost in both treatments during days 8-36 (Fig. 2.7B). In contrast, we observed a significant relationship between the amount of Chl and PRI during days 0-4, and the relationship was maintained in both treatments during days 8-36 (Fig. 2.7D). Similarly, we observed a significant relationship between the amount of carotenoids Chl^{-1} and PRI during days 0-4, with R^2 values of 0.42 (P<0.001) and 0.51 (P<0.001) in SD/LT and SD/HT seedlings, respectively (Fig. 2.7E). During days 8-36, the relationships were conserved with R^2 values of 0.53 (P<0.001) in SD/LT seedlings and 0.68 (P<0.001) in SD/HT seedlings (Fig. 2.7F). Significant relationships that were conserved throughout the entire experiment were also observed between PRI and the amount of xanthophylls Chl^{-1} (Fig. 2.7G,H), the amount of β-carotene Chl^{-1} (Fig. 2.7I,J) and the amount of lutein Chl^{-1} (Fig. 2.7K,L).

A mixed linear model including data from the SD/LT and SD/HT confirmed that the amount of xanthophylls Chl^{-1} best explains PRI variation at a seasonal scale (Table 2.1). The next three best predictors for PRI were carotenoids Chl^{-1}, lutein Chl^{-1} and VAZ Chl^{-1}. Total Chls appeared on the list only as the fifth best predictor, before DEPS and β-carotene Chl^{-1} (Table 2.1).

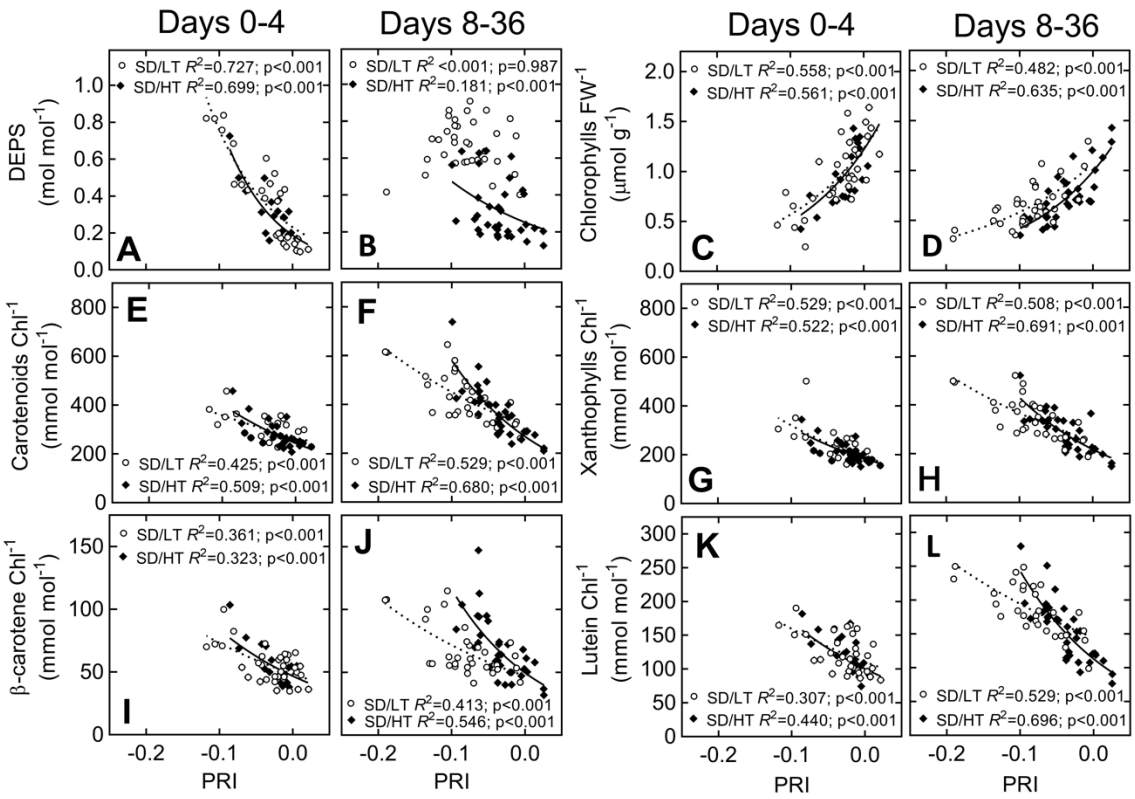

Figure 2.7 Relationship between PRI and DEPS (A-B), chlorophylls FW^{-1} (C-D), carotenoids Chl^{-1} (E-F), xanthophylls Chl^{-1} (G-H), β-carotene Chl^{-1} (I-J), and lutein Chl^{-1} (K-L) during the downregulation of photosynthesis of *P. strobus* exposed to LD/HT, SD/LT or SD/HT conditions. The relationships were considered significant when $p<0.05$. For each parameter, left and right panels present data from days 0-4 and days 8-36 of the experiment, respectively.

Table 2.1 Summary of mixed linear modelling to identify the best predictors of PRI variation in *P. strobus* seedlings on a seasonal scale. Data from SD/LT and SD/HT were pooled together. AIC scores provided for goodness of fit of each predictor model, with high ΔAIC values indicating high goodness of fit (see Materials and Methods for details).

Rank	Predictor	AIC	ΔAIC	Significance
	Null model	-532.37		
1	Xanthophylls Chl^{-1}	-600.54	68.18	$P < 0.001$
2	Carotenoids Chl^{-1}	-596.57	64.20	$P < 0.001$
3	Lutein Chl^{-1}	-590.45	58.08	$P < 0.001$
4	VAZ Chl^{-1}	-583.40	51.04	$P < 0.001$
5	Chlorophylls FW^{-1}	-571.86	39.49	$P < 0.001$
6	Zeaxanthin Chl^{-1}	-566.58	34.21	$P < 0.001$
7	DEPS	-560.23	27.87	$P < 0.001$
8	β-carotene Chl^{-1}	-547.71	15.34	$P < 0.001$

2.5 Discussion

Downregulation of photosynthesis upon exposure to short photoperiod

In autumn, short photoperiod and cold temperature act as signals for growth cessation and/or downregulation of photosynthesis in conifers, with individual species differing in their responses to each signal (Green 2007, Busch *et al*. 2007, 2008, Way & Montgomery 2014). For example, growth cessation can induce the downregulation of photosynthesis through feedback response to reduced sink capacity for photoassimilates (Savitch *et al*. 2002, Ensminger *et al*. 2006). In our experiment, the greatest declines in photosynthetic carbon assimilation and stomatal conductance were observed in seedlings exposed to both short photoperiod and cold temperature (SD/LT; Fig. 2.4D,E), reflecting the effect of cold temperature on general metabolism, membrane viscosity and enzymatic reactions involved in the reduction of carbon (Hüner *et al*. 1998). Interestingly, we also observed a considerable decline in net photosynthetic CO_2 assimilation under SD/HT conditions, which essentially represents a shift from long day to short day photoperiod (Fig. 2.1, 2.4, 2.5). This suggests that photoperiod is an important signal in the autumn downregulation of photosynthesis in *P. strobus*. Most remarkably, the response of carbon assimilation to a decrease in photoperiod was already observed on the first short day of the experiment, with a loss of almost half of the photosynthetic activity that was observed under LD/HT conditions (long day). In *P. sylvestris*, Busch *et al*. (2007) also observed a decline in CO_2 assimilation of approximately 40% after 4 weeks exposure to a short photoperiod treatment. In *Arabidopsis*, short photoperiod, or longer nights, results in a temporary period of sugar starvation at the end of the night (Gibon *et al*. 2009). Sugar starvation causes hormonal inhibition of growth (Paparelli *et al*. 2013) and a decrease in protein and amino acid content of *Arabidopsis* leaves (Gibon *et al*. 2009). It is likely that photosynthesis in needles of our *P. strobus* seedlings was inhibited through a reduced metabolic sink capacity due to repressed growth (Savitch *et al*. 2002, Busch *et al*. 2007), but also by carbon starvation at the end of the night, that can inhibit the turnover of enzymes and proteins involved in carbon fixation (Osuna *et al*. 2007).

Sustained NPQ is induced by low temperature exposure but repressed by warm temperature

Exposure to shorter photoperiod and warm temperature did not affect the efficiency of PSII, as reflected by unchanged F_v/F_m values throughout the experiment (Fig. 2.4A). Light absorption by the light harvesting complexes of PSII (LHCII) combined with a decreased sink capacity for photoassimilates creates energetic imbalances which are potentially harmful to thylakoid membranes (Barber & Andersson 1992, Hüner *et al.* 1998, Ensminger *et al*. 2006). Levels of excess light energy increased on day 1 after shifting seedlings from LD/HT to SD/HT conditions. This was caused by a decline in assimilation rates and reduced metabolic sink capacity (Fig. 2.4). Under SD/HT conditions, it appears that excess light energy was mostly quenched via dynamic NPQ (Fig. 2.3). Sustained NPQ was not observed under SD/HT, indicating that cold temperature is necessary for its induction. In contrast, under SD/HT conditions sustained NPQ was induced over the first 8 days of exposure to cold temperature, gradually replacing dynamic NPQ (Fig. 2.3). In conifers, sustained NPQ is activated by long-term limitations in carbon export capacity (Demmig-Adams & Adams 2006a). Under SD/LT conditions, these conditions were reflected by very low photosynthetic activity along with high excitation pressure values (Fig. 2.4). Interestingly, dynamic NPQ retained functionality even with exposure to cold temperature, and long after photosynthetic downregulation and the induction of sustained NPQ (Fig. 2.3). During the autumn downregulation of field grown *P. sylvestris*, Porcar-Castell (2011) also observed the accumulation of sustained NPQ at temperatures much higher than those at which dynamic NPQ is strongly inhibited. This confirms that sustained and dynamic NPQ are additive rather than exclusive, conferring flexibility to photoprotection with changing environmental conditions throughout the year.

Differences in adjustments of pigment pool sizes and in energy partitioning characteristics between cold and warm conditions

The initial decline of photosynthetic activity after shifting seedlings to both SD/LT and SD/HT conditions was paralleled by adjustments in photosynthetic pigment pools, e.g. by a 50% decrease of Chl (Fig. 2.5A). It is remarkable that this loss occurred in both treatments,

and with this initial decline in Chl being only slightly larger under SD/LT than under SD/HT conditions. This suggests that chlorophyll degradation was mostly a result of a short day-induced decline in metabolic sink capacity. However, beyond the initial chlorophyll degradation it appears that cold-induced photoinhibition (Ensminger *et al*. 2004) further contributed to the decrease of chlorophylls under SD/LT conditions (Fig. 2.5A, days 16 to 36; Sveshnikov *et al*. 2006).

Carotenoids Chl^{-1} increased under both SD/LT and SD/HT treatments, although exposure to cold temperature had a larger effect on carotenoid accumulation (Fig. 2.5C), which concurs with the observed increase in thermal dissipation of light energy under SD/LT conditions. Exposure to cold temperature resulted in increased zeaxanthin Chl^{-1} and DEPS values (Fig. 2.5E,F). In contrast, under SD/HT conditions the pool of zeaxanthin did not significantly increase, and DEPS remained similar to LD/HT values. This indicates that plants exposed to SD/HT conditions did not enhance dissipation of excess energy via the xanthophyll cycle, despite reduced CO_2 assimilation and a decrease in LUE. Instead, under SD/HT conditions we observed a moderate decrease in light-harvesting Chl, resulting in the physical reduction of the size of the light harvesting complexes (Ensminger *et al*. 2004, 2006), a significant increase in the ratio of lutein and β-carotene to Chls (Fig. 2.5G,H; Table 2.S1) as well as a 24% increase of β-carotene on a per fresh weight basis (Table 2.S1). Recently it was shown that lutein and β-carotene act as important radical scavengers, with lutein having the ability to quench both the ^{3}Chl and ^{1}Chl*states (Dall'Osto *et al*. 2006, Avenson *et al*. 2009, Jahns and Holzwarth 2012), and β-carotene quenching the singlet oxygen generated via the triplet state of the primary electron donor pheophytin (Young and Frank 1996, Trebst 2003, Telfer 1994, 2005, 2014, Krieger-Liszkay 2008). This indicates that these pigments can act as alternative quenchers of excess energy, as suggested by Busch *et al*. (2007), who observed low DEPS and elevated levels of β-carotene in *P. banksiana* seedlings exposed to SD/HT conditions. Busch *et al*. (2007) concluded that β-carotene must play a role in quenching of singlet oxygen, as previously documented (Trebst 2003, Telfer 1994, 2005, 2014, Krieger-Liszkay 2008). Although these xanthophyll cycle independent mechanisms were observed in both the cold and warm treated seedlings, they can serve under SD/HT conditions to balance the reduced metabolic sink capacity when exposed to short autumn photoperiod in the absence of sustained NPQ.

At a diurnal timescale, the range of PRI variation reflects the capacity for photoconversion of the xanthophyll cycle pigments violaxanthin and zeaxanthin

Variations of xanthophyll de-epoxidation are reflected by the PRI at a diurnal scale (Gamon *et al*. 1992, 1997). In needles acclimated to LD/HT we observed a difference of 0.037 between the dark state of PRI and the PRI obtained under saturating light conditions (ΔPRI; Fig. 2.1F), which is similar to values observed on other conifer species such as *P. menziesii*, *T. heterophylla*, *P. banksiana*, *P. contorta* and *P. ponderosa* (Gamon & Berry 2012, Wong & Gamon 2015a). Gamon & Berry (2012) demonstrated that within a tree canopy ΔPRI is larger in sun needles than in shade needles, attributing large ΔPRI to a greater capacity for dynamic NPQ. This supports our observation of smaller ΔPRI in needles acclimated to SD/LT conditions, reflecting a partial deactivation of the dynamic regulation of the xanthophyll cycle in the cold (Fig. 2.1D). This is consistent with Wong & Gamon (2015b), who observed winter time ΔPRI values close to 0, which coincided with photosynthetic downregulation. This lowered capacity for photoconversion of xanthophyll pigments in our cold seedlings was reflected by lower Φ_{NPQ} and higher $\Phi_{f,D}$ (Fig. 2.1, 2.3), indicating a shift from dynamic NPQ to sustained NPQ in the cold.

The PRI-LUE relationship is impaired by exposure to both simulated cold and warm autumn conditions

Over diurnal timescales, the fraction of energy used for photochemistry (Φ_{PSII}), the light-use efficiency of CO_2 assimilation (LUE_A) and the rate of CO_2 assimilation all correlated significantly with PRI. The fraction of light quenched via dynamic NPQ (Φ_{NPQ}) was the parameter that showed the strongest correlation with PRI (R^2=0.59, P<0.001 in LD/HT seedlings; Fig. 2.2D). Interestingly, this relationship was impaired under both SD/LT and SD/HT conditions. In conifer needles acclimated to LD/HT, a large fraction of NPQ is facilitated by dynamic conversions of xanthophyll pigments. In contrast, in cold-acclimated needles the xanthophyll cycle is arrested in a sustained photoprotective state where zeaxanthin no longer reconverts into violaxanthin in the dark and the photosynthetic apparatus remains primed for thermal dissipation (Demmig-Adams & Adams 2006a). This

sustained NPQ is achieved through structural reorganization of PSII. This reorganization includes the aggregation of LHCII, which constitutes a major energy dissipation pathway (Horton *et al*. 1991, 2005, Ottander *et al*. 1995). Cold-acclimated conifers also dissipate excess light energy via PSII reaction centre quenching, which is maximal in winter-acclimated needles (Ivanov *et al*. 2002). Savitch *et al*. (2010) also suggested that plastid terminal oxidase (PTOX) mediated electron transport to oxygen might be a major component of winter time sustained NPQ. Cyclic electron transport around PSI, contributing to ATP production, was also proposed to be a significant energy sink in winter-acclimated needles (Ivanov *et al*. 2001, Fréchette *et al*. 2015). This might explain why under cold conditions PRI did not correlate well with NPQ, and hence the efficiency of photosynthesis. Although exposure to elevated temperature prevented the induction of sustained NPQ, an impairment of the PRI-LUE relationship was observed in seedlings exposed to SD/HT conditions. As mentioned above, our pigment data indicate that this impairment is likely caused by the involvement of alternative NPQ mechanisms in seedlings acclimated to SD/HT, likely via radical scavenging by carotenoid pigments such as β-carotene and lutein (Busch *et al*. 2007).

Cold temperature induces long-term adjustments of pigment pools, which are a larger source of PRI variation than the photoconversion of xanthophyll pigments

Apart from the interconversion of xanthophyll pigments, PRI was also affected by seasonal adjustments of pigment pools. Since PRI integrates the relative reflectance on either side of the green reflectance bump, it compares the reflectance in the blue region of the spectrum (chlorophylls and carotenoids absorption) with the reflectance in the red (carotenoids only) (Garbulsky *et al*. 2011). Therefore, adjustments in Car Chl^{-1} ratios of conifer leaves will exert a strong influence on the PRI, particularly as they undergo physiological changes associated with winter acclimation. In our study, PRI variation resulting from long-term pigment pool adjustments was almost 3 times larger than PRI variation resulting from changes in the de-epoxidation state of the xanthophyll cycle (Fig. 2.1, 2.4). This ratio suggests that on an annual scale, seasonal pigment adjustments mask diurnal variations in PRI, especially during the transition between dynamic NPQ and sustained NPQ. This

finding is consistent with recent reports of a strong contribution of pigment pools on the PRI in boreal pine species (Porcar-Castell *et al*. 2012, Fréchette *et al*. 2015, Wong & Gamon 2015a,b). The relative contributions of dynamic effects and long-term seasonal effects on PRI variation vary throughout the year, causing variation in the strength of the PRI-LUE relationship on an annual scale. For instance, our data indicate a greater contribution of dynamic effects on the PRI compared to long-term effects under SD/HT conditions, and a greater contribution of long-term effects under SD/LT conditions.

At a seasonal timescale, PRI is mostly controlled by the ratio of carotenoids to chlorophylls

Over the 36 days of simulated autumn the strength of the PRI-LUE_A relationship varied considerably. During the initial phase of the experiment we observed a significant relationship under both SD/LT and SD/HT conditions between PRI and LUE_A as well as PRI and the fraction of light used for photochemistry (Φ_{PSII}; days 0-4). However, under prolonged exposure to the cold temperature the relationships became non-significant (days 8-36, Fig. 2.6B,C,D). Our data also clearly demonstrate a significant relationship between PRI and DEPS during the initial response to SD/LT and SD/HT conditions, which is absent during the second phase of the experiment in both cases (Fig. 2.7A,B). The data obtained during the initial 4 days of the experiment confirm the suitability of PRI as an index for LUE of evergreen foliage during the growing season and in the absence of conditions that induce sustained NPQ. However, under environmental conditions where the predominant mode of NPQ does not involve a dynamic operation of the xanthophyll-cycle, such as prolonged exposure to low temperature leading to cold acclimation, PRI must be used with caution as a proxy for LUE. Instead, at a seasonal timescales, the PRI is much better correlated with the pool sizes of chlorophylls and carotenoids (Fig. 2.7, days 8-36). Mixed linear modelling analysis identified the four best predictors of the variation observed in PRI on a seasonal scale, confirming the role of carotenoid pigments, including total xanthophylls Chl^{-1} as the single best predictor. DEPS, however, ranked low compared to the other predictors (Table 2.1). In field grown *P. sylvestris*, Porcar-Castell *et al*. (2012) reported a stronger correlation between PRI and VAZ Chl^{-1} than DEPS at a seasonal scale, while Wong and Gamon (2015a) observed Car Chl^{-1} to match PRI more closely throughout the year. Our

results provide strong evidence for the dominance of long-term pigment pool adjustments over diurnal changes in the de-epoxidation state of xanthophyll pigments at a seasonal timescale.

Our study shows that understanding the effects of different environmental conditions on various quenching mechanisms and, in turn, their effects on PRI will be crucial to properly interpret the PRI signal at different times of the year. While our study sheds new light on the mechanisms introducing a discrepancy in the PRI-LUE relationships under simulated autumn conditions, field studies will be necessary to quantify the contribution of these mechanisms under naturally fluctuating light and temperature regimes. In addition, it will be important to further validate the mechanisms identified here on mature trees and in natural systems where additional causes of PRI variation, such as sun angle or canopy structure, are likely to be present and add further complexity to the signal detected from leaf reflectance measurements.

2.6 Conclusions

We demonstrated that seedlings exposed to different photoperiod and temperature conditions use different strategies for dissipating excess energy. Under cold temperature and short photoperiod, a large proportion of excess energy was dissipated via sustained NPQ and presumably concomitant aggregation of light-harvesting complexes. In contrast, under warm temperature and short photoperiod sustained NPQ was not induced and excess energy was largely avoided via decreases in chlorophylls, increases in the ratio of β-carotene and lutein to chlorophylls and increases in β-carotene needle content. The variation in PRI associated with seasonal changes in pigment pool sizes was approximately threefold that of the variation in PRI attributable to the dynamic diurnal adjustments of xanthophyll pigments. In both treatments, the presence of these alternative NPQ mechanisms, which are independent of dynamic xanthophyll cycle activity, were undetected by the PRI and impaired the PRI-LUE relationship.

2.7 Acknowledgements

Authors are grateful to Laura Verena Junker for her expertise on pigment analysis and Dhyani Patel for her continuous help and assistance in the lab. Financial support from NSERC and Canada Foundation for Innovation to IE is gratefully acknowledged. EF acknowledges the receipt of a Graduate Student Research Award from the University of Toronto Center for Global Change Science, Ph.D. funding from the Department of Cell and Systems Biology at the University of Toronto and Ontario Graduate Scholarships.

2.8 Supplementary material

Table 2.S1 Results of an ANOVA for the determination of differences in pigment contents between day 0 and day 36 of the experiment in both treatments (n=10 seedlings; *P<0.05; ** P<0.01; ***P<0.001).

		Sp_C			Sp_W		
	Day 0 mean	Day 36 mean	Diff.	Signif.	Day 36 mean	Diff.	Signif.
Chlorophylls/FW[a]	1.30	0.54	-0.76	*P* <0.001 ***	0.78	-0.52	*P* <0.001 ***
Chlorophyll a/b[b]	3.40	3.18	-0.22	*P* <0.048 *	3.38	-0.02	*P* = 0.686 n.s.
Carotenoids/FW[a]	328.4	246.7	-81.6	*P* = 0.603 n.s.	244.4	-83.9	*P* = 0.489 n.s.
Carotenoids/Chl[c]	250.4	519.5	269.2	*P* <0.001 ***	369.4	119.1	*P* <0.001 ***
Xanthophylls/FW[a]	179.2	162.6	-16.6	*P* = 0.288 n.s.	164.8	-14.4	*P* = 0.032 *
Xanthophylls/Chl[c]	192.9	428.6	235.8	*P* <0.001 ***	303.4	110.5	*P* <0.001 ***
Zeaxanthin/Fw[a]	8.2	37.5	29.3	*P* <0.001 ***	6.1	-2.1	*P* = 0.740 n.s.
Zeaxanthin/Chl[c]	6.8	76.7	69.9	*P* <0.001 ***	7.3	0.5	*P* = 0.538 n.s.
DEPS[b]	0.25	0.64	0.39	*P* <0.001 ***	0.26	0.01	*P* = 0.367 n.s.
β-carotene/FW[a]	40.7	42.5	1.8	*P* = 0.628 n.s.	50.6	9.9	*P* = 0.010 **
β-carotene/Chl[c]	40.0	87.0	47.0	*P* <0.001 ***	84.8	44.8	*P* <0.001 ***
Lutein/FW[a]	102.2	121.5	19.4	*P* = 0.015 **	95.5	-6.7	*P* = 0.530 n.s.
Lutein/Chl[c]	103.2	230.3	127.1	*P* <0.001 ***	170.9	67.6	*P* <0.001 ***

a: expressed in ng mg FW^{-1}; b: expressed in mol $mol^{-1;}$ c: expressed in mmol mol^{-1}

Chapter 3

3 Zeaxanthin-independent energy quenching and alternative electron sinks cause a decoupling of the relation between the photochemical reflectance index (PRI) and photosynthesis in an evergreen conifer during spring

Fréchette E, Wong CYS, Junker LV, Chang CY, Ensminger I (2015) Zeaxanthin-independent energy quenching and alternative electron sinks cause a decoupling of the relation between the photochemical reflectance index (PRI) and photosynthesis in an evergreen conifer during spring. Journal of Experimental Botany 66(22):7309-7323.

Status: published.

3.1 Abstract

In evergreen conifers, the winter downregulation of photosynthesis and its recovery during spring are the result of a reorganisation of the chloroplast and adjustments of energy quenching mechanisms. These phenological changes may remain undetected by remote sensing, as conifers retain green foliage during periods of photosynthetic downregulation. We aimed to assess if the timing of the spring recovery of photosynthesis and energy quenching characteristics are accurately monitored by the photochemical reflectance index (PRI) in the evergreen conifer *Pinus strobus*. We studied the recovery of photosynthesis using chlorophyll fluorescence, leaf gas exchange, leaf spectral reflectance and photosynthetic pigment measurements. To assess if climate change might affect the recovery of photosynthesis, we exposed seedlings to cold spring conditions or warm spring conditions with elevated temperature. We observed an early spring decoupling of the relationship between photosynthesis and PRI in both treatments. This was caused by differences between the timing of the recovery of photosynthesis, and the timing of carotenoid and chlorophyll pool size adjustments, which are the main factors controlling PRI during spring. We also demonstrate that zeaxanthin-independent NPQ mechanisms undetected by PRI further contributed to the early spring decoupling of the PRI-LUE relationship. An important mechanism undetected by PRI seems to involve increased electron transport around photosystem I, which was a significant energy sink during the entire spring transition, particularly in needles exposed to a combination of high light and cold temperatures.

3.2 Introduction

Recent increases in global temperature are causing large-scale changes in carbon cycling of conifer dominated northern forest ecosystems (IPCC 2014, Piao *et al*. 2008, Zhang *et al*. 2013). Since photosynthesis is highly variable in space and time, its assessment with high spatial and temporal resolution is essential to accurately assess the actual and projected effects of global climate change on the carbon budget of these forests. Remote sensing can provide data across a range of spatial scales and has become an important source of information for modelling global carbon cycling. In particular, the photochemical reflectance index (PRI), a parameter that can be derived from remotely sensed spectral reflectance data, has recently received considerable attention for its ability to detect changes in photosynthetic efficiency of leaves, canopies, and entire ecosystems (Garbulsky *et al.* 2011).

The biological basis of PRI is its capacity to detect the spectral signature of pigments involved in the dissipation of excess light and hence, the efficiency of photosynthesis. To ensure optimum plant performance in ever-changing light environments, leaves constantly acclimate to balance the amount of light absorbed and their requirements for energy utilization (Ensminger *et al*. 2006). While it is advantageous to maximize absorption of light energy to fuel photosynthesis, the absorption of excess light that exceeds the capacity of photosynthesis can produce harmful reactive oxygen species (Barber and Andersson 1992, Hüner *et al.* 1998, Niyogi 2000). Plants use different strategies to maintain a balance between the energy they absorb and the energy utilized for photochemistry. One strategy is to regulate light absorption capacity by e.g. chloroplast relocation (Kodama *et al.* 2008). Another strategy is the regulation of light-use efficiency (LUE), i.e. the partitioning of absorbed light energy between photochemical and non-photochemical pathways (Demmig-Adams and Adams 2006a, Ensminger *et al.* 2006). Evergreen conifers retain most of their chlorophyll content throughout the year and adjust LUE by various mechanisms in response to environmental conditions and depending on the season. During summer, the harmless removal of excess light, referred to as non-photochemical quenching (NPQ), is mediated by xanthophyll cycle pigments. Excess light energy rapidly induces the de-epoxidation of xanthophyll cycle pigments, i.e. the conversion of violaxanthin into the energy quenching antheraxanthin and zeaxanthin (Niyogi *et al*. 2005, Demmig-Adams and Adams 2006a,

Verhoeven 2014). Changes in the de-epoxidation status of xanthophyll cycle pigments (DEPS) affect leaf spectral reflectance at 531 nm. This change in reflectance amplitude at 531 nm is used to derive PRI by comparing it to the xanthophyll-insensitive band at 570 nm (Gamon *et al*. 1992, 1997, Peñuelas *et al*. 1995). During winter, however, the xanthophyll cycle is arrested in a state primed for sustained energy quenching where zeaxanthin is retained, chlorophylls are partially degraded, photosystem (PS) II core units are reorganized (Ensminger *et al*. 2006, Demmig-Adams and Adams 2006a, Verhoeven 2014) and photoprotective pigments such as lutein and β-carotene are upregulated (Adams and Demmig-Adams, 1994, Ottander *et al*. 1995, Filella *et al*. 2009, Verhoeven 2014). These long-term, slowly reversible pigment adjustments are associated with this sustained mode of NPQ (Demmig-Adams and Adams, 2006).

Both short- and long-term pigment adjustments lead to changes in leaf spectral properties. These changes can be detected through leaf spectral reflectance measurements and have been used to measure PRI. In evergreen conifers PRI was reported to be a good proxy for xanthophyll cycle dynamics over the course of a day (Nakaji *et al*. 2006, Harris *et al*. 2014), although there are reports that PRI has limitations to reflect the diurnal variation of xanthophyll de-epoxidation under excessive light (Kováč *et al*. 2013). Recent studies have also reported good correlations between PRI and LUE over longer timescales, e.g. seasons (Garbulsky *et al*. 2011). It was suggested that PRI varies not only as a consequence of dynamic changes in xanthophyll pigments, but also as a result of long-term adjustments of pigment pools that allow plants to acclimate to changing environmental conditions throughout the year (Sims and Gamon 2002, Garrity *et al*. 2011, Wong and Gamon 2015a,b, Hmimina *et al.* 2015). Besides adjustments of pigment pools, it is also important to note that on the canopy scale changes in leaf area, foliage clumping and distribution of shadow fraction affect the PRI signal that is detected from canopy spectral measurements (Hilker *et al.* 2008, 2010). Long-term adjustments of chlorophyll and carotenoid pool sizes can be observed during spring in conifers, when photosynthesis recovers from winter stress (Ensminger *et al*. 2004, 2008). These adjustments were shown to be a considerable source of PRI variation during the spring transition (Busch *et al.* 2009, Wong and Gamon, 2015a,b, Porcar-Castell *et al*. 2012). Over the course of the year, Wong and Gamon (2015a) observed that PRI variation in lodgepole and ponderosa pine (*Pinus contorta* D. and *P. ponderosa*)

correlated better with the ratio of carotenoids per chlorophyll than xanthophyll cycle activity. In boreal Scots pine (*P. sylvestris* L.), Porcar-Castell *et al*. (2012) came to the same conclusion and reported that PRI was a good proxy for LUE during most of the year except during severe cold stress in early spring. Similarly, Busch *et al*. (2009) observed that PRI could not explain variations in the quantum yield of PSII of Jack pine (*P. banksiana* Lamb.) seedlings during spring, when excess energy was predominantly dissipated via sustained quenching. The inability of the PRI to accurately detect changes in LUE during the winter-spring transition reflects the reorganization of the chloroplast during spring, that involves replacement of sustained NPQ by the rapidly reversible, flexible energy dissipation via the xanthophyll cycle (Demmig-Adams and Adams 2006a, Zarter *et al.* 2006, Ensminger *et al*. 2008).

In addition to sustained quenching, several zeaxanthin-independent NPQ mechanisms and alternative electron sinks might contribute to a discrepancy in the PRI-LUE relationship in conifers throughout the year (Busch *et al*. 2009, Porcar-Castell *et al*. 2012), although there is no direct evidence yet. NPQ mechanisms might include PSII and PSI reaction centre quenching (Öquist and Hüner, 2003), quenching of singlet excited chlorophyll by carotenoid pigments (Trebst 2003, Tefler 2005, Jahns and Holzwarth 2012) and quenching via the lutein epoxide cycle (Matsubara *et al*. 2012). Alternative electron sinks can include plastid terminal oxidase (PTOX) mediated electron transport to oxygen (Savitch *et al*. 2010), or photorespiration (Takahashi & Badger, 2011). Cyclic electron transport around PSI can also contribute significantly to the removal of excess energy during winter and early spring (Ivanov *et al*. 2002). Recently it was suggested that the provision of ATP produced from cyclic electron transport maintains chloroplast integrity during chilling stress (Huang *et al*. 2010) and supports the recovery from chilling stress. Furthermore, it has been established that the stoichiometry of the two photosystems adjusts to balance electron transport under cold conditions (Ivanov *et al.* 2001, Ensminger *et al*. 2004). Because some of these processes have the potential to adjust LUE downstream of PSII, they will remain undetected by PRI. Assessing the contribution of zeaxanthin-independent mechanisms to NPQ during the spring recovery of photosynthesis can therefore reveal sources of the decoupling observed in the PRI-LUE relationship during that season (Busch *et al*. 2009, Porcar-Castell *et al*. 2012, Wong and Gamon 2015b).

In the boreal zone, the spring recovery of photosynthesis is largely driven by air temperature, which determines the physiological state of the chloroplast (Ensminger *et al.* 2004). This includes the excitation pressure on PSII and PSI, energy partitioning between the photosystems, and the requirement for excess energy dissipation. The phenology of these events, and in turn the PRI-LUE relationship, are likely to change as spring temperatures increase in the future (IPCC 2014). For instance, the effects of warmer spring conditions on the transition from sustained NPQ to energy dependent NPQ are uncertain, but will most likely affect the PRI-LUE relationship during that transitory period.

In the present study we followed the photosynthetic recovery of winter-acclimated Eastern white pine (*Pinus strobus* L.) seedlings exposed to cold or warm simulated spring conditions in controlled growth environments to (1) investigate the effect of spring temperature on the transition from the sustained quenching mode of NPQ to energy-dependent quenching in conifer needles (2) determine whether the spring timing of seasonal carotenoid and chlorophyll pool size adjustments, and thus of PRI recovery, are consistent with the recovery of LUE and (3) identify zeaxanthin-independent NPQ mechanisms that contribute to the decoupling of the PRI-LUE relationship during the winter-spring transition.

3.3 Materials and Methods

Plant material and growth conditions

Three-year-old Eastern white pine (*P. strobus* L.) seedlings were obtained in April 2011 and 2013 from a local nursery (Somerville Seedlings, Everett, Ontario, Canada), planted in a mixture of sand and sphagnum peat moss (1:3 v/v) and fertilized with 28:10:10 mineral fertilizer (Miracle-Gro, Scotts, Marysville, OH, USA). Seedlings were kept outside in an experimental garden at the University of Toronto Mississauga (Ontario, Canada) until transfer to environmental growth chambers (Biochambers, Winnipeg, Canada) during December. The seedlings were acclimated for 6 weeks to simulated winter conditions (2/-5˚C day/night; 8h photoperiod at 400 μmol quanta $m^{-2}s^{-1}$). Winter-acclimated seedlings (Wi) were then shifted for 36 days to either a cold spring (Sp_C) or warm spring (Sp_W) treatment. The temperature in Sp_C was set to 10/5˚C (day/night) and in Sp_W it was set to 15/10˚C (day/night) and photoperiod was 12 hours in both spring treatments (Table 1). Light

intensity was constantly monitored with a PAR sensor mounted at the top of the seedling canopy and maintained at an intensity of 1400 µmol quanta $m^{-2}s^{-1}$ (Table 1). Incident sunlight under fluctuating natural conditions may reach light intensities well above 1800 µmol quanta $m^{-2}s^{-1}$. However, preliminary experiments showed that a constant light intensity higher than 1500 µmol quanta $m^{-2}s^{-1}$ over the full course of the photoperiod caused severe photodamage in our seedlings and light intensity in our growth chambers was therefore set to values not exceeding 1400 µmol quanta $m^{-2}s^{-1}$. Wi seedlings were sampled and measured one day prior to transfer to spring conditions (day 0). Subsequent sampling and measurements of spring plants was done after transfer to spring conditions on days 1, 3, 6, 12, 18, 24 and 36 of the experiment. Measurements and samples of summer-acclimated needles were obtained from summer seedlings (Su) that had been kept outdoors in the experimental garden and were then acclimated for six weeks to simulated summer conditions (22/15˚C day/night; 14h photoperiod at 1400 µmol quanta $m^{-2}s^{-1}$ light intensity). All measurements and needle sampling were performed on previous year needles of the topmost portion of the leader shoot. All data were obtained from two independent experiments performed in 2012 and 2014 using identical settings and protocols. In order to further minimize chamber effects, we rotated seedlings between chambers every two weeks.

Table 3.1 Overview of growth conditions within the chambers during the spring simulation.

Exerimental treatment	Air temperature (°C; day/night)	Photoperiod (hour)	Light intensity (µmol m^{-2} s^{-1})
Wi, winter	2/-5	8	400
Sp_C, cold spring	10/5	12	1400
Sp_W, warm spring	15/10	12	1400
Su, summer	22/15	14	1400

Chlorophyll fluorescence measurements

At each time point, chlorophyll-fluorescence measurements were performed using a Dual-PAM-100 (Walz, Effeltrich, Germany). Measurements were done on bundles of 10-15 needles that were aligned in parallel to form a single layer of needles in the leaf clip holder of the Dual-PAM-100. A saturating light pulse (SP) was applied to dark-adapted (pre-dawn)

needles for determination of F_o and F_m (minimal and maximum fluorescence). Maximum quantum yield of PSII (F_v/F_m) was calculated according to Genty *et al*. (1989):

$$F_v/F_m = \left(\frac{F_m - F_o}{F_m}\right) \quad \text{Equation 3.1}$$

The needles were then exposed to a sequence of 2.5-min intervals with actinic light of increasing intensity (0-2000 μmol quanta $m^{-2}s^{-1}$), each step followed by a 400 ms saturating pulse of 10000 μmol quanta $m^{-2}s^{-1}$ for determination of F_m' (maximum fluorescence of light-adapted needles), and a weak pulse of far-red light for determination of F_o' (minimal fluorescence of light-adapted needles). Energy partitioning parameters were calculated according to Hendrickson *et al*. (2004). The effective quantum yield of PSII of light-adapted needles (Φ_{PSII}) reflects the proportion of light absorbed by PSII which is used for photochemistry and was calculated as:

$$\Phi_{PSII} = 1 - \frac{F_s}{F_{m'}} \quad \text{Equation 3.2}$$

where F_s is the yield of fluorescence of a light-adapted sample. The proportion of light that is absorbed by PSII antenna and quenched via dynamic NPQ (Φ_{NPQ}) was calculated as:

$$\Phi_{NPQ} = \frac{F_s}{F_{m'}} - \frac{F_s}{F_m} \quad \text{Equation 3.3}$$

The sum of fluorescence and sustained NPQ ($\Phi_{f,D}$) was calculated as:

$$\Phi_{f,D} = \frac{F_s}{F_m} \quad \text{Equation 3.4}$$

The electron transport rate of PSII (ETR_{II}, in μmol electron $m^{-2}s^{-1}$) was calculated according to Genty *et al*. (1989):

$$ETR_{II} = \Phi_{PSII} \cdot PPFD \cdot \alpha \cdot d_{II} \quad \text{Equation 3.5}$$

where PPFD is the applied light intensity (μmol quanta $m^{-2}s^{-1}$), α is the absorptance, i.e. the fraction of incident light absorbed by leaves, and d_{II} the fraction of light directed to PSII. Values of α were calculated as α = 1 – transmittance – reflectance. Given the thickness of pine needles, transmittance was assumed to be 0. However, it should be noted that a small proportion of light can be transmitted through conifer needles (Lukeš *et al*. 2013).

Reflectance was measured with a Unispec-SC spectrometer over the 400-700 nm wavelengths range (Huang *et al*. 2012). Values of d_{II} were calculated using the ratio of Φ_{II}:Φ_I (see below) at low light intensity (60 μmol quanta $m^{-2}s^{-1}$), where CET is assumed to be absent and $ETR_{II}=ETR_I$ (Huang *et al*. 2012).

The excitation pressure of PSII (1-qP) was calculated as:

$$1 - qP = 1 - \frac{F_m' - F_s}{F_m' - F_o} \qquad \text{Equation 3.6}$$

To assess energy partitioning characteristics at a diurnal timescale, light response curves were measured on day 0 as well as on day 12 of the experiment. A dark-adapted bundle of needles was exposed to 10-min. steps of increasing actinic light intensity (0-2000 μmol quanta $m^{-2}s^{-1}$). At each light step, Φ_{PSII}, Φ_{NPQ} and $\Phi_{f,D}$ were recorded.

PSI absorbance measurements

Absorbance changes of the reaction centre chlorophyll of PSI (P700) were assessed simultaneously with chlorophyll fluorescence measurements using a Dual-PAM-100. The P700 signal (*P*) was calculated as the difference of the 875 nm and 830 nm transmittance signals. Firstly, P700 oxidation was transiently induced by applying a saturating pulse after far-red pre-illumination of dark-adapted needles. Briefly after the SP, the minimal P700 signal was measured to capture a state of full P700 reduction. The difference between the fully reduced and fully oxidized states is denoted P_m. Secondly, actinic illumination was applied with the same actinic light intensities and SPs used for fluorescence. Upon application of each maximum change of the P700 signal (P_m') was determined. Each saturating pulse was followed by a 1s dark interval for full reduction of P700 and determination of the minimal P700 signal (P_o).

The three types of quantum yields of energy conversion in PSI were assessed according to Klughammer and Schreiber (1994) and calculated according to Pfündel *et al.* (2008). The effective quantum yield of PSI (Φ_{PSI}) in the light was calculated as:

$$\Phi_{PSI} = \frac{P_m' - P}{P_m} \qquad \text{Equation 3.7}$$

The fraction of overall P700 that is oxidized due to a lack of electron donors (donor side limitation; Φ_{ND}), was calculated as:

$$\Phi_{ND} = \frac{P - P_o}{P_m} \quad \text{Equation 3.8}$$

The fraction of overall P700 that cannot be oxidized by a saturation pulse due to a lack of electron acceptors (acceptor side limitation, Φ_{NA}), was calculated as:

$$\Phi_{NA} = \frac{P_m - P_m'}{P_m} \quad \text{Equation 3.9}$$

Analogous to ETR_{II}, the electron transport rate of PSI (ETR_I, in μmol electron $m^{-2}s^{-1}$) was calculated as:

$$ETR_I = \Phi_{PSI} \cdot PPFD \cdot \alpha \cdot d_I \quad \text{Equation 3.10}$$

where d_I was calculated as $d_I = 1 - d_{II}$ (Huang *et al.* 2012). Cyclic electron transport (CET, in μmol electron $m^{-2}s^{-1}$) was calculated according to Huang *et al.* (2012) as:

$$CET = ETR_I - ETR_{II} \quad \text{Equation 3.11}$$

Photosynthetic gas exchange measurements

To assess variations in photosynthetic activity at a seasonal timescale, photosynthetic gas exchange was measured at each time point (GFS-3000, Walz, Effeltrich, Germany). Measurements started 2 hours after the lights were turned on inside the growth chambers. A bundle of attached needles was oriented to form a flat plane and inserted in the leaf cuvette. CO_2 concentration in the cuvette was set to 400 ppm, temperature was set to growth temperature (Table 1) and humidity was set 60% RH. Net CO_2 assimilation (*A*, in μmol CO_2 $m^{-2}s^{-1}$) was measured at growth light intensity (1400 μmol quanta $m^{-2}s^{-1}$) once steady-state assimilation was achieved. Immediately after the measurements, needles were detached from the seedling and measured for surface area using the WinSEEDLE software package (Regent Instruments Inc., Québec, Canada). The light-use efficiency of CO_2 assimilation (LUE_A, in mol CO_2 mol $quanta^{-1}$) was calculated as:

$$LUE_A = \frac{\text{Assimilation}}{\text{PPFD}}$$ Equation 3.12

To assess variations in photosynthetic activity at a diurnal timescale, light response curves were measured on days 0 and 12 in both treatments. A fully dark-adapted bundle of needles was exposed to a sequence of eight 10-min. light steps of increasing actinic light intensity (0-2000 μmol quanta $m^{-2}s^{-1}$). Measurement and cuvette conditions were identical to those used for assessing variation of photosynthetic activity at a seasonal timescale (see above). At each light step, *A* was measured and LUE_A was calculated.

Spectral reflectance measurements

Seasonal variations in PRI were assessed from leaf spectral reflectance measurements using a Unispec-SC spectrometer (UNI007, PP Systems, Haverhill, MA, USA) equipped with an internal tungsten halogen light source. The spectrometer was connected to a bifurcated fiberoptic (UNI400) and a leaf clip (UNI500) maintaining the fiberoptic on the needle surface at a fixed angle of 60° relative to needle axis (2 mm diameter spot size). Leaf bidirectional reflectance was computed by dividing reflected irradiance by the radiance obtained from a white reflectance standard (Spectralon, Labsphere, North Sutton, NH, USA) taken immediately before each leaf measurement. Dark current instrument noise was subtracted from white standard and leaf radiance measurements. Reflectance was measured on needles of the topmost part of the leader shoot. Needles were in bundles of approximately 10-15 needles arranged in parallel to form a single layer flat plane. The integration time was set to 10 ms and 40 scans were averaged for each measurement followed by interpolation of the ~3.3 nm resolution output of the spectrometer to 1 nm bandwidths using the software Multispec v. 5.1.0 (Purdue University, Indiana, USA). Finally, PRI was calculated according to Peñuelas *et al*. (1995):

$$PRI = \frac{R_{531} - R_{570}}{R_{531} + R_{570}}$$ Equation 3.13

where R_{531} and R_{570} represent leaf reflectance at 531 and 570 nm, respectively. In order to compare seasonal PRI variation, we used pre-dawn PRI measurements to separate the effects of long-term and short-term pigment variations on PRI (Gamon and Berry, 2012).

To assess the effect of short-term xanthophyll pigment variations on PRI and infer the magnitude of diurnal PRI variation light response curves were measured on days 0 and 12. A bundle of needles was set up in the leaf clip and exposed to eight 10-min. light steps of increasing actinic light intensity (0-2000 µmol quanta $m^{-2}s^{-1}$) using the Unispec-SC internal light source. 3 scans were averaged at each light step. To assess the range of diurnal PRI variation, we calculated ΔPRI as the difference between PRI of dark-adapted needles and PRI measured at 2000 µmol quanta $m^{-2}s^{-1}$ (Gamon and Berry, 2012).

Pigment analysis

Needle samples for pigment analysis were collected after at least 2 hours of exposure to growth light. The samples were immediately frozen in liquid nitrogen and stored at -80°C. The needles were then ground to a fine powder in liquid nitrogen. Pigments were extracted in dim light conditions in 98% methanol buffered with 2% 0.5M ammonium acetate for 2 hours. The extracts were filtered through a 0.45 µm PTFE filter prior to high-performance liquid chromatography (HPLC) analysis. HPLC analysis was performed with an Agilent 1260 system (Agilent Technologies, Santa Clara, CA, USA) with a quaternary pump, autosampler set to 4 °C, column oven set to 25°C and photodiode array detector. Pigments were detected at 450 nm and 656 nm wavelengths and separated using a reverse-phase C_{30}-column (5 µm, 250*4.6 mm; YMC Co. Ltd., Kyoto, Japan) protected by a 20*4.6 mm guard column. Three solvents, i.e. A: 100% methanol, B: 100% methyl-tert-butyl-ether and C: water buffered with 0.2% ammonium acetate, were used to run a gradient starting with 92% A, 5% B and 3% C. During each run solvent A was gradually replaced by solvent B to a minimum of 5% B. Every run was followed by a 5 min reconditioning phase with initial solvent concentrations. For calibration and peak detection, commercially available standards were obtained from Sigma Aldrich (St. Louis, MO, USA) and DHI Lab products (Hørsholm, Denmark). Peak detection and pigment quantification was performed using ChemStation software (Agilent Technologies, Santa Clara, CA, USA).

Total chlorophylls (Chl) were determined as the sum of chlorophyll a and b concentration on a fresh weight basis (µmol g^{-1}), as the water content of *P. strobus* needles varies less than 10% year-round (Verhoeven *et al.* 2009). The ratio of Chl a/b was expressed in mol mol^{-1}

and the concentration of carotenoid pigments was normalized to chlorophyll levels and was expressed in mmol carotenoids mol Chl^{-1}. Total carotenoids (Car) were expressed (in mmol mol Chl^{-1}) as the sum of violaxanthin, antheraxanthin, zeaxanthin, neoxanthin, lutein, α-carotene and β-carotene concentrations. Total xanthophyll cycle pigments (VAZ) were calculated as the sum of violaxanthin, antheraxanthin and zeaxanthin. DEPS (in mol mol Chl^{-1}) was expressed as:

$$\mathrm{DEPS} = \frac{0.5\mathrm{A}+\mathrm{Z}}{\mathrm{V}+\mathrm{A}+\mathrm{Z}} \qquad \text{Equation 3.14}$$

Statistical analyses

The effects of treatments on individual parameters at each time point were estimated using mixed model analysis of variance (ANOVA). For all statistical analyses the data from two experiments ran on two different years were pooled together. Year was included as a random effect in the mixed model to account for the two replicate experiments. The analysis was performed using the difflsmeans function in the lmerTest package, using R version 3.1.1 (R Core team, 2014).

In order to evaluate the strength of the relationship between PRI and physiological parameters, we obtained R^2 values from linear regressions with log-transformed variables and considered the slope significantly different from zero when $p<0.05$. Regressions were performed using GraphPad Prism 6 software version 6.05 (GraphPad Software, Inc., La Jolla, CA, USA).

3.4 Results

Seasonal variation in energy partitioning of PSII and PSI

Winter-acclimated seedlings (Wi) were assessed on day 0 of the experiment and then transferred to simulated spring growth conditions. Following transfer to spring conditions, a clear response of energy partitioning to longer photoperiod and warmer temperature was observed. In both spring treatments, the recovery of photosynthesis reached a steady state by day 12 of the experiment (Fig. 3.1A). By that time the effective quantum yield of PSII

(Φ_{PSII}) was approximately twice as high in the warm spring treatment (Sp_W) as in the cold spring treatment (Sp_C). After photosynthetic recovery, 60% of absorbed energy in Sp_C was quenched via dynamic NPQ (Φ_{NPQ}) and 40% via fluorescence and sustained NPQ ($\Phi_{f,D}$; Fig. 3.1B,C). In Sp_W, however, the majority (75%) of NPQ was facilitated by Φ_{NPQ} (Fig. 3.1B). In Wi seedlings, more than 90% of all light energy absorbed was dissipated via $\Phi_{f,D}$, but after 18 days of exposure to spring conditions this value had declined to approximately 40% in Sp_C and 20% in Sp_W (Fig. 3.1C).

In addition to measurements of energy partitioning in PSII, we assessed energy conversion in PSI (Fig. 3.1D,E,F). Upon transfer to spring conditions, the effective quantum yield of PSI (Φ_{PSI}) quickly recovered, with a faster rate in Sp_W compared to Sp_C (Fig. 3.1D). However, by day 18 of the experiment Φ_{PSI} was higher in Sp_C and remained so until the end of the experiment. During that period, quantum yield in Sp_C was 5 times higher in PSI compared to PSII. In contrast, in Sp_W seedlings quantum yield of PSI was only 1.5 times higher than in PSII (Fig. 3.1A,D). In both spring treatments, the fraction of overall P700 oxidized due to a lack of electron donors (Φ_{ND}) transiently increased on the first day of the experiment, and then gradually declined in the following days (Fig. 3.1E). Φ_{ND} stabilized to a steady state by day 18 of the experiment to values significantly higher in Sp_C than in Sp_W. In both treatments, the fraction of overall P700 that cannot be oxidized by a saturation pulse due to a lack of electron acceptors (Φ_{NA}) dropped on the first day of exposure to spring conditions (Fig. 3.1F). In Sp_C, Φ_{NA} continued to decrease until the end of the experiment. In contrast, Φ_{NA} in Sp_W increased after day 1, until it reached a plateau by day 12 and then remained significantly higher than in Sp_C until the end of the experiment.

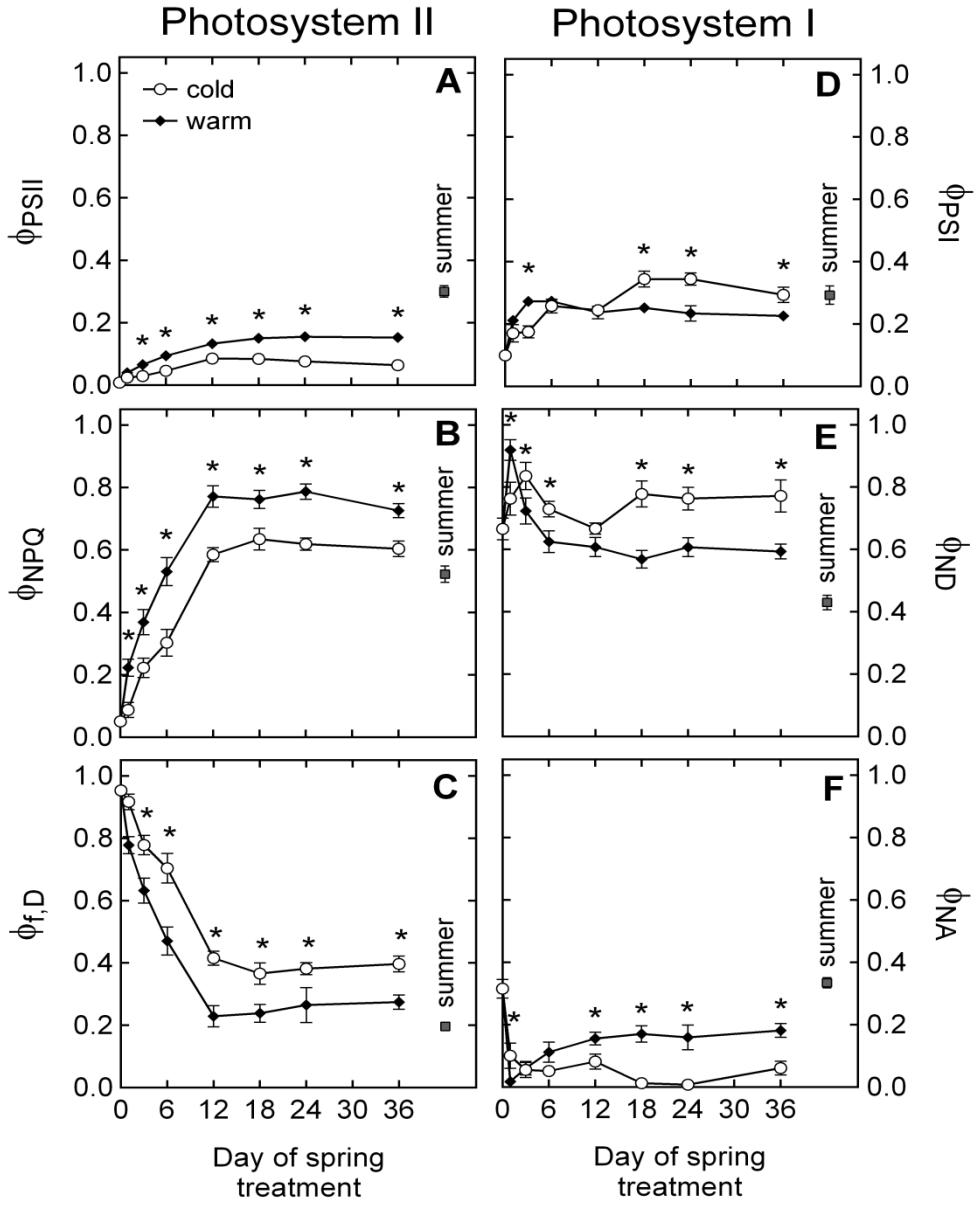

Figure 3.1 Time course of energy partitioning characteristics of *P. strobus* needles exposed to cold and warm spring treatments. A) Φ_{PSII}, fraction of absorbed light at PSII used for photochemistry; B) Φ_{NPQ}, fraction of absorbed light at PSII quenched via dynamic NPQ; C) $\Phi_{f,D}$, sum of fluorescence and sustained NPQ; D) Φ_{PSI}, effective quantum yield of PSI; E) Φ_{ND}, fraction of P700 oxidized due to a lack of electron donors and F) Φ_{NA}, fraction of P700 that cannot be oxidized by a saturation pulse due to a lack of electron acceptors. Measurements taken at 1400 µmol quanta $m^{-2}s^{-1}$ light intensity. Each data point represents n=10-11 seedlings ±SE and asterisks indicate significant differences ($\alpha<0.05$) between treatments at a given time point.

Acclimation to Wi conditions resulted in high d_I values (0.88 ± 0.02) compared to d_{II} (0.12 ± 0.02). Exposure to both spring treatments resulted in a gradual increase in d_{II} and decline in d_I as the experiment progressed, with generally higher d_I values in Sp_C than in Sp_W (Table 2). Throughout the experiment, the electron transport rate of PSI (ETR_I) was higher than the electron transport rate of PSII (ETR_{II}) in both spring treatments (Fig. 3.2A,B). The highest ETR_I values were observed in Sp_C between days 12 and 24 of the experiment. Cyclic electron transport (CET) was significantly higher in Sp_C than in Sp_W from day 12 of the experiment, with CET approximately 300% higher in Sp_C than in Sp_W during the second half of the experiment (Fig. 3.2C).

Table 3.2 Fraction of light absorbed by PSII and PSI (d_{II} and d_I) and absorptance (α) of *P. strobus* needles exposed to winter, cold spring, warm spring and summer treatments. N=11 seedlings ± SE.

Day	d_{II}	d_I	α
winter	0.12 ± 0.02	0.88 ± 0.02	0.87 ± 0.01
cold spring			
1	0.12 ± 0.01	0.88 ± 0.01	0.86 ± 0.01
3	0.19 ± 0.03	0.81 ± 0.03	0.88 ± 0.01
6	0.15 ± 0.02	0.85 ± 0.02	0.88 ± 0.01
12	0.25 ± 0.02	0.74 ± 0.02	0.87 ± 0.01
18	0.20 ± 0.02	0.80 ± 0.02	0.88 ± 0.01
24	0.18 ± 0.02	0.82 ± 0.02	0.87 ± 0.01
36	0.22 ± 0.02	0.78 ± 0.02	0.86 ± 0.01
warm spring			
1	0.13 ± 0.02	0.87 ± 0.02	0.88 ± 0.01
3	0.19 ± 0.02	0.81 ± 0.02	0.89 ± 0.01
6	0.27 ± 0.03	0.73 ± 0.03	0.87 ± 0.01
12	0.34 ± 0.03	0.66 ± 0.03	0.88 ± 0.004
18	0.37 ± 0.03	0.63 ± 0.03	0.87 ± 0.004
24	0.44 ± 0.03	0.56 ± 0.03	0.87 ± 0.01
36	0.44 ± 0.02	0.55 ± 0.02	0.86 ± 0.01
summer	0.53 ± 0.01	0.47 ± 0.01	0.85 ± 0.01

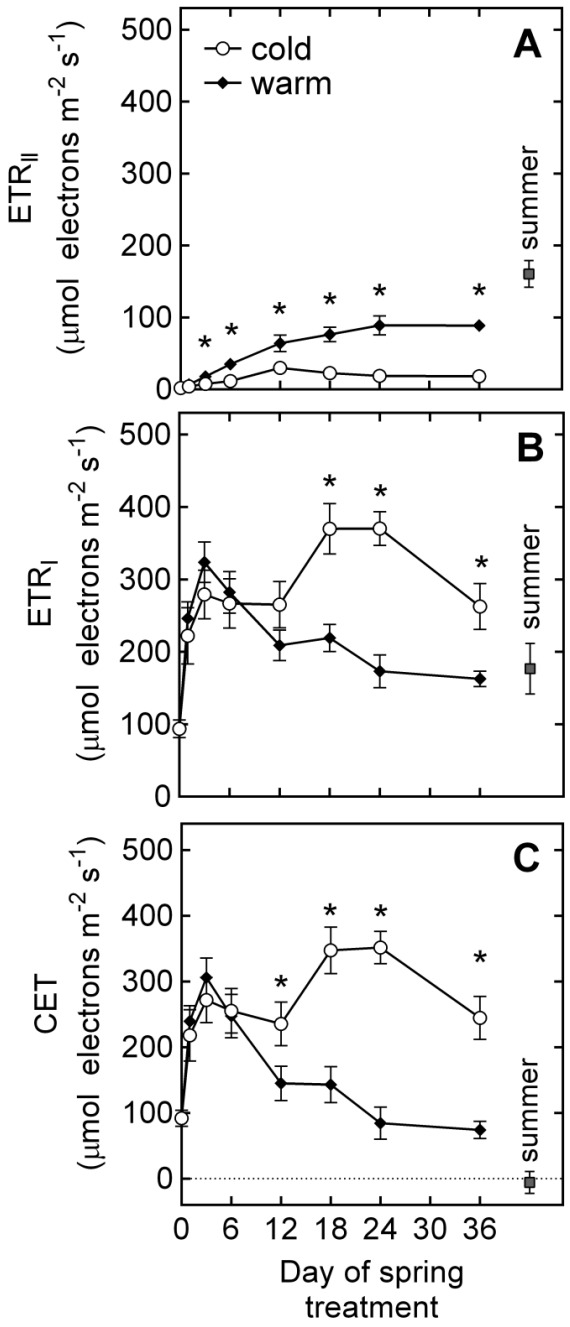

Figure 3.2 Time course of A) electron transport rate of PSII; B) electron transport rate of PSI and C) cyclic electron transport rate of *P. strobus* needles exposed to cold and warm spring treatments. Measurements taken at 1400 μmol quanta $m^{-2}s^{-1}$ light intensity. Each data point represents n=10-11 seedlings ±SE and asterisks indicate significant differences ($\alpha<0.05$) between treatments at a given time point.

Photosynthetic recovery and seasonal changes in PRI

Consistent with the pattern observed in energy partitioning (Fig 3.1), we observed a recovery of photosynthetic activity over the 36 days of our experiment (Fig. 3.3). By the end of the experiment the maximum quantum yield of PSII (F_v/F_m) had recovered from a value of 0.13 in Wi seedlings (day 0) to values of 0.46 in Sp_C and 0.70 in Sp_W (Fig. 3.3A). From day 3, F_v/F_m was significantly higher in Sp_W than in Sp_C. In both treatments, the excitation pressure of PSII (1-qP) declined from day 1 of the experiment until day 18, but then recovered considerably until day 36 of the experiment (Fig. 3.3B). Values of 1-qP were significantly higher in Sp_C during most of the experiment. In both treatments, the light-use efficiency of CO_2 assimilation (LUE_A) recovered quickly during the first 12 days of spring treatment, with a faster rate of recovery in Sp_W than in Sp_C (Fig. 3.3C). LUE_A was consistently higher in Sp_W compared to Sp_C (Fig. 3.3C). Under winter conditions, we recorded a PRI value of -0.168. In Sp_C, PRI slightly declined until day 6 of the experiment and then increased again by day 12 and remained at winter-like values until the end of the experiment (Fig. 3.3D). In Sp_W, PRI was also relatively stable for the first 12 days of the experiment, with most of its recovery occurring between days 12 and 24 of the experiment, and final values of approximately -0.05. After day 24, PRI was significantly higher in Sp_W than in Sp_C.

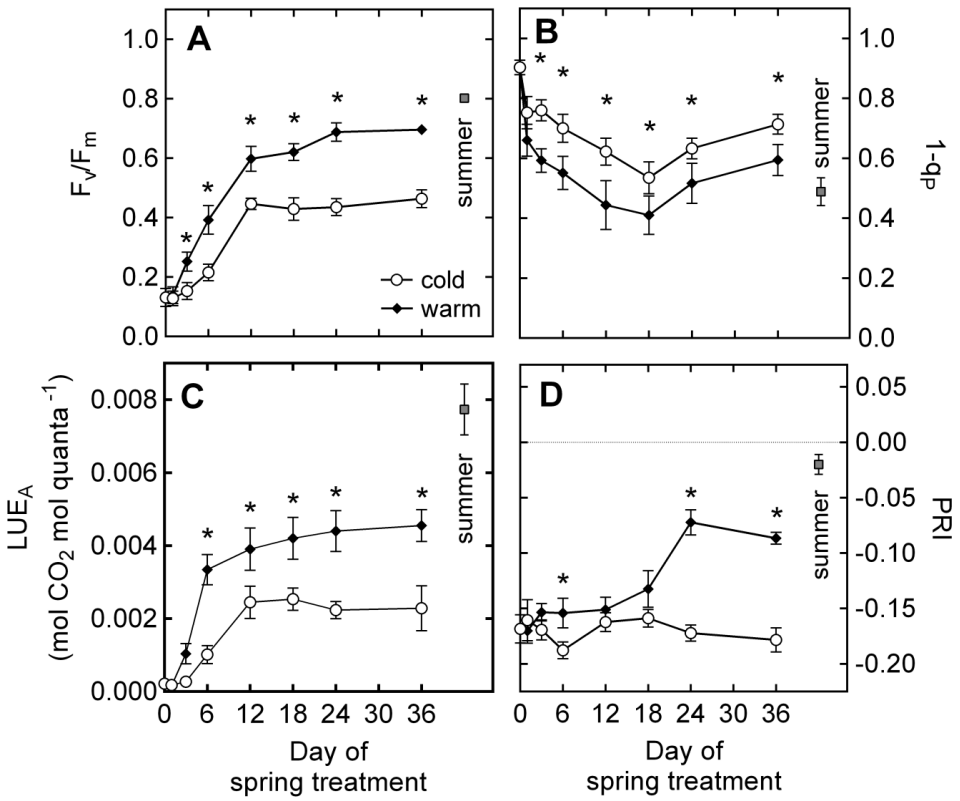

Figure 3.3 Time course of photosynthetic recovery in *P. strobus* exposed to cold and warm spring treatments. A) F_v/F_m, maximum quantum yield of PSII; B) 1-qP, excitation pressure of PSII; C) LUE_A, light-use efficiency of CO_2 assimilation and D) PRI. F_v/F_m and PRI were measured on dark-acclimated needles and 1-qP and LUE_A were measured at 1400 μmol quanta $m^{-2}s^{-1}$ light intensity. Each data point represents n=10-11 seedlings ±SE and asterisks indicate significant differences ($\alpha<0.05$) between treatments at a given time point.

Seasonal changes in foliar pigment content

Transfer of seedlings from winter to spring conditions resulted in a clear response of photosynthetic pigment composition in both treatments (Fig. 3.4). Chlorophyll (Chl) FW^{-1} remained stable until day 12 of the experiment, but recovered to summer levels after day 18 (Fig. 3.4A). By the end of the experiment, the pool of Chl had increased by 30% in Sp_C and by 53% in Sp_W. In both treatments, Chl a/b increased over the course of the experiment and as of day 12 we observed higher Chl a/b in Sp_W than in Sp_C (Fig. 3.4B). In contrast, carotenoid (Car) Chl^{-1} peaked in Sp_C on day 18 of the experiment, and remained significantly higher in Sp_C than in Sp_W until day 36 (Fig. 3.4C). Xanthophyll cycle pigments (VAZ) Chl^{-1} remained fairly stable over the course of the experiment in Sp_C but declined in

Sp_W seedlings after day 3 (Fig. 3.4D). The amount of zeaxanthin Chl^{-1} decreased over the first 6 days of the experiment in both treatments, increased again until day 24 in Sp_C, and was significantly higher in Sp_C than in Sp_W for most of the experiment (Fig. 3.4E). By day 36, zeaxanthin had decreased by 44% in Sp_C, and by 66% in Sp_W compared to Wi seedlings on day 0. A similar trend was observed for the de-epoxidation status of the xanthophyll cycle (DEPS; Fig. 3.4F), which was higher in Sp_C compared to Sp_W throughout most of the experiment. For instance, by day 36 DEPS was 0.75 and 0.61 mol mol Chl^{-1} in Sp_C and Sp_W, respectively. In both treatments, the amount of β-carotene Chl^{-1} also declined throughout the experiment. Most of the β-carotene Chl^{-1} was lost after day 24 of the experiment, with 21% of the winter β-carotene pool lost in Sp_C, and 38% lost in Sp_W (Fig. 3.4G). At any time during the experiment, the amount of β-carotene did not significantly differ between treatments. Lutein Chl^{-1} in Sp_C initially declined on the first days of the experiment, and then increased until day 18, before it decreased again until the end of the experiment. In Sp_W, lutein Chl^{-1} decreased consistently throughout the experiment (Fig. 3.4H). From day 18, significantly higher levels of lutein were observed in Sp_C compared to Sp_W.

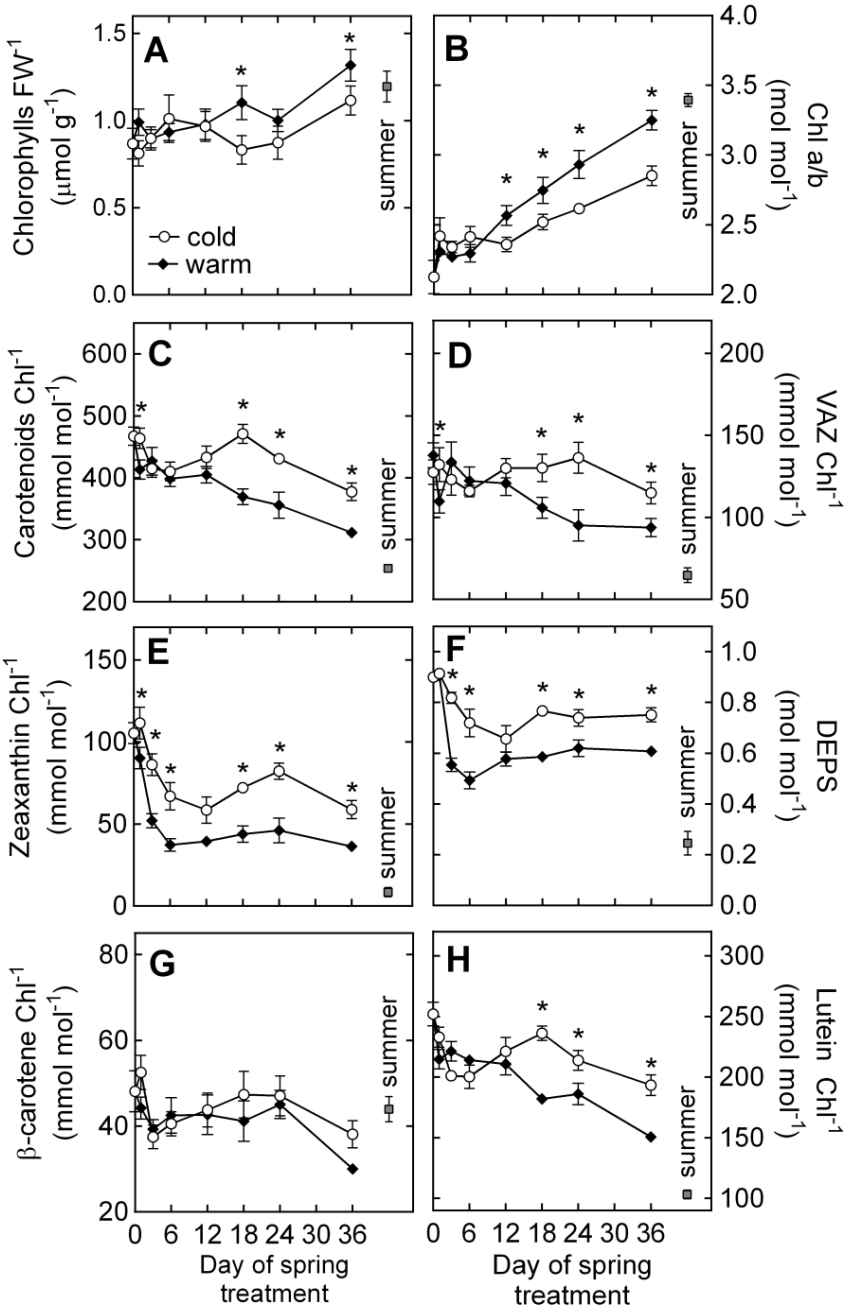

Figure 3.4 Time course of photosynthetic pigment dynamics in *P. strobus* needles exposed to cold and warm spring treatments. A) Chl FW^{-1}; B) ratio of Chl a to Chl b; C) Car Chl^{-1} D) VAZ Chl^{-1}; E) zeaxanthin Chl^{-1}; F) DEPS G) β-carotene Chl^{-1} and H) lutein Chl^{-1}. Each data point represents n=10-11 seedlings ±SE and asterisks indicate significant differences ($\alpha<0.05$) between treatments at a given time point.

Variation in the relationships between PRI and physiological parameters during the winter-spring transition

The relationship between PRI and energy partitioning varied depending on exposure time to the treatments (Fig. 3.5). For all energy partitioning parameters, we observed no relationship with PRI during days 0-3 of the experiment, but significant relationships for days 6-36 and/or the entire experiment (Fig. 3.5). Similar trends were observed for DEPS, where samples from days 0-3 were clearly separated from samples taken between days 6-36 (Fig. 3.6E,F). In contrast, relationships between PRI and Chl FW^{-1} or Car Chl^{-1} were significant for all time periods (Fig. 3.6A-D).

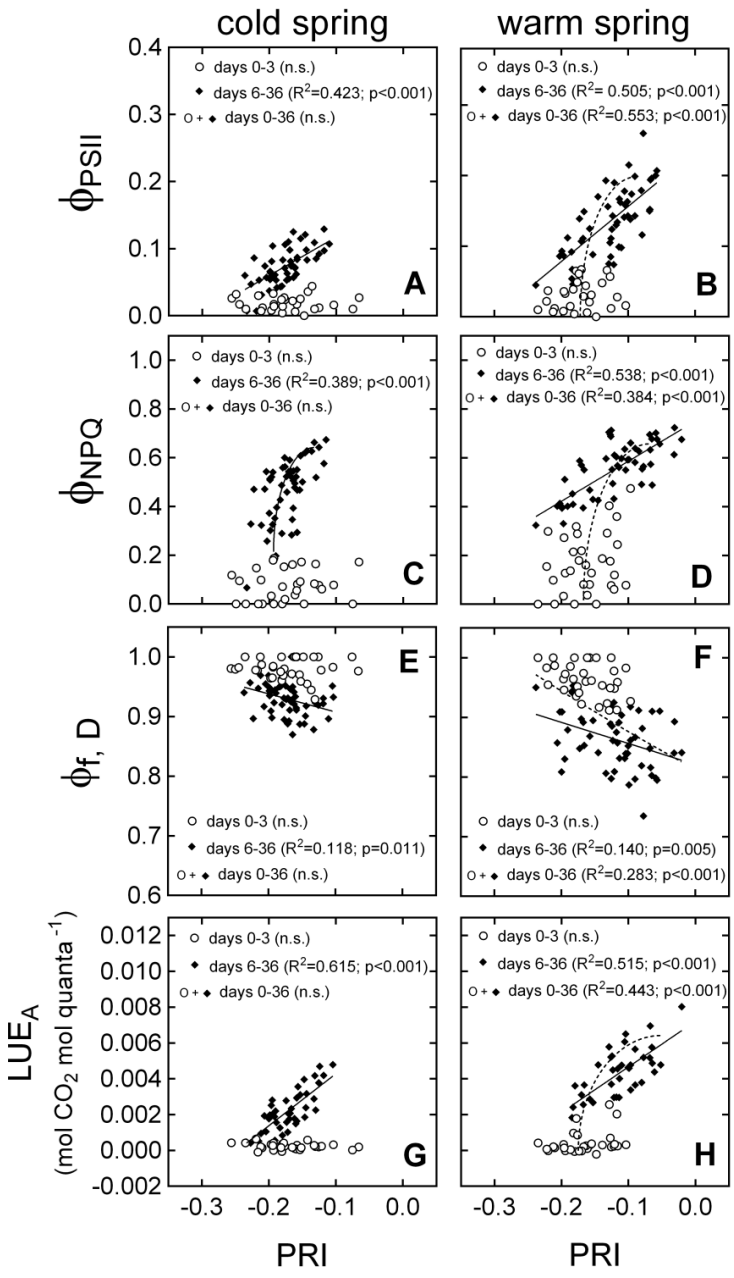

Figure 3.5 Relationship between PRI and A-B) Φ_{PSII}, fraction of absorbed light used for photochemistry; C-D) Φ_{NPQ}, fraction of absorbed light quenched via dynamic NPQ; E-F) $\Phi_{f, D}$, sum of fluorescence and constitutive thermal dissipation; G-H) LUE_A, light-use efficiency of CO_2 assimilation during the photosynthetic recovery of *P. strobus* exposed to cold and warm spring treatments. R^2 values indicate goodness of fit for linear, logarithmic or exponential relationships during days 0-3 of the experiment (circles), days 6-36 (diamonds, full line) or the entire experiment (circles and diamonds, dashed line). The left and right panels present data from the cold and warm treatments, respectively.

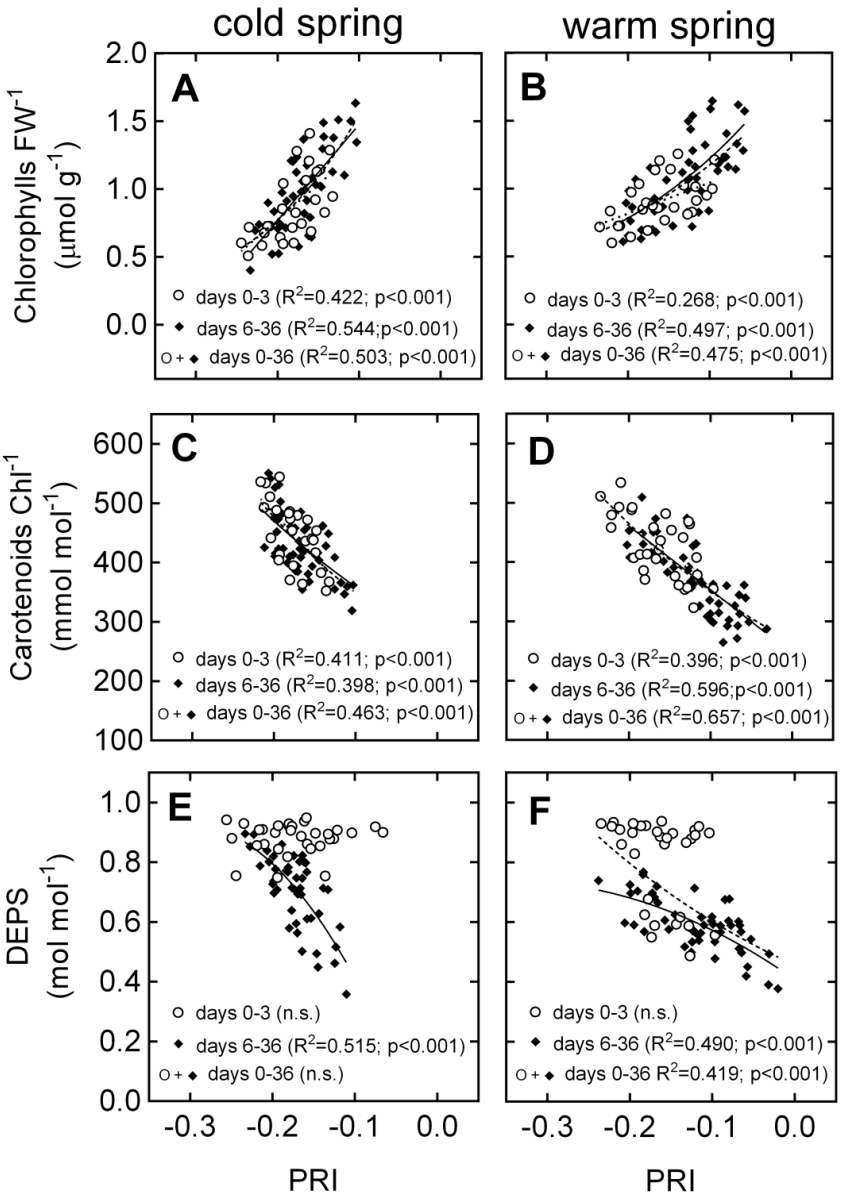

Figure 3.6 Relationship between PRI and A-B) Chl FW^{-1}; C-D) Car Chl^{-1} and E-F) DEPS during the photosynthetic recovery of *P. strobus* exposed to cold and warm spring treatments. R^2 values indicate goodness of fit for exponential or linear relationships for days 0-3 of the experiment (circles, dotted line), days 6-36 (diamonds, full line) or the entire experiment (circles and diamonds, dashed line). The left and right panels present data from the cold and warm treatments, respectively.

Response of photosynthesis to short term variations in light intensity of seedlings acclimated to winter, spring or summer conditions

After 12 days of acclimation to simulated spring conditions, the seedlings exhibited different responses to increasing light intensity compared to winter conditions (Fig. 3.7). Assimilation increased from almost 0 μmol CO_2 $m^{-2}s^{-1}$ in Wi seedlings to approximately 3 μmol CO_2 $m^{-2}s^{-1}$ in Sp_C and 7 μmol CO_2 $m^{-2}s^{-1}$ in Sp_W at 2000 μmol quanta $m^{-2}s^{-1}$ light intensity (Fig. 3.7A). Assimilation in Sp_C and Sp_W had recovered 31% and 76% of the capacity observed in Su at 2000 μmol quanta $m^{-2}s^{-1}$ light intensity. The higher maximum rate of assimilation in spring seedlings was accompanied by lower light compensation points compared to Wi (122.7± 42.9 μmol quanta $m^{-2}s^{-1}$), with 80.7±23.1 μmol quanta $m^{-2}s^{-1}$ in Sp_C and 14.2± 8.6 μmol quanta $m^{-2}s^{-1}$ in Sp_W. Compared to winter, LUE_A was slightly higher in Sp_C, while LUE_A in Sp_W was only slightly lower than Su values (Fig. 3.7B). Assessing changes in energy partitioning via chlorophyll-fluorescence revealed a different pattern. The short term light response of Φ_{PSII} in Sp_W was very close to Su values, but we observed considerably higher Φ_{NPQ} and lower $\Phi_{f,D}$ values over the full range of light intensities in Sp_W (Fig. 3.7C,D,E). In contrast, Sp_C seedlings showed Φ_{NPQ} values similar to Wi, but considerably higher Φ_{PSII} and lower $\Phi_{f,D}$. PRI was still very close to winter values in both spring treatments, which had recovered approximately 18% of their Su values (Fig. 3.7F). The range of diurnal PRI variation differed between treatments, with a ΔPRI of -0.033 in Su, a ΔPRI of -0.0076 in Sp_C, a ΔPRI of -0.022 in Sp_W, and a ΔPRI of -0.0032 in Wi.

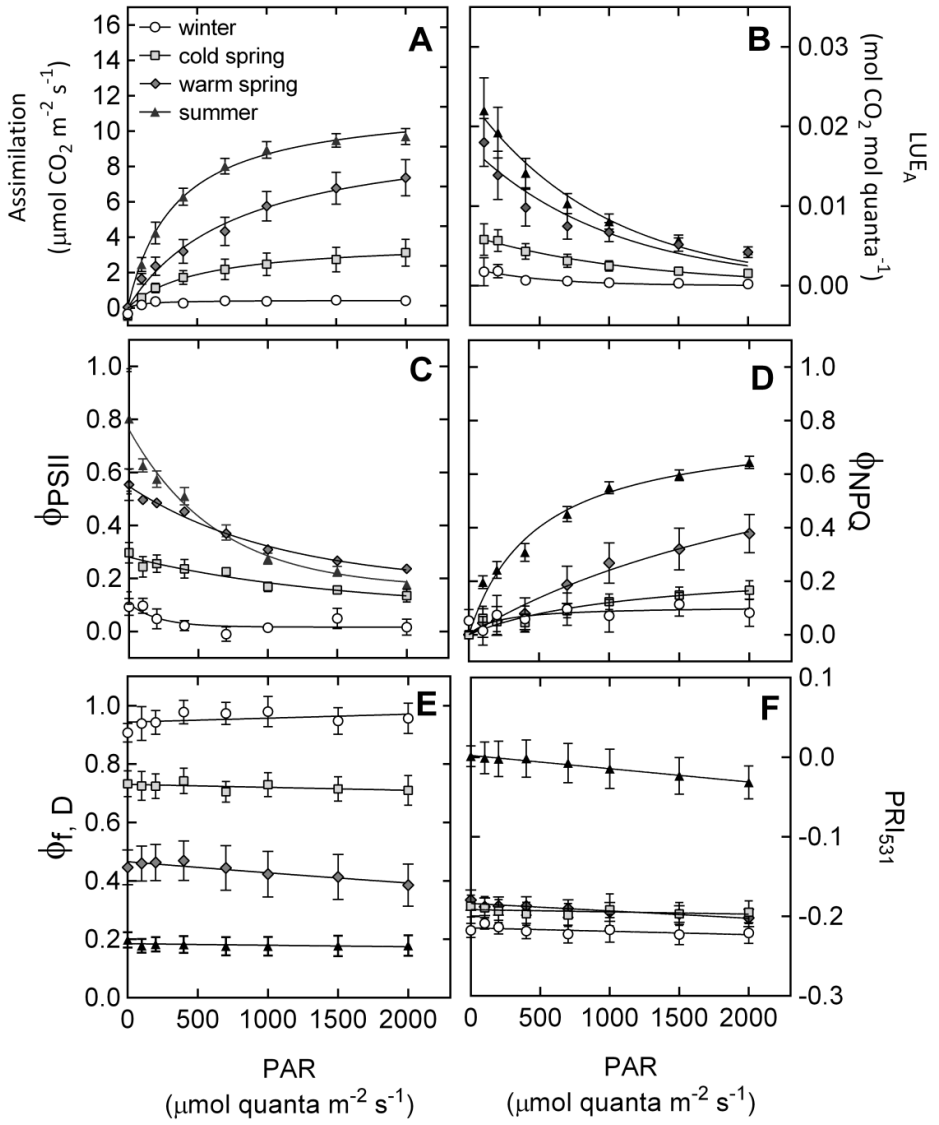

Figure 3.7 The response to light of *P. strobus* needles acclimated to winter, cold spring, warm spring or summer conditions for (A) photosynthetic CO_2 assimilation; (B) LUE_A, light-use efficiency of CO_2 assimilation; (C) Φ_{PSII}, fraction of absorbed light used for photochemistry, (D) Φ_{NPQ}, fraction of light quenched via dynamic NPQ; (E) $\Phi_{f,D}$, sum of fluorescence and sustained NPQ; and (F) PRI. Each data point represents n=6–8 seedlings ±SE.

3.5 Discussion

Conifers undergo a reorganisation of components of the chloroplast during winter stress

Winter conditions simulated in our experiment induced complete downregulation of photosynthesis in pine seedlings (Fig. 3.3C), including a 30% reduction of the chlorophyll that was present in summer-acclimated needles (Fig. 3.4A). Light absorption by chlorophylls remaining in the winter-acclimated needles resulted in high excitation pressure of PSII, as indicated by 1-qP values close to 1 (Fig. 3.3B). Low F_v/F_m values observed under winter conditions indicated that the chlorophyll pigments were retained in a quenched, photoprotected state (Ottander *et al*. 1995, Ensminger *et al*. 2004). Under winter conditions approximately 90% of all energy absorbed by pine needles was dissipated thermally via sustained NPQ (Fig. 3.1C) as reported in winter-acclimated *P. strobus* trees (Verhoeven 2013). This sustained capacity for NPQ was facilitated by xanthophyll cycle pigments maintained in a highly de-epoxidized state compared to the summer seedlings (Fig. 3.4D,F). Accumulation of xanthophylls was also accompanied by larger amounts of lutein and β-carotene, reflecting an increased capacity for triplet Chl quenching (Fig. 3.4G,H) that has been observed in several other overwintering conifer species (Adams and Demmig-Adams 1994, Ottander *et al*. 1995, Sveshnikov *et al.* 2006). This winter state concurred with highly negative PRI values of approximately -0.2 (Fig. 3.3D), which is comparable to PRI values reported in winter downregulated pine species (Wong and Gamon, 2015a,b).

Although the functionality of both photosystems was impaired under winter conditions, PSI was less affected than PSII (Table 2; Fig. 3.1, 3.2). While PSII electron transport was suppressed almost completely (Fig. 3.2A), approximately 50% of the capacity observed in summer needles was preserved in PSI (Fig. 3.2B). This is in accordance with Ivanov *et al*. (2001) who observed that PSI has a higher level of resistance to winter stress compared to PSII. The repression of linear electron transport downstream of PSII was accompanied by marked donor-side limitation of PSI, as indicated by high Φ_{ND} values (Fig. 3.1E). Interestingly, Φ_{NA} in winter-acclimated needles was the same as observed during summer, suggesting retention of the pool size of PSI electron acceptors during winter-acclimation,

possibly as a strategy to facilitate rapid recovery of carbon fixation in early spring. The observed imbalance between electron transport at PSII and PSI points to enhanced cyclic electron transport around PSI (Johnson, 2011). This indicates that in winter-acclimated seedlings, electron flow around PSI plays a considerable role in the removal of excess light. Oxidized P700 can efficiently quench chlorophyll fluorescence (Öquist and Hüner 2003); thus, we conclude that PSI was likely an important quencher of absorbed light in our winter-acclimated seedlings.

It is important to note that in this study needle absorptance (α) was calculated with the assumption that needle transmittance is zero. Recently it was shown that a small proportion of light (<5% of the visible spectrum) can be transmitted through conifer needles (Lukeš *et al*. 2013). The absorptance values presented in Table 2 might therefore slightly overestimate the true α, which can potentially result in a minor overestimation of ETR. However, the error is minimal and equally affects ETR_{II} and ETR_{I} and the overall trends observed in our data are not affected. We recommend that future studies include measurements of reflectance and transmittance to facilitate estimation of leaf absorptance and the calculation of α and ETR.

Different rates of recovery cause decoupling of PRI and LUE during early stages of spring

Immediately after transfer to our spring treatments, we observed a decrease of the excitation pressure of PSII (1-qP, Fig. 3.3B), reflecting the role of air temperature in restoring the redox state of the chloroplast (Demmig-Adams and Adams 2006a, Ensminger *et al.* 2008). In both spring treatments, the maximum quantum yield of PSII recovered rapidly, indicating a fast re-organization of the photosynthetic apparatus under warmer conditions. A considerable recovery of assimilation was also observed within the first days of exposure to spring treatments (Fig. 3.3C). We further observed a concomitant decrease in zeaxanthin pools and a decrease in the de-epoxidation state of the xanthophyll cycle (Fig. 3.4E,F), both indicating a decreased requirement for photoprotection. In *P. sylvestris*, Ensminger *et al*. (2008) also reported rapid recovery of photosynthetic capacity, along with rapid relaxation of DEPS during the first few days of exposure to a simulated spring treatment. In our

experiment the quick decline in zeaxanthin Chl^{-1} and DEPS occurred concomitantly with the transition from sustained quenching to dynamic quenching mediated by xanthophyll cycle pigments (Fig 3.1B,C).

Interestingly, under warm spring conditions, it took more than 18 days before PRI recovered from winter stress, while under cold spring conditions, no PRI recovery was observed. Similarly, levels of Chl FW^{-1} and Car Chl^{-1} did not recover from winter stress until after day 12 (Fig. 3.4A,C). In the field, boreal spring conditions are characterized by large day-to-day variations in air temperature, and photosynthesis recovers quickly and opportunistically with increasing air temperature. Conversely, photosynthesis can rapidly revert back to a downregulated state with the occurrence of cold episodes (Ensminger *et al*. 2004, 2008). Maintaining large pools of carotenoids in needles after photosynthetic recovery reflects a strategy that allows for rapid photoprotection during sudden low temperature episodes. On the other hand, the delay in Chl synthesis during the early stages of photosynthetic recovery prevents the absorption of excess light and photooxidative stress. This is supported by the fact that the timing of Car downregulation and Chl upregulation coincided with the occurrence of the maximum rates of photosynthesis after day 12 of the experiment (Figs 3.3, 3.4). A mismatch in the timing of the spring recovery was also reported by Wong and Gamon (2015b). They observed that the recovery of electron transport, LUE and the epoxidation status of the xanthophyll cycle (EPS) occurred approximately 2-3 weeks earlier than the recovery of PRI in *P. ponderosa* and *P. contorta* seedlings exposed to natural spring conditions. These differences in the timing of recoveries indicate that during the early stages of photosynthetic recovery, xanthophyll cycle dynamics are not the main factor controlling PRI. PRI therefore insufficiently detects variations in LUE during that time.

At a seasonal timescale, PRI is mostly controlled by carotenoid and chlorophyll pool sizes

Previous studies on boreal pine species have reported a strong contribution of pigment pools on PRI. For instance, Porcar-Castell *et al.* (2012) reported that variations in the pool size of xanthophyll cycle pigments over the year control the dynamics of PRI in *P. sylvestris*, while Wong and Gamon (2015a,b) reported a combined effect of all carotenoid pigments in *P.*

ponderosa and *P. contorta*. Our experiment revealed that PRI and DEPS did not correlate well during the early stages of spring recovery (days 0-3), when NPQ was predominantly facilitated via the sustained quenching mode. In contrast, PRI correlated consistently with Chl and Car pigment pool sizes throughout the spring transition, regardless of the degree of photosynthetic recovery (Fig. 3.6A-D). Furthermore, Chl and Car were responsible for a large proportion of the PRI variation observed. The range of PRI variation between winter and summer seedlings was 0.22 while the largest range of PRI variation observed at a diurnal scale was only 0.033 (Fig. 3.7F). Accordingly, the magnitude of variation in PRI due to long-term pigment pool adjustments was more than six times higher than the magnitude caused by short-term changes in xanthophyll cycle pigments. This ratio suggests that on an annual scale, the PRI signal reflects the small contribution of xanthophyll cycle dynamics superimposed on the much larger effects of seasonal pigment adjustments. Thus, the adjustments in pigment pools conceal the diurnal variations in PRI, especially during the winter-spring transition from sustained NPQ to energy-dependent NPQ.

Alternative energy sinks contribute to the early spring discrepancy in the PRI-LUE relationship

During the spring transition from sustained to reversible zeaxanthin-dependent NPQ, adjustments in NPQ may occur independently of xanthophyll pigment conversions and decouple PRI from NPQ. This was observed during the entire duration of the spring simulation, where sustained quenching was retained to some extent in both the cold and warm treatments, and particularly during the first days of exposure to spring conditions. What causes the delay of the release of sustained quenching? Sustained NPQ or the thermal dissipation of excess energy is achieved through structural reorganization of PSII. These changes include the aggregation of LHCII as a major energy dissipation pathway (Horton *et al*. 1991, 2005, Ottander *et al*. 1995). Unlike the xanthophyll-regulated LHCII aggregation associated with energy-dependent quenching (Horton *et al*. 2005, Ruban *et al*. 2012), this cold-induced reorganisation reflects a zeaxanthin-independent quenching mechanism, which is not detected by PRI. In addition to LHCII aggregation, another zeaxanthin-independent electron sink that remains undetected by PRI is the diversion of excess energy to PSI-driven cyclic electron transport. In *P. strobus* seedlings, the recovery of PSII function was

generally slowed down and impaired in the cold spring treatment. PSII electron transport in the cold spring treatment recovered to values approximately half of that observed in the warm spring treatment and at a slower recovery rate (Fig. 3.2A). Interestingly, PSI electron transport in the cold spring treatment greatly surpassed the amount recorded in the warm treatment during the second half of the experiment (Fig. 3.2B). Ivanov *et al*. (2001) suggested that PSI photochemistry in early spring supplies the ATP required to maintain the integrity of chloroplasts while supporting the recovery from winter stress. In this experiment, enhanced PSI-driven electron transport coincided with high excitation pressure of PSII (Fig. 3.2C, 3.3B). High light and low temperature in our cold spring treatment imposed increased excitation pressure and likely photodamage to the D1 protein of PSII. Because *de novo* synthesis of the D1 protein requires a large amount of ATP (Murata *et al*. 2007), cyclic electron flow was proposed to be an essential component in the recovery of PSII under conditions of impaired linear electron transport (Huang *et al*. 2010). This may indicate that in the cold spring treatment, a larger fraction of absorbed energy was invested in ATP production via PSI-driven electron transport, rather than being dissipated as heat via the xanthophyll cycle as was the case in the warm spring treatment.

Under conditions of cold stress, both PSII and PSI may be important non-radiative quenchers through charge recombination events (Lunde *et al*. 2000, Öquist and Hüner 2003). In addition, Savitch *et al*. (2010) suggested that PTOX mediated electron transport to oxygen is a major electron sink during winter. However, such measurements were outside the scope of this experiment, but these energy sinks likely contribute to NPQ during the winter-spring transition without apparent effect on PRI. This early-spring decoupling of PRI and LUE seems to result in the overestimation of LUE (Fig. 3.5A,B), as reported by Porcar-Castell *et al*. (2012) in *P. sylvestris* during early spring, when foliage was downregulated due to severe cold stress.

3.6 Conclusions

Our results demonstrate an early spring decoupling in the PRI-LUE relationship caused by differences between the timing of the recovery of photosynthesis, and the timing of carotenoid and chlorophyll pigment pool size adjustments, which are the main controlling factors of PRI during spring. We also demonstrate that zeaxanthin-independent NPQ

mechanisms undetected by PRI further contributed to this decoupling. One of the main mechanisms contributing to the decoupling of the PRI-LUE relationship likely involves PSI-driven electron transport, which appears to be a significant energy sink during the entire spring transition, and particularly in needles exposed to a combination of high light and cold temperatures.

Future studies should also aim to validate the mechanisms identified here on mature trees and in natural systems where additional causes of PRI variation, such as illumination angle or canopy structure, are likely to impose additional complexity to the signal detected from leaf reflectance measurements.

3.7 Acknowledgements

Financial support from NSERC and the Canada Foundation for Innovation to IE is gratefully acknowledged. EF acknowledges the receipt of a Graduate Student Research Award from the University of Toronto Center for Global Change Science and PhD funding from the Department of Cell and Systems Biology at the University of Toronto and Ontario Graduate Scholarships. The authors are also grateful to Christopher Juliao and Daniel Marsden for their help and assistance in the laboratory.

Chapter 4

4 Intraspecific variation in the phenology of photosynthesis of field grown *Pinus strobus* L. provenances in response to artificial warming

Fréchette E, Chang CYY, Ensminger I. Intraspecific variation in the phenology of photosynthesis of field grown *Pinus strobus* L. provenances in response to artificial warming.

Status: To be submitted to a peer-reviewed journal.

4.1 Abstract

In northern-latitude trees, temperature and photoperiod control the beginning and end of the photosynthetically active season. Rising temperature in the northern hemisphere has advanced spring warming and delayed autumn cooling while photoperiod remained unchanged. We aimed to assess the effects of elevated temperature on the length of the photosynthetically active season of Eastern white pine (*Pinus strobus* L.) seedlings adapted to the photoperiod and temperature of different latitudes. Also, we aimed to verify whether the photochemical reflectance index (PRI) and the chlorophyll/carotenoid index (CCI) could accurately track the phenology of photosynthesis during spring and autumn. Three year-old seedlings from three provenances of *P. strobus* were obtained, representing a 1000 km latitudinal gradient. Using a Temperature Free-Air-Controlled Enhancement (T-FACE) experiment we exposed the seedlings to elevated temperature (+1.5/3°C; day/night). Over 18 months, we measured chlorophyll fluorescence, photosynthetic gas exchange, spectral reflectance and foliar pigment content in seedlings. During autumn all seedlings regardless of provenance revealed the same sequence of phenological events with the initial downregulation of photosynthesis, followed by the modulation of NPQ and subsequent adjustment of pigment pool sizes. Seedlings from the southern provenance were delayed by up to two weeks with this sequence, while seedlings from the northern provenance were up to two weeks early compared to local seedlings, indicating genetic controls of autumn photosynthesis dictated by photoperiod. A provenance effect during spring was also observed but was generally not significant. During autumn a greater potential for additional photosynthesis in response to warming was observed in the southern provenance, while the northern provenance was genetically constrained to terminate photosynthesis earlier. The vegetation indices PRI and CCI were both effective at tracking the seasonal variations of the light-use efficiency of *P. strobus* needles, and the amounts of the carotenoid pigments indicative of the stress status of needles throughout the year.

4.2 Introduction

In northern forest ecosystems, low temperature is the most important climatic constraint to photosynthesis (Nemani *et al.* 2003, Öquist and Hüner 2003). The timing and duration of the photosynthetically active season are tightly coupled with above-zero temperature and the absence of a snow cover. During the last decades, conifer-dominated northern-latitude ecosystems have experienced more rapid warming compared to other regions of the globe, particularly during winter and spring (IPCC 2014). Yet, there is no consensus on the effects of a warmer climate on the timing of the beginning and end of the photosynthetically active season of evergreen conifers, and, in turn, on the changes in the amount of carbon sequestrated by boreal and temperate forests. Some authors predict enhanced photosynthesis in response to warming (Myneni *et al.* 1997, Bergh *et al.* 2003, Tanja *et al*. 2003) while others have postulated that trees might be unable to fully exploit warmer temperatures in the spring and/or autumn due to photoperiodic control of the beginning, and particularly the end of the photosynthetically active season (Busch *et al*. 2006, Piao *et al.* 2008, Barichivich *et al.* 2013, Trahan and Schubert 2016).

Eastern white pine (*Pinus strobus* L.), the most valuable softwood lumber in eastern Canada (Farrar 2003), expands longitudinally from western Ontario to the Atlantic provinces in Canada, and latitudinally throughout most of north central and the northeastern U.S.A. (Farrar 2003). Tree species with broad latitudinal distributions, such as *P. strobus*, encompass diverse regional climates. This gives rise to potential for local adaptation (Savolainen *et al.* 2007), i.e. intraspecific variation between populations of the same species in response to selective pressures imposed by some aspect of the local environment (Lepais and Bacles 2014). Intraspecific variation in photoperiod and/or temperature responses between *P. strobus* provenances from different latitudes is expected, as was reported in other trees such as *Populus* (Fracheboud *et al.* 2009, Ma *et al*. 2010, Soolanayakanahally *et al.* 2015), *Pinus sylvestris* (Kujala and Savolainen 2012, Kujala *et al.* 2017) and *Picea sitchensis* (Holliday *et al.* 2008, Dauwe *et al.* 2012).

Climate envelope models predict a northward shift of the range of suitable conditions for *P. strobus* in the next decades (Rehfeldt *et al.* 2012). As suitable ranges shift, plants can adjust to novel climatic conditions by adapting through natural selection (Liepe *et al.* 2015) or

migrating to follow conditions to which they are adapted (Hamann and Aitken 2013; Savolainen *et al.* 2007). Alternatively, plants may acclimate through phenotypic plasticity, i.e. the range of observable traits a single genotype can express as a function of its environment (Nicotra *et al.* 2010; Franks *et al*. 2013). In the case of long-lived species like *P. strobus*, phenological responses to rapid climate warming, such as the spring recovery or autumn downregulation of photosynthesis, will depend largely on the degree of phenotypic plasticity exhibited in response to temperature and photoperiod, and the extent to which the species relies on photoperiodic cues for determining phenology (Ensminger *et al.* 2015). Species that are highly sensitive to photoperiod will not be able to track climate warming, i.e. the lengthening of the potential growing season, unless they exhibit enough phenotypic plasticity to acclimate to new conditions.

During autumn many tree species downregulate photosynthesis in response to shortening photoperiod weeks before temperature becomes a limiting factor to photosynthesis. In evergreen conifers, shortening days at the end of the summer were reported to induce growth cessation and/or photosynthetic downregulation in species such as Scots pine (*Pinus sylvestris* L.; Vogg *et al*. 1998, Repo *et al*. 2000), Norway spruce (*Picea abies* (L.) H. Karst.; Asante *et al.* 2011) and Eastern white pine (*P. strobus*; Fréchette *et al.* 2016). Low temperatures as autumn progresses further inhibit growth by reducing cell growth and differentiation (Rossi *et al.* 2008). The resulting decrease in sink capacity for photosynthates negatively regulates photosynthetic carbon assimilation. To compensate for the decreased energy sink, evergreen conifers reduce their capacity for harvesting sunlight by reducing the size of chlorophyll pools, and increase their capacity for photoprotection (Ensminger *et al*. 2006). Increased photoprotection is achieved by replacing dynamic qE type non-photochemical quenching (NPQ), where dissipation of excess light energy is dynamically regulated via rapid adjustments of the de-epoxidation state of xanthophyll cycle pigments, by qI type NPQ (Demmig-Adams & Adams 2012). The sustained and slowly reversible qI type NPQ involves the arrest of the xanthophyll cycle in a state primed for sustained energy quenching where zeaxanthin is retained and no longer reconverts to violaxanthin upon dark-relaxation. Sustained qI type NPQ was reported to occur concomitantly with partial chlorophyll degradation (*P. sylvestris*; Ensminger *et al*. 2006, *P. strobus*; Chang *et al.* 2015; Fréchette *et al.* 2016), photosystem (PS) II core unit reorganization (*P. sylvestris*; Ottander

et al. 1995, Ensminger *et al*. 2006) and upregulation of photoprotective pigments such as lutein and β-carotene (*Pinus banksiana* Lamb., Busch *et al.* 2007, *P. strobus*, Fréchette *et al*. 2016). This ensures photoprotection as photosynthesis almost completely downregulates during winter.

The effects of warmer autumn temperatures have been investigated both in growth chambers and field experiments, with contrasting results depending on the magnitude of warming. For instance, in a controlled, factorial experiment using *P. banksiana* seedlings, Busch *et al.* (2007) did not observe an increase in photosynthetic carbon uptake under a +15/12°C (day/night) autumn warming treatment, but observed instead enhanced NPQ of excess light energy via the xanthophyll cycle. In a temperature free-air controlled experiment (T-FACE), Chang *et al.* (2015) reported that an additional 1.5°C/3°C (day/night) above ambient field temperature was not enough to delay photosynthetic downregulation or delay the transition from qE type NPQ to sustained qI type NPQ in *P. strobus* seedlings. In contrast, Stinziano *et al.* (2015) observed delayed photosynthetic downregulation in Norway spruce (*Picea abies*) seedlings growing in a greenhouse and exposed to a +4°C warming treatment. This suggests variation in the sensitivity of photosynthetic downregulation to photoperiod among species.

During spring, the recovery of photosynthesis in conifers was reported to be closely linked to the increase of air temperature above 0°C (Tanja *et al*. 2003, Sevanto *et al.* 2006) which facilitates biochemical reactions involved in repair and reorganization of the photosynthetic apparatus (Ensminger *et al*. 2004, 2006). In contrast, the timing of spring developmental events, such as vegetative bud burst and flowering, is irreversible and was reported to be both temperature- and photoperiod-sensitive (Hänninen and Tanino 2011). A whole-tree chamber experiment recently revealed that an elevated temperature treatment of +2.8–5.6°C advanced the onset of photosynthetic recovery by approximately 8 days, and advanced the completion of photosynthetic recovery by 22 days in *P. abies* (Hall *et al.* 2013, Wallin *et al.* 2013). Intermittent frost during the recovery period delayed the recovery of photosynthesis, as was reported for other boreal conifers such as *P. abies* (Bergh and Linder 1999), *P. sylvestris* (Strand *et al*. 2002; Ensminger *et al.* 2008) and *Picea mariana* (Mill.) Britton, Sterns & Poggenburg (Fréchette *et al.* 2011).

Although substantial developments have been made in assessing growing season length using remote sensing of forests dominated by deciduous trees, important limitations remain for the transfer of these techniques to coniferous forests. In deciduous forests, growing season phenology is typically monitored with vegetation greenness indices derived from spectral reflectance data, most commonly NDVI or EVI (Garrity *et al*. 2011, Sonnentag *et al*. 2012). Greenness indices, however, present important limitations in forests dominated by evergreen trees, which show little variation in canopy greenness throughout the year (Guyon *et al*. 2011, Hufkens *et al*. 2012, Melaas *et al.* 2013, Walther *et al.* 2016), making it difficult to detect the beginning and, particularly, the end of the photosynthetically active season. An alternative to greenness indices for the detection of the "invisible" phenology of evergreen conifers is the use of indices that actually track the efficiency of photosynthesis, such as the photochemical reflectance index (PRI). The biological basis of PRI is its capacity to detect, over short timespans, the spectral signature of xanthophyll cycle pigments involved in the dissipation of excess light, and, hence, the efficiency of photosynthesis (Gamon *et al.* 1992, 1997, Peñuelas *et al.* 1995). However, recent studies on evergreen conifers suggest that changes in energy partitioning occurring during the spring and autumn seasons result in discrepancies between the PRI and the efficiency of photosynthesis, and that variations in leaf carotenoid pigment pool sizes appear to be the main driver of PRI changes over seasonal timespans (Busch *et al.* 2009, Porcar-Castell *et al.* 2012; Fréchette *et al*. 2015, 2016, Wong and Gamon 2015a,b). More recently, the chlorophyll/carotenoid index (CCI), which tracks seasonal changes in leaf carotenoid pigment pools, has been proposed as a new way to assess the phenology of photosynthesis (Gamon *et al*. 2016). Indeed, since carotenoid pigments are upregulated with environmental stress, including cold stress occurring during winter, detecting the variations in their pool sizes might be the key to a better understanding of the spring and autumn phenology of photosynthesis. Still, the suitability of the PRI and CCI to track variations in photosynthesis during those transitionary seasons needs to be clarified for accurate assessments of variations in the photosynthetically active season length of conifer-dominated ecosystems.

In the present study, we assessed the spring and autumn phenology of photosynthesis of three provenances of *P. strobus* seedlings originating from northern, central and southern locations within the species range under either ambient temperature or an elevated

temperature treatment in the field. We aimed to (1) investigate whether the phenology of photosynthesis differs between provenances of *P. strobus* seedlings growing under the same temperature and photoperiod regimes, (2) investigate whether *P. strobus* provenances differ in their response to elevated temperature, and (3) determine whether the PRI and CCI can be used to detect differences observed in photosynthesis, energy partitioning and photosynthetic pigment pool sizes during spring and autumn.

4.3 Materials and Methods

Field site and plant material

The experiment was carried out at the Koffler Scientific Reserve of the University of Toronto located in King City, Ontario, Canada (44°01'44"N, -79°32'21"W; Fig. 4.1). A Temperature Free-Air-Controlled Enhancement (T-FACE) system was set up according to Kimball *et al.* (2008), and consisted of 10 circular plots, each with a diameter of 3m (Fig. 4.2). Ambient canopy temperature was recorded using infrared temperature sensors (Model IRT-P5, Apogee Instruments, Logan, UT, USA) in five unheated control plots (ambient temperature; AT). For the elevated temperature treatment (ET), five plots were equipped with six 100W infrared heaters (Mor Electric Heating Association, Comstock Park, MI, USA) in a hexagonal array, where leaf temperature was raised by +1.5°C during the day and +3°C at night to mimic predicted air temperature for 2050 in southern Ontario (Price *et al.* 2011, Peng *et al.* 2013, Fig. 4.2). Ambient air and canopy temperatures were recorded using a CR1000 datalogger (Campbell Scientific Inc., Edmonton, AB, Canada). Precipitation data were obtained from the Buttonville Airport weather station in Newmarket, Ontario (Environment Canada 2014), located 25 km from the field site.

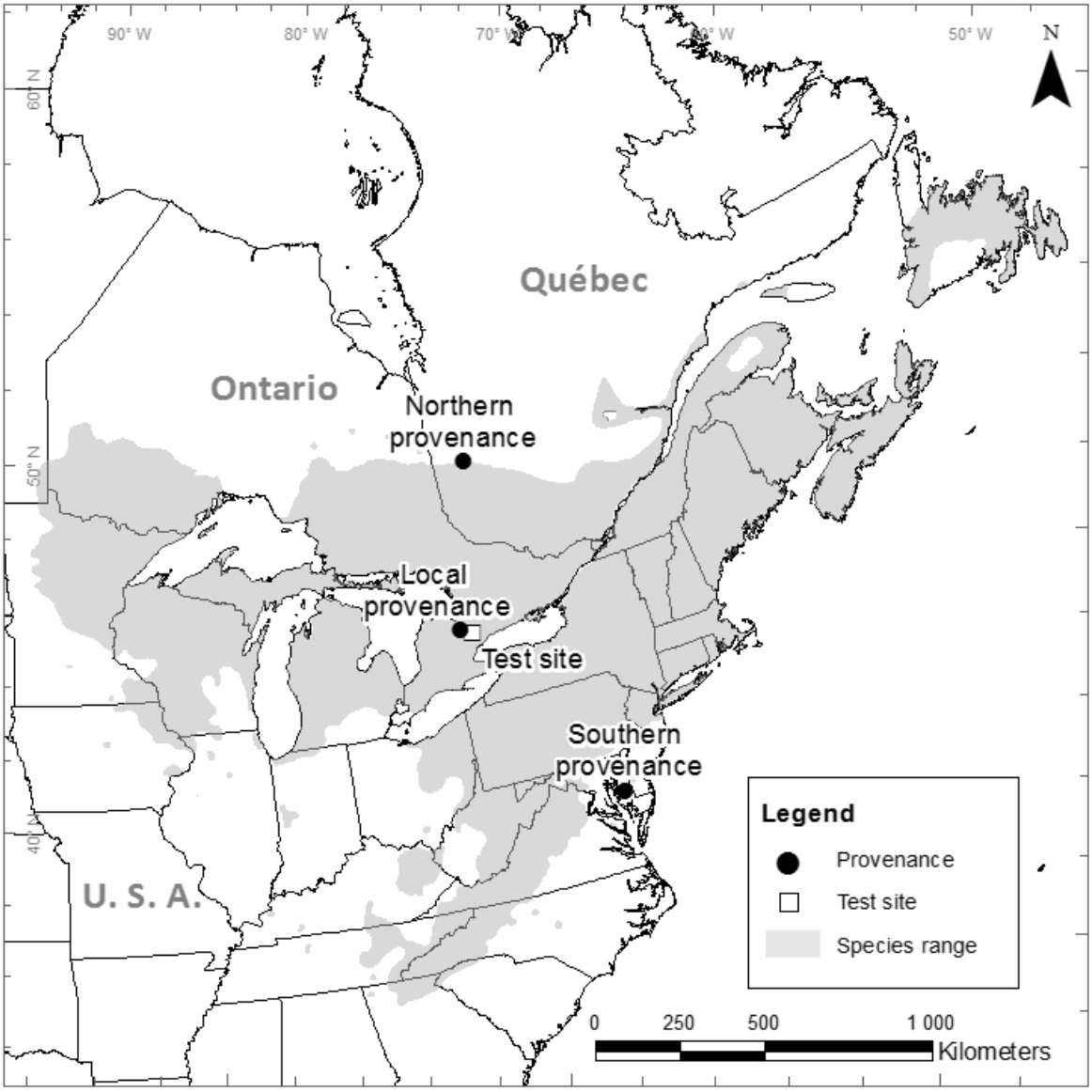

Figure 4.1 Locations of the test site at Koffler Scientific Reserve in Ontario, Canada and of the three *P. strobus* provenances in Québec and Ontario, Canada, and Maryland, U.S.A.

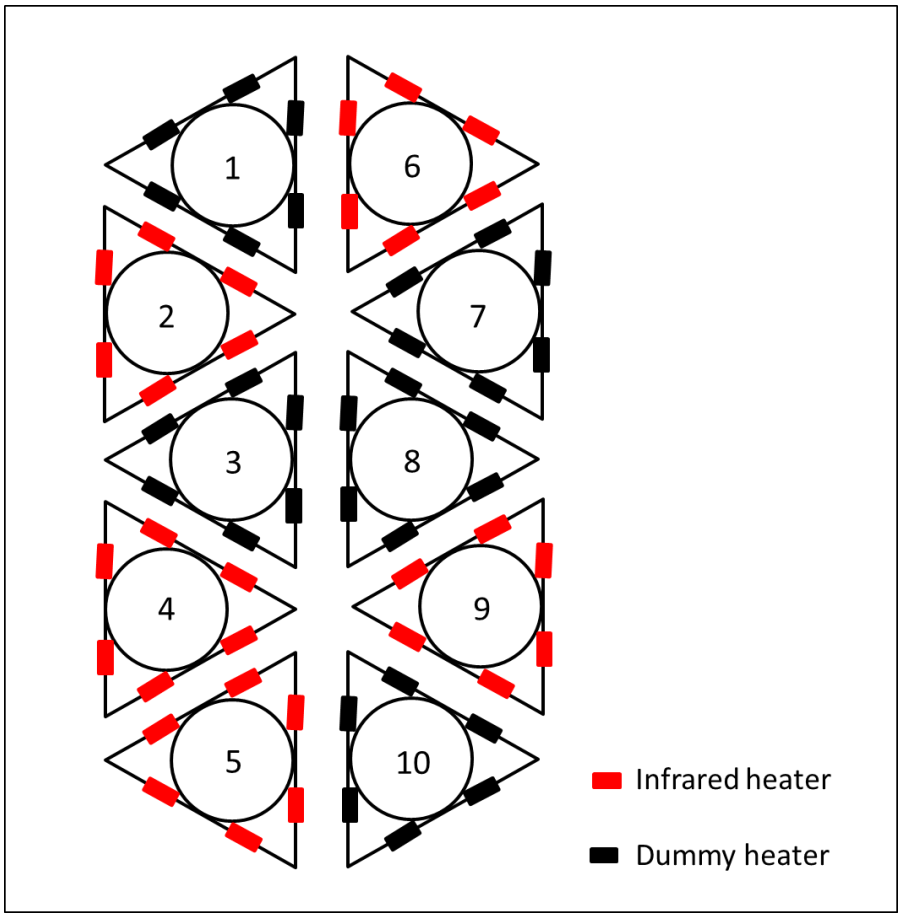

Figure 4.2 Scheme of the Temperature Free-Air-Controlled Enhancement (T-FACE) system set up at the Koffler Scientific Reserve. Ten circular plots, each with a diameter of 3m, were either heated (+1.5°C /+3°C; day/night) with 100W infrared heaters or equipped with dummy heaters and left at ambient temperature.

Plots were excavated 30cm deep and filled with a mixture composed of one-third peat, one-third sand and one-third local soil prior to planting. Three-year-old (3+0) bare-rooted Eastern white pine (*Pinus strobus* L.) seedlings were obtained from a northern (NP; Trécesson Nursery, Amos, QC, Canada; 48°34'36"N, -78°15'21"W; Fig. 4.1), local (LP; Somerville Nurseries, Everett, ON, Canada; 44°10'46"N, -79°56'30"W; Fig. 4.1) and southern provenance (SP; John S. Ayton State Tree Nursery, Preston, MD, USA; 38°42'05"N, -75°54'51"W; Fig. 4.1). The seedlings were selected from local seed orchards at each provenance to ensure adaptation to local environmental conditions. In early May 2012, 210 seedlings were planted per plot at a distance of 30 cm. Gas exchange, fluorescence and spectral measurements started in September 2012 after seedlings were established, and monthly measurement campaigns were carried out until January 2014. At

each time point, two seedlings per provenance were selected in each of the 5 plots for measurement, yielding 5 replicate plots per treatment.

Climatic and environmental conditions at sites of origin

The sites of origin of the three *P. strobus* provenances selected for this experiment are located along a latitudinal transect of approximately 1000 km or 10 degrees of latitude (Fig. 4.1). The provenances were chosen because of the contrasting temperature and photoperiod regimes at the three locations (Fig. 4.3). Temperature records for the period 1981-2010 indicate that annual mean temperatures range from 1.5 to 14.7°C from the northern to the southern sites of origin (Environment Canada, 2018; US Climate Data 2018). Such differences result in lengths of the thermal potential growing season, i.e. the frost-free season, ranging from 5.5 to 9.5 months from the northern to the southern sites of origin (Fig. 4.3). In addition, at the beginning of the thermal potential growing season in the spring, photoperiods range from 14.7 to 11h from the northern to the southern site (Fig. 4.3), whereas at the end of the potential growing season in autumn, photoperiods range from 10.7 to 9.4h (Fig. 4.3).

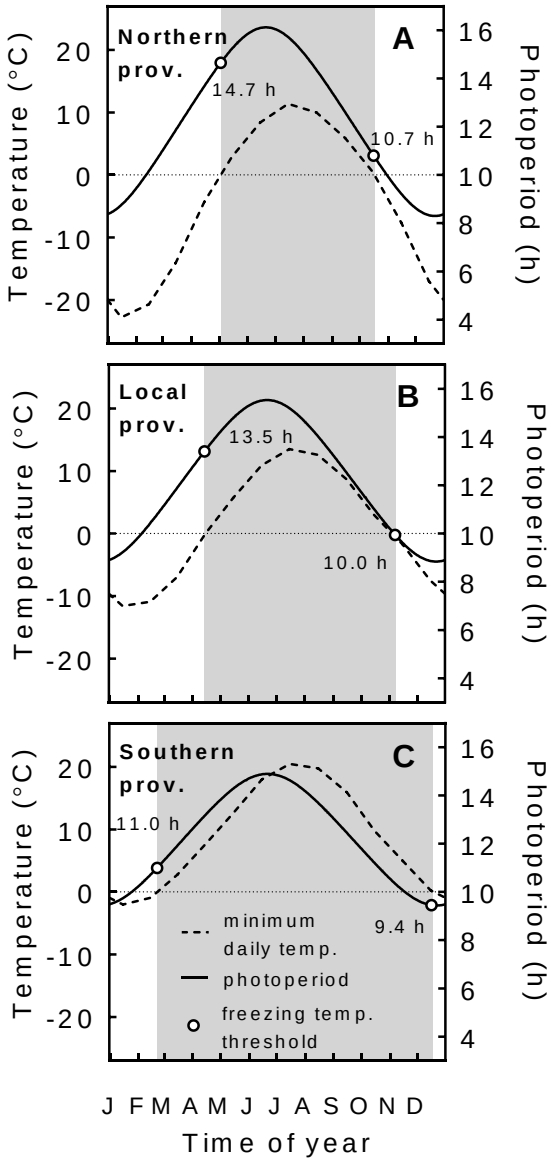

Figure 4.3 The link between photoperiod and seasonal temperatures at (A) the northern (Amos, QC, Canada, 48°34'36"N, -78°15'21"W); (B) local (Everett, ON, Canada; 44°10'46"N, -79°56'30"W) and (C) southern (Preston, MD, USA; 38°42'05"N, -75°54'51"W) provenances of *P. strobus*. Dashed lines indicate average minimum daily temperature for the period 1970-2010, full lines indicate photoperiod, circles indicate the photoperiod at which temperatures cross the freezing threshold and the shaded area represents the frost-free season.

Chlorophyll fluorescence measurements

Chlorophyll fluorescence was used to assess energy utilization by the seedlings. A Dual-PAM-100 (Walz, Effeltrich, Germany) was used for the measurements, with a fiberoptic mounted on a leaf holder (2030-B). A saturating light pulse was first applied to dark-adapted (pre-dawn) needles for determination of F_o and F_m (minimal and maximal fluorescence). Maximal quantum yield of photosystem (PS) II was calculated according to Genty *et al*. (1989):

$$F_v/F_m = \left(\frac{F_m - F_o}{F_m}\right) \qquad \text{Equation 4.1}$$

The needles were then exposed to 1200 μmol photon $m^{-2}s^{-1}$ actinic light for a period of 12 minutes, which previous testing on *P. strobus* has revealed sufficient to induce full light acclimation in needles. During that period a 400 ms saturating pulse of 10000 μmol photon $m^{-2}s^{-1}$ was applied every 40 s for determination of F_m' (maximal fluorescence of light-adapted needles), and a weak pulse of far-red light for determination of F_o' (minimal fluorescence of light-adapted needles). Energy partitioning parameters, presented as equations 2-4 below, were calculated according to Hendrickson *et al*. (2004). Effective quantum yield of PSII of a light-adapted sample (Φ_{PSII}) reflects the proportion of light absorbed by PSII which is used for photochemistry and was calculated as:

$$\Phi_{PSII} = 1 - \frac{F_s}{F_m'} \qquad \text{Equation 4.2}$$

where F_s is the yield of fluorescence in a light-adapted sample. The proportion of light that is absorbed by PSII antenna and thermally dissipated via xanthophyll-regulated NPQ (Φ_{NPQ}) was calculated as:

$$\Phi_{NPQ} = \frac{F_s}{F_m'} - \frac{F_s}{F_m} \qquad \text{Equation 4.3}$$

The proportion of energy quenched by fluorescence and dissipated constitutively ($\Phi_{f,D}$) was calculated as:

$$\Phi_{f,D} = \frac{F_s}{F_m} \qquad \text{Equation 4.4}$$

Photosynthetic gas exchange measurements

To assess variations in photosynthetic activity over the course of the experiment, photosynthetic gas exchange was measured using a GFS-3000 (Walz, Effeltrich, Germany). A bundle of needles attached to the main twig was oriented to form a flat plane and inserted in the leaf cuvette. CO_2 concentration in the cuvette was set to 400 ppm, humidity was set 60% RH and cuvette temperature was set to ambient temperature, which was selected based on field temperature. Net CO_2 assimilation (A) and stomatal conductance (g_s) were measured in the dark and at 1200 μmol photon $m^{-2}s^{-1}$ once steady-state assimilation was achieved. Immediately after the measurements, needles were detached from the seedling and measured for surface area using the Winseedle software package (Regent Instruments Inc., Québec, Canada).

Spectral reflectance measurements

Seasonal variations in PRI were assessed from leaf spectral reflectance measurements using a Unispec-SC spectrometer (UNI007, PP Systems, Haverhill, MA, USA) equipped with an internal tungsten halogen light source. The spectrometer was connected to a bifurcated fiberoptic (UNI400) and mounted on the Dual-PAM-100 leaf holder, therefore measuring the same needles as for fluorescence measurements and maintaining the fiberoptic on the needle surface at a fixed angle of 60° relative to needle axis (2 mm diameter spot size). Leaf bidirectional reflectance was computed by dividing reflected irradiance by the radiance obtained from a white reflectance standard (Spectralon, Labsphere, North Sutton, NH, USA) taken immediately before each leaf measurement. Dark current instrument noise was subtracted from white standard and leaf radiance measurements. Reflectance was measured on previous-year needles of the topmost part of the leader shoot. For each measurement, 3 scans were averaged from dark-adapted needles, and 1 scan was recorded every 40 s over a period of 12 minutes. The integration time was set to 10 ms and interpolation of the ~3.3 nm resolution output of the spectrometer to 1 nm bandwidths was computed using the software Multispec v. 5.1.0 (Purdue University, Indiana, USA). PRI was calculated according to Peñuelas *et al*. (1995):

$$\mathrm{PRI} = \frac{R_{531} - R_{570}}{R_{531} + R_{570}} \qquad \text{Equation 4.5}$$

where R_{531} and R_{570} represent leaf reflectance at 531 and 570 nm, respectively. CCI was calculated according to Gamon *et al.* (2016):

$$\mathrm{CCI} = \frac{R_{531} - R_{645}}{R_{531} + R_{645}} \qquad \text{Equation 4.6}$$

where R_{645} represents leaf reflectance at 645 nm.

Photosynthetic pigment analysis

Needle samples for pigment analysis were collected following the fluorescence, spectral and gas exchange measurements. The samples were immediately frozen in liquid nitrogen and stored at -80°C until they were ground to a fine powder in liquid nitrogen. Photosynthetic pigments were analyzed according to Junker and Ensminger (2016). Briefly, pigments were first extracted in dim light conditions in 98% methanol with water buffered with 2% 0.5M ammonium acetate for 2 hours. The extracts were then filtered through a 0.45 µm PTFE filter prior to high-performance liquid chromatography (HPLC) analysis. HPLC analysis was performed with an Agilent 1260 system (Agilent Technologies, Santa Clara, CA, USA) with a quaternary pump, autosampler set to 4°C, column oven set to 25°C and photodiode array detector. Pigments were detected at 450 nm and 656 nm wavelengths and separated using a reverse-phase C_{30} column (5 µm, 250*4.6 mm; YMC America, Inc., Allentown, PA, USA) protected by a 20*4.6 mm guard column. Three solvents, i.e. A: 100% methanol, B: 100% methyl-tert-butyl-ether and C: water buffered with 0.2% ammonium acetate, were used to run a gradient starting with 92% A, 5% B and 3% C. During each run solvent A was gradually replaced by solvent B to a minimum of 5% A. Every run was followed by a 5 min reconditioning phase with initial solvent concentrations. For calibration and peak detection, commercially available standards were obtained from Sigma Aldrich (St. Louis, MO, USA) and DHI Lab products (Hørsholm, Denmark). Peak detection and pigment quantification was performed using ChemStation software (Agilent Technologies, Santa Clara, CA, USA).

HPLC data was used to determine total chlorophylls (Chl), as the sum of chlorophyll a and b concentration on a fresh weight basis (µmol g^{-1}), since the water content of *P. strobus*

needles varies less than 10% year-round (Verhoeven *et al.* 2009). The concentration of carotenoid pigments was normalized to chlorophyll levels and was expressed in mmol mol^{-1}. Total carotenoids (Car) were expressed as the sum of violaxanthin, antheraxanthin, zeaxanthin, neoxanthin, lutein, α-carotene and β-carotene concentrations. DEPS was expressed according to Thayer and BJörkman (1990):

$$\mathrm{DEPS} = \frac{0.5\mathrm{A}+\mathrm{Z}}{\mathrm{V}+\mathrm{A}+\mathrm{Z}} \qquad \text{Equation 4.7}$$

Deriving phenology metrics from time series

Spring and autumn phenology metrics were derived from our physiological, pigment and vegetation indices time series by fitting the data to logistic functions using a method described in Gonsamo *et al*. (2012, 2013). Firstly, for each physiological and optical parameter (i.e., F_v/F_m, Φ_{II}, A, g_s, R_d, Φ_{NPQ} Φ_{fD}, Carotenoids Chl^{-1}, Zeaxanthin Chl^{-1}, DEPS, PRI and CCI), time series were divided into spring or autumn transition sub-datasets. Spring subdatasets were fit to the following logistic function (Gonsamo *et al.* 2012, 2013):

$$y(t) = \alpha_1 + \frac{\alpha_2}{1+e^{-\delta_1(t-\beta_1)}} \qquad \text{Equation 4.8}$$

where $y(t)$ is the observed parameter at day of year (DOY) t, α_1 is the background (winter) parameter value, α_2 is the early summer plateau value, δ_1 is the spring transition normalized slope coefficient and β_1 is the midpoint in DOY of the spring transition (Fig. 4.4A). Autumn subdatasets were fit to the following logistic function (Gonsamo *et al.* 2012, 2013):

$$y(t) = \alpha_1 - \frac{\alpha_3}{1+e^{\delta_2(t-\beta_2)}} \qquad \text{Equation 4.9}$$

where α_3 is the late summer plateau value of the observed parameter, δ_2 is the autumn transition normalized slope coefficient and β_2 is the midpoint in DOY of the autumn transition (Fig. 4.4B). Data were fitted to the logistic functions with nonlinear regressions ran with the first guess values of the seven parameters in equations 7 and 8 and solved with maximum of 1000 iterations using GraphPad Prism 7.03 (GraphPad Software, Inc., La Jolla, CA, USA). First guess values were based on field observations.

Two key transition dates were then computed, i.e. start of recovery (SOR) and start of downregulation (SOD), in DOY, as the third (f"(x)) derivatives of the logistic function according to (Gonsamo *et al*. 2012, 2013) as:

$$\mathrm{SOR} = \beta_1 - (4.562/2\delta_1) \qquad \text{Equation 4.10}$$

and

$$\mathrm{SOD} = \beta_2 - (4.562/2\delta_2) \qquad \text{Equation 4.11}$$

with SOR representing the point in time during the spring transition where the parameter initiates recovery (Fig. 4.4A), and SOD representing the point in time during the autumn transition where the parameter initiates downregulation (Fig. 4.4B). SOD and SOR values were obtained for each treatment x provenance group (6 groups) for each plot (n=5). Group differences were tested using one-tailed unpaired Student's t-test with seedlings from the local provenance growing at ambient temperature (LP/AT) used as a control group.

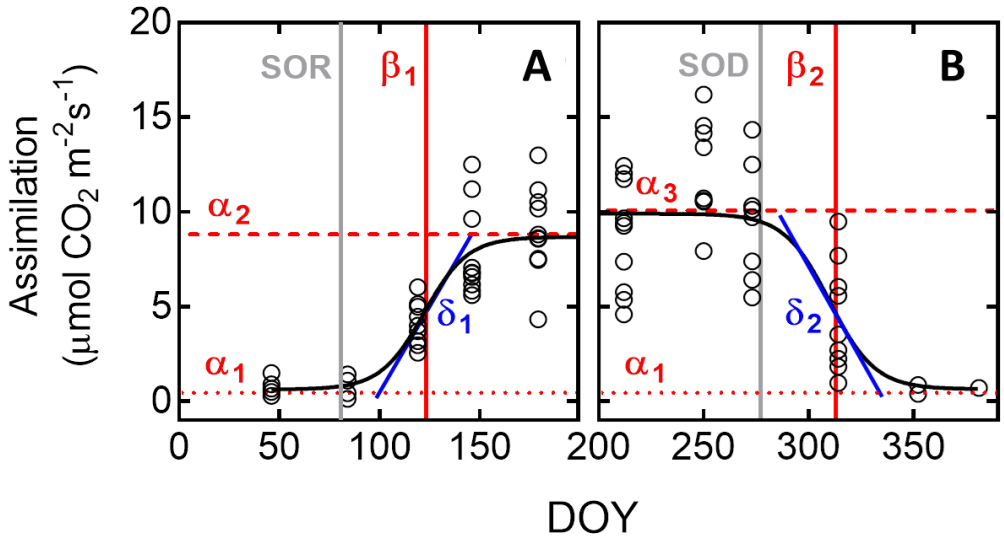

Figure 4.4 Scheme of the curve-fitting mechanism for a seasonal assimilation (*A*) time series during (A) spring and (B) autumn 2013. Adapted from Gonsamo *et al.* (2012).

In order to evaluate the strength of the relationship between PRI or CCI and other physiological and pigment parameters, R^2 values were obtained from linear regressions with parameter values and the slope was considered significantly different from zero when $P < 0.05$. Regressions were performed using GraphPad Prism 7 software version 7.03 (GraphPad Software, Inc., La Jolla, CA, USA). For autumn relationships, regressions were performed using data points from the 2012 and 2013 seasons pooled together.

4.4 Results

Seasonal weather patterns

The years of 2012 and 2013 were both characterized by warm autumns. In 2012, daily maximum temperatures remained above 20°C until the end of September and above 0°C until mid-November, with the first night frost recorded on October 8 (Fig. 4.5A). Winter 2012-2013 was warmer than normal, with above zero temperatures until mid-January. The lowest temperature recorded during winter was -20°C at the end of February (Fig. 4.5A). During spring 2013 the last night frost was recorded on 26 April and daily maximum temperatures above 20°C were recorded starting in early-May (Fig. 4.5A). The summer of 2013 was wetter than normal, with a total of 447 mm of rain from June to September (Fig. 4.5B). The highest temperature recorded during summer was 36°C in mid-July (Fig. 4.5A). During autumn 2013 daily maximum temperatures remained above 20°C until mid-October and above 0°C until early-December, with the first night frost recorded on 27 October (Fig. 4.5A).

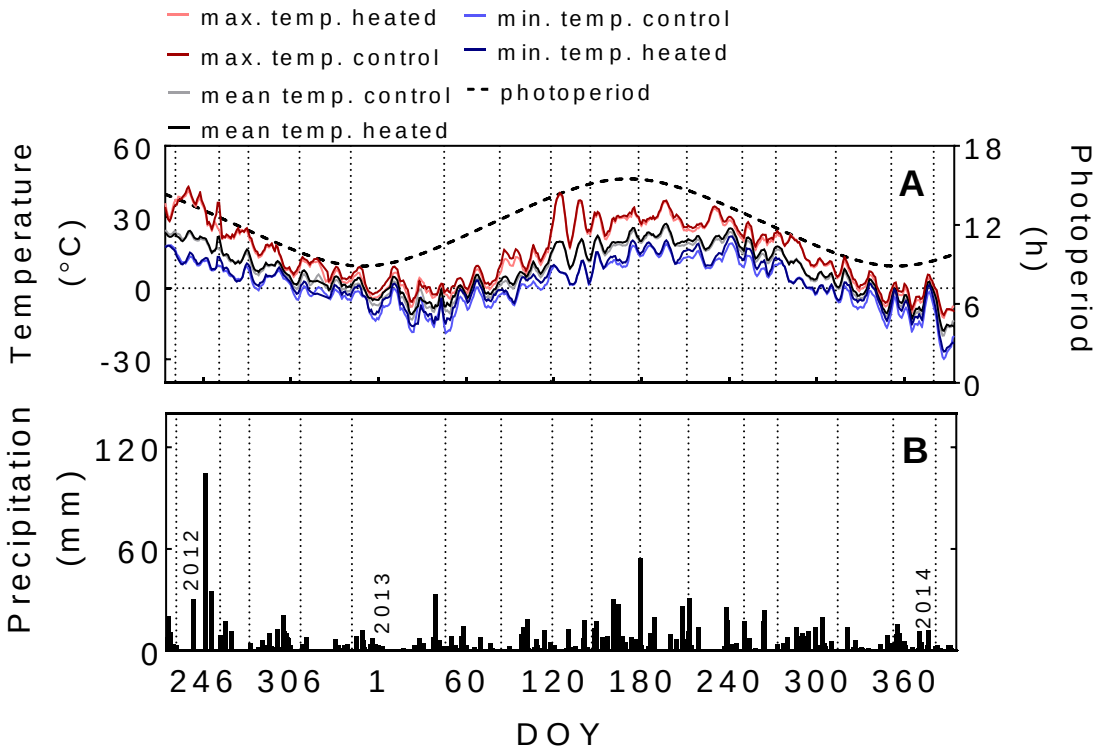

Figure 4.5 Seasonal variations in temperature, photoperiod and precipitation from 1 August, 2012 to 1 February, 2014 at Koffler Scientific Reserve in Ontario, Canada. (A) photoperiod (dashed line) and 5-day running average for minimum (light and dark blue lines), maximum (light and dark red lines) and mean (light and dark grey lines) daily temperature in the heated and control plots and (B) daily precipitation. Vertical dotted lines indicate sampling dates.

Seasonal variation of physiological and pigment parameters, as well as vegetation indices

During both autumns 2012 and 2013, maximal quantum yield of PSII (F_v/F_m) in local seedlings growing at ambient temperature (LP/AT) downregulated during October to December from summer values around 0.85 to winter values close to 0.1, while the recovery of F_v/F_m during spring 2013 occurred mainly during the months of April and May (Fig. 4.6A). Variations in the fraction of absorbed light used for photochemistry (Φ_{PSII}) followed similar timing, with winter values close to 0 and summer values close to 0.35. At the end of July, Φ_{PSII} values declined by approximately half (0.17) before rising back to 0.35 in August and September (Fig. 4.6B). This July Φ_{PSII} depression was paralleled by similar drops in assimilation (*A*) and stomatal conductance (g_s; Fig. 4.6C,D). *A* almost downregulated

completely during winter, declining from summer values around 12 μmol CO_2 $m^{-2}s^{-1}$ to winter values below 1 μmol CO_2 $m^{-2}s^{-1}$ (Fig. 4.6C). Patterns of g_s variation closely followed those of *A*, with typical summer values of 150 mmol H_2O $m^{-2}s^{-1}$ and winter values below 25 mmol H_2O $m^{-2}s^{-1}$ (Fig. 4.6D). Summer values for dark respiration (R_d) were approximately 1.5 μmol CO_2 $m^{-2}s^{-1}$ in 2012, and 1.2 μmol CO_2 $m^{-2}s^{-1}$in 2013, with winter values close to 0.2 μmol CO_2 $m^{-2}s^{-1}$ (Fig. 4.6E). The fraction of absorbed light dissipated via xanthophyll-regulated thermal dissipation (Φ_{NPQ}) was close to 0.6 during the summer months, but was downregulated to near zero values in winter (Fig. 4.6F). In contrast, the sum of fluorescence and constitutive thermal dissipation ($\Phi_{f,D}$) was at its lowest during summer months but peaked during winter, with values close to 1 (Fig. 4.6G). Carotenoid pigments (Car Chl^{-1}) rose from summer levels of approximately 250 mmol mol^{-1} to their maximal levels of 550 mmol mol^{-1} during winter 2013, but did not rise as much during winter 2014, where we observed maximal levels close to 400 mmol mol^{-1} (Fig. 4.6H). Similarly, zeaxanthin Chl^{-1} (Zea Chl^{-1}) rose from summer levels of 15 mmol mol^{-1} to its maximal level of approximately 140 mmol mol^{-1} during winter 2013, and to only 100 mmol mol^{-1} during winter 2014 (Fig. 4.6I). The de-epoxidation status of the xanthophyll cycle (DEPS) was close to 0.35 during summer months and rose to maximal values of 0.85 during winter months (Fig. 4.6J). We recorded PRI values of approximately 0 during summer months, and a decline to values of approximately -0.20 during winter (Fig. 4.6K). Finally, we recorded CCI values of approximately 0.3 during summer, and winter values slightly above 0 during winter (Fig. 4.6L). The July 2013 depression observed in Φ_{PSII}, *A* and g_s was also observed in CCI (Fig. 4.6B,C,D,L). Considering all parameters, mean SOD values for autumn ranged from 2 September to 6 October in 2012 and from 23 August to 15 October in 2013. In spring, mean SOR values ranged between 13 February and 13 March (Fig. 4.6).

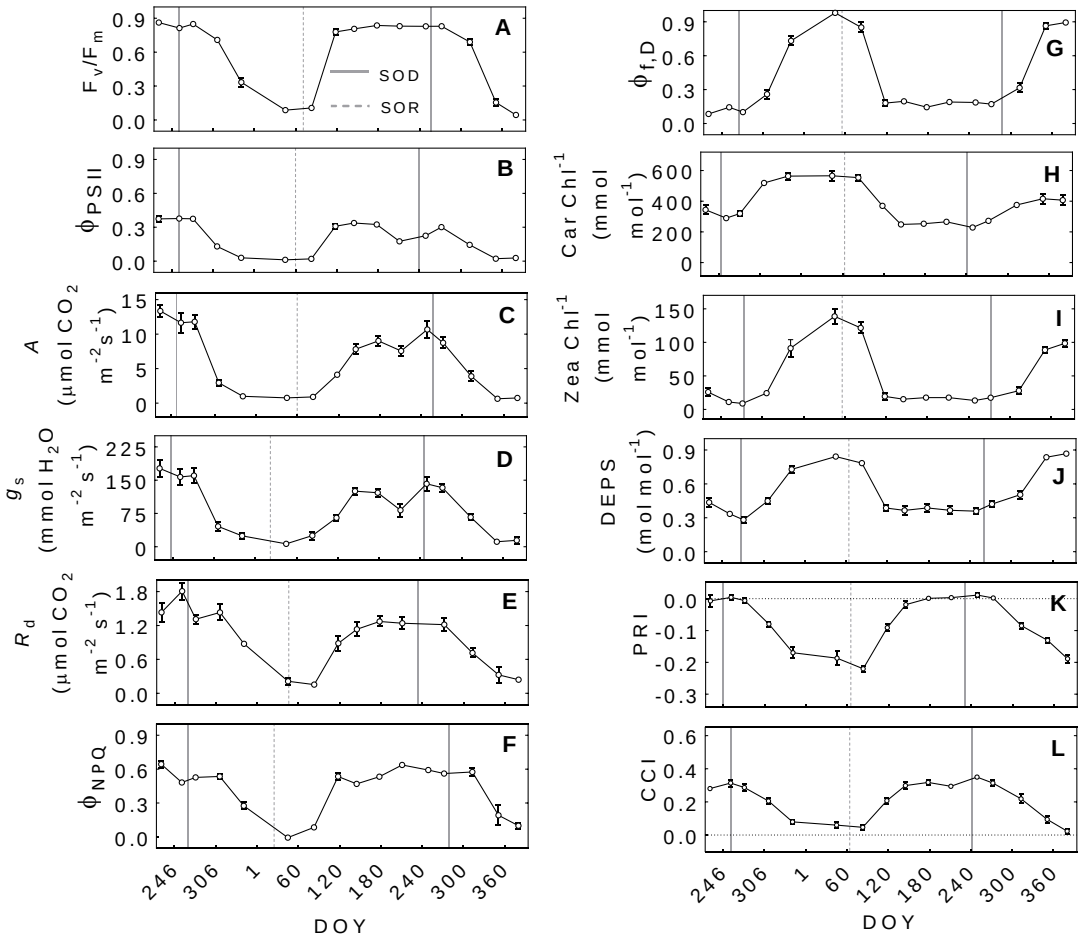

Figure 4.6 Time course of physiological and pigment parameters as well as vegetation index variation in seedlings from the local provenance (LP) of *P. strobus* growing at ambient temperature (AT). (A) F_v/F_m, maximal quantum yield of PSII; (B) Φ_{PSII}, fraction of absorbed light used for photochemistry at 1200 µmol $m^{-2}s^{-1}$ light intensity; (C) *A*, assimilation at 1200 µmol $m^{-2}s^{-1}$ light intensity; (D) g_s, stomatal conductance at 1200 µmol $m^{-2}s^{-1}$ light intensity; (E) R_d, dark respiration; (F) Φ_{NPQ}, fraction of absorbed light dissipated via xanthophyll-regulated thermal dissipation at 1200 µmol $m^{-2}s^{-1}$ light intensity; (G) $\Phi_{f,D}$, sum of fluorescence and constitutive thermal dissipation at 1200 µmol $m^{-2}s^{-1}$ light intensity; (H) Car Chl^{-1}, carotenoids Chl^{-1}; (I) Zea Chl^{-1}, zeaxanthin Chl^{-1}; (J) DEPS, the de-epoxidation status of the xanthophyll cycle, (K) PRI and (L) CCI. Each data point represents n = 6-10 seedlings ±SE. Vertical solid grey lines indicate mean start of downregulation (SOD) dates in autumn and dotted grey lines indicate start of recovery (SOR) in spring for each parameter.

Effect of seedling provenance on the phenology of photosynthesis during autumn

During both autumns 2012 and 2013, we generally observed a later start of downregulation (SOD) in most studied parameters for southern provenance seedlings growing at ambient temperature (SP/AT) compared to local provenance seedlings growing at ambient temperature (LP/AT), and earlier SOD for northern provenance seedlings growing at ambient temperature (NP/AT) compared to LP/AT seedlings (Fig. 4.7). Indeed, during autumn 2012, SOD for F_v/F_m was 15 days earlier ($p \leq 0.1$) in NP/AT seedlings than in LP/AT seedlings, whereas in autumn 2013, SOD for F_v/F_m was 17 days later ($p \leq 0.01$) in SP/AT seedlings than in LP/AT seedlings. During both autumns 2012 and 2013, SOD for the fraction of absorbed light used for photochemistry (Φ_{PSII}) followed the same trend as F_v/F_m (Fig. 4.7). During autumn 2012, SOD for assimiliation (A) was 14 days later ($p \leq 0.1$) in SP seedlings than in LP/AT seedlings. During autumns 2012 and 2013, SOD for stomatal conductance (g_s) and dark respiration (R_d) followed the same trend as A. During autumn 2012, SOD for the fraction of absorbed light dissipated via xanthophyll-regulated thermal dissipation (Φ_{NPQ}) was 9 days later ($p \leq 0.1$) in SP/AT seedlings than in LP/AT seedlings and 9 days later in 2013, although not significantly (Fig. 4.7), with $\Phi_{f,D}$ following the same trend in both years. During autumn 2012, SOD for carotenoids Chl^{-1} ($Car\ Chl^{-1}$) were 12 days later ($p \leq 0.05$) in SP/AT seedlings compared to LP/AT seedlings, and in 2013 it was 17 days earlier ($p \leq 0.01$) in NP/AT seedlings than in LP/AT seedlings (Fig. 4.7). In autumns 2012 and 2013, SOD for zeaxanthin Chl^{-1} ($Zea\ Chl^{-1}$) and the de-epoxidation status of the xanthophyll cycle (DEPS) followed the same trend as $Car\ Chl^{-1}$. During autumns 2012 and 2013, SOD for the photochemical reflectance index (PRI) was between 7 and 8 days earlier in SP/AT seedlings than in LP/AT seedlings, and between 7 and 10 days later in NP/AT seedlings, although the differences were not significant. Finally, during autumn 2012 SOD for the chlorophyll/carotenoid index (CCI) was 16 days earlier ($p \leq 0.1$) in NP/AT seedlings than in LP/AT seedlings (Fig. 4.7).

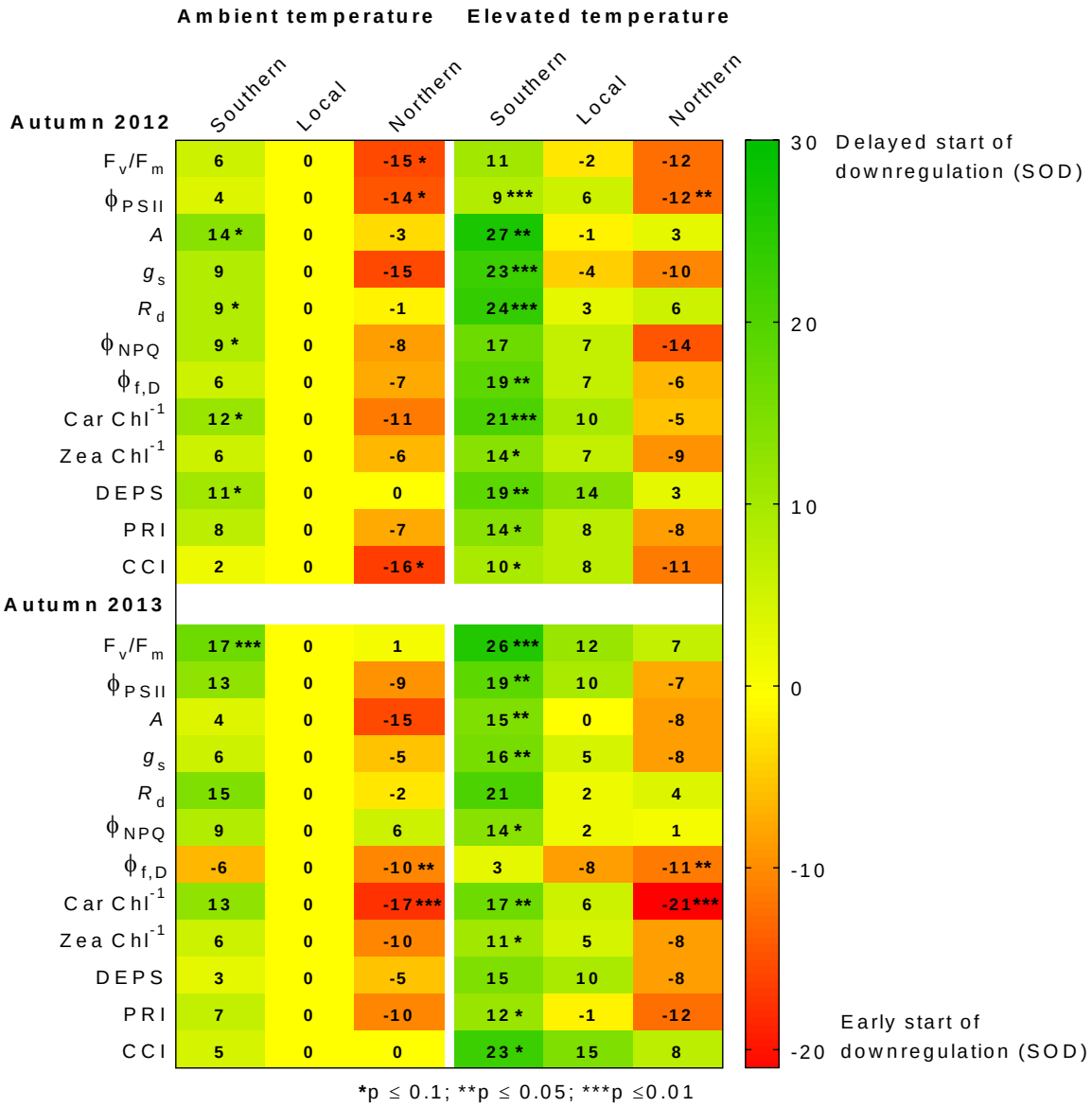

Figure 4.7 Effect of provenance and elevated temperature on the start of downregulation (SOD) of F_v/F_m, the maximal quantum yield of PSII; Φ_{PSII}, the fraction of absorbed light used for photochemistry at 1200 µmol m^{-2} s^{-1} light intensity; *A*, assimilation at 1200 µmol m^{-2} s^{-1} light intensity; g_s, stomatal conductance at 1200 µmol m^{-2} s^{-1} light intensity; R_d, dark respiration; Φ_{NPQ}, the fraction of absorbed light dissipated via xanthophyll-regulated thermal dissipation at 1200 µmol m^{-2} s^{-1} light intensity; $\Phi_{f,D}$, the sum of fluorescence and constitutive thermal dissipation at 1200 µmol m^{-2} s^{-1} light intensity; Car Chl^{-1}, carotenoids Chl^{-1}; Zea Chl^{-1}, zeaxanthin Chl^{-1}; DEPS, the de-epoxidation status of the xanthophyll cycle, PRI and CCI during autumns 2012 and 2013. Values represent differences between mean SOD in DOY calculated for LP/AT (control) seedlings and mean SOD calculated for each treatment and asterisks indicate significant differences with *$p \leq 0.1$; **$p \leq 0.05$ and ***$p \leq 0.01$. Positive values (green shades) indicate delayed SOD compared to LP/AT seedlings, whereas negative values (red shades) indicate early SOD.

Effect of seedling provenance on the phenology of photosynthesis during spring

When considering all studied parameters, the phenology of photosynthesis was less sensitive to seedling provenance during spring than during autumn. Still, during spring 2013, a major trend observed among our studied parameters was early start of recovery (SOR) in southern provenance seedlings growing at ambient temperature (SP/AT) and late SOR in northern provenance seedlings growing at ambient temperature (NP/AT) compared to control seedlings, i.e. local provenance seedlings growing at ambient temperature (LP/AT; Fig. 4.8). Specifically, SOR for the maximal quantum yield of PSII (F_v/F_m) was 10 days earlier ($p \leq 0.05$) in SP/AT seedlings than in LP/AT seedlings. SORs for other parameters were between 0 and 12 days earlier in SP seedlings than in LP seedlings, although the differences were not significant (Fig. 4.8). On the other hand, SORs for other parameters were between 0 and 13 days later in NP seedlings than in LP seedlings, although not significantly, with the exception of the SOR for g_s, which was 3 days earlier in NP seedlings than in LP seedlings, again not significantly (Fig. 4.8).

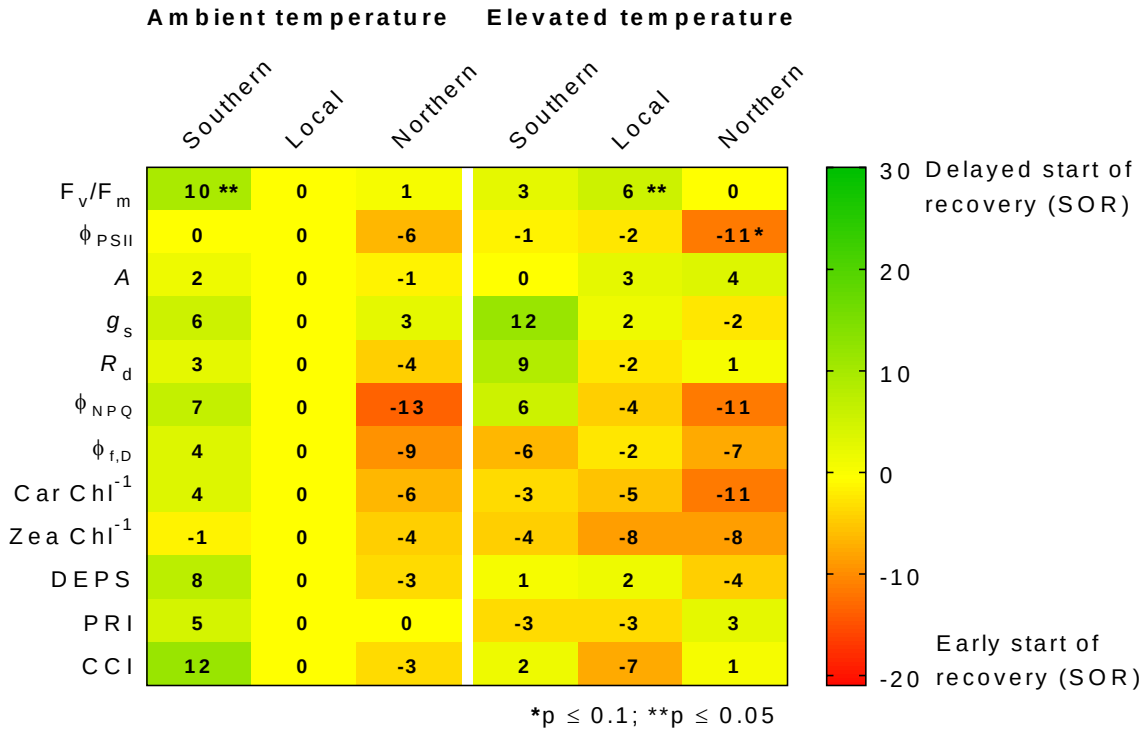

Figure 4.8 Effect of provenance and elevated temperature on the start of recovery (SOR) of F_v/F_m, the maximal quantum yield of PSII; Φ_{PSII}, the fraction of absorbed light used for photochemistry at 1200 µmol m^{-2} s^{-1} light intensity; *A*, assimilation at 1200 µmol m^{-2} s^{-1} light intensity; g_s, stomatal conductance at 1200 µmol m^{-2} s^{-1} light intensity; R_d, dark respiration; Φ_{NPQ}, the fraction of absorbed light dissipated via xanthophyll-regulated thermal dissipation at 1200 µmol m^{-2} s^{-1} light intensity; $\Phi_{f,D}$, the sum of fluorescence and constitutive thermal dissipation at 1200 µmol m^{-2} s^{-1} light intensity; Car Chl^{-1}, carotenoids Chl^{-1}; Zea Chl^{-1}, zeaxanthin Chl^{-1}; DEPS, the de-epoxidation status of the xanthophyll cycle; PRI and CCI during spring 2013. Values represent the difference between the SOR in DOY calculated for LP/AT (control) seedlings and the SOR calculated for each treatment. Positive values (green shades) indicate early SOR compared to LP/AT seedlings, whereas negative values (red shades) indicate delayed SOR. Asterisks indicate significant differences with *p ≤ 0.1 and **p ≤ 0.05. Positive values (green shades) indicate early SOR compared to LP/AT seedlings, whereas negative values (red shades) indicate late SOR.

Effect of seedling provenance on the response to elevated temperature during autumn and spring

During autumns 2012 and 2013, our elevated temperature treatment generally caused delayed SOD in all three provenances (Fig. 4.7; Table 4.1). Provenances, however, did not respond to warming to the same extent, with the southern provenance (SP) seedlings gaining the most extra days of physiological activity with warming, and the northern provenance

(NP) gaining the least extra days (Table 4.1). Specifically, considering all studied parameters, southern provenance seedlings growing at elevated temperature (SP/ET) gained on average 9 extra days during autumn 2012, which is significantly higher ($p \leq 0.05$) than the amount of extra days gained by local provenance seedlings growing at elevated temperature (LP/ET) and northern provenance seedlings growing at elevated temperature (NP/ET). During autumn 2013, SP/ET seedlings also gained on average 9 extra days, which was significantly higher ($p \leq 0.05$) than the amount of extra days gained by NP/ET seedlings. Finally, during spring 2013, there was no significant difference between the numbers of extra days gained by each provenance (Table 4.1).

Table 4.1 Effect of elevated temperature on the physiological activity of seedlings from southern (SP), local (LP) and northern (NP) provenances. Numbers indicate the difference in SOD during autumn or SOR during spring between seedlings of a given provenance growing at ambient temperature (AT) and seedlings of the same provenance growing at elevated temperature (ET). Different letters following means in the last column indicate significantly different means with $p \leq 0.05$.

	F_v/F_m	Φ_{II}	A	g_s	R_d	Φ_{NPQ}	$\Phi_{f,D}$	Car Chl^{-1}	Zea Chl^{-1}	DEPS	PRI	CCI	**Mean**
Autumn 2012													
SP	5	5	13	14	15	9	12	10	8	8	6	8	**9 a**
LP	-1	6	-1	-4	3	7	7	10	7	14	8	8	**5 b**
NP	3	2	6	5	7	-5	1	6	-3	3	-1	5	**2 b**
Spring 2013													
SP	7	2	2	-5	-6	6	10	7	3	6	9	11	**4 a**
LP	-6	2	-3	-2	2	2	2	5	7	-2	3	7	**1 a**
NP	1	5	-4	5	-4	-5	-1	5	4	2	-3	-3	**0 a**
Autumn 2013													
SP	8	7	11	9	6	6	10	4	5	12	7	18	**9 a**
LP	12	10	0	5	-8	2	-8	6	5	10	-1	15	**4 ab**
NP	6	2	7	-3	6	-4	1	-4	2	-3	-3	8	**1b**

Effectiveness of PRI and CCI for detecting physiological activity during autumn

During autumns 2012 and 2013, both PRI and CCI correlated significantly ($p \leq 0.05$) with all fluorecence, gas exchange and pigment parameters (Fig. 4.9). Of all parameters, we recorded the strongest relationships with F_v/F_m, for both PRI and CCI. Among the strongest

relationships also figured $\Phi_{f,D}$ and Φ_{PSII} (Fig. 4.9). In contrast, the weakest relationships we recorded were between PRI and CCI and the gas exchange parameters *A*, g_s and R_d. During autumn, PRI generally performed better than CCI at tracking all parameters. Indeed, while PRI performed similarly than CCI at tracking fluorescence parameters (F_v/F_m, Φ_{PSII}, Φ_{NPQ}, $\Phi_{f,D}$), it performed better than CCI at tracking gas exchange parameters (*A*, g_s, R_d) as well as photosynthetic pigment parameters (Car Chl^{-1}, Zea Chl^{-1} and DEPS; Fig. 4.9).

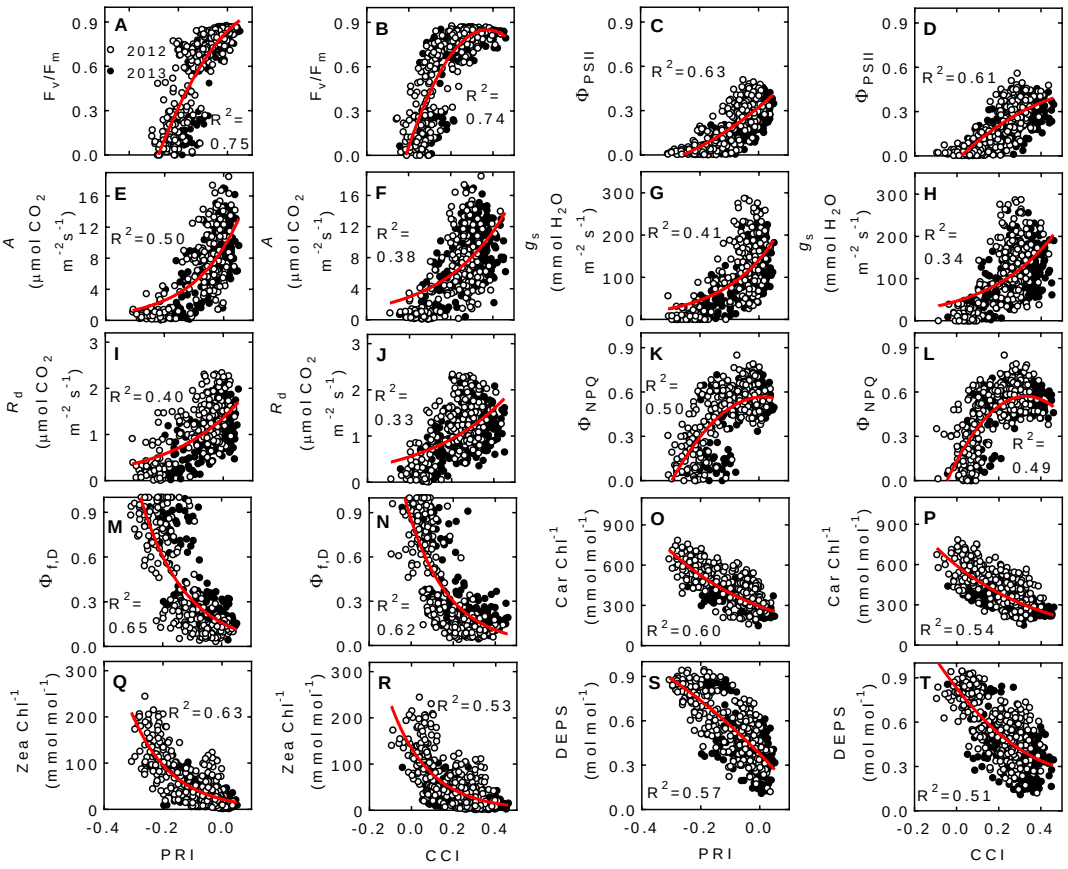

Figure 4.9 Relationships between the vegetation indices PRI and CCI and the physiological parameters (A-B) F_v/F_m, maximal quantum yield of PSII; (C-D) Φ_{PSII}, fraction of absorbed light used for photochemistry at 1200 μmol m^{-2} s^{-1} light intensity; (E-F) *A*, assimilation at 1200 μmol m^{-2} s^{-1} light intensity; (G-H) g_s, stomatal conductance at 1200 μmol m^{-2} s^{-1} light intensity; (I-J) R_d, dark respiration; (K-L) Φ_{NPQ}, fraction of absorbed light dissipated via xanthophyll-regulated thermal dissipation at 1200 μmol m^{-2} s^{-1} light intensity; (M-N) $\Phi_{f,D}$, sum of fluorescence and constitutive thermal dissipation at 1200 μmol m^{-2} s^{-1} light intensity; (O-P) Car Chl^{-1}, carotenoids Chl^{-1}; (Q-R) Zea Chl^{-1}, zeaxanthin Chl^{-1}; (S-T) DEPS, the de-epoxidation status of the xanthophyll cycle during autumn 2012 (empty circles) and 2013 (solid circles). All relationships were considered significant with $P < 0.05$.

Effectiveness of PRI and CCI for detecting physiological activity during spring

As was the case during the autumn season, both PRI and CCI showed a significant correlation ($p \leq 0.05$) with all studied parameters during spring 2013 (Fig. 4.10). Again, the strongest relationships were recorded for the parameter F_v/F_m, for both PRI and CCI. Strong relationships were also recorded for $\Phi_{f,D}$, Car Chl^{-1} as well as Zea Chl^{-1} (Fig. 4.10). As was the case during autumn, the gas exchange parameters A, g_s and R_d correlated poorly with PRI and CCI. Again, during spring PRI and CCI did not perform equally for different groups of parameters. For instance, CCI performed better than PRI with fluorescence parameters (F_v/F_m, Φ_{PSII}, Φ_{NPQ}, $\Phi_{f,D}$; Fig. 4.10). In contrast, PRI performed better than CCI tracking gas exchange parameters (A, g_s, R_d). During spring, two distinct clusters of data points were observed for the relationships between PRI and CCI and the fluorescence parameters F_v/F_m, Φ_{PSII}, Φ_{NPQ}, $\Phi_{f,D}$ and DEPS (Fig.4.10A,B,C,D,K,L,M,N,S,T). Indeed, parameter values either very low or very high, with an absence of intermediate values.

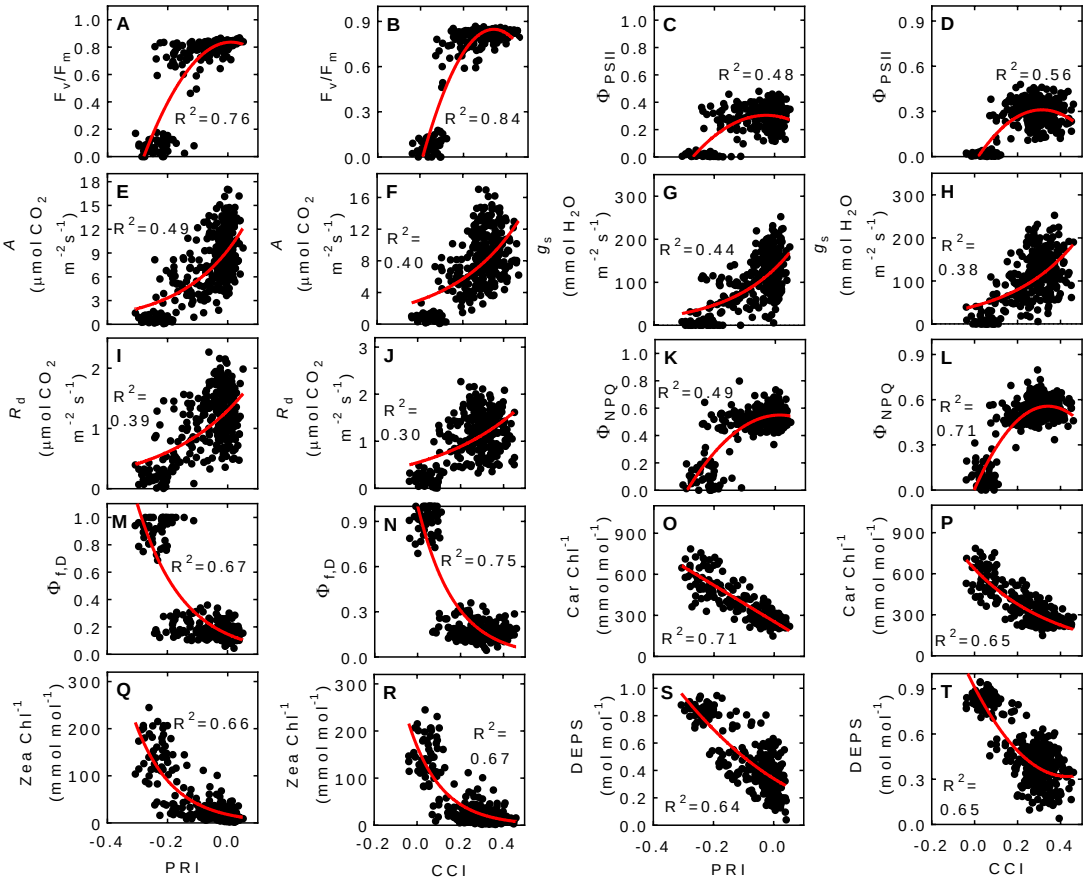

Figure 4.10 Relationships between the vegetation indices PRI and CCI and the physiological parameters (A-B) F_v/F_m, maximal quantum yield of PSII; (C-D) Φ_{PSII}, fraction of absorbed light used for photochemistry at 1200 μmol m^{-2} s^{-1} light intensity; (E-F) *A*, assimilation at 1200 μmol m^{-2} s^{-1} light intensity; (G-H) g_s, stomatal conductance at 1200 μmol m^{-2} s^{-1} light intensity; (I-J) R_d, dark respiration; (K-L) Φ_{NPQ}, fraction of absorbed light dissipated via xanthophyll-regulated thermal dissipation at 1200 μmol m^{-2} s^{-1} light intensity; (M-N) $\Phi_{f,D}$, sum of fluorescence and constitutive thermal dissipation at 1200 μmol m^{-2} s^{-1} light intensity; (O-P) Car Chl^{-1}, carotenoids Chl^{-1}; (Q-R) Zea Chl^{-1}, zeaxanthin Chl^{-1}; (S-T) DEPS, the de-epoxidation status of the xanthophyll cycle during spring 2013. All relationships were considered significant with $P < 0.05$.

4.5 Discussion

Seasonal peaks of photosynthetic activity coincide with peaks of qE type NPQ

At northern latitudes, plants are exposed to extremely contrasting weather conditions over the course of a year. For instance, at our field site in Southern Ontario, Canada (44°01'44"N, -79°32'21"W; Fig. 4.1), plants experience days of 15.5h sunlight at summer solstice, with daily temperatures commonly exceeding 30°C (Fig. 4.3, 4.5). At the opposite end of the year, plants receive as little as 8h sunlight per day at winter solstice, with temperatures generally remaining below zero during the entire winter season (Fig. 4.3, 4.5). Plant leaves that experience both climatic extremes, and all conditions in between, such as conifer needles, need to partition absorbed light energy between photochemistry and non-photochemical quenching (NPQ) to optimize photosynthesis while ensuring protection against potentially damaging elements such as excess light or freezing temperature (Müller *et al.* 2001, Demmig-Adams & Adams 2006a, Ensminger et al. 2006). Over the time course of this study, highest rates of photochemistry, as indicated by highest rates of CO_2 assimilation (A; approx. 10 μmol CO_2 m^{-2} s^{-1}; Fig. 4.6C), stomatal conductance (g_s; approx. 140 mmol H_20 m^{-2} s^{-1}; Fig. 4.6D) and of the fraction of absorbed light used for photochemistry (Φ_{PSII}; approx. 0.35; Fig. 4.6B) coincided with the period of the year with frost-free nights, i.e. the end of May until the end of September (Fig. 4.5). This reflects the limitations imposed by cold temperature on photosynthesis via decreased fluidity of the thylakoid membrane which limits the light reactions of photosynthesis (Vogg *et al*. 1998), limitations in the repair of the PSII reaction centre protein D1 (Kanervo *et al*. 1997), inhibited regeneration of ribulose 1,5-biphosphate (RuBP) and reduced efficiency of Ribulose-1,5-bisphosphate carboxylase/oxygenase (Rubisco) carboxylation, which limit carbon fixation in the Calvin-Benson cycle (Sage 2002). Further limitations on photosynthesis in the cold are due to inhibited plant water uptake (Kauffman 1975, Kramer 1983), slowed down cell division and differentiation (Rossi *et al*. 2008), and enzymatic reactions essential to growth and metabolism (Hüner *et al.* 1998). Concomitantly with high rates of photosynthesis, we recorded in our seedlings the highest rates of dynamic qE type NPQ, as indicated by a high fraction of absorbed light dissipated via xanthophyll-regulated

thermal dissipation values (Φ_{NPQ}; approx. 0.6; Fig. 4.6F). This indicates that although the warmth of summer months was favourable to photosynthesis, 60% of all light energy absorbed by needles was in excess of the sink capacity of photosynthesis, hence creating a need for safe dissipation of this excess light. This is consistent with other reports of large proportions of qE type NPQ in summer-adapted needles of *P. strobus* (Fréchette *et al.* 2015, 2016) and other conifer species such as *P. banksiana* (Busch *et al*. 2009). This also emphasizes the high capacities for qE type NPQ of slow-growing, long-lived evergreen species (Demmig-Adams *et al.* 2006a) such as *P. strobus*. Indeed, in order to survive in temperate and boreal climates, evergreens show a high propensity for photoprotection, along with a limited intrinsic capacity for photosynthesis and the ability to downregulate photosynthesis under stress. Because evergreens largely retain their chlorophyll, light energy is absorbed throughout the year, even when photosynthesis is downregulated during severe winter stress. The ability to dissipate absorbed light energy efficiently through thermal dissipation is therefore a prerequisite for winter survival.

Seasonal acclimation of dynamic and sustained non-photochemical processes

During both autumns 2012 and 2013, downregulation of photosynthesis occurred mainly during the months of October and November, period during which photoperiod lost 2 hours (11.7h to 9.6h) and daily mean temperature declined from approximately 13°C to 0°C (Fig. 4.5). During those months, *A* values declined to winter values just inferior to 1 μmol CO_2 m^{-2} s^{-1} (Fig. 4.6C). Following the initiation of photosynthetic downregulation, we observed the initiation of a gradual transition from qE type NPQ to the sustained qI type of NPQ as indicated by steadily increasing $\Phi_{f,D}$ values (Fig. 4.6G). By February 2013, just above 97% of all sunlight absorbed by needles was dissipated via qI type NPQ. This primed state of sustained energy dissipation was achieved through a doubling of the total carotenoids pool size (Fig. 4.6H), and a 10-fold increase of the photoprotective pigment zeaxanthin (Fig. 4.6I). Also, the xanthophyll cycle became arrested in its photoprotective form, with zeaxanthin no longer reconverting to violaxanthin upon dark-relaxation (Demmig *et al.* 1987, Öquist & Huner 2003; Zarter *et al*. 2006), as indicated by de-epoxidation status of the xanthophyll cycle (DEPS) values remaining above 0.8 during winter months (Fig. 4.6J). A

similar rise in sustained NPQ, coupled with the upregulation of the photoprotective carotenoid pigments lutein, neoxanthin, and the xanthophylls was reported by Chang *et al.* (2015) during the downregulation of photosynthesis of *P. strobus* seedlings exposed to natural autumn conditions. Interestingly, during both autumns 2012 and 2013 we observed a 3-week delay between the initiation of photosynthetic downregulation, and the initiation of Φ_{NPQ} decline (Fig. 4.6C,F). Similarly, the initiation of the rise of $\Phi_{f,D}$ occurred 3 weeks after photosynthesis initiated its downregulation, as well as the initiation of the rise of zeaxanthin and DEPS (Fig. 4.6G,I,J). This indicates that excess light energy resulting from the reduced sink for photosynthates after photosynthetic downregulation was initially dissipated via qE type NPQ, but replaced by qI type NPQ only after several days of stress caused by excess light. Since qI type NPQ is associated with sustained rearrangement or degradation of PSII core proteins degradation of PSII core proteins (Ensminger *et al*. 2004, Demmig-Adams and Adams 2006a) and *de novo* synthesis of zeaxanthin pigments (Adams & Demmig-Adams 1994, Filella *et al*. 2009), it is expected to take over only as other more reversible forms of NPQ are no longer sufficient for photoprotection (Demmig-Adams and Adams 2006a). Also, in this experiment qI type NPQ accumulated during autumn at temperatures much higher than those at which qE type NPQ is strongly inhibited (Fig. 4.5, 4.6). This was also reported by Porcar-Castell (2011) for field grown *P. sylvestris* and Fréchette *et al*. (2016) for *P. strobus* growing in controlled environments. This confirms that qE type and qI type NPQ are additive rather than exclusive, ensuring flexibility to photoprotection with fluctuating environmental conditions throughout the year.

Latitude of origin affects phenology of photosynthesis during autumn

Over two successive autumn seasons we observed in our seedlings a consistent provenance effect in the timing of downregulation of fluorescence, gas exchange, pigment parameters and vegetation indices. Indeed, seedlings originating from the southern site downregulated studied parameters up to 17 days later than seedlings from the local site, while seedlings from the northern site downregulated parameters up to 17 days earlier (Fig. 4.7). Interestingly, seedlings from all provenances followed the same sequence of autumn events, starting with photosynthetic downregulation, followed by the modulation of NPQ as indicated by declining qE type NPQ and upregulated qI type NPQ, as well as upregulated zeaxanthin and DEPS (Fig. 4.6). Provenances were simply naturally delayed or early with

this sequence, which suggests an inherent genetic control of the termination of photosynthesis. As is the case for the phenology of several developmental events such as bud set or growth cessation in a number of long-lived, late-successional tree species (Körner and Basler 2010; Hamilton *et al.* 2016), the genetic controls of autumn photosynthesis in *P. strobus* appear to be to some extent dictated by photoperiod. Indeed, seedlings originating from the southern latitude experience shorter photoperiods at the time when temperature is no longer favourable for photosynthesis (9.4h; Fig 4.3C), while seedlings from the northern latitude experience longer photoperiods (10.7h; Fig. 4.3A) at that cardinal time of the season. It is expected that seedlings adapted to the temperature and photoperiod regimes from their southern and northern sites keep exhibiting adaptive traits from their origin once transplanted to different latitudes (Savolainen *et al.* 2007). Previous studies reported genetic controls of autumn photosynthesis by photoperiod in trees. Under controlled conditions, authors have reported photosynthetic declines in summer-acclimated seedlings after sudden switches to short day conditions in *P. banksiana* (Busch *et al.* 2007) and *P. strobus* (Fréchette *et al.* 2016). In the field, Bauerle *et al.* (2012) observed peaks in photosynthetic capacity just after the summer solstice, and consistent declines with decreasing photoperiod in 23 temperate and boreal tree species from the genera *Acer*, *Betula*, *Gleditsia*, *Fraxinus*, *Paulownia*, *Prunus* and *Quercus*. On the other hand, Stinziano *et al.* (2015) did not conclude to photoperiodic regulation of the autumn decline of photosynthetic capacity of *Picea abies* growing under a +4°C autumn warming treatment. This suggests variation in the importance of photoperiodic control of photosynthesis during autumn among species. This highlights the need for a better understanding of photoperiod controls on photosynthesis in different tree species.

Latitude of origin affects phenology of photosynthesis during spring to a lesser extent

During spring 2013 we also observed a provenance effect in the timing of recovery of our fluorescence, gas exchange and pigment parameters, as well as vegetation indices, but to a lesser extent compared to the provenance effect observed during autumn (Fig. 4.6, 4.7). Seedlings originating from the southern site recovered parameters up to 10 days earlier than seedlings from the local site, while seedlings from the northern site recovered parameters up

to 13 days later, with most differences in recovery time not significant (Fig. 4.7). This indicates that the genetic controls of autumn photosynthesis by photoperiod are more prominent during autumn than during spring. A number of previous studies have reported the spring phenology of other developmental events such as budburst to be more strongly controlled by temperature than photoperiod (e.g. Bronson *et al.* 2009; Laube *et al.* 2014). We suggest that this difference is due to the necessity for conifers to cold-acclimate and build up frost-hardiness in time during autumn to prevent damage to tissues before the first frost episodes. Indeed, in early autumn the buildup of frost hardiness is initiated as short photoperiod induces dormancy and the termination of growth, even before exposure to low temperatures (Strand and Öquist 1998; Öquist and Hüner 2003). Upon exposure to low temperatures later in the season, full frost hardiness is induced and causes a strong suppression of photosynthesis during the day as was demonstrated in *P. contorta* (Savitch *et al.* 2002). Strong photoperiodic control of frost hardiness was demonstrated by Rostad *et al.* 2006 in *Picea abies* exposed to a combination of natural and artificial photoperiod, and recently by Chang *et al*. (2015) in field-grown *P. strobus* seedlings exposed to natural declining autumn photoperiod. On the other hand, the spring de-hardening and recovery of photosynthesis of evergreen conifers were reported to be closely linked to the increase of air temperature above 0°C (Tanja *et al*. 2003, Sevanto *et al.* 2006), as was the case in this study (Fig. 4.5, 4.6). Above-zero temperatures facilitate biochemical reactions involved in repair and reorganization of the photosynthetic apparatus (Ensminger *et al*. 2004, 2006).. Weak or absent photoperiodic control of spring photosynthesis allows for *P. strobus* to take advantage of warm temperature early on during the spring season.

Greater potential for elongated photosynthetically active season during autumn in southern provenance with elevated temperature

During both autumn seasons, the sensitivity of seedlings to our elevated temperature treatment differed depending on provenance, with seedlings from the southern provenance benefiting the most from elevated temperature with the most extra days of photosynthesis while seedlings from the northern provenance benefitting the least (Table 4.1). Genetic controls of autumn photosynthesis by photoperiod are likely to explain this trend, with northern seedlings being adapted to a long photoperiod threshold of 10.7h (Fig. 4.3A) at the

time when temperature is no longer favorable to photosynthesis (Fig. 4.3B) at it site of origin, and, therefore, constrained to terminate photosynthesis once it was reached. Conversely, once temperature became unfavorable to photosynthetic activity, southern seedlings had not yet reached their shorter, critical autumn photoperiod threshold of 9.4h (Fig 4.3C) and could, therefore, benefit from elevated temperature. This implies that in a future climate, generally warmer autumn temperatures should have a positive effect on photosynthesis until photoperiod thresholds are met, after which new genotypes will have to emerge, which will likely take a few tree generations to achieve (Körner and Basler 2010). The observed differences between the capacities of genotypes from different latitudes to exploit warming will have important implications for forestry, such as the need to reassess the suitability of provenances used in forest regeneration (Hänninen and Tanino 2011). In the light of our results, assisted migration initiatives that aim to transfer southern genotypes northward will prevent photoperiodic regulation of photosynthesis during autumn, allowing trees to benefit from warmer conditions. However, moving genotypes northward might result in tree populations with increased sensitivity to cold episodes during spring and autumn, which might offset extra carbon gains due to warmer climate (Hänninen *et al*. 2005; Man *et al.* 2009; Chang *et al*. 2015).

PRI and CCI can track the photoprotective status of needles throughout the year

This study aimed to assess the suitability of two vegetation indices, the photochemical reflectance index (PRI) and the chlorophyll/carotenoid index (CCI) to track the phenology of photosynthesis and the associated changes in energy partitioning and photosynthetic pigment contents during spring and autumn. Our results indicate that both indices constitute good proxies for our studied parameters, i.e. F_v/F_m, Φ_{PSII}, A, g_s, R_d, Φ_{NPQ}, $\Phi_{f,D}$, Car Chl^{-1}, Zea Chl^{-1} and DEPS, as all correlated significantly ($p \leq 0.05$) with both PRI and CCI during spring and autumn (Fig. 4.9, 4.10). Specifically, both indices generally performed best tracking the metrics F_v/F_m, Φ_{PSII} and $\Phi_{f,D}$ (Fig. 4.9, 4.10), which are indicative of the energy partitioning status of needles. The parameter F_v/F_m indicates the potential for light absorption by the light-harvesting complexes (LHC) of PSII, and declines from its maximal value of 0.85 at the first signs of plant stress (Fig. 4.6; Maxwell and Johnson 2000; Baker

2008). Under cold stress, declines in F_v/F_m to values close to 0 reflect a reorganisation of the thylakoid membrane and associated membrane-bound proteins (Verhoeven *et al.* 2009; Ensminger *et al.* 2004). The metrics Φ_{PSII} and $\Phi_{f,D}$ are direct indicators of the photoprotective state of needles, with Φ_{PSII} declining to near-zero values under cold stress and $\Phi_{f,D}$ rising to values close to 1 with the buildup of cold-induced qI type NPQ (Fig. 4.6). The results indicate that PRI and CCI can both be indicators of the degree of cold stress imposed on the photosynthetic apparatus throughout the year.

During spring, our data indicate differences in the rate of recovery of fluorescence, gas exchange and pigment parameters. Indeed, fluorescence parameters generally recovered to near summer values very quickly once maximal daily air temperature rose above freezing, along with rapid relaxation of the de-epoxidation status of the xanthophyll cycle (DEPS). Gas exchange and other pigment parameters, on the other hand, recovered much more gradually after maximum daily temperatures rose above freezing, taking several weeks to recover to summer values. This trend is illustrated in Fig. 4.6 and also in Fig. 4.10, where point clouds for the parameters F_v/F_m, Φ_{PSII}, Φ_{NPQ}, $\Phi_{f,D}$ and DEPS (Fig. 4.10A,B,C,D,K,L,M,N,S,T) form two distinct clusters, with values either very low, indicative of downregulated vegetation, or very high, as typically observed in vegetation acclimated to summer conditions. This trend was not observed for gas exchange and other pigment parameters, with the presence of intermediate values indicating a much slower recovery of gas exchange processes as well as slower adjustments of chorophyll and carotenoid pool sizes. During spring, recovery of the quantum yield of photosynthesis, along with the relaxation of DEPS values were reported by Ensminger *et al.* (2008) within the first 24h of warming episodes in winter-acclimated Scots pine (*P. sylvestris*). This reflects the fast rearrangement of the thylakoid membrane system, and the slower rate of the changes required to completely restore carbon fixation and metabolism (Ensminger *et al.* 2008). Fréchette *et al.* (2015) also reported such differences in the rate of recovery of spring processes, with the recovery of quantum yield, the relaxation of DEPS and the transition from qI type NPQ to qE type NPQ occurring very quickly upon exposure to above-zero temperatures during a simulated winter-spring transition in *P. strobus.* As was the case in the present study, adjustments of chlorophyll and carotenoid pool sizes occurred at a much slower rate than other processes, which reflects the need for photoprotection with air

temperature fluctuations during the spring season, even after photosynthetic recovery. While our measurements were performed on a monthly basis, future work should aim to characterize the spring recovery of fast-recovering parameters such as fluorescence parameters, as well as DEPS, with higher temporal resolution measurements. This will allow a more accurate characterization of the relationship between these parameters and PRI and CCI.

PRI and CCI can also track the variation of photoprotective pigment pools throughout the year

It is not surprising that PRI and CCI also correlated strongly with the metrics Car Chl^{-1} and Zea Chl^{-1}, since PRI was initially formulated for the detection of the diurnal variations of xanthophyll cycle pigments to assess the light-use efficiency of photosynthesis (Gamon *et al.* 1992, 1997, Peñuelas *et al.* 1995), while CCI was formulated to detect seasonal variations in the ratios of chlorophylls to carotenoids pool sizes as a proxy for plant stress (Gamon *et al.* 2016). In this study, the observed doubling under winter conditions of the total carotenoids pool size, including the pigments violaxanthin, antheraxanthin, zeaxanthin, neoxanthin, lutein, α-carotene and β-carotene (Fig. 4.6H), and the 10-fold increase of the photoprotective pigment zeaxanthin (Fig. 4.6I) occurred concomitantly with photosynthetic downregulation and the increase of qI type quenching. Indeed, carotenoids play a two-fold role in photoxidative damage avoidance under cold stress by (1) being active thermal energy quenchers (Niyogi et al. 2005, Demmig-Adams and Adams 2006b) and (2) being important reactive oxygen species (ROS) scavengers (Jahns and Holzwarth 2012; Trebst 2003; Telfer 1994, 2005, 2014). At seasonal timescales, close relationships between PRI and carotenoid to chlorophyll ratios were reported for conifers such as *P. sylvestris* (Filella *et al.* 2009), *P. strobus* (Fréchette *et al.* 2015, 2016), *P. contorta* and *P. ponderosa* (Wong and Gamon 2015a). Recently, similar results were reported in *P. contorta* using CCI (Gamon *et al.* 2016) and in *P. mariana*, *P. banksiana* and *P. glauca* for both indices (Springer *et al*. 2017). Our results suggest that the remote detection of carotenoid pigments using either PRI or CCI can help infer the phenology of photosynthesis by detecting yearly variations in the stress status of *P. strobus* subjected to severe cold stress during winter.

Photosynthetic carbon assimilation is not well detected by PRI and CCI

During both autumn and spring, the metrics that correlated the least with PRI and CCI were those of photosynthetic gas exchange, i.e. A, g_s and R_d (Fig. 4.9, 4.10). The biological basis of both PRI and CCI is their capacity to detect the spectral signature of pigments involved in the dissipation of excess light and, hence, the efficiency of photosynthesis. However, seasonal adjustments of energy sinks that do not directly involve the xanthophyll cycle pigments might cause a decoupling between the amount of energy dissipated by a plant and its photosynthetic efficiency. For instance, Porcar-Castell *et al.* (2012) reported such decoupling in the relationship between photosynthetic efficiency and PRI in early spring when the foliage of *P. sylvestris* was deeply downregulated and most NPQ was facilitated by qI type quenching. Also in early spring, Fréchette *et al.* (2015) recently demonstrated that in *P. strobus* an important proportion of absorbed energy is used for ATP production via cyclic electron transport around PSI. Other alternative energy sinks that could potentially introduce a decoupling in the relationship between PRI and photosynthetic efficiency include photorespiration during summer (Ögren 1984), state transition quenching (Lunde *et al.* 2000), as well as PSII and PSI reaction centre quenching (Öquist and Hüner 2003). It is expected that these energy sinks introduce a decoupling in the relationship between photosynthetic efficiency and CCI as well. Finally, while both indices correlated significantly with all studied parameters, PRI and CCI performed differently depending on the season of the year. For instance, both indices performed similarly tracking fluorescence parameters (F_v/F_m, Φ_{PSII}, Φ_{NPQ}, $\Phi_{f,D}$) during autumn (Fig. 4.9) while CCI performed better than PRI during spring (Fig. 4.10). During both autumn and spring, PRI correlated more strongly than CCI with gas exchange parameters (A, g_s, R_d) and photosynthetic pigment parameters (Car Chl^{-1}, Zea Chl^{-1} and DEPS; Fig. 4.9, 4.10). Furthermore, when photosynthesis was impaired by a dry spell during July 2013, CCI was able to detect the lower A, g_s and Φ_{PSII} values while PRI could not. Both PRI and CCI are integrated using bands of the spectrum located on either side of the green reflectance 'bump' (531 and 570 nm for PRI, 531 nm and 645 nm for CCI). Both, therefore, compare reflectance in the blue, i.e. the chlorophylls and carotenoids absorption region of the spectrum, with the reflectance in the orange and red regions of the spectrum, where absorption is limited to chlorophylls. Because CCI is integrated using reflectance at 645 nm, which is more strongly absorbed by

chlorophylls, an enhanced sensitivity to chlorophyll pool sizes is expected with the CCI, which might explain the observed differences in our data. Furthermore, Springer *et al.* (2017) reported the presence of snow to be confounding in the seasonal interpretation of the CCI, which is also sensitive to structural changes in canopies. What is clear from our data is that both indices appear to provide complementary information and should be used together for optimal detection performance at different times of year.

4.6 Conclusions

Our results demonstrate genetic controls of autumn and spring photosynthesis by photoperiod in *P. strobus* as indicated by differences in the phenology of seedlings originating from northern, local and southern provenances located along a 1000 km latitudinal gradient. We also show that seedlings follow the same sequence of autumn events regardless of provenance, starting with photosynthetic downregulation, followed by the modulation of NPQ and adjustments of pigment chlorophyll and carotenoid pool sizes. The differences in phenology were more important during autumn than during spring, indicating stronger genetic controls of photosynthesis by photoperiod during autumn than spring. We also demonstrate a greater potential for elongated photosynthetically active season during autumn with elevated temperature in seedlings originating from the southern latitude, and photoperiodic constraints in the northern latitude seedlings. Our results indicate that assisted migration initiatives that will consist in moving genotypes northward will prevent photoperiodic regulation of photosynthesis during autumn, allowing trees to benefit from warmer conditions. The vegetation indices PRI and CCI were both effective at tracking the seasonal variations of the energy partitioning status of *P. strobus* needles, as well as the amounts of the carotenoid pigments indicative of the stress status of needles throughout the year.

4.7 Acknowledgements

Financial support from NSERC and Canada Foundation for Innovation to IE is gratefully acknowledged. EF acknowledges the receipt of a Graduate Student Research Award from the University of Toronto Center for Global Change Science, Ph.D. funding from the Department of Cell and Systems Biology at the University of Toronto and Ontario Graduate Scholarships. Authors are also grateful to Laura Junker for her contribution on pigment

analysis, Attey Rostami and Ziguo Zhao for help in the field, Christopher Juliao, Daniel Marsden and Dhyani Patel for their assistance in the laboratory and Petra D'Odorico for assistance with data analysis.

Chapter 5

5 Conclusions and Future Directions

In this thesis, we investigated the potential for additional photosynthesis during warmer springs and autumns in the evergreen conifer *Pinus strobus* L. as well as the suitability of the photochemical reflectance index (PRI) to detect changes in the phenology of photosynthesis during spring and autumn. Specifically, we studied the impacts of temperature and photoperiod on photosynthetic efficiency, energy partitioning and photosynthetic pigment content during spring and autumn transitions, and the seasonal variations in their relationships to PRI. The presented results establish that photosynthesis in the evergreen conifer *P. strobus* might be enhanced in the spring and autumn in warmer climates. However, a certain degree of photoperiodic regulation of photosynthesis is to be expected during autumn, which might prevent a linear increase of photosynthesis with increasing temperature. Also, the interpretation of PRI in evergreen vegetation should take into account alternative energy sinks present during spring and autumn transitions, especially under cold conditions. This last chapter discusses our findings in the context of three main research hypotheses and proposes avenues for future research that develop from the presented work.

5.1 Hypothesis 1 : Photoperiodic constraints on the initiation of photosynthetic recovery in the spring and, particularly, photosynthetic downregulation in the autumn might prevent trees from benefiting from warmer conditions during those seasons, partly offsetting any potential for prolonged carbon gain due to warm temperatures.

Downregulation of photosynthesis in *P. strobus* is induced upon exposure to short photoperiod

In the work presented in this thesis we demonstrate that the downregulation of photosynthesis is not only regulated by cold temperature, but is also regulated by photoperiod. During autumn, short photoperiod and cold temperature act as signals for growth cessation and/or downregulation of photosynthesis in conifers. It has been widely established in the literature that low temperature is a major constraint to photosynthesis (e.g. Öquist and Hüner 2003). At northern latitudes, photosynthesis decreases upon exposure to cold autumn days before being completely suppressed at subfreezing temperatures during winter (Lloyd *et al*. 2002, Ensminger *et al*. 2004). Cold temperature imposes limitations on both the light and dark reactions of photosynthesis by decreasing the fluidity of membranes, the availability of liquid water, and inhibiting the rate of reactions involved in photochemistry, growth and metabolism. Exposure to short photoperiod, on the other hand, was shown to result in sugar starvation in species such as *Arabidopsis* (Gibon *et al*. 2009) and *Populus* (Hoffman *et al*. 2010), and induce hormonal inhibition of growth (Paparelli *et al*. 2013), reduced rate of starch turnover, and a decrease in protein and amino acid content of leaves (Gibon *et al*. 2009).

The sensitivity of photosynthetic downregulation to photoperiod seems, however, to vary widely among species. Körner and Basler (2010) reported long-lived, late-successional species (such as *P. strobus*) to be generally sensitive to photoperiod, while shorter-lived, early-successional species generally adopt a more risky life-strategy and respond mainly to variations in air temperature. In evergreen conifers, decreasing temperature was often reported to be the main environmental signal that drives the downregulation of photosynthesis (Lundmark *et al.* 1998, Öquist and Huner 2003, Ensminger *et al.* 2006,

Stinziano *et al.* 2015, Chang *et al.* 2016). A few studies, however, have suggested that photosynthesis may be downregulated in response to short photoperiod (Busch *et al.* 2007).

In the experiment presented in Chapter 2 of this thesis, the greatest declines in photosynthetic carbon assimilation and stomatal conductance were observed in seedlings exposed to both short photoperiod and cold temperature (SD/LT; Fig. 2.4D,E). However, we also observed a considerable decline in net photosynthetic CO_2 assimilation with exposure to short photoperiod only (Fig. 2.1, 2.4, 2.5). This suggests that photoperiod indeed plays a role in the autumn downregulation of photosynthesis in *P. strobus*. Most remarkably, the response of carbon assimilation to a decrease in photoperiod was already observed on the first short day of the experiment, with a loss of almost half of the photosynthetic activity that was observed under simulated summer conditions.

While drastic and sudden photoperiod declines such as that imposed in the experiment presented in Chapter 2 never occur in nature, photoperiodic control of autumn photosynthetic downregulation in *P. strobus* was validated in the field under exposure to natural photoperiod declines in the experiment presented in Chapter 4. Indeed, in seedlings from a northern, local and southern provenance, we observed a clear provenance effect in the timing of downregulation of photosynthesis and other related physiological, and pigment parameters, as well as vegetation indices, which downregulated more than two weeks earlier in the northern provenance and more than 2 weeks later in the southern provenance. This indicates adaptation to photoperiods of the sites of origin, and genetic controls of autumn photosynthesis dictated by photoperiod that remain after being transplanted to a new site, as reported for a number of other adaptive traits in common garden experiments (Savolainen *et al.* 2007).

Photoperiodic control of photosynthesis in *P. strobus* is not as strong in the spring as it is in the autumn

In the field experiment presented in Chapter 4 of this thesis, the weak provenance effect observed in the timing of the spring recovery of our physiological and pigment parameters, as well as vegetation indices, was not statistically significant, in contrast to the autumn downregulation of photosynthesis. A number of previous studies have reported the spring

phenology of other developmental events such as budburst to be more strongly controlled by temperature than photoperiod (e.g. Bronson *et al.* 2009; Laube *et al.* 2014). During spring, the recovery of photosynthesis in conifers was reported to be opportunistic and closely linked to the increase of air temperature above 0°C (Tanja *et al.* 2003, Sevanto *et al.* 2006) which facilitates biochemical reactions involved in repair and reorganization of the photosynthetic apparatus (Ensminger *et al*. 2004, 2006). This concurs with results from Ensminger *et al.* (2004, 2008) and Zarter *et al.* 2006, who reported quick recovery of photosynthesis with increasing air temperature during spring, as well as rapid downregulation with the occurrence of cold episodes.

P. strobus partitions energy differently under cold and warm autumn conditions

In Chapter 2 of this thesis, we show that seedlings exposed to different combinations of temperature and photoperiod utilize different strategies to regulate the light use efficiency of photosynthesis. To ensure optimum plant performance in ever-changing light environments, leaves constantly acclimate to balance the amount of light absorbed and their requirements for energy utilization (Ensminger *et al*. 2006). Plants use different strategies to maintain a balance between the energy they absorb and the energy utilized for photochemistry. One strategy is the regulation of light-use efficiency (LUE), i.e. the partitioning of absorbed light energy between photochemical and non-photochemical pathways (Demmig-Adams and Adams 2006a, Ensminger *et al.* 2006). During summer, the harmless removal of excess light, referred to as non-photochemical quenching (NPQ), is mediated by xanthophyll cycle pigments. Excess light energy rapidly induces the de-epoxidation of xanthophyll cycle pigments, i.e. the conversion of violaxanthin into the energy quenching antheraxanthin and zeaxanthin (Niyogi *et al*. 2005, Demmig-Adams and Adams 2006a, Verhoeven 2014). As temperatures decline during autumn, the xanthophyll cycle is arrested in a state primed for sustained energy quenching where zeaxanthin is retained, chlorophylls are partially degraded, photosystem (PS) II core units are reorganized (Ensminger *et al*. 2006, Demmig-Adams and Adams 2006a, Verhoeven 2014) and photoprotective pigments such as lutein and β-carotene are upregulated (Adams and Demmig-Adams, 1994, Ottander *et al*. 1995, Filella *et al*. 2009, Verhoeven 2014).

In the growth chamber experiment presented in Chapter 2, seedlings exposed to cold autumn conditions (SD/LT) showed increased zeaxanthin Chl^{-1} and DEPS values, indicating enhanced dissipation of excess energy via the xanthophyll cycle. On the other hand, plants exposed to warm autumn conditions (or short day only) did not show enhanced dissipation of excess energy via the xanthophyll cycle, despite reduced CO_2 assimilation and a decrease in LUE. Instead, we observed a moderate decrease in light-harvesting Chl, indicating a physical reduction of the size of the light harvesting complexes (Ensminger *et al*. 2004, 2006), a significant increase in the ratio of lutein and β-carotene to Chls (Fig. 2.5G,H; Table 2.S1) as well as an increase of β-carotene (Table 2.S1). It has been established that lutein and β-carotene act as important radical scavengers (e.g. Jahns and Holzwarth 2012, Trebst 2003, Telfer 1994, 2005, 2014). These pigments can act as alternative quenchers of excess energy, as suggested by Busch *et al*. (2007), who observed low DEPS and elevated levels of β-carotene in *P. banksiana* seedlings exposed to a warm autumn (short day) treatment. Although these xanthophyll cycle independent mechanisms were observed in both the cold and warm treated seedlings, they were enhanced under warm autumn (short day) conditions to balance the reduced metabolic sink capacity when exposed to short autumn photoperiod in the absence of sustained NPQ.

When considered altogether, these results suggest that in the future, warmer temperatures during autumn will allow for photosynthesis in *P. strobus* to carry on longer into the season. A certain degree of photoperiodic regulation of autumn photosynthesis is, however, to be expected, and will not allow for a linear increase of carbon assimilation with increasing temperature. Photoperiodic regulation will occur once temperature thresholds fall outside the natural range of variation of genotypes, becoming out of phase with photoperiod thresholds. Trees exposed to warm temperatures and constraining photoperiods during autumn might exhibit xanthophyll cycle independent mechanisms, such as enhanced radical scavenging by carotenoid pigments. Our results also indicate that photoperiodic limitation is likely to be minimal in *P. strobus* during spring, which will allow for additional carbon uptake at the beginning of the growing season.

Given the potential for elongated photosynthetically active season, especially in the spring, future research should investigate the effects of regulation by temperature sum accumulation, which was shown to regulate other phenologic processes such as growth

cessation in other tree species (Viherä-Aarnio *et al.* 2005, Hänninen and Tannino 2011), and which might introduce additional variation in the timing of photosynthetic downregulation during autumn. Additionally, the effects of respiration during spring and, particularly during autumn should be further investigated. Indeed, the possibility of enhanced respiration due to increased temperature (Piao *et al.* 2008) at a time when photosynthesis in constrained by photoperiod might temporarily convert forest ecosystems into carbon sources, especially during autumn, thereby affecting atmospheric carbon.

5.2 Hypothesis 2 : During spring and autumn, NPQ mechanisms that are independent of zeaxanthin-regulated qE type NPQ might be an important proportion of NPQ. Since these zeaxanthin independent mechanisms are undetected by spectral measurements, photochemical quenching and LUE are likely overestimated by the PRI during those seasons.

At a diurnal timescale, the range of PRI variation reflects the capacity for photoconversion of xanthophyll cycle pigments

In the experiments presented in Chapter 2 and 3 of this thesis, we confirm previous observations by Gamon *et al.* (1992, 1997) that variations of xanthophyll de-epoxidation are reflected by PRI at a diurnal scale. Non-photochemical quenching (NPQ) contributes to photoprotection and ROS formation avoidance by safely dissipating excess excitation energy in the form of heat. As mentioned above, during summer the main component of NPQ is the energy-dependent component, qE (Müller *et al*. 2001, Demmig-Adams and Adams 2006a). This component is triggered at a timescale of seconds by light-induced proton transport across the thylakoid membrane, which creates a pH gradient and conformational change of photosystem (PS) II (Ruban *et al*. 2012). In addition, the de-epoxidation of the xanthophyll cycle pigments, i.e. the conversion of the pigment violaxanthin into antheraxanthin and zeaxanthin (Demmig-Adams & Adams 2005, Niyogi *et al*. 2005) occurs at a timescale of minutes and is quickly reversible upon dark-relaxation (Müller *et al*. 2001). Since changes in the de-epoxidation state (DEPS) of xanthophyll cycle pigments modify leaf spectral reflectance at 531 nm, variations in the qE component of NPQ

is detectable with the photochemical reflectance index (PRI). The other major component of NPQ is called qI, and replaces qE under prolonged and severe light stress, such as that experienced during winter when photosynthesis is arrested (Müller *et al*. 2001, Demmig-Adams and Adams 2006a). The qI type quenching involves the upregulation of xanthophyll cycle pigments and the retention of zeaxanthin upon dark-relaxation.

In the autumn growth chamber experiments presented in Chapter 2 of this thesis, we observed in summer-acclimated seedlings ΔPRI, i.e. the difference between the dark state of PRI and the PRI obtained under saturating light conditions, of 0.037 (Fig. 2.1F). This value gradually declined with photosynthetic downregulation to values close to 0. This shows that a reduction of ΔPRI in needles acclimating to cold conditions reflect the deactivation of the dynamic regulation of the xanthophyll cycle in the cold, i.e. of qE type NPQ (Fig. 2.1D). This was validated in the spring growth chamber experiment presented in Chapter 3, where we observed ΔPRI values corresponding to the proportion of qE type quenching in our spring treatments. Gamon & Berry (2012) previously reported ΔPRI values in needles exposed to different light environments within a tree canopy, but in the present experiments we compared for the first time ΔPRI values of needles during seasonal transitions to/from cold-induced qI type NPQ.

Different rates of recovery cause decoupling of PRI and LUE during early stages of spring

A significant finding of the work presented in Chapter 3 is the observation of different rates of recovery of spring processes, which caused a decoupling of PRI and LUE in early spring. Indeed, immediately after transfer to our spring treatments, we observed that the recovery of the light reactions of photosynthesis and of CO_2 assimilation, as well as the reduction of zeaxanthin pools and a relaxation of DEPS, which occurred concomitantly with the transition from qI type NPQ to qE type NPQ (Fig. 3.3, 3.4). On the other hand, levels of Chl FW^{-1} and Car Chl^{-1} did not recover from winter stress until after day 12 of the experiment, as was the case for PRI (Fig. 3.3, 3.4). These differences in the timing of recoveries indicate that during the early stages of photosynthetic recovery, xanthophyll cycle dynamics are not

the main factor controlling PRI. Variations in LUE are, therefore, not accurately detected during that time.

The PRI–LUE relationship is impaired by exposure to cold conditions due to the presence of cold-induced alternative energy sinks

Authors have previously observed a discrepancy between PRI and variations in photosynthesis during early spring in *Pinus banksiana* Lamb (Busch *et al.* 2009) and *Pinus* sylvestris (Porcar-Castell *et al.* 2012). Despite these observations, it was unclear which mechanisms were responsible for the discrepancy in the relationship between PRI and LUE under cold conditions. In the experiments presented in Chapters 2 and 3, by combining fluorescence and spectral reflectance measurements we could demonstrate that the discrepancy in the LUE-PRI relationship occurs with the cold-induced buildup of sustained qI type NPQ. We demonstrated that under cold conditions, a large proportion of excess light energy is dissipated via qI type NPQ, but that this mechanism is not reflected at the wavelengths used to integrate the PRI signal, making it undetectable by the PRI. With most dissipated energy undetected by the PRI under cold conditions, we confirmed our hypothesis that the PRI overestimates the LUE of photosynthesis in cold-acclimated needles.

In addition to qI type sustained NPQ, we identified additional electron sinks likely to contribute to the PRI-LUE discrepancy reported under cold conditions. One such mechanism is radical scavenging by carotenoid pigments, which was enhanced under cold conditions as indicated by increased pool sizes of carotenoid pigments such as beta-carotene and lutein (Fig. 2.5 and 3.4).

Furthermore, in the experiment presented in Chapter 3, we demonstrate the presence of another mechanism, cyclic electron transport around PSI, further contributing to the discrepancy in the PRI-LUE relationship. Indeed, under winter conditions, we observed that the functionality of PSI was much less affected than PSII (Table 2; Fig. 3.1, 3.2). While PSII electron transport was suppressed almost completely (Fig. 3.2A), approximately 50% of the capacity observed in summer needles was preserved in PSI (Fig. 3.2B), which concurs with results from Ivanov *et al*. (2001) who observed that PSI has a higher level of resistance to winter stress compared to PSII. The observed imbalance between electron transport at PSII

and PSI pointed to enhanced cyclic electron transport around PSI (Johnson, 2011). This indicated that in winter-acclimated seedlings, electron flow around PSI plays a considerable role in the removal of excess light. In addition, since oxidized P700 can efficiently quench chlorophyll fluorescence (Öquist and Hüner 2003), we concluded that PSI was likely an important quencher of absorbed light in winter-acclimated seedlings, further contributing to the discrepancy in the PRI-LUE relationship.

At seasonal time-scales, PRI is mostly controlled by cold-induced variations in carotenoid and chlorophyll pigment pool sizes

Early studies on the photochemical reflectance index (PRI) have established that both short- and long-term pigment adjustments lead to changes in leaf spectral properties. In evergreen conifers, PRI was reported to be a good proxy for xanthophyll cycle dynamics over the course of a day (Nakaji *et al.* 2006; Harris *et al.* 2014). Recent studies have also reported good correlations between PRI and LUE over longer timescales, i.e. seasons (Filella *et al.* 2009, Garbulsky *et al.* 2011, Wong and Gamon 2015a,b). In Chapters 2 and 3 of this thesis, we reported for the first time a combination of both sources of PRI variation, i.e. diurnal and seasonal, thereby allowing a direct comparison of the patterns and extent of both sources. We showed that PRI variation resulting from long-term pigment pool adjustments was almost three times larger during autumn and six times larger during spring than PRI variation resulting from changes in the DEPS of the xanthophyll cycle (Figures 2.1, 2.4, 3.3 and 3.7). Specifically, we identified the ratio of Car to Chls to be the single most important factor controlling PRI variation at seasonal timescales. This new evidence suggests that on an annual scale, seasonal pigment adjustments simply mask diurnal variations in PRI, especially during the transition between qE type NPQ and qI type NPQ.

In Chapter 4, we validate this observation in field-grown *P. strobus* seedlings during one spring season and two autumn seasons. For instance, during both autumn seasons, PRI varied closely along with the doubling of the total carotenoids pool size (Fig. 4.6H), and the 10-fold increase in zeaxanthin (Fig. 4.6I). These pigment adjustments occurred concomitantly with photosynthetic downregulation and the build-up of qI type quenching, reflecting the essential role of carotenoids in photoxidative damage avoidance under cold

stress. In Chapter 4, we also investigated the chlorophyll/carotenoid index (CCI), a vegetation index recently formulated to detect seasonal variations in the ratios of chlorophylls to carotenoids pool sizes as a proxy for plant stress (Gamon *et al.* 2016). During our spring and autumn transitions, CCI varied very closely with PRI, and exhibited the same strong relationships with total carotenoids and zeaxanthin pool sizes.

These results suggest that the PRI and CCI can both be useful proxies for seasonal variations in conifer photosynthetic efficiency, not for their capacity to detect the LUE of photosynthesis *per se*, but for their capacity to detect variations in the carotenoid pigments that are indicative of conifer stress status. In that context, both indices can constitute helpful tools for tracking the spring and autumn phenology of photosynthesis. We conclude that the PRI and CCI should be used together, since our results suggest a complementarity between both indices, with one of them performing better than the other at different times of year. Future research should, therefore, focus on determining optimal vegetation index combinations for specific species combinations, seasons of the year and other environmental conditions (e.g. presence of snow, stand age, canopy structure) that are likely to introduce additional sources of variation in spectral signals.

5.3 Hypothesis 3: Because genotypic characteristics determine phenology, yearly photosynthetic capacity will not increase linearly with an increase in temperature. Both temperature and photoperiodic cues might be necessary to initiate photosynthetic recovery in the spring and photosynthetic downregulation in the autumn. When transferred to a common garden, tree seedlings adapted to northern and southern conditions will face photoperiodic constraints on photosynthesis, unless they exhibit enough phenotypic plasticity to acclimate to local temperature and photoperiod regimes.

Latitude of origin affects phenology of photosynthesis during autumn

In the field experiment presented in Chapter 4, we studied the phenology of photosynthesis in seedlings from three provenances of *P. strobus* – a northern, a local and a southern

provenance - representing a 1000 km latitudinal gradient, to test the hypothesis of photoperiodic regulation of photosynthesis during spring and autumn. Over two successive autumn seasons, we observed a consistent provenance effect in the timing of downregulation of photosynthesis, as well as related physiological and pigment parameters, and vegetation indices. Interestingly, seedlings from all provenances followed the same sequence of autumn events, starting with photosynthetic downregulation, followed by the modulation of NPQ and adjustments of chlorophyll and carotenoid pool sizes (Fig. 4.6). Provenances were simply naturally delayed or early with this sequence, which suggests an inherent genetic control of the termination of photosynthesis. Seedlings from the southern site downregulated photosynthesis later than seedlings from the local site, while seedlings from the northern site downregulated photosynthesis earlier (Fig. 4.7). These results indicate that the genetic controls of autumn photosynthesis in *P. strobus* appear to be to some extent dictated by photoperiod, as indicated by results obtained in the growth chamber experiment presented in Chapter 2 of this thesis. In our field experiment, seedlings originating from the southern latitude experienced shorter photoperiods at the time when temperature was no longer favorable for photosynthesis (9.4h; Fig 4.3C), while seedlings from the northern latitude experienced longer photoperiods (10.7h; Fig. 4.3A) at that cardinal time of the season. It is expected that seedlings adapted to the temperature and photoperiod regimes from their southern and northern sites keep exhibiting adaptive traits from their origin once transplanted to different latitudes (Savolainen et al. 2007). During spring, however, the provenance effect observed in the timing of recovery of photosynthesis and other physiological and pigment parameters, as well as vegetation indices, was not statistically significant (Fig. 4.6, 4.7). Again, this indicates that the genetic controls of autumn photosynthesis by photoperiod are more prominent during autumn than during spring.

Greater potential for elongated photosynthetically active season during autumn in southern provenance with elevated temperature

During both autumn seasons studied in Chapter 4, the sensitivity of *P. strobus* to our elevated temperature treatment differed depending on provenance, with seedlings from the southern provenance benefiting the most from elevated temperature with the most extra days of photosynthesis while seedlings from the northern provenance benefitting the least (Table

4.1). Genetic controls of autumn photosynthesis by photoperiod are likely to explain this trend, with northern seedlings being adapted to a longer photoperiod threshold than seedlings at the local site at the time when temperature is no longer favorable to photosynthesis at the northern site and, therefore, constrained to terminate photosynthesis once it was reached. Conversely, once temperature became unfavorable to photosynthetic activity, southern seedlings had not yet reached their shorter, critical autumn photoperiod threshold and could, therefore, benefit from elevated temperature.

These results imply that in a future climate, generally warmer temperatures should have a positive effect on photosynthesis during spring, which will offer the greatest potential for extra carbon assimilation throughout the year. During autumn, warmer temperatures will allow for extra photosynthesis until photoperiod thresholds are met, after which new genotypes will have to emerge, which will likely take a few tree generations to achieve (Körner and Basler 2010). The observed differences between the capacities of genotypes from different latitudes to exploit warming will have important implications for forestry, such as the need to reassess the suitability of provenances used in forest regeneration (Hänninen and Tanino 2011). In the light of our results, assisted migration initiatives that will consist in planting *P. strobus* genotypes from southern locations will prevent photosynthesis from being limited during warmer autumns due to photoperiodic regulation of photosynthesis. However, moving *P. strobus* genotypes northward might result in tree populations with increased sensitivity to cold episodes during spring and autumn, which might offset extra carbon gains due to warmer climate (Hänninen *et al*. 2005; Man *et al.* 2009; Chang *et al*. 2015). Furthermore, while this thesis focused on the effects of temperature and photoperiod on the spring and autumn phenology of photosynthesis, the interactions between these factors and other important environmental factors likely to vary with the ongoing climate change will introduce additional variation in the response of trees to future climate. Such factors include, among others, rising atmospheric concentrations of CO_2, varying soil water availability, as well as increased frequency of extreme climatic events such as droughts and ice storms. Future research initiatives should, through provenance trials, aim to identify species and genotypes with the highest degree of phenotypic plasticity exhibited in response to predicted climate for specific regions, to increase the potential for extra carbon assimilation under future climates.

5.4 Future directions

The results presented in this thesis establish that photosynthesis in the evergreen conifer *P. strobus* might be enhanced in the spring and autumn in warmer climates. However, a certain degree of photoperiodic regulation of photosynthesis is to be expected during autumn, which might prevent a linear increase of photosynthesis with increasing temperature. Due to the absence of photoperiodic regulation of photosynthesis during spring, this season will offer the greatest potential for increased annual carbon uptake when climate warms in the future.

Photoperiodic regulation of photosynthesis, as indicated in our study by differences in the start and end of the photosynthetically active season in provenances from different latitudes, offers the opportunity to identify genotypes able to exploit warmer temperatures at the beginning, and, especially, end of the season. Future research should, therefore, study larger tree populations through provenance trials for identifying the genotypes that will perform better in future climates. Such trials will allow the identification of genotypes most suited not only for the predicted temperatures of future climates but also for predicted atmospheric CO_2 concentrations, soil water availability, as well as predicted extreme climatic events such as drought episodes and ice storms. Such studies should be conducted over several growing seasons to investigate, among other things, the effects of regulation by temperature sum accumulation, which might introduce additional variation in the timing of photosynthetic downregulation during autumn.

The interpretation of PRI in evergreen vegetation should take into account alternative energy sinks present during spring and autumn transitions, especially under cold conditions. Indeed, in *P. strobus*, energy sinks that do not involve energy dissipation via the dynamic of xanthophyll cycle pigments introduce a discrepancy in the relationship between PRI and photosynthetic efficiency. This implies that the use of the PRI for assessments of the light use efficiency of photosynthesis of northern-latitude conifers will lead to its overestimation, especially in the cold, where a number of non-photochemical quenching mechanisms and energy sinks act in concert to ensure photoprotection. In fact, a single vegetation index is unlikely to reflect the higly integrated photoprotective responses of conifers throughout the year. Future research initiatives should focus on identifying other combinations of

wavelengths or combinations of vegetation indices indicative of the actual light-use efficiency of evergreen conifers for different times of year.

Our research demonstrated that PRI varies seasonally with variations of the carotenoid pigments indicative of the stress status of needles throughout the year. In that context, the PRI constitutes a helpful tool for tracking the spring and autumn phenology of photosynthesis, but not for its capacity to detect the light-use efficiency of photosynthesis *per se*. Instead, the PRI is rather useful to detect variations in the carotenoid pigments that are indicative of conifer stress status. Again, our research suggests that optimal results are attained by using the PRI together with other vegetation indices such as the CCI.

Finally, investigating the relationship between the photosynthetic efficiency of vegetation and PRI at the needle level allowed for a deeper understanding of the physiological mechanisms, e.g. variations in photosynthetic pigments, adjustments in energy partitioning strategies, behind the relationship. Ultimately, the understanding of the physiological mechanisms should help to improve remote sensing of vegetation at larger spatial scales. This requires validation of our findings at the stand and ecosystem scales, where solar angle, canopy and stand structure or soil cover represent additional sources of variation in spectral reflectance and are likely to introduce scatter in the relationship between the physiological state of vegetation and spectral signals. When derived using spectral data collected by sensors mounted on remote platforms such as flux towers, aircrafts or satellites, the PRI will constitute a useful proxy for tracking changes in the spring and autumn phenology of photosynthesis at spatial scales ranging from a few meters to several kilometers. Ultimately, such knowledge will be crucial in understanding the spatial and temporal patterns of carbon fluxes between the biosphere and the atmosphere in a changing climate.

Bibliography

Adams III WW, Demmig-Adams B (1994) Carotenoid composition and down regulation of photosystem II in three conifer species during the winter. Physiologia Plantarum 92:451-458.

Aitken SN, Bemmels JB (2016) Time to get moving: assisted gene flow of forest trees. Evolutionary Applications 9: 271–290.

Asada K. (2000) The water–water cycle as alternative photon and electron sinks. Philosophical Transactions of the Royal Society B 355:1419–1431.

Avenson T, Ahn T, Niyogi K, Ballottari M, Bassi R, Fleming G (2009) Lutein Can Act as a Switchable Charge Transfer Quencher in the CP26 Light-harvesting Complex. Journal of Biological Chemistry 284:2830–2835.

Baker NR (2008) Chlorophyll Fluorescence: A Probe of Photosynthesis In Vivo. Annual Review of Plant Biology 59:89–113.

Barber J, Andersson B (1992) Too much of a good thing: light can be bad for photosynthesis. Trends in biochemical sciences 17:61–6.

Barichivich J, Briffa KR, Ranga B, Myneni RB, Osborn TJ, Melvin TM, Ciais P, Piao S and Tucker C (2013) Large-scale variations in the vegetation growing season and annual cycle of atmospheric CO_2 at high northern latitudes from 1950 to 2011. Global Change Biology 19(10): 3167-3183.

Bauerle W, Oren R, Way D, Qian S, Stoy P, Thornton P, Bowden J, Hoffman F, Reynolds R (2012) Photoperiodic regulation of the seasonal pattern of photosynthetic capacity and the implications for carbon cycling. Proceedings of the National Academy of Sciences of the United States of America 109:8612–8617.

Bergh J, Linder S (1999) Effects of soil warming during spring on photosynthetic recovery in boreal Norway spruce stands. Global Change Biology 5:245–253.

Bergh J, Freeman M, Sigurdson B, Kellomäki S, Laitinen K, Niinistö S, Peltola H, and Linder S (2003) Modelling the short-term effects of climate change on the productivity of selected tree species in Nordic countries. Forest Ecology and Management 183: 327–340

Bolhàr-Nordenkampf HR, Haumann J, Lechner EG, Postl WF, Schreier V (1993) Seasonal changes in photochemical capacity, quantum yield, P700-absorbance and carboxylation efficiency in needles from Norway spruce. In Photosynthetic Responses to the Environment, ed. HY Yamamoto, CM Smith, pp. 193–200. Rockville, MD: Am. Soc. Plant Physiol.

Bonan G (2008) Forests and Climate Change: Forcings, Feedbacks, and the Climate Benefits of Forests. Science 320:1444-1449.

Bräutigam K, Vining K, Lafon-Placette C, Fossdal C, Mirouze M, Marcos J, Fluch S, Fraga M, Guevara M, Abarca D, Johnsen O, Maury S, Strauss SH, Campbell MM, Rohde A, Díaz-Sala C, Cervera MT (2013) Epigenetic regulation of adaptive responses of forest tree species to the environment. Ecology and evolution 3:399–415.

Bronson DR, Gower ST, Tanner M, Van Herk I (2009) Effect of ecosystem warming on boreal black spruce bud burst and shoot growth. Global Change Biology 15:1534–1543.

Busch F, Hüner NP, Ensminger I (2007) Increased air temperature during simulated autumn conditions does not increase photosynthetic carbon gain but affects the dissipation of excess energy in seedlings of the evergreen conifer Jack pine. Plant Physiology 143:1242–51.

Busch F, Hüner NP, Ensminger I (2008) Increased air temperature during simulated autumn conditions impairs photosynthetic electron transport between photosystem II and photosystem I. Plant Physiology 147:402–14.

Busch F, Hüner NPA, Ensminger I (2009) Biochemical constrains limit the potential of the photochemical reflectance index as a predictor of effective quantum efficiency of photosynthesis during the winter spring transition in Jack pine seedlings. Functional Plant Biology 36:1016-1026.

Butler WL (1978) Tripartite and bipartite models of the photochemical apparatus of photosynthesis. Ciba Foundation symposium 61:237-256.

Chang C, Unda F, Zubilewich A, Mansfield S, Ensminger I (2015) Sensitivity of cold acclimation to elevated autumn temperature in field-grown *Pinus strobus* seedlings. Frontiers in Plant Science 6:165.

Cheng YB, Middleton EM, Hilker T, Coop, NC, Black TA, Krishnan P (2009) Dynamics of spectral bio-indicators and their correlations with light use efficiency using directional observations at a douglas-fir forest. Measurement Science and Technology 20(9):095107.

Ciais P, Tans PP, Trolier M, White JWC, Francey RJ (1995) A large Northern Hemisphere terrestrial CO_2 sink indicated by the 13C 12C ratio of atmospheric CO_2. Science 269:1098-1102.

Dall'Osto L, Lico C, Alric J, Giuliano G, Havaux M, Bassi R (2006) Lutein is needed for efficient chlorophyll triplet quenching in the major LHCII antenna complex of higher plants and effective photoprotection in vivo under strong light. BMC Plant Biology 6:32.

Dauwe R, Holliday JA, Aitken SN, Mansfield SD (2012) Metabolic dynamics during autumn cold acclimation within and among populations of Sitka spruce (*Picea sitchensis*). New Phytologist 194**:** 192–205.

de Boeck H, Kimball B, Miglietta F, Nijs I (2012) Quantification of excess water loss in plant canopies warmed with infrared heating. Global Change Biology 18: 2860–2868.

Demmig B, Winter K, Krüger A, Czygan F-C (1987) Photoinhibition and zeaxanthin formation in intact leaves. A possible role of the xanthophyll cycle in the dissipation of excess light. Plant Physiology 84: 218–224.

Demmig-Adams B (1990) Carotenoids and photoprotection in plants: A role for the xanthophyll zeaxanthin. Biochimica et Biophysica Acta 1020:1-24.

Demmig-Adams B, Adams W (1990) The carotenoid zeaxanthin and 'high-energy-state quenching' of chlorophyll fluorescence. Photosynthesis Research 25:187-197.

Demmig-Adams B, Adams III WW (2006a) Photoprotection in an ecological context: the remarkable complexity of thermal energy dissipation. New Phytologist 172:11–21.

Demmig-Adams B, Ebbert V, Mellman DL, Mueh KE, Schaffer L, Funk C, Zarter CR, Adamska I, Jansson S, Adams WW (2006b) Modulation of PsbS and flexible versus sustained energy dissipation by light environment in different species. Physiologia Plantarum 127**:** 670–680.

Demmig-Adams B, Cohu CM, Muller O, Adams WW (2012) Modulation of photosynthetic energy conversion efficiency in nature: from seconds to seasons. Photosynthesis Research 113: 75-88.

Drolet GG, Huemmrich KF, Hall FG, Middleton EM, Black TA, Barr AG, Margolis, HA (2005) A MODIS-derived photochemical reflectance index to detect inter-annual variations in the photosynthetic light-use efficiency of a boreal deciduous forest. Remote Sensing of Environment 98(2-3):212-224.

Drolet GG, Middleton EM, Huemmrich KF, Hall FG, Amiro BD, Barr AG, Black TA, McCaughey JH, Margolis HA (2008) Regional mapping of gross light-use efficiency using MODIS spectral indices. Remote Sensing of Environment 112(6):3064-3078.

Ensminger I, Sveshnikov D, Campbell D, Funk C, Jansson S, Lloyd J, Shibistova O, Öquist G (2004) Intermittent low temperatures constrain spring recovery of photosynthesis in boreal Scots pine forests. Global Change Biology 10:995-1008.

Ensminger I, Foerster J, Hagen C, Braune W (2005) Plasticity and acclimation to light reflected in temporal and spatial changes of small-scale macroalgal distribution in a stream. Journal of Experimental Botany 56(418):2047-2058.

Ensminger I, Busch F, Hüner N (2006) Photostasis and cold acclimation: sensing low temperature through photosynthesis. Physiologia Plantarum 126:28-44.

Ensminger I, Schmidt L, Lloyd J (2008) Soil temperature and intermittent frost modulate the rate of recovery of photosynthesis in Scots pine under simulated spring conditions. New Phytologist 177:428-42.

Ensminger I, Chang CYY, Bräutigam K (2015) Tree Responses to environmental cues. In Adam-Blondon A-F & Plomion C (Eds), Land Plants - Trees (pp. 229-263). Elsevier Ltd.

Environment Canada (2018**)** Canadian Climate Normals 1981-2010. [online] Available at: http://climate.weather.gc.ca/climate_normals/index_e.html [Accessed 31 Jul. 2018].

Farrar, JL (2003) Trees in Canada. 3rd Ed. Fitzhenry & Whiteside Ltd. 502 pp.

Filella I, Porcar-Castell A, Munné-Bosch S, Bäck J, Garbulsky M, Peñuelas J (2009) PRI assessment of long-term changes in carotenoids/chlorophyll ratio and short-term changes in de-epoxidation state of the xanthophyll cycle. International Journal of Remote Sensing 30(17):4443–4455.

Fracheboud Y, Luquez V, Björkén L, Sjödin A, Tuominen H, and Jansson S (2009) The control of autumn senescence in European Aspen. Plant Physiology 149:1982–1991.

Franks S, Weber J, Aitken S (2013) Evolutionary and plastic responses to climate change in terrestrial plant populations. Evolutionary Applications 7:123-139.

Fréchette E, Ensminger I, Bergeron Y, Gessler A, Berninger F (2011) Will changes in root-zone temperature in boreal spring affect recovery of photosynthesis in *Picea mariana* and *Populus tremuloides* in a future climate? Tree Physiology 31(11):1204-1216.

Fréchette E, Wong CY, Junker LV, Chang CYY, Ensminger I (2015) Zeaxanthin-independent energy quenching and alternative electron sinks cause a decoupling of the relationship between the photochemical reflectance index (PRI) and photosynthesis in an evergreen conifer during spring. Journal of Experimental Botany 66(22):7309-7323.

Fréchette E, Chang CYY, Ensminger I (2016) Photoperiod and temperature constraints on the relationship between the photochemical reflectance index and the light use efficiency of photosynthesis in *Pinus strobus*. Tree Physiology 36 (3): 311-324.

Gamon JA, Peñuelas J, Field CB (1992) A narrow-waveband spectral index that tracks diurnal changes in photosynthetic efficiency. Remote Sensing of Environment 41:35-44.

Gamon J, Serrano L, Surfus J (1997) The photochemical reflectance index: an optical indicator of photosynthetic radiation use efficiency across species, functional types, and nutrient levels. Oecologia 112:492-501.

Gamon JA, Berry JA (2012) Facultative and constitutive pigment effects on the Photochemical Reflectance Index (PRI) in sun and shade conifer needles. Israel Journal of Plant Sciences 60(1-2):85-95.

Gamon JA, Huemmrich KF, Wong CYS, Ensminger I, Garrity S, Hollinger DY, Noormets A, Peñuelas J (2016) A remotely sensed pigment index reveals photosynthetic phenology in evergreen conifers. Proceedings of the National Academy of Sciences of the United States of America 113:1387-1392.

Garbulsky MF, Peñuelas J, Papale D, Filella I (2008) Remote estimation of carbon dioxide uptake by a Mediterranean forest. Global Change Biology 14(12):2860-2867

Garbulsky MF., Peñuelas J, Gamon J, Inoue Y, Filella I (2011) The photochemical reflectance index (PRI) and the remote sensing of leaf, canopy and ecosystem radiation use efficiencies - A review and meta-analysis. Remote Sensing of Environment 115:281-297.

Garrity SR, Eitel JUH, Vierling LA (2011) Disentangling the relationships between plant pigments and the photochemical reflectance index reveals a new approach for remote estimation of carotenoid content. Remote Sensing of Environment 115:628-635.

Garrity S, Bohrer G, Maurer K, Mueller K, Vogel C, Curtis P (2011) A comparison of multiple phenology data sources for estimating seasonal transitions in deciduous forest carbon exchange. Agricultural and Forest Meteorology 151:1741-1752.

Genty B, Briantais J-M, Baker NR (1989) The relationship between the quantum yield of photosynthetic electron transport and quenching of chlorophyll fluorescence. Biochimica et Biophysica Acta 990(1):87-92.

Gibon Y, Pyl E-T, Sulpice R, Lunn J, Höhne M, Günther M, Stitt M (2009) Adjustment of growth, starch turnover, protein content and central metabolism to a decrease of the carbon supply when Arabidopsis is grown in very short photoperiods. Plant, Cell & Environment 32:859-874.

Goerner A, Reichstein M, Rambal S (2008) Estimation of photosynthetic light use efficiency in Semi-arid ecosystems with the MODIS-derived photochemical reflectance index. International Geoscience and Remote Sensing Symposium (IGARSS) 3(1):756-758.

Goerner A, Reichstein M, Rambal S (2009) Tracking seasonal drought effects on ecosystem light use efficiency with satellite-based PRI in a Mediterranean forest. Remote Sensing of Environment 113(5):1101-1111.

Gonsamo A, Chen JM, Price DT, Kurz WA, Wu C (2012) Land surface phenology from optical satellite measurement and CO_2 eddy covariance technique. Journal of Geophysical Research 117:G03032.

Gonsamo A, Chen JM, D'Odorico P (2013) Deriving land surface phenology indicators from CO_2 eddy covariance measurements. Ecological Indicators 29:203–207.

Govindjee, Shevela D, Björn LO (2017) Evolution of the Z-scheme of photosynthesis: a perspective. Photosynthesis Research 133(1-3):5-15.Green DS (2007) Controls of growth phenology vary in seedlings of three, co-occurring ecologically distinct northern conifers. Tree Physiology 27:1197-1205.

Guo JM, Trotter CM (2006) Assessing light-dependent down-regulation of photosynthesis using the photochemical reflectance index (PRI). Journal of Spatial Science 51(2):67-78

Guyon D, Guillot M, Vitasse Y, Cardot H, Hagolle O, Delzon S, Wigneron J-P (2011) Monitoring elevation variations in leaf phenology of deciduous broadleaf forests from SPOT/VEGETATION time-series. Remote Sensing of Environment 115:615-627.

Hall DO, Rao KK (1999) Photosynthesis (Studies in Biology). Cambridge University Press. 214 pp.

Hall FG, Hilker T, Coops NC, Lyapustin A, Huemmrich, KF, Middleton E, Margolis H, Drolet G, Black TA (2008) Multi-angle remote sensing of forest light use efficiency by observing PRI variation with canopy shadow fraction. Remote Sensing of Environment 112(7):3201-3211.

Hall M, Medlyn B, Abramowitz G, Franklin O, Rantfors M, Linder S, Wallin G (2013) Which are the most important parameters for modelling carbon assimilation in boreal Norway spruce under elevated [CO_2] and temperature conditions? Tree Physiology 33:1156-1176.

Hamann A, Aitken S (2013) Conservation planning under climate change: accounting for adaptive potential and migration capacity in species distribution models. Diversity and Distributions 19:268-280.

Hamilton JA, El Kayal W, Hart AT, Runcie DE, Arango-Velez A, Cooke JEK (2016) The joint influence of photoperiod and temperature during growth cessation and development of dormancy in white spruce (*Picea glauca*). Tree Physiology 36: 1432-1448.

Hänninen H, Beuker E, Johnsen Ø, Leinonen I, Murray M, Sheppard L, Skrøppa T (2001) Impacts of climate change on cold hardiness of conifers. In Conifer Cold Hardiness. Bigras, F. J. & Colombo, S. J. (eds.). Kluwer Academic Publishers, p. 305-333.

Hänninen H (2006) Climate warming and the risk of frost damage to boreal forest trees: Identification of critical ecophysiological traits. Tree Physiology 26(7): 889-898.

Hänninen H, Tanino K (2011) Tree seasonality in a warming climate. Trends in Plant Science 16: 412-416.

Harris A, Gamon J, Pastorello G, Wong C (2014) Retrieval of the photochemical reflectance index for assessing xanthophyll cycle activity: a comparison of near-surface optical sensors. Biogeosciences 11:6277-6292.

Heldt HW and Piechulla B (2011) Plant Biochemistry, Fourth Edition. Academic Press, ISBN 9780123849861.

Hendrickson L, Furbank R, Chow W (2004) A simple alternative approach to assessing the fate of absorbed light energy using chlorophyll fluorescence. Physiologia Plantarum 8:73-81.

Hilker T, Coops N, Hall F, Black T, Wulder M, Nesic Z, Krishnan P (2008) Separating physiologically and directionally induced changes in PRI using BRDF models. Remote Sensing of Environment 112:2777-2788.

Hilker T, Lyapustin A, Hall FG, Wang Y, Coops NC, Drolet G, Black TA (2009) An assessment of photosynthetic light use efficiency from space: Modeling the atmospheric and directional impacts on PRI reflectance. Remote Sensing of Environment 113(11):2463-2475.

Hilker T, Hall F, Coops N, Lyapustin A, Wang Y, Nesic Z, Grant N, Black A, Wulder M, Kljun N (2010) Remote sensing of photosynthetic light-use efficiency across two forested biomes: Spatial scaling. Remote Sensing of Environment 114:2863-2874.

Hmimina G, Merlier E, Dufrêne E, Soudani K (2015) Deconvolution of pigment and physiologically related photochemical reflectance index variability at the canopy scale over an entire growing season. Plant, Cell & Environment 38(8):1578-1590.

Hoffman D, Jonsson P, Bylesjö M, Trygg J, Antti H, Eriksson M, Moritz T (2010) Changes in diurnal patterns within the Populus transcriptome and metabolome in response to photoperiod variation. Plant, Cell & Environment 33:1298-1313.

Holliday JA, Ralph SG, White R, Bohlmann J, Aitken SN (2008) Global monitoring of autumn gene expression within and among phenotypically divergent populations of Sitka spruce (*Picea sitchensis*) New Phytologist 178: 103–122.

Horton P, Ruban A, Rees D, Pascal AA, Noctor G, Young AJ (1991) Control of the light-harvesting function of chloroplast membranes by aggregation of the LHCII chlorophyll-protein complex. FEBS Letters 292(1-2):1-4

Horton P, Wentworth M, Ruban A (2005) Control of the light harvesting function of chloroplast membranes: the LHCII-aggregation model for non-photochemical quenching. FEBS letters 579:4201-4206.

Hossain MS, Dietz KJ (2016) Tuning of Redox Regulatory Mechanisms, Reactive Oxygen Species and Redox Homeostasis under Salinity Stress. Frontiers in Plant Science 7:548.

Huang W, Zhang S-B, Cao K-F (2010) Stimulation of Cyclic Electron Flow During Recovery After Chilling-Induced Photoinhibition of PSII. Plant and Cell Physiology 51:1922-1928.

Huang W, Yang S-J, Zhang S-B, Zhang J-L, Cao K-F (2012) Cyclic electron flow plays an important role in photoprotection for the resurrection plant *Paraboea rufescens* under drought stress. Planta 235:819–828.

Hufkens K, Friedl M, Sonnentag O, Braswell B, Milliman T, Richardson A (2012) Linking near-surface and satellite remote sensing measurements of deciduous broadleaf forest phenology. Remote Sensing of Environment 117:307-321.

Hüner N, Öquist G, Sarhan F (1998) Energy balance and acclimation to light and cold. Trends in Plant Science 3(6):224-230.

Inoue Y, Peñuelas J (2006) Relationship between light use efficiency and photochemical reflectance index in soybean leaves as affected by soil water content. International Journal of Remote Sensing 27(22):5109-5114.

IPCC (2014) Summary for policymakers. In: Climate Change 2014: Impacts, Adaptation, and Vulnerability. Part A: Global and Sectoral Aspects. Contribution of Working Group II to the Fifth Assessment Report of the Intergovernmental Panel on Climate Change [Field, C.B., V.R. Barros, D.J. Dokken, K.J. Mach, M.D. Mastrandrea, T.E. Bilir, M. Chatterjee, K.L. Ebi, Y.O. Estrada, R.C. Genova, B. Girma, E.S. Kissel, A.N. Levy, S. MacCracken, P.R. Mastrandrea, and L.L.White (eds.)]. Cambridge University Press, Cambridge, United Kingdom and New York, NY, USA.

Ivanov A, Sane P, Zeinalov Y, Malmberg G, Gardeström P, Huner N, Öquist G (2001) Photosynthetic electron transport adjustments in overwintering Scots pine (*Pinus sylvestris* L.). Planta 213:575–585.

Ivanov A, Sane P, Zeinalov Y, Simidjiev I, Huner N, Öquist G (2002) Seasonal responses of photosynthetic electron transport in Scots pine (*Pinus sylvestris* L.) studied by thermoluminescence. Planta 215:457–465.

Ivanov AG, Hurry V, Sane PV, Öquist G, and Huner NPA (2008) Reaction Centre Quenching of Excess Light Energy and Photoprotection of Photosystem II. Journal of Plant Biology 51(2):85-96.

Jahns P, Holzwarth A (2012) The role of the xanthophyll cycle and of lutein in photoprotection of photosystem II. Biochimica et Biophysica Acta 1817:182–93.

Johnsen K, Seiler J, Major J (1996) Growth, shoot phenology and physiology of diverse seed sources of black spruce: II. 23-year-old field trees. Tree Physiology 16: 375–380.

Johnson G (2011) Physiology of PSI cyclic electron transport in higher plants. Biochimica et Biophysica Acta 1807:384–389.

Junker LV and Ensminger I (2016) Fast detection of leaf pigments and isoprenoids for ecophysiological studies, plant phenotyping and validating remote-sensing of vegetation. Physiologia Plantarum 158(4):369–381.

Kanervo E, Tasaka Y, Murata N, Aro E-M (1997) Membrane lipid unsaturation modulates processing of the photosystem II reaction-center protein D1 at low temperatures. Plant Physiology 114(3):841-849.

Kanervo E, Suorsa M, Aro E-M (2005) Functional flexibility and acclimation of the thylakoid membrane. Photochemical and Photobiological Sciences 4(12):1072-1080.

Kaufmann MR (1975) Leaf water stress in Engelmann Spruce. Influence of the root and shoot environments. Plant Physiology 56:841-844.

Kimball B (2005) Theory and performance of an infrared heater for ecosystem warming. Global Change Biology 11: 2041–2056.

Kimball B, Conley M, Wang S, Lin X, Luo C, Morgan J, Smith D (2008) Infrared heater arrays for warming ecosystem field plots. Global Change Biology 14: 309–320.

Klughammer C, Schreiber U (1994) An improved method, using saturating light pulses, for the determination of photosystem I quantum yield via $P700^{+}$-absorbance changes at 830nm. Planta 192:261-268.

Kodama Y, Tsuboi H, Kagawa T, Wada M (2008) Low temperature-induced chloroplast relocation mediated by a blue light receptor, phototropin 2, in fern gametophytes. Journal of Plant Research 121:441-448.

Körner C, Basler D (2010) Plant science. Phenology under global warming. Science 327:1461-1462.

Kováč D, Malenovsky Z, Urban O, Spunda V, Kalina J, Ac A, Kaplan V, Hanus J (2013) Response of green reflectance continuum removal index to the xanthophyll de-epoxidation cycle in Norway spruce needles. Journal of Experimental Botany 64:1817-1827

Kramer PJ (1983) Water relations in plants. Academic Press, Orlando, FL, pp. 489.

Kramer K (1995) Phenotypic plasticity of the phenology of seven European tree species in relation to climatic warming. Plant, Cell and Environment 18(2):93-104.

Krieger-Liszkay A, Fufezan C, Trebst A (2008) Singlet oxygen production in photosystem II and related protection mechanism. Photosynthesis Research 98:551-564.

Kujala ST, Savolainen O (2012) Sequence variation patterns along a latitudinal cline in Scots pine (*Pinus sylvestris*): signs of clinal adaptation? Tree Genetics & Genomes 8:1451–1467.

Kujala ST, Knürr T, Kärkkäinen K, Neale DB, Sillanpää MJ, Savolainen O (2017) Genetic heterogeneity underlying variation in a locally adaptive clinal trait in *Pinus sylvestris* revealed by a Bayesian multipopulation analysis. Heredity 118:413–423.

Laube J, Sparks TH, Estrella N, Höfler J, Ankerst DP, Menzel A (2014) Chilling outweighs photoperiod in preventing precocious spring development. Global Change Biology 20:170–182.

Lee CM, Thomashow MF (2012) Photoperiodic regulation of the C-repeat binding factor (CBF) cold acclimation pathway and freezing tolerance in *Arabidopsis thaliana*. PNAS 109(37):15054-15059.

Lepais O, Bacles CF (2014) Two are better than one: Combining landscape genomics and common gardens for detecting local adaptation in forest trees. Molecular Ecology 23(19):4671-4673.

Liepe K, Hamann A, Smets P, Fitzpatrick C, Aitken S (2016) Adaptation of lodgepole pine and interior spruce to climate: implications for reforestation in a warming world. Evolutionary Applications 9:409-419.

Lloyd J, Shibistova O, Zolotoukhine D, Kolle O, Arneth A (2002) Seasonal and annual variations in the photosynthetic productivity and carbon balance of a central Siberian pine forest. Tellus 54B:590-610.

Louis J, Ounis A, Ducruet J-M, Evain S, Laurila T, Thum T, Aurela M, Wingsle G, Alonso L, Pedros R, Moya I (2005) Remote sensing of sunlight-induced chlorophyll fluorescence and reflectance of Scots pine in the boreal forest during spring recovery. Remote Sensing of Environment 96(1):37-48.

Lu P, Joyce D, Sinclair R (2003) Geographic variation in cold hardiness among eastern white pine (*Pinus strobus* L.) provenances in Ontario. Forest Ecology and Management 178(3): 329-340.

Lukeš P, Stenberg P, Rautiainen M, Mõttus M, Vanhatalo K (2013) Optical properties of leaves and needles for boreal tree species in Europe. Remote Sensing Letters 4:667-676.

Lunde C, Jensen PE, Haldrup A, Knoetzel J, Scheller HV (2000) The PSI-H subunit of photosystem I is essential for state transitions in plant photosynthesis. Nature 408:613-615.

Lundmark T, Bergh J, Strand M, Koppel A (1998) Seasonal variation of maximum photochemical efficiency in boreal Norway spruce stands. Trees 13:63-67.

Ma X-F, Hall D, St. Onge KR, Jansson S, Ingvarsson PK (2010) Genetic differentiation, clinal variation and phenotypic associations with growth cessation across the *Populus tremula* photoperiodic pathway. Genetics 186:1033–1044.

Maibam P, Nawkar GM, Park JH, Sahi VP, Lee SY, and Kang CH (2013) The Influence of Light Quality, Circadian Rhythm, and Photoperiod on the CBF-Mediated Freezing Tolerance International Journal of Molecular Sciences 14(6):11527–11543.

Man R, Kayahara GJ, Dang Q-L, Rice JA (2009) A case of severe frost damage prior to budbreak in young conifers in Northeastern Ontario: Consequence of climate change? *The Forestry Chronicle* 85(3):453-462.

Markiet V, Hernández-Clemente R, Mõttus M (2007) Spectral similarity and PRI variations for a boreal forest stand using multi-angular airborne imagery. Remote Sensing 9:1005.

Matsubara S, Forster B, Waterman M, Robinson S, Pogson B, Gunning B, Osmond B (2012) From ecophysiology to phenomics: some implications of photoprotection and shade-sun acclimation in situ for dynamics of thylakoids in vitro. Philosophical Transactions of the Royal Society B: Biological Sciences 367:3503-3514.

Maxwell K, Johnson GN (2000) Chlorophyll fluorescence--a practical guide. Journal of Experimental Botany 51:659-68.

Melaas E, Friedl M, Zhu Z (2013) Detecting interannual variation in deciduous broadleaf forest phenology using Landsat TM/ETM+ data. Remote Sensing of Environment 132:176-185.

Middleton EM, Cheng Y-B, Hilker T, Black TA, Krishnan P, Coops NC, Huemmrich KF (2009) Linking foliage spectral responses to canopy-level ecosystem photosynthetic light-use efficiency at a Douglas-fir forest in Canada. Canadian Journal of Remote Sensing 35(2):166-188.

Minagawa J (2013) Dynamic reorganization of photosynthetic supercomplexes during environmental acclimation of photosynthesis. Frontiers in Plant Science 4:513.

Miyake C, Horiguchi S, Makino A, Shinzaki Y, Yamamoto H, Tomizawa K (2005) Effects of Light Intensity on Cyclic Electron Flow Around PSI and its Relationship to Non-photochemical Quenching of Chl Fluorescence in Tobacco Leaves. Plant and Cell Physiology 46:1819-1830.

Monteith JL (1972) Solar radiation and productivity in tropical ecosystems. Journal of Applied Ecology 9:747-766.

Monteith JL (1977) Climate and the efficiency of crop production in Britain. Philosophical Transactions of the Royal Society of London B 281:277-294.

Moran JA, Mitchell AK, Goodmanson G, Stockburger KA (2000) Differentiation among effects of nitrogen fertilization treatments on conifer seedlings by foliar reflectance: A comparison of methods. Tree Physiology 20(16):1113-1120.

Mõttus M, Hernández-Clemente R, Perheentupa V, Markiet V (2017) In situ measurement of Scots pine needle PRI. Plant Methods 13(1):35.

Mõttus M, Hernández-Clemente R, Perheentupa V, Markiet V (2018) Measurement of diurnal variation in needle PRI and shoot photosynthesis in a boreal forest. Remote Sensing 10:1019.

Müller P, Li X-P, Niyogi K (2001) Non-photochemical quenching. A response to excess light energy. Plant Physiology 125:1558-1566.

Murata N, Takahashi S, Nishiyama Y, Allakhverdiev S (2007) Photoinhibition of photosystem II under environmental stress. Biochimica et Biophysica Acta (BBA) - Bioenergetics 1767:414-421.

Myneni RB, Keeling CD, Tucker CJ, Asrar G, Nemani RR (1997) Increased plant growth in the northern high latitudes from 1981 to 1991. Nature 386(6626):698-702.

Myneni RB, Dong J, Tucker CJ, Kaufmann RK, Kauppi PE, Liski J, Zhou L, Alexeyev V, Hughes MK (2001) A large carbon sink in the woody biomass of northern forests. Proceedings of the National Academy of Sciences of the United States of America 98:14784-14789.

Nakaji T, Oguma H, Fujinuma Y (2006) Seasonal changes in the relationship between photochemical reflectance index and photosynthetic light use efficiency of Japanese larch needles. International Journal of Remote Sensing 27:493-509.

Nakaji T, Ide R, Oguma H, Saigusa N, Fujinuma Y (2007) Utility of spectral vegetation index for estimation of gross CO_2 flux under varied sky conditions. Remote Sensing of Environment 109(3):274-284.

Nakaji T, Ide R, Takagi K, Kosugi Y, Ohkubo S, Nasahara KN, Saigusa N, Oguma H (2008) Utility of spectral vegetation indices for estimation of light conversion efficiency in coniferous forests in Japan. Agricultural and Forest Meteorology 148(5):776-787.

Nemani RR, Keeling CD, Hashimoto H, Jolly WM, Piper SC, Tucker CJ, Myneni RB, Running SW (2003) Climate-Driven Increases in Global Terrestrial Net Primary Production from 1982 to 1999. Science 300:1560-1563.

Nichol CJ, Huemmrich KF, Black TA, Jarvis PG, Walthall CL, Grace J, Hall FG (2000) Agricultural and Forest Meteorology 101(2-3):131-142.

Nichol CJ, Lloyd J, Shibistova O, Arneth A, Röser C, Knohl A, Matsubara S, Grace J (2002) Remote sensing of photosynthetic-light-use efficiency of a Siberian boreal forest. Tellus, Series B: Chemical and Physical Meteorology 54(5):677-687.

Nichol CJ, Rascher U, Matsubara S, Osmond B (2006) Assessing photosynthetic efficiency in an experimental mangrove canopy using remote sensing and chlorophyll fluorescence. Trees - Structure and Function 20(1):9-15.

Nicotra A, Atkin O, Bonser S, Davidson A, Finnegan E, Mathesius U, Poot P, Purugganan M, Richards C, Valladares F, van Kleunen M. (2010) Plant phenotypic plasticity in a changing climate. Trends in Plant Science 15:684-692.

Niyogi KK (2000) Safety valves for photosynthesis. Current Opinion in Plant Biology 3:455-460.

Niyogi K, Li X-P, Rosenberg V, Jung H-S (2005) Is PsbS the site of non-photochemical quenching in photosynthesis? Journal of Experimental Botany 56:375–382.

Ögren WL (1984) Photorespiration: pathways, regulation, and modification. Annual Review of Plant Physiology 35:415–442.

Öquist G, Huner NP (2003) Photosynthesis of overwintering evergreen plants. Annual Review of Plant Biology 54:329–55.

Ottander C, Campbell D, Öquist G (1995) Seasonal changes in photosystem II organisation and pigment composition in *Pinus sylvestris*. Planta 197:176-183.

Pan Y, Birdsey R, Fang J, Houghton R, Kauppi P, Kurz W, Phillips OL, Shvidenko A, Lewis SL, Canadell JG, Ciais P, Jackson RB, Pacala SW, McGuire AD, Piao S, Rautiainen A, Sitch S, Hayes, D (2011) A large and persistent carbon sink in the world's forests. Science 333(6045):988–993.

Paparelli E, Parlanti S, Gonzali S, Novi G, Mariotti L, Ceccarelli N, Dongen J, Kölling K, Zeeman S, Perata P (2013) Nighttime sugar starvation orchestrates gibberellin biosynthesis and plant growth in Arabidopsis. The Plant Cell 25:3760–3769.

Peguero-Pina JJ, Morales F, Flexas J, Gil-Pelegrín E, Moya I (2008) Photochemistry, remotely sensed physiological reflectance index and de-epoxidation state of the xanthophyll cycle in *Quercus coccifera* under intense drought. Oecologia 156(1):1-11.

Peng S, Piao S, Ciais P, Myneni R, Chen A, Chevallier F, Dolman A, Janssens I, Peñuelas J, Zhang G, Vicca S, Wan S, Wang S, Zeng H (2013) Asymmetric effects of daytime and night-time warming on Northern Hemisphere vegetation. Nature 501: 88–92.

Peñuelas J, Filella I, Gamon J (1995) Assessment of photosynthetic radiation-use efficiency with spectral reflectance. New Phytologist 131:291-296.

Pfündel E, Klughammer C Schreiber U (2008) Monitoring the effects of reduced PS II antenna size on quantum yields of photosystems I and II using the Dual-PAM-100 measuring system. PAM Application Notes 1:21-24.

Piao S, Ciais P, Friedlingstein P, Peylin P, Reichstein M, Luyssaert S, Margolis H, Fang J, Barr A, Chen A (2008) Net carbon dioxide losses of northern ecosystems in response to autumn warming. Nature 451:49-52.

Porcar-Castell A (2011) A high-resolution portrait of the annual dynamics of photochemical and non-photochemical quenching in needles of *Pinus sylvestris*. Physiologia Plantarum 143:139-153.

Porcar-Castell A, Garcia-Plazaola J, Nichol C, Kolari P, Olascoaga B, Kuusinen N, Fernández-Marín B, Pulkkinen M, Juurola E, Nikinmaa E (2012) Physiology of the seasonal relationship between the photochemical reflectance index and photosynthetic light use efficiency. Oecologia 170:313-23.

Price DT, McKenney DW, Joyce LA, Siltanen RM, Papadopol P, Lawrence K (2011) High-Resolution Interpolation of Climate Scenarios for Canada Derived from General Circulation Model Simulations. Natural Resources Canada, Canadian Forest Service, Northern Forestry Center, Edmonton, Alberta. Information Report NOR-X-421.

R Core Team (2014) R: A language and environment for statistical computing. R foundataion for Statistical Computing, Vienna, Austria URL http://www.R-project.org/.

Rahman AF, Gamon JA, Fuentes DA, Roberts DA, Prentiss D (2001) Modeling spatially distributed ecosystem flux of boreal forest using hyperspectral indices from AVIRIS imagery. Journal of Geophysical Research Atmospheres 106(D24):33579-33591

Rahman AF, Cordova VD, Gamon JA, Schmid HP, Sims DA (2004) Potential of MODIS ocean bands for estimating CO_2 flux from terrestrial vegetation: A novel approach. Geophysical Research Letters 31(10):L10503 1-4

Rehfeldt G, Crookston N, Sáenz-Romero C, Campbell E (2012) North American vegetation model for land-use planning in a changing climate: a solution to large classification problems. Ecological Applications 22:119-141.

Repo T, Zhang G, Ryyppö A, Rikala R, Vuorinen M (2000) The relation between growth cessation and frost hardening in Scots pines of different origins. Trees 14:456–464

Richardson AD, Berlyn GP, Gregoire TG (2001) Spectral reflectance of Picea rubens (pinaceae) and Abies balsamea (Pinaceae) needles along an elevational gradient, Mt. Moosilauke, New Hampshire, USA. American Journal of Botany 88(4):667-676.

Rossi S, Deslauriers A, Griçar J, Seo J, Rathgeber C, Anfodillo T, Morin H, Levanic T, Oven P, Jalkanen R (2008) Critical temperatures for xylogenesis in conifers of cold climates. Global Ecology and Biogeography 17:696–707.

Rostad H, Granhus A, Fløistad IS, Morgenlie S (2006) Early summer frost hardiness in *Picea abies* seedlings in response to photoperiod treatment. Canadian Journal of Forest Research 36:1966–1973.

Ruban A, Johnson M, Duffy C (2012) The photoprotective molecular switch in the photosystem II antenna. Biochimica et Biophysica Acta (BBA) - Bioenergetics 1817:167-181.

Sage RF (2002) Variation in the kcat of Rubisco in C3and C4plants and some implications for photosynthetic performance at high and low temperature. Journal of Experimental Botany 53:609-620.

Savitch L, Leonardos E, Krol M, Jansson S, Grodzinski B, Hüner N, Öquist G (2002) Two different strategies for light utilization in photosynthesis in relation to growth and cold acclimation. Plant, Cell & Environment 25:761-771.

Savitch L, Ivanov A, Krol M, Sprott D, Öquist G, Huner N (2010) Regulation of Energy Partitioning and Alternative Electron Transport Pathways During Cold Acclimation of Lodgepole Pine is Oxygen Dependent. Plant and Cell Physiology 51:1555-1570.

Savolainen O, Pyhäjärvi T, Knürr T (2007) Gene Flow and Local Adaptation in Trees. Annual Review of Ecology, Evolution, and Systematics 38:595-619.

Sevanto S, Suni T, Pumpanen J, Grönholm T, Kolari P, Nikinmaa E, Hari P, Vesala T (2006) Wintertime photosynthesis and water uptake in a boreal forest. Tree Physiology 26:749-757.

Sims D, Gamon J (2002) Relationships between leaf pigment content and spectral reflectance across a wide range of species, leaf structures and developmental stages. Remote Sensing of Environment 81:337-354.

Sonnentag O, Hufkens K, Teshera-Sterne C, Young A, Friedl M, Braswell B, Milliman T, O'Keefe J, Richardson A (2012) Digital repeat photography for phenological research in forest ecosystems. Agricultural and Forest Meteorology 152:159-177.

Soolanayakanahally RY, Guy RD, Street NR, Robinson KM, Silim SN, Albrectsen BR, Jansson S (2015) Comparative physiology of allopatric *Populus* species: geographic clines in photosynthesis, height growth, and carbon isotope discrimination in common gardens. Frontiers in Plant Science 6:528.

Springer KR, Wang R, Gamon JA (2017) Parallel seasonal patterns of photosynthesis, fluorescence, and reflectance indices in boreal trees. Remote Sensing 9:691.

Stinziano JR, Hüner NPA, Way DA (2015) Warming delays autumn declines in photosynthetic capacity in a boreal conifer, Norway spruce (*Picea abies*). Tree Physiology 35, 1303–1313.

Strachan IB, Pattey E, Boisvert JB (2002) Impact of nitrogen and environmental conditions on corn as detected by hyperspectral reflectance. Remote Sensing of Environment 80(2):213-224.

Strachan IB, Pattey E, Salustro C, Miller JR (2008) Use of hyperspectral remote sensing to estimate the gross photosynthesis of agricultural fields. Canadian Journal of Remote Sensing 34 (3):333-341.

Strand M, Öquist G (1998) Effects of frost hardening, dehardening and freezing stress on in vivo chlorophyll fluorescence of seedlings of Scots pine (*Pinus sylvestris* L.). Plant, Cell & Environment 11(4):231-238.

Strand M, Lundmark T, Söderbergh I, Mellander P-E (2002) Impacts of seasonal air and soil temperatures on photosynthesis in Scots pine trees. Tree Physiology 22: 839–47.

Stylinsky CD, Gamon JA, Oechel WC (2002) Seasonal patterns of reflectance indices, carotenoid pigments and photosynthesis of evergreen chaparral species. Oecologia 131:366-374.

Sveshnikov D, Ensminger I, Ivanov AG (2006) Excitation energy partitioning and quenching during cold acclimation in Scots pine. Tree Physiology 26:325-336.

Taniguchi M, Miyake H (2012) Redox-shuttling between chloroplast and cytosol: integration of intra-chloroplast and extra-chloroplast metabolism. Current Opinion in Plant Biology 15:252–260.

Tanja S, Berninger F, Vesala T, Markkanen T, Hari P, Mäkelä A, Ilvesniemi H, Hänninen H, Nikinmaa E, Huttula T, Laurila T, Aurela M, Grelle A, Lindroth A, Arneth A, Shibistova O, Lloyd J (2003) Air temperature triggers the recovery of evergreen boreal forest photosynthesis in spring. Global Change Biology 9:1410-1426.

Telfer A, Dhami S, Bishop S, Phillips D, Barber J (1994) β-Carotene Quenches Singlet Oxygen Formed by Isolated Photosystem II Reaction Centers. Biochemistry 33:14469-14474.

Telfer A (2005) Too much light? How β-carotene protects the photosystem II reaction centre. Photochemical & Photobiological Sciences 4:950-956.

Telfer A (2014) Singlet Oxygen Production by PSII Under Light Stress: Mechanism, Detection and the Protective role of β-Carotene. Plant and Cell Physiology 55:1216-1223.

Thayer S, Björkman O (1990) Leaf xanthophyll content and composition in sun and shade determined by HPLC. Photosynthesis Research 23:331-343.

Trahan MW, Schubert BA (2016) Temperature-induced water stress in high-latitude forests in response to natural and anthropogenic warming. Global Change Biology 22(2):782–791.

Trebst A (2003) Function of beta-carotene and tocopherol in photosystem II. Zeitschrift für Naturforschung. C, Journal of Biosciences 58:609-620.

U. S. Climate Data (2018) 1981-2010 Normals - Weather. [online] Available at: https://usclimatedata.com/ [Accessed 31 Jul. 2018].

Ustin S, Gitelson AA, Jacquemoud S, Schaepman M, Asner G, Gamon J, Zarco-Tejada P (2009) Retrieval of foliar information about plant pigment systems from high resolution spectroscopy. Remote Sensing of Environment 113:S67-S77.

Verhoeven A, Osmolak A, Morales P, Crow J (2009) Seasonal changes in abundance and phosphorylation status of photosynthetic proteins in eastern white pine and balsam fir. Tree Physiology 29:361-374.

Verhoeven A (2013) Recovery kinetics of photochemical efficiency in winter stressed conifers: the effects of growth light environment, extent of the season and species. Physiologia Plantarum 147:147-58.

Verhoeven A (2014) Sustained energy dissipation in winter evergreens. New Phytologist 201:57-65.

Viherä-Aarnio A, Häkkinen R, Partanen J, Luomajoki A, Koski V (2005) Effects of seed origin and sowing time on timing of height growth cessation of *Betula pendula* seedlings. Tree Physiology 25:101–108.

Vogg G, Heim R, Gotschy B, Beck E, Hansen J (1998) Frost hardening and photosynthetic performance of Scots pine (*Pinus sylvestris* L.). II. Seasonal changes in the fluidity of thylakoid membranes. Planta 204(2):201-206.

Wallin G, Hall M, Slaney M, Räntfors M, Medhurst J, Linder S (2013) Spring photosynthetic recovery of boreal Norway spruce under conditions of elevated [CO_2] and air temperature. Tree Physiology 33:1177-1191.

Walther S, Voigt M, Thum T, Gonsamo A, Zhang Y, Köhler P, Jung M, Varlagin A, Guanter L. (2016) Satellite chlorophyll fluorescence measurements reveal large-scale decoupling of photosynthesis and greenness dynamics in boreal evergreen forests. Global Change Biology 22(9):2979-2996.

Way DA and Montgomery R (2015) Photoperiod constraints on tree migration in a warmer world. Plant, Cell & Environment 38(9):1725-1736.

Wong CYS, Gamon J (2015) Three causes of variation in the photochemical reflectance index (PRI) in evergreen conifers. New Phytologist 206(1):187-195.

Wong CYS, Gamon JA (2015) The photochemical reflectance index provides an optical indicator of spring photosynthetic activation in evergreen conifers. New Phytologist 206(1):196-208.

Young A, Frank H (1996) Energy transfer reactions involving carotenoids: quenching of chlorophyll fluorescence. Journal of Photochemistry and Photobiology B: Biology 36:315.

Zarter CR, Demmig-Adams B, Ebbert V, Adamska I, Adams WW (2006) Photosynthetic capacity and light harvesting efficiency during the winter-to-spring transition in subalpine conifers. New Phytologist 172:283-92.

Zhang X, Gurney KR, Peylin P, Chevallier F, Law RM, Patra PK, Rayner PJ, Röedenbeck C, Krol M (2013) On the variation of regional CO_2 exchange over temperate and boreal North America. Global Biogeochemical Cycles 27:991-1000.

Appendix
Experimental Conditions and Methods

A1 Experimental conditions

Plant materials (Chapters 2-3)

For the growth chamber experiments, three-year-old (3+0) bare-rooted Eastern white pine (*Pinus strobus* L.) seedlings were obtained in April 2011 and 2012 from a local seed orchard (Ontario seed zone 37, Somerville Seedlings, Everett, Ontario, Canada).

The seedlings were potted in 3L containers in a mixture of sand and sphagnum peat moss (1:2 v/v) and fertilized with 28:10:10 (N:P:K) mineral fertilizer (Miracle-Gro, Scotts, Marysville, OH, USA). Seedlings were kept outside in an experimental garden at the University of Toronto at Mississauga (Ontario, Canada) until transferred to the growth chambers (Biochambers, Winnipeg, Canada) during July (Chapter 2) or December (Chapter 3).

Plant materials (Chapter 4)

For the T-FACE array experiment, three-year-old (3+0) bare-rooted Eastern white pine (*Pinus strobus* L.) seedlings were obtained from a northern (Trécesson Nursery, Amos, QC, Canada; 48°34'36"N, -78°15'21"W), local (Somerville Nurseries, Everett, ON, Canada; 44°10'46"N, -79°56'30"W) and southern provenance (John S. Ayton State Tree Nursery, Preston, MD, USA; 38°42'05"N, -75°54'51"W). At each provenance, the seedlings were selected from local seed orchards to ensure adaptation to local environmental conditions.

In early May 2012, 210 seedlings from the three provenances were planted per plot with a distance of 30 cm between them. Two rows of buffer seedlings were planted at the periphery of each plot to ensure similar micro-environments for all test seedlings.

Sampling and measurements started in September 2012 after seedlings were established. At each field campaign, two seedlings per provenance were randomly selected in each plot for sampling and measurement.

Chamber settings (Chapter 2)

For the autumn growth chamber experiment (Chapter 2), seedlings were acclimated for 6 weeks to simulated summer conditions with long days and high temperature (LD/HT; 14h photoperiod; 22/15˚C day/night) and then exposed for 36 days of simulated cold or warm autumn conditions. The cold autumn simulation consisted of short days and low temperature (SD/LT; 8h photoperiod; 12/5˚C day/night) and the warm autumn simulation consisted of short days and high temperature (SD/HT; 8h photoperiod; 22/15˚C day/night). Under LD/HT, SD/LT and SD/HT, seedlings were exposed to a light intensity of 1500 µmol quanta $m^{-2}s^{-1}$, with a period of 30 minutes at 400 µmol quanta $m^{-2}s^{-1}$ at the beginning and end of the day. Humidity was set to 60% RH (Table A1). Two independent experiments were performed in two consecutive years, using identical settings and protocols, with rotations of treatments between the chambers to minimize chamber-specific effects.

Table A1. Summary of chamber settings for the autumn experiment (Chapter 2)

	Long day / high temp. (LD/HT; summer)	Short day / low temp. (SD/LT; cold autumn)	Short day / high temp. (SD/HT; warm autumn)
Photoperiod (h)	14	8	8
Daytime light intensity (µmol quanta $m^{-2}s^{-1}$)	1500	1500	1500
Nighttime light intensity (µmol quanta $m^{-2}s^{-1}$)	0	0	0
Daytime temperature (˚C)	22	12	22
Nighttime temperature (˚C)	15	5	15
Relative humidity (%)	60	60	60

Chamber settings (Chapter 3)

For the spring growth chamber experiment (Chapter 3), seedlings were acclimated for 6 weeks to simulated winter conditions (2/-5˚C day/night; 8h photoperiod at 400 µmol quanta $m^{-2}s^{-1}$). Winter-acclimated seedlings (Wi) were then shifted for 36 days to either a cold spring (Sp_C) or warm spring (Sp_W) treatment. The temperature in Sp_C was set to 10/5˚C (day/night) and in Sp_W it was set to 15/10˚C (day/night) and photoperiod was 12 hours in both spring treatments. Light intensity was constantly monitored with a PAR sensor mounted at the top of the seedling canopy and maintained at an intensity of 1400 µmol quanta $m^{-2}s^{-1}$. Measurements and samples of summer-acclimated needles were obtained from summer seedlings (Su) that had been kept outdoors in the experimental garden and were then acclimated for six weeks to simulated summer conditions (22/15˚C day/night; 14h photoperiod at 1400 µmol quanta $m^{-2}s^{-1}$ light intensity). Two independent experiments were performed in 2012 and 2014 using identical settings and protocols. In order to minimize chamber effects, we rotated seedlings between chambers every two weeks.

Table A2. Summary of chamber settings for the spring experiment (Chapter 3)

	Winter (Wi)	Cold spring (Sp_C)	Warm spring (Sp_W)	Summer (Su)
Photoperiod (h)	8	12	12	14
Daytime light intensity (µmol quanta $m^{-2}s^{-1}$)	400	1400	1400	1500
Nighttime light intensity (µmol quanta $m^{-2}s^{-1}$)	0	0	0	0
Daytime temperature (˚C)	2	10	15	22
Nighttime temperature (˚C)	-5	5	10	15
Relative humidity (%)	60	60	60	60

T-FACE array settings (Chapter 4)

The warming arrays were set up at the Koffler Scientific Reserve of the University of Toronto located in King City, Ontario, Canada (44°01'44"N, -79°32'21"W). A Temperature Free-Air-Controlled Enhancement (T-FACE) system was set up according to Kimball *et al.* (2008), and consisted of 10 circular plots, each with a diameter of 3m. Ambient canopy temperature was recorded using infrared sensors (Model IRT-P5, Apogee Instruments, Logan, UT, USA) in five unheated control plots (ambient temperature; AT). For the elevated temperature treatment (ET), five plots were equipped with six 100W infrared heaters (Mor Electric Heating Association, Comstock Park, MI, USA) in a hexagonal array, where leaf temperature was raised by +1.5°C during the day and +3°C at night to mimic predicted air temperature for 2050 in southern Ontario (Kimball *et al.* 2008, Price *et al.* 2011, Peng *et al.* 2013). Ambient air and canopy temperatures were recorded using a CR1000 datalogger (Campbell Scientific Inc., Edmonton, AB, Canada). Precipitation data were obtained from the Buttonville Airport weather station in Newmarket, ON (Environment Canada, 2014), located 25 km from the field site.

A2 Photosynthetic gas exchange protocols

Seasonal gas exchange time series using the Walz GFS-3000 (Chapters 2 and 3)

For the autumn and spring growth chamber experiments, photosynthetic gas exchange was measured using a GFS-3000 (Walz, Effeltrich, Germany). Measurements started 2 hours after the lights were turned on in the morning. A bundle of attached needles was oriented to form a flat plane and inserted in the leaf cuvette. Net CO_2 assimilation (A) and stomatal conductance (g_s) were measured at growth light intensity (1500 µmol quanta $m^{-2}s^{-1}$) once steady-state assimilation was achieved. Immediately after the measurements, needles were detached from the seedling and measured for surface area using the Winseedle software package (Regent Instruments Inc., Québec, Canada). The light use efficiency of CO_2 assimilation (LUE_A, in mol CO_2 mol^{-1}) was calculated as the ratio of assimilation (in µmol CO_2 $m^{-2}s^{-1}$) and the intensity of the actinic light (in µmol quanta m^2s^{-1}) during measurements.

Table A3. GFS-3000 settings for the growth chamber seasonal time series

Flow rate	750 µmol min^{-1}
CO_2 concentration	400 ppm
H_2O concentration	60% RH
Cuvette temperature	2, 10, 12, 15 or 22°C, according to treatment measured
Impeller speed	7 steps
Light intensity	PARtop 0, 1400 or 1500 µmol quanta $m^{-2}s^{-1}$, according to experiment or measurement taken

Seasonal gas exchange time series using the Walz GFS-3000 (Chapter 4)

In Chapter 4, variations in photosynthetic activity over the course of the experiment were also measured using a GFS-3000 (Walz, Effeltrich, Germany). A bundle of attached needles was oriented to form a flat plane and inserted in the leaf cuvette. CO_2 concentration in the cuvette was set to 400 ppm, humidity was set 60% RH and temperature was set to a value corresponding to daily ambient temperature on the day of the measurement (Table A4). Net CO_2 assimilation (*A*) and stomatal conductance (g_s) were measured in the dark and at 1200 µmol photon $m^{-2}s^{-1}$ once steady-state assimilation was achieved. Immediately after the measurements, needles were detached from the seedling and measured for surface area using the Winseedle software package (Regent Instruments Inc., Québec, Canada).

Table A4. GFS-3000 settings for the warming array experiment

Flow rate	750 µmol min^{-1}
CO_2 concentration	400 ppm
H_2O concentration	60% RH
Cuvette temperature	Set to value corresponding to daily ambient temperature
Impeller speed	7 steps
Light intensity	PARtop 0 or 1200 µmol quanta $m^{-2}s^{-1}$, according to measurement taken

A3 Chlorophyll fluorescence protocols

Chlorophyll fluorescence using the Walz Dual-PAM-100 (Chapters 2 and 3)

For the autumn and spring growth chamber experiments, chlorophyll-fluorescence was used to assess energy partitioning using a Dual-PAM-100, Walz, Effeltrich, Germany. A saturating light pulse was first applied to dark-adapted (pre-dawn) needles for determination of F_o and F_m (minimal and maximal fluorescence) and calculation of maximum quantum yield of PSII. The needles were then exposed to a sequence of 2.5-min intervals with actinic light of increasing intensity (0-2000 µmol quanta $m^{-2}s^{-1}$). Each step was followed by a 400 ms saturating pulse of 10000 µmol quanta $m^{-2}s^{-1}$ preceded by determination of $F_{s,}$ the yield of steady state fluorescence in a light-adapted sample recorded immediately before the saturation pulse, and followed by determination of F_m', the maximal fluorescence of light-adapted needles. Finally, and a weak pulse of far-red light for determination of F_o', the minimal fluorescence of light-adapted needles.

Energy partitioning using the parameters Φ_{PSII}, Φ_{NPQ} and $\Phi_{f,D}$ was calculated according to Hendrickson *et al*. (2004; Table A5).

The electron transport rate of PSII was calculated as $ETR_{II} = \Phi_{PSII} \cdot PPFD \cdot \alpha \cdot d_{II}$, where PPFD is the applied light intensity (μmol quanta $m^{-2}s^{-1}$), α is the absorptance, i.e. the fraction of incident light absorbed by leaves, and d_{II} the fraction of light directed to PSII. Values of α were calculated as α = 1 – transmittance – reflectance. Given the thickness of pine needles, transmittance was assumed to be 0. Reflectance was measured with a Unispec-SC spectrometer over the 400-700 nm wavelengths range (Huang *et al*. 2012). In Chapter 2, d_{II} was set to 0.5, assuming even distribution of excitation energy between the two photosystems (Maxwell and Johnson, 2000). In Chapter 3, values of d_{II} were calculated using the ratio of Φ_{II}:Φ_I at low light intensity (60 μmol quanta $m^{-2}s^{-1}$), where CET is assumed to be absent and ETR_{II}=ETR_I (Huang *et al*. 2012).

The excitation pressure of PSII was calculated as 1–qP according to Hüner *et al*. (1998, Table A5).

Table A5. Summary of fluorescence parameters used in Chapters 2, 3 and 4.

Fluorescence parameter	Formula	Reference
Maximum quantum yield of PSII	$F_v/F_m = \left(\frac{F_m - F_o}{F_m}\right)$	Genty *et al*. (1989)
Effective quantum yield of PSII of a light-adapted sample	$\Phi_{PSII} = 1 - \frac{F_s}{F_m'}$	Hendrickson *et al*. (2004)
Proportion of light absorbed by PSII antenna and thermally dissipated via dynamic NPQ	$\Phi_{NPQ} = \frac{F_s}{F_m'} - \frac{F_s}{F_m}$	Hendrickson *et al*. (2004)
Proportion energy quenched by fluorescence and sustained NPQ	$\Phi_{f,D} = \frac{F_s}{F_m}$	Hendrickson *et al*. (2004)
Electron transport rate of PSII	$ETR_{II} = \Phi_{PSII} \cdot PPFD \cdot \alpha \cdot d_{II}$	Huang *et al*. 2012
Excitation pressure of PSII	$1 - qP = 1 - \frac{F_m' - F_s}{F_m' - F_o}$	Hüner *et al*. (1998)

Chlorophyll fluorescence using the Walz Dual-PAM-100 (Chapter 4)

To assess chlorophyll fluorescence in the field, a Dual-PAM-100 (Walz, Effeltrich, Germany) was used for the measurements, with a fiberoptic mounted on a leaf holder (2030-B). A saturating light pulse was first applied to dark-adapted (pre-dawn) needles for determination of F_o and F_m. The needles were then exposed to 1200 µmol photon $m^{-2}s^{-1}$ actinic light for a period of 12 minutes. During that period a 400 ms saturating pulse of 10000 µmol photon $m^{-2}s^{-1}$ was applied every 40 s for determination of F_s and F_m', and a weak pulse of far-red light for determination of F_o'. Fluorescence and energy partitioning parameters were calculated according to Table A5.

A4 PSI absorbance protocols

PSI absorbance using the Walz Dual-PAM-100 (Chapter 3)

In Chapter 3, absorbance changes of the reaction centre chlorophyll of PSI (P700) were assessed simultaneously with chlorophyll fluorescence measurements using a Dual-PAM-100. The P700 signal (P) was calculated as the difference of the 875 nm and 830 nm transmittance signals. Firstly, P700 oxidation was transiently induced by applying a saturating pulse after far-red pre-illumination of dark-adapted needles. Briefly after the SP, the minimal P700 signal was measured to capture a state of full P700 reduction. The difference between the fully reduced and fully oxidized states is denoted P_m. Secondly, actinic illumination was applied with the same actinic light intensities and SPs used for fluorescence. Upon application of each saturating pulse maximum change of the P700 signal (P_m') was determined. Each saturating pulse was followed by a 1s dark interval for full reduction of P700 and determination of the minimal P700 signal (P_o).

The three types of quantum yields of energy conversion in PSI, Φ_{PSI}, Φ_{ND} and Φ_{NA} were assessed according to Klughammer and Schreiber (1994) and calculated according to Pfündel *et al.* (2008, Table A6).

Analogous to ETR_{II}, the electron transport rate of PSI (ETR_I, in µmol electron $m^{-2}s^{-1}$) was calculated as $ETR_I = \Phi_{PSI} \cdot \alpha \cdot d_I$ where d_I was calculated as $d_I = 1 - d_{II}$ (Huang *et al.* 2012).

Cyclic electron transport (CET, in μmol electron $m^{-2}s^{-1}$) was calculated according to Huang *et al.* (2012) as $CET = ETR_I - ETR_{II}$.

Table A6. Summary of P700 parameters used in Chapter 3.

P700 parameter	Formula	Reference
Effective quantum yield of PSI	$\Phi_{PSI} = \frac{P_m' - P}{P_m}$	Pfündel *et al.* (2008)
Fraction of overall P700 that is oxidized in a given state due to a lack of electron donors (donor side limitation)	$\Phi_{ND} = \frac{P - P_o}{P_m}$	Pfündel *et al.* (2008)
Fraction of overall P700 that cannot be oxidized by a saturation pulse in a given state due to a lack of electron acceptors (acceptor side limitation)	$\Phi_{NA} = \frac{P_m - P_m'}{P_m}$	Pfündel *et al.* (2008)
Electron transport rate of PSI	$ETR_I = \Phi_{PSI} \cdot PPFD \cdot \alpha \cdot d_I$	Huang *et al.* 2012
Cyclic electron transport	$CET = ETR_I - ETR_{II}$	Huang *et al.* (2012)

A5 Spectral reflectance protocols

PRI measurements using the Unispec-SC (Chapters 2 and 3)

For the autumn and spring growth chamber experiments, needle spectral reflectance was measured with a Unispec-SC spectrometer (UNI007, PP Systems, Haverhill, MA, USA). The spectrometer was connected to a bifurcated fiberoptic (UNI400) and a leaf clip (UNI500) maintaining the fiberoptic on the needle surface at a fixed angle of 60° relative to needle axis (2 mm diameter spot size). Needle reflectance was computed by dividing each needle scan by the radiance obtained from a white reflectance standard (Spectralon, Labsphere, North Sutton, NH, USA) taken immediately before each needle measurement.

Dark current instrument noise was subtracted from white standard and needle radiance measurements.

Reflectance was measured on needles of the topmost part of the leader shoot. Needles were in bundles of approximately 10-15 needles arranged in parallel to form a single layer flat plane. For each measurement, 30 scans were averaged, followed by interpolation of the ~3.3 nm resolution output of the spectrometer to 1 nm bandwidths using the software Multispec v. 5.1.0 (Purdue University, Indiana, USA). Finally, PRI was calculated according to Peñuelas *et al*. (1995) as PRI = $(R_{531}-R_{570})/(R_{531}+R_{570})$ where R_{531} and R_{570} represent needle reflectance at 531 and 570 nm, respectively. At each time point, reflectance was measured at pre-dawn and at midday. In order to compare PRI variation at a seasonal timescale, we used pre-dawn PRI measurements to separate the effects of sustained and dynamic pigment variations on PRI (Gamon & Berry 2012).

PRI measurements using the Unispec-SC (Chapter 4)

In the field, seasonal variations in PRI were also assessed using a Unispec-SC spectrometer connected to a bifurcated fiberoptic (UNI400) and mounted on the Dual-PAM-100 leaf holder. This ensured that the same needles were measured as for fluorescence measurements and maintained the fiberoptic on the needle surface at a fixed angle of 60° relative to needle axis (2 mm diameter spot size). For each measurement, 3 scans were averaged from dark-adapted needles, and 1 scan was recorded every 40 s over a period of 12 minutes. The integration time was set to 10 ms and 40 scans were averaged for each measurement. Reflectance was measured on previous-year needles of the topmost part of the leader shoot. Leaf reflectance was computed as explained above and calculated in the same way.

A6 Light-response curves protocol

Gas exchange, fluorescence and PRI light-response curves (Chapters 2 and 3)

In Chapters 2 and 3, to assess LUE_A, energy partitioning and PRI at a diurnal timescale, light response curves were measured on day 0 as well as on day 16 of the experiment. A pre-dawn dark-adapted bundle of needles was exposed to 10-minute steps of increasing actinic

light intensity (0-2000 µmol quanta $m^{-2}s^{-1}$). At each light step, Φ_{PSII}, Φ_{NPQ} and $\Phi_{f,D}$ were recorded with the Dual-PAM-100. Then, assimilation was measured with the GFS-3000 and LUE_A was calculated, with measurement and cuvette conditions identical to those used for assessing variation of photosynthetic activity at a seasonal timescale (see above). Finally, spectral reflectance was assessed using the Unispec-SC, with 3 scans averaged at each light step. To assess the range of diurnal PRI variation, we calculated ΔPRI as the difference between PRI dark-adapted needles and PRI measured at 2000 µmol quanta $m^{-2}s^{-1}$ according to Gamon & Berry (2012).

A7 Photosynthetic pigment protocols

Recipe

Pigment extraction buffer (0.01M ammonium acetate in methanol)

2 ml 0.5 M ammonium acetate, pH 7.1

98 ml methanol

Photosynthetic pigment extraction and HPLC analysis (Chapters 2-4)

Photosynthetic pigment extraction and analysis was performed according to Junker and Esminger (2016). Needle samples for pigment analysis were collected after at least 2 hours of exposure to growth light. The samples were immediately frozen in liquid nitrogen and stored at -80°C. The needles were then ground to a fine powder in liquid nitrogen. Pigments were extracted in dim light conditions in 98% methanol buffered with 2% 0.5M ammonium acetate for 2 hours. The extracts were filtered through a 0.45 µm PTFE filter prior to high-performance liquid chromatography (HPLC) analysis. HPLC analysis was performed with an Agilent 1260 system (Agilent Technologies, Santa Clara, CA, USA) with a quaternary pump, autosampler set to 4 °C, column oven set to 25°C and photodiode array detector. Pigments were detected at 450 nm and 656 nm wavelengths and separated using a reverse-phase C_{30}-column (5 µm, 250*4.6 mm; YMC Co. Ltd., Kyoto, Japan) protected by a 20*4.6 mm guard column. Three solvents, i.e. A: 100% methanol, B: 100% methyl-tert-butyl-ether and C: ultrapure water buffered with 0.2% ammonium acetate and set to pH 6, were used to run a gradient starting with 92% A, 5% B and 3% C. During each run solvent

A was gradually replaced by solvent B to a minimum of 5% B. Every run was followed by a 5 min reconditioning phase with initial solvent concentrations. For calibration and peak detection, commercially available standards were obtained from Sigma Aldrich (St. Louis, MO, USA) and DHI Lab products (Hørsholm, Denmark). Peak detection and pigment quantification was performed using ChemStation software (Agilent Technologies, Santa Clara, CA, USA).

Total chlorophylls (Chl) were determined as the sum of chlorophyll a and b concentration on a fresh weight basis (μmol g^{-1}), as the water content of *P. strobus* needles varies less than 10% year-round (Verhoeven *et al.* 2009). The ratio of Chl a/b was expressed in mol mol^{-1} and the concentration of carotenoid pigments was normalized to chlorophyll levels and was expressed in mmol carotenoids mol Chl^{-1}. Total carotenoids (Car) were expressed (in mmol mol Chl^{-1}) as the sum of violaxanthin, antheraxanthin, zeaxanthin, neoxanthin, lutein, α-carotene and β-carotene concentrations. Total xanthophyll cycle pigments (VAZ) were calculated as the sum of violaxanthin, antheraxanthin and zeaxanthin. DEPS (in mol mol Chl^{-1}) was expressed as DEPS = (0.5A + Z)/(V + A + Z).

A8 Statistical methods

Analysis of variance (Chapters 2 and 3)

In Chapters 2 and 3, the effects of treatments on individual parameters at each time point were estimated using mixed model analysis of variance (ANOVA). The mixed model analysis included the data of two independent experiments. Each experiment was included in the mixed model as a random effect. The mixed model analysis was performed using the difflsmeans function in the lmerTest package, using R version 3.1.1 (R Core team, 2014).

Linear regression curve fitting (Chapters 2, 3 and 4)

In chapters 2 and 3, in order to evaluate the strength of the relationship between PRI and physiological parameters both at diurnal and seasonal timescales, we obtained R^2 values from linear regressions with log-transformed variables and considered the slope significantly different from zero when $P<0.05$. Regressions were performed using GraphPad Prism 6 software version 6.05 or version 7.03 (GraphPad Software, Inc., La Jolla, CA, USA).

Generalized linear mixed modelling (Chapter 2)

In Chapter 2, for the estimation of the best predictors for PRI at a seasonal timescale, we pooled data from both treatments and used mixed regression models and the Akaike information criterion (AIC) scores as a measure of model goodness of fit using the lmer function in the lme4 package in R version 3.1.1 (R Core team, 2014). ΔAIC values were calculated by subtracting the AIC score of each predictor model from the AIC score of the null model. Predictors were ranked according to ΔAIC values, with high ΔAIC representing high goodness of fit. Each experiment was included as a random effect to account for the two independent sets of experiments in both years. Significance of predictors was calculated comparing the null model to the predictor model using ANOVA.

Deriving phenology metrics from time series (Chapter 4)

In Chapter 4, spring and autumn phenology metrics were derived from our physiological and optical time series by fitting the data to a logistic function using a method described in Gonsamo *et al*. (2012, 2013). Firstly, for each parameter (i.e., F_v/F_m, Φ_{II}, A, g_s, R_d, Φ_{NPQ} Φ_{fD}, Carotenoids Chl^{-1}, Zeaxanthin Chl^{-1}, DEPS, PRI and CCI), time series were divided into spring or autumn transition sub-datasets. Spring and autumn subdatasets were fit according to the logistic functions presented in table A7 with parameters summarized in table A8.

Table A7 Logistic regression formulae used in Chapter 4

Season	**Logistic function**	**References**
Spring	$y(t) = \alpha_1 - \frac{\alpha_3}{1+e^{\delta_2(t-\beta_2)}}$	Gonsamo *et al.* (2012, 2013)
Autumn	$y(t) = \alpha_1 - \frac{\alpha_3}{1+e^{\delta_2(t-\beta_2)}}$	Gonsamo *et al.* (2012, 2013

Table A8 Summary of the logistic function parameters used in Chapter 4.

Parameter	Description
$y(t)$	observed parameter at day of year (DOY) t
α_1	background (winter) parameter value
α_2	early summer plateau value
δ_1	spring transition normalized slope coefficient
β_1	midpoint in DOY of the spring transition
α_3	late summer plateau value of the observed parameter
δ_2	autumn transition normalized slope coefficient
β_2	midpoint in DOY of the autumn transition

Data were fitted to the logistic functions with nonlinear regressions ran with the first guess values of the seven parameters in equations 7 and 8 and solved with maximum of 1000 iterations using GraphPad Prism 7.03 (GraphPad Software, Inc., La Jolla, CA, USA). First guess values were based on field observations.

Two key transition dates were then computed, i.e. start of recovery (SOR) and start of downregulation (SOD), in DOY, as the third (f"(x)) derivatives of the logistic function according to the formulae presented in table A9 (Gonsamo *et al*. 2012, 2013).

Table A9 Formulae used to derive SOR and SOD in Chapter 4.

Parameter	Description	Formula
SOR	Start of recovery	$\beta_1 - (4.562/2\delta_1)$
SOD	Start of downregulation	$\beta_2 - (4.562/2\delta_2)$

SOR represents the point in time during the spring transition where the parameter initiates recovery and SOD representing the point in time during the autumn transition where the parameter initiates downregulation. SOD and SOR values were obtained for each treatment*provenance group (6 groups) for each plot (n=5). Group differences were tested using one-tailed unpaired Student's t-test with seedlings from the local provenance growing at ambient temperature (LP/AT) used as a control group.

Publications

From this thesis:

Chapter 1 is in preparation to be submitted to a peer-reviewed journal as a review article.

Chapter 2 was published in the journal *Tree Physiology*.

Fréchette E, Chang CY and Ensminger I (2016) Photoperiod and temperature constraints on the relationship between the photochemical reflectance index and the light use efficiency of photosynthesis in *Pinus strobus*. Tree Physiology 36(3):311-324.

Chapter 3 was published in the *Journal of Experimental Botany*.

Fréchette E, Wong CYS, Junker LV, Chang CY and Ensminger I (2015) Zeaxanthin-independent energy quenching and alternative electron sinks cause a decoupling of the relation between the photochemical reflectance index (PRI) and photosynthesis in an evergreen conifer during spring. Journal of Experimental Botany 66(22):7309-7323.

Chapter 4 is in preparation to be submitted to a peer-reviewed journal as an original research article.

Other articles:

Chang, C. Y., Fréchette E., Unda, F., Mansfield, S. D., Ensminger, I. Elevated temperature and elevated CO_2 stimulate late season photosynthesis but impair freezing resistance in Eastern white pine seedlings. Plant Physiology 172(2) 802-818.